

**Reconstruction of past bottom water conditions of the
Peruvian Oxygen Minimum Zone for the last 22,000 years and
the benthic foraminiferal response to (de)oxygenation**

Dissertation

Submitted for the degree of
Doctorate in Natural Sciences

Dr. rer. nat. der
zur Erlangung des Doktorgrades

Dr. rer. nat. der

Faculty of Mathematics and Nature Science
Christian-Albrechts-University of Kiel
Mathematisch Naturwissenschaftlichen Fakultät
der ChristianAlbrechts Universität
zu Kiel

submitted by

vorgelegt von

Zeynep Erdem

Kiel, May 2016

Erster Gutachter: Prof. Dr. Wolf-Christian Dullo

Zweiter Gutachter: Prof. Dr. Dirk Nürnberg

Tag der Disputation: 16.06.2016

Zum Druck genehmigt:

Declaration

I, Zeynep Erdem, hereby declare that apart from the guidance of my supervisors, I have independently and entirely conducted this doctoral work and written the dissertation without any kind of unauthorized aid. Neither this nor a similar work has been published, submitted for publication, or submitted for an examination procedure to another department or institution. I assure that the presented research project has been conducted in full compliance with the rules of good scientific practice laid by the German Research Foundation (DFG).

Kiel,

Zeynep Erdem, M.Sc.

Erklärung

Hiermit erkläre ich, Zeynep Erdem, dass ich, abgesehen von der Unterstützung meiner Betreuer, diese Doktorarbeit eigenständig und ohne unerlaubte Hilfe durchgeführt habe. Weder diese noch eine ähnliche Arbeit wurde an einer anderen Abteilung oder Hochschule im Rahmen eines Prüfungsverfahrens vorgelegt, veröffentlicht oder zur Veröffentlichung vorgelegt. Ich versichere, dass die Arbeit unter Einhaltung der guten wissenschaftlichen Praxis der Deutschen Forschungsgemeinschaft entstanden ist.

Kiel,

Zeynep Erdem, M.Sc.

Contents

Abstract	iii
Zusammenfassung	vi
Abbreviations	ix
1. INTRODUCTION.....	1
1.1. Motivation and previous work.....	1
1.2. Outline	3
1.3. Declaration of contribution.....	4
1.4. Study Area	5
1.4.1. Present Hydrodynamics of the Eastern Equatorial Pacific.....	5
1.4.2. The Peruvian OMZ & Upwelling.....	8
1.4.3. Sediment distribution along the Peruvian margin	10
1.5. Micropaleontological proxies: benthic foraminifera	11
1.5.1. Benthic foraminifera in oxygen depleted habitats.....	12
1.5.2. Benthic foraminifera of the Eastern Equatorial Pacific OMZs	15
2. METHODOLOGY AND STRATIGRAPHIES OF THE SEDIMENT CORES.....	17
2.1. Age models of the sediment cores	19
2.2. Core specific information	22
3. PERUVIAN SEDIMENTS AS RECORDERS OF AN EVOLVING HIATUS FOR THE LAST 22 THOUSAND YEARS.....	33
3.1. Introduction	35
3.2. Regional setting	35
3.2.1. Physical Oceanography	36
3.2.2. Sediments and topography of Peruvian margin	39
3.3. Material and Methods	40
3.3.1. Chronostratigraphy.....	40
3.3.2. Determination of critical slope areas.....	43
3.4. Results	45
3.4.1. General facies distribution	45
3.4.2. Sediments of the time windows: Recent, late and early Holocene, BA, HS1 and LGM	46
3.4.3. Distribution of phosphorites.....	48
3.4.4. Near critical slope areas	49
3.5. Discussion.....	50
3.5.1. Phosphorites as erosion indicators	52

3.5.2.	Evolving sedimentary dynamics at the Peruvian margin.....	54
3.5.3.	Potential effects of mid-depth hydrodynamic change.....	55
3.6.	Conclusions	56
4.	DOWNCORE BENTHIC FORAMINIFERAL DISTRIBUTIONS FROM THE PERUVIAN MARGIN FOR THE LAST 22,000 YEARS.....	59
4.1.	General trends.....	59
4.2.	The most abundant species and their indications	68
5.	BOTTOM-WATER DEOXYGENATION AT THE PERUVIAN MARGIN DURING THE LAST DEGLACIATION RECORDED BY BENTHIC FORAMINIFERA	71
5.1.	Introduction	72
5.1.1.	Benthic foraminifera as oxygen proxy	74
5.1.2.	Regional setting.....	77
5.2.	Materials and Methods	78
5.2.1.	Sediment cores	78
5.2.2.	Surface samples and living benthic foraminifera.....	78
5.2.3.	Statistical analyses	82
5.3.	Results and Discussion.....	83
5.3.1.	Living benthic foraminiferal distributions	83
5.3.2.	Results and interpretation of statistical analyses.....	85
5.3.3.	Quantification of BWO concentrations: downcore records	89
5.3.4.	Comparison with other proxies and records from the EEP.....	94
5.4.	Summary and Conclusions.....	97
6.	SUMMARY AND OUTLOOK.....	99
6.1.	Summary	99
6.2.	Outlook.....	102
	REFERENCES.....	105
	APPENDIX.....	123
	Thank you	195
	Curriculum Vitae.....	197

Abstract

The Eastern Equatorial Pacific (EEP) is characterized by oxygen depleted waters as result of intense upwelling, enhanced surface primary productivity and sluggish ventilation of the subsurface waters. The dynamics of these oxygen minimum zones (OMZs) are closely related to changing climatic conditions with recent observations indicating these zones are expanding as the atmosphere and oceans warm. To advance our understanding of the OMZs and improve modelling under future warming, we need to decipher the dynamics of dissolved oxygen during past periods of temperature fluctuation, such as during glacial-interglacial transitional periods.

The Peruvian margin hosts one of the strongest OMZs in the today's oceans and has long been in the focus of (paleo)-oceanographic investigations. Many paleo-proxy records from the region indicate increased oxygen depletion during the last deglaciation, Termination I. This present study investigated the potential changes in the structure and shape of the OMZ since the Last Glacial Maximum (LGM) using downcore distributions of the benthic foraminiferal assemblages. The sediment cores considered in this study were recovered from the lower oxic-suboxic boundary of the OMZ in order to reconstruct temporal and spatial changes in the extension of the OMZ. Using benthic foraminifera to quantify past bottom-water oxygen concentrations was a particular focus of this study. In addition to oxygen reconstruction, this study focused on the erosional features and gaps found in the sediment records in order to investigate the potential changes in the mid-depth hydrodynamics since the LGM. Variations within the subsurface and intermediate waters might lead changes in the ventilation of bottom-waters, thus the oxygenation.

Chronostratigraphies of nine sediment cores which were recovered during M77 during Leg 1 & 2 from the region between 3°S and 18°S are considered for this study. The age models and stratigraphic information of four cores were previously reported. The stratigraphic information of the remaining cores, methods and measurements (e.g., $\delta^{18}\text{O}$, $\delta^{13}\text{C}$, TOC, TN) done are presented in Chapter 2. Analysis of the chronostratigraphies revealed gaps and short-term interruptions of the stratigraphical records at cores from the southern part of the region, consistent with earlier studies. Hence, the bottom-water oxygen concentrations could not be determined in these cores using the benthic foraminifera approach. The extent of the hiatus and the responsible mechanisms are investigated in Chapter 3. Stratigraphic information from 31 sediment cores was compiled with a focus on the time intervals from the late Holocene (LH; 3-5 cal ka BP), the early Holocene (EH; 8-10 cal ka BP), the Bølling Ållerød/Antarctic Cold

Reversal (BA/ACR; 13-14.5 cal ka BP), the Heinrich Stadial-1 (HS1; 15-17.5 cal ka BP) and the Last Glacial Maximum (LGM; 20-22 cal ka BP). Erosional features were mainly observed in the sediment cores from the areas south of 7°S. These structures together with the hiatus found in the sediment cores depict a prograding feature on the continental slope from south to north during the deglaciation. In addition to downcore investigations, the recent oceanographic and sedimentological observations were combined. This analysis showed that tide-topography interactions result in non-linear internal waves (NLIWs) which shape the continental slope by erosion and remobilization of the sediments. Resuspended material is carried further south by the poleward flowing undercurrent, the Peru-Chile Undercurrent (PCUC), which causes non-deposition in the northern part of the continental shelf whereas in the south a depocenter forms. The compilation of downcore records and the northward expanding feature of the hiatus revealed that the tide-topography interactions, therefore enhanced bottom water activities and currents, have progressively evolved since the LGM. Elevated tidal amplitudes and changes in the mid-depth water masses during the Termination I are two potential explanations for this process.

Benthic foraminiferal investigations were done at four cores from the north between 3°S and 8°S and at one core from 17°S to compare the assemblage distributions during the LGM (Chapter 4). In total of 190 species were identified with *Bolivina costata*, *Bolivinita minuta*, *Cassidulina delicata* and *Epistominella exigua*, the four most abundant species. The oxygen quantification approach was validated using multiple regression analysis on three datasets of living (Rose Bengal stained) calcareous benthic foraminiferal distributions and measured oxygen concentrations from 1°S to 18°S. Analysis indicated that the composition of benthic foraminiferal assemblages is primarily governed by the availability of the oxygen in the bottom waters rather than the amount of deposited particulate organic matter. It was later followed by application of a transfer function to the four sediment cores from the northern part of the region. Estimated bottom water oxygen concentrations were low compared to measured modern values however the trend of decreasing oxygen levels during the Termination I and slight increase in the Holocene was consistent across all cores. The overall change in the bottom water oxygen levels from the LGM and the Holocene was reckoned to be 25 $\mu\text{mol/kg}$. Deoxygenation was observed first in the southern core at the onset of the HS1 and gradually spread to cores from deeper waters and to further north implying a gradual expansion of the northern OMZ boundary during the last deglaciation. Additionally, the comparison of the bottom water oxygen estimates with other proxies from the region showed that the deoxygenation did not always co-occur with enhanced surface productivity. Hence, parameters other than primary productivity may govern oxygen dynamics on the Peruvian margin, for instance, changes in the hydrodynamics or

ventilation of the subsurface and intermediate waters. This might be due to reduced oxygen advection from the EEP or from less ventilated intermediate water masses. The sedimentological features and the benthic foraminiferal distributions showed that the Peruvian margin hosts a complex setting with distinct regional differences between north and south of 5-7°S. The impact of the hydrodynamics in the region should not be neglected in order to better understanding the changes in bottom water oxygenation and redox conditions.

Zusammenfassung

Der östliche, äquatoriale Pazifik charakterisiert sich durch sauerstoffarme Wassermassen als Ergebnis von starkem Küstenauftrieb, erhöhter Primärproduktivität an der Oberfläche und einer trägen Ventilation des Tiefenwassers. Die dynamischen Eigenschaften einer solchen Sauerstoffminimumzone (SMZ) sind eng gekoppelt an den Klimawandel und jüngste Beobachtungen deuten darauf hin, dass sich diese Zonen als Resultat der Erwärmung von Atmosphäre und Ozeanen ausdehnen. Eine Rekonstruktion der Dynamik der Sauerstoffsättigung in der Vergangenheit ist unabdingbar zum Fortschritt des Verständnisses von SMZs und zur Modellierung möglicher Zukunftsszenarien. Untersuchungen von Glazial-Interglazial Zyklen an marinen Sedimentkernen aus SMZs sind demnach unerlässlich. Die SMZ am Kontinentalhang vor Peru gehört zu den sauerstoffärmsten Gebieten der gegenwärtigen Weltmeere und steht schon lange im Fokus vieler (paleo-)ozeanographischer Studien. Viele der Paleorekonstruktionen aus dieser Region deuten während der letzten Deglaziation (Termination I) eine Intensivierung und Ausdehnung der SMZ an. Das Hauptaugenmerk der hier präsentierten Studie liegt auf der Untersuchung potentieller Änderungen von Struktur und Form der peruanischen SMZ seit dem letzten glazialen Maximum (LGM) mittels Verteilung von benthischen Foraminiferenvergesellschaftungen kernabwärts. Die untersuchten Sedimentkerne stammen von der unteren Grenze der SMZ, um Änderungen in der Ausdehnung sowohl in Zeit als auch im Raum zu erfassen. Es soll hervorgehoben werden, dass in diesem Ansatz Änderungen der Sauerstoffkonzentration im Bodenwasser quantitativ erfasst werden sollen.

In der vorliegenden Studie wurden neun Sedimentkerne aus dieser Region untersucht, die während M77 Teilabschnitt 1 & 2 genommen wurden. Von vier Kernen wurden Altersmodell und stratigraphische Informationen bereits früher veröffentlicht. Die stratigraphischen Informationen der verbleibenden Kerne werden inklusive aller Methoden und Messungen ($\delta^{18}\text{O}$, $\delta^{13}\text{C}$, TOC, TN) in Kapitel 2 dieser Arbeit präsentiert. Der Vollständigkeit halber und für einen Vergleich regionaler Unterschiede aus erster Hand werden auch die Informationen aus den vorhergehenden Studien in diesem Kapitel beschrieben. Die Chronostratigraphien zeigten Lücken und kurzzeitige Unterbrechungen in den stratigraphischen Datensätzen aus dem südlichen Teil der Region. Derartige Lücken wurden schon in vorhergehenden Studien dargelegt. Zwecks Untersuchung der Ausdehnung dieses Hiatus und der verantwortlichen Mechanismen wird in Kapitel 3 eine Kompilation der stratigraphischen Informationen von 31 Sedimentkernen präsentiert. Der Fokus der hier präsentierten Studie liegt auf folgenden Zeitabschnitten: Spätes Holozän (LH; 3-5 cal ka BP), frühes Holozän (EH; 8-10 cal ka BP), Bølling

Ållerød/Antarktischer Kälterückfall (BA/ACR; 13-14.5 cal ka BP), Heinrich Stadial-1 (HS1; 15-17.5 cal ka BP) und das letzte glaziale Maximum (LGM; 20-22 cal ka BP). Die Erosionsmerkmale zeigt sich am deutlichsten südlich von 7°S. Am Kontinentalhang deutete sich eine nordwärtige Ausdehnung des Hiatus und der erosiven Fläche im Verlauf der letzten Deglaziation an. Ergänzend zu den Paleountersuchungen wurden rezente ozeanographische und sedimentologische Untersuchungen kombiniert und zeigen, dass durch Wechselwirkungen von Tiden mit der Topographie des Kontinentalhangs nicht lineare interne Wellen (NLIWs) entstehen, die zu einer Erosion und Remobilisation von Sedimenten führen. Das in Suspension gebrachte Material wird durch den polwärts gerichteten Peru-Chile Unterstrom (PCUC) nach Süden transportiert, wodurch sich ein Depozentrum am südlicher gelegenen Teil des Kontinentalhangs bildet. Eine Kompilation der Paleodaten und des nordwärts expandierenden Hiatus zeigte, dass die Wechselwirkung zwischen Tiden und Topographie des Kontinentalhangs seit dem LGM fortlaufend zugenommen haben. Die Hauptgründe für diesen Prozess liegen vermutlich in erhöhten Tidenamplituden und Veränderungen in den Wassermassen der mittleren Tiefen während der Termination I.

Aufgrund der weitverbreiteten Erosion und des damit verbundenen Hiatus wurden die Studien hinsichtlich der benthischen Foraminiferenvergesellschaftungen beschränkt auf vier Kerne zwischen 3°S und 8°S und einen Kern aus 17°S zum Vergleich der Vergesellschaftungen während des LGM. Insgesamt wurden 190 Arten identifiziert. Die häufigsten Arten waren *Bolivina costata*, *Bolivinita minuta*, *Cassidulina delicata* und *Epistominella exigua*. In Kapitel 4 werden die Vergesellschaftungen kernabwärts dokumentiert. Drei Datensätze von lebenden (mit Bengalrosa angefärbten), kalkschaligen Foraminiferenvergesellschaftungen wurden zusammengefasst als Ausgangspunkt für die quantitative Rekonstruktion von Sauerstoffkonzentrationen im Bodenwasser kernabwärts. Ausgehend von diesem Gesamtdatensatz und den Sauerstoffkonzentrationen im Bodenwasser als abhängige Variable wurden multiple Regressionsanalysen durchgeführt. Diese Tests gaben deutliche Indikationen dafür, dass die Zusammensetzung der Foraminiferenvergesellschaftungen hauptsächlich von der Sauerstoffkonzentration und nicht von der Ablagerung von partikulärem, organischem Material reguliert wird. Die auf der Regression basierende Transferfunktion wurde auf die vier nördlichen Sedimentkerne angewandt. Verglichen mit den modernen Sauerstoffkonzentrationen im Bodenwasser waren die rekonstruierten Werte relativ gering. In jedem Kern zeigte sich allerdings ein Trend zu sinkenden Sauerstoffkonzentrationen im Verlauf von Termination I gefolgt von einem geringen Anstieg während des Holozäns. Insgesamt nahm der Sauerstoffgehalt zwischen LGM und Holozän um ca. 25 $\mu\text{mol/kg}$ ab. Die Deoxygenierung wurde

zu Beginn von HS1 zuerst im Süden beobachtet und dehnte sich allmählich in tiefere Wassermassen und nach Norden aus. Dieser Trend impliziert generell eine Ausdehnung der SMZ im Verlauf der letzten Deglaziation und ist vermutlich als Folge reduzierter Sauerstoffadvektion aus dem ostäquatorialem Pazifik oder anderer weniger gut ventilerter Wassermassen. Ein Vergleich mit anderen Proxydatensätzen aus dieser Region zeigte außerdem, dass die Deoxygenierung nicht immer gekoppelt war an eine erhöhte Primärproduktion. Dies lässt vermuten, dass zusätzlich zur Primärproduktion andere Parameter die Dynamik von Sauerstoffkonzentrationen in der peruanischen SMZ antreiben, beispielsweise Änderungen in der Hydrodynamik oder der Ventilation der Wassermassen aus flachen und mittleren Tiefen. Die Sedimentologie und die Zusammensetzung der Foraminiferenvergesellschaftungen zeigen demnach, dass die peruanische SMZ eine Umgebung mit komplexen dynamischen Eigenschaften und ausgeprägten regionalen Unterschieden nördlich und südlich von 5-7°S darstellt. Zum Verständnis von Änderungen der Redoxbedingungen darf der hydrodynamische Einfluss in dieser Region nicht außer Betracht gelassen werden.

Abbreviations

AABW – Antarctic Bottom Waters
AAIW – Antarctic Intermediate Waters
ACC – Antarctic Circumpolar Current
ACR – Antarctic Cold Reversal
AMS – Accelerator Mass Spectrometer
AR – Accumulation rates
BA – Bølling Ållerød
BP – Before present
BWO – Bottom water oxygen
CCA - Canonical Correspondence Analysis
CPDCC – Chile-Peru Deep Coastal Current
CTD – Conductivity-Temperature-Density (*instrument*)
EEP – Eastern Equatorial Pacific
EH – early Holocene
ENSO – El Niño-Southern Oscillation
EPICA – European Project for Ice Coring in Antarctica
EUC – Equatorial Undercurrent
GC – Gravity core
GUC – Gunther Undercurrent
HS1 – Heinrich Stadial-1
ITCZ – Intertropical Convergence Zone
LGM – Last Glacial Maximum
LH – late Holocene
NECC – North Equatorial Countercurrent
NLIW – Non-linear Internal Wave
MUC - Multicore
OMZ – Oxygen Minimum Zone
PAST - PAleontological STatistics
PC – Piston core
PCC – Peru Coastal Current
PCCC – Peru Chile Countercurrent
PCUC – Peru Chile Undercurrent
PDW – Pacific Deep Waters

POC – Peru Oceanic Current
RRPOC – Rain Rates of Particulate Organic Carbon
SAMW – Sub-Antarctic Mode Waters
SEC – South Equatorial Current
SEM – Scanning Electron Microscope
SFB – Sonderforschungsbereich
SR – Sedimentation rates
SSCCs – Southern Subsurface Countercurrents
SST – Sea Surface Temperature
TN – Total nitrogen
TOC – Total organic carbon
TROX – TRophic OXYgen
UPGMA - Unweighted Pair Group Method
WOD – World Ocean Database

1. INTRODUCTION

1.1. Motivation and previous work

The Earth's climate is undergoing drastic changes due to increasing anthropogenic impact. Meanwhile deoxygenation in the world oceans also became a growing concern. Recent observations reported an increasing trend of the Oxygen Minimum Zones' (OMZs) expansion in accordance with the warming world (Stramma et al., 2008; Stramma et al., 2010). The interdisciplinary project, Collaborative Research Centre (SFB: Sonderforschungsbereich) 754 "Climate-Biogeochemistry Interactions in the Tropical Oceans" focuses on these zones in order to understand the dynamics in relation with the changing climate with the following questions:

- 1) How does subsurface dissolved oxygen in the tropical ocean respond to variability in ocean circulation and ventilation?
- 2) What are the sensitivities and feedbacks linking low or variable oxygen levels and key nutrient source and sink mechanisms? In the benthos? In the water column?
- 3) What are the magnitudes and time scales of past, present and likely future variations in oceanic oxygen and nutrient levels? On the regional scale? On the global scale?

The present study, taking part in the second phase of the SFB and subproject B7, focused on question 3 and investigated the past variations in bottom water oxygen concentrations on a regional scale. Today, there are few places in the world oceans where these variations could be studied. The Peruvian margin is characterized by one of the most pronounced and persistent OMZs in the tropical oceans (Figure 1.1). Consequently, this study presents results obtained from sediment cores which were collected from the Peruvian margin in 2008 during expeditions M77 Leg 1 & Leg 2 aboard *R/V Meteor*. The main goal of the present study is a reconstruction of the bottom-water oxygen (BWO) concentrations for the last 22,000 years by using benthic foraminiferal assemblages.

Paleoceanographic and paleoclimatic reconstructions are needed for a better understanding of the changing climate, ocean and atmospheric circulation, hydrodynamics and the influence of all these changes on the living Earth. The elucidating past conditions would help us to formulize and model the future scenarios. Particularly investigating the last warming period (Termination I) at the end of the Last Glacial using marine sediment cores is crucial to obtain a sound understanding of today's warming atmosphere and oceans. Thanks to their global distribution, quick response to environmental changes, and tests preserved in the fossil record,

benthic foraminifera have served as important tools in paleoceanography and paleoclimatology. Their distributions in oxygen depleted environments have been matter of discussion and interest over the past decades. Some species were observed to be resistant to extremely low oxygen levels (e.g., Sen Gupta and Machain-Castillo, 1993; Bernhard and Sen Gupta, 1999; Gooday, 2003). Some of them have morphological features, such as pore structures, facilitating them to adapt to these extreme conditions (e.g., Piña-Ochoa et al., 2010; Glock et al., 2012b; Kuhnt et al., 2013). Certain species were used to assess the relative changes in the bottom water oxygenation during the last deglaciation at different parts of the Pacific Ocean (e.g., Moffitt et al., 2014; Praetorius et al., 2015).

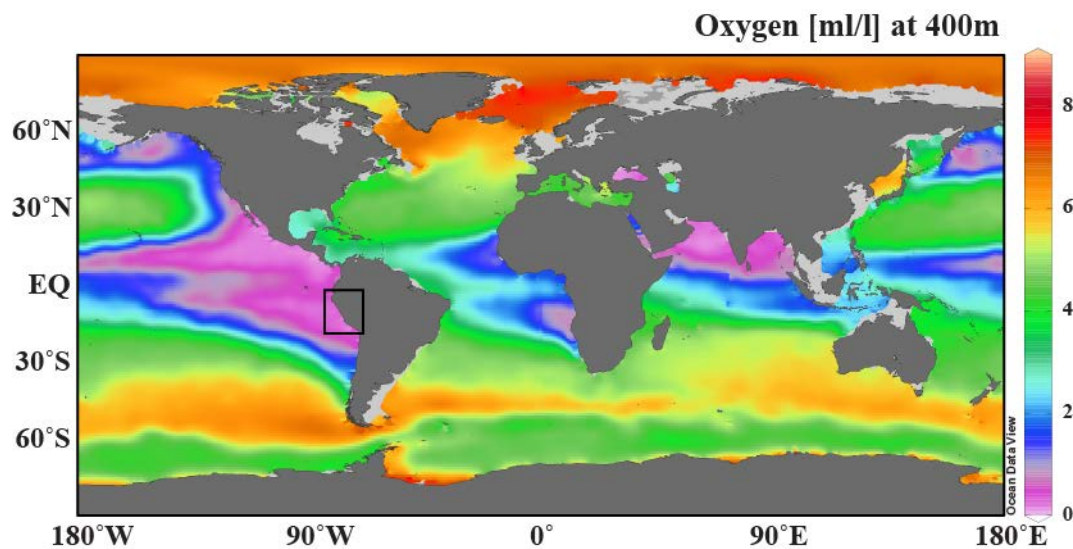


Figure 1. Global map showing the dissolved oxygen concentrations in the water column at 400 m water depths. The study area is depicted with a square; it is located in southern part of the Eastern Equatorial Pacific (EEP). Data is obtained from World Ocean Database, WOD2013 (Boyer et al., 2013).

In order to understand the recent processes and to create calibration datasets for downcore applications regarding to all these motivations mentioned above, surface sediment samples and cores were collected with a Multi-Corer, MUC from the Peruvian margin during the first phase of the project SFB754 in 2008. The living (rose Bengal stained) benthic foraminiferal distributions, taxonomy and morphological characteristics developed under the prevailing bottom-water conditions (e.g., oxygen concentrations) were previously documented as Ph.D. theses and related articles (Glock, 2011; Glock et al., 2011; Mallon, 2012; Mallon et al., 2012). To accomplish this dataset, living benthic foraminiferal faunas from 12 additional stations were included (Pérez et al., unpublished; Cardich et al., 2015). Using this information, the present study presents a comprehensive dataset of the benthic foraminiferal distribution along the

continental shelf and slope and attempts a reconstruction of their dynamics in relation with changing BWO concentrations.

The application to the fossil record mainly considers sediment cores recovered from the lower boundary of today's OMZ in order to investigate potential changes in shape and extension of the OMZ during the deglaciation, and to quantify past oxygen levels. The main aims of the study were to: 1) to assess the stratigraphies of previously disregarded sediment cores and to combine the new information with existing cores, 2) to extend the knowledge and provide additional information on potential changes in bottom-water oxygenation such as total organic carbon accumulation, 3) to accomplish the benthic foraminiferal taxonomy of the sediment cores and to reconstruct past BWO levels using a benthic foraminiferal quantification approach based on the living-foraminifera dataset.

1.2. Outline

In addition to the motivation and previous works, **Chapter 1** gives information on the study area, the present hydrodynamics and sedimentological characteristics of the Peruvian margin. A brief introduction on benthic foraminifera from the Peruvian margin and other Oxygen Minimum Zones is also included in this chapter.

In **Chapter 2**, basic information and stratigraphies of the sediment cores used for this study are described. Detailed information on cores, methods and materials used can be found in this chapter. Information given here is already published by (Schönfeld et al., 2015) and Erdem et al. (2016). It is used in preparation of different chapters of this thesis.

Chapter 3 presents a published paper (Erdem et al., 2016). The publication combines stratigraphical information from literature and the results from the new sediment cores. A ubiquitous hiatus and gaps in stratigraphical record were found in sediment cores from the Peruvian margin indicating an evolving structure since the LGM. The present publication focuses on the potential reasons of this non-deposition considering the present hydrodynamics of the region such as tide-topography interactions and non-linear internal wave formations and the impact of the Peru-Chile Undercurrent (PCUC) on the seabed and sediment transport.

Chapter 4 presents the downcore distribution of the benthic foraminiferal assemblages in each core separately. It includes the results obtained from the benthic foraminiferal investigations emphasizing on the most abundant species with comparisons between different cores and time intervals. Taxonomic reference list with supporting real colour pictures and SEM images can be found in the Appendix.

Chapter 5 presents the extended dataset of the living (rose Bengal stained) benthic foraminifera from the Peruvian margin. It describes BWO quantification approach in details which was applied to four sediment cores from the region using the information described in Chapter 4. Estimated BWO concentrations were later compared with previous records from the Eastern Equatorial Pacific.

All results and findings of this study are summarized in **Chapter 6**.

1.3. Declaration of contribution

Chapter 2: Parts of the results reported in this chapter are already published in Schönfeld et al., (2015) in which Zeynep Erdem is one of the co-authors. This paper is not considered as part of this Ph.D. thesis.

Data acquisition: Zeynep Erdem, Nicolaas Glock; Age Models: Zeynep Erdem

Chapter 3: Published manuscript

Idea: Zeynep Erdem

Data acquisition: Zeynep Erdem, Nicolaas Glock, data of present day hydrodynamics by Marcus Dengler, Stefan Sommer, Thomas Mosch, seismic profile processing and interpretation by Judith Elger

Interpretation: Zeynep Erdem with major input from Joachim Schönfeld and Marcus Dengler

Manuscript preparation: Zeynep Erdem with comments from co-authors.

Chapter 4: Draft manuscript

Idea: Zeynep Erdem, Joachim Schönfeld

Data acquisition: Zeynep Erdem

Interpretation, manuscript preparation: Zeynep Erdem, with comments from Joachim Schönfeld

Chapter 5: Draft manuscript (in preparation for submission)

Idea: Zeynep Erdem, Joachim Schönfeld

Data acquisition: Zeynep Erdem and input from co-authors regarding to their earlier works.

Methodology, Interpretation, Manuscript preparation: Zeynep Erdem with major in put from Joachim Schönfeld and with comments from co-authors.

1.4. Study Area

The Eastern Equatorial Pacific (EEP) comprises the tropical and subtropical areas off the western coasts of North and South America (Wyrcki, 1967; Kessler, 2006). This study focuses in particular on the southern part of the EEP offshore Peru and southern Ecuador, comprising the region between 1° and 18°S (Figure 1.1). The Peruvian coastal region is characterized by wind driven upwelling of cold and nutrient-rich water masses creating one of the most pronounced OMZs in today's world oceans. The strength and extension of the Peruvian OMZ is maintained by the combination of a sluggish ocean circulation and high primary productivity in the surface mixed layer, leading to increased organic carbon export and enhanced consumption of dissolved oxygen in the water column (Wyrcki, 1962; Fuenzalida et al., 2009). The area regarded in this study comprises the continental shelf and slope off Peru and the southern part of Ecuador. It is characterized by an active continental margin with a narrow continental shelf up to 100 km width (Strub et al., 1998). A major part of the study area is under the influence of the Peruvian OMZ extending from 50 to 500 m water depth.

1.4.1. *Present Hydrodynamics of the Eastern Equatorial Pacific*

The EEP comprises the area between the California Peninsula in the North and Peru in the South where the North and South Pacific subtropical gyres move in which eastern boundary currents prevail, e.g., the California Current from north and the Peru Current from south (Fiedler and Talley, 2006). Most of the early oceanographic studies described the tropical Pacific, its currents, winds and thermal structure, only as function of latitude. For the EEP, the situation is different from open ocean settings, because the American continent on the eastern side of the region shapes the wind and circulation systems (Kessler, 2006; and the references therein).

There are two major current systems in the area; the Equatorial Current System (Wyrcki, 1967) and the Peru Current System (Gunther, 1936; Strub et al., 1998). The Equatorial Current System is composed of the westward-flowing near-surface South Equatorial Current (SEC), the Equatorial Undercurrent (EUC) and the primary and secondary Southern Subsurface Countercurrents (pSSCC and sSSCC) flowing eastwards underneath SEC (Figure 1.2; Montes et al., 2010). The SEC is a surface current that flows along Equator with a maximum velocity and shallowest thickness of 50 cm/s and 20 to 50 m. It gets thicker to around 200 m and slower further south extending to ~10°S in direction of west-southwest with irregular velocities (Wyrcki, 1967). The EUC is the northernmost subsurface current in the area and it flows underneath the SEC along the Equator (1.5°N to 1.5°S) between water depths of 30 and 200 m with maximum mean velocities of 20 to 30 cm/s (Montes et al., 2010). The Galapagos Islands act as a barrier for

the EUC splitting the current as north and south branches flowing around the islands. They merge again on the eastern side whereas a third branch flows southeastward converging with pSSCC at around 91°W (Figure 1.2; Karnauskas et al., 2007; Montes et al., 2010). The EUC water masses are characterized by high salinity, high nutrient content and oxygen depletion that make them a main nutrient source of the upwelling of the Peruvian OMZ (Strub et al., 1998). Subsurface currents pSSCC and sSSCC flow eastwards at south of the EUC at 3-4°S and 6-8°S and with velocities of 5 cm/s and 15 cm/s, respectively (Figure 1.2; Montes et al., 2010).

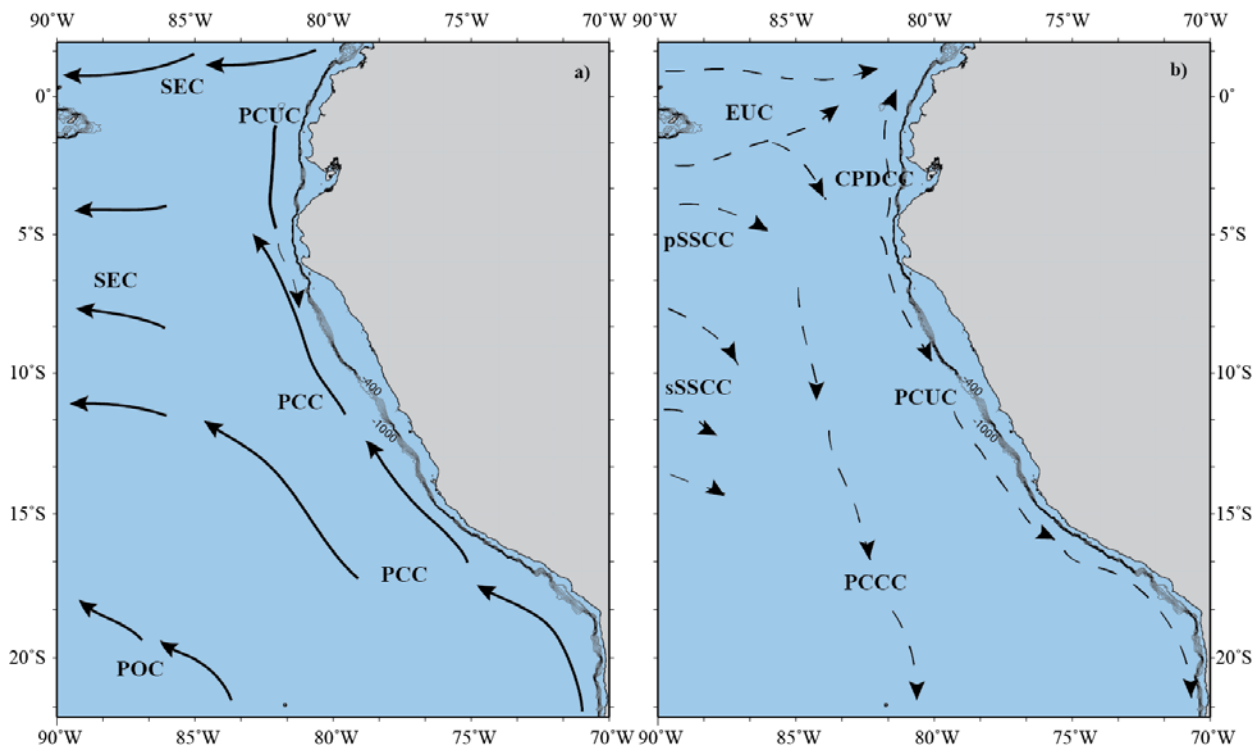


Figure 1.2. Generalized map of the surface and subsurface current systems of South EEP (modified after Montes et al., 2010; Chaigneau et al., 2013); a) surface currents; SEC: South Equatorial Current; PCC: Peru Coastal Current; POC: Peru Oceanic Current, b) subsurface currents shown as dashed lines; EUC: Equatorial Undercurrent; pSSCC: primary Southern Subsurface Countercurrent; sSSCC: secondary Southern Subsurface Countercurrent; PCUC: Peru-Chile Undercurrent; PCCC: Peru-Chile Countercurrent and CPDCC: Chile-Peru Deep Coastal Current.

The other major system, the Peru Current System is composed of the Peru Coastal Current (PCC) and the Peru Oceanic Current (POC) near the surface, the deep equatorward Chile-Peru Deep Coastal Current (CPDCC; Chaigneau et al., 2013), the Peru Chile Countercurrent (PCCC) and the Peru Chile Undercurrent (PCUC) in the subsurface, which is also called Gunther Undercurrent (GUC) (Figure 1.2; Montes et al., 2010). The northward

extension of the Humboldt Current originates from the Antarctic Circumpolar Current (ACC) and this northern flow splits off into PCC and POC at around 100-300 km offshore Chile (Mohtadi et al., 2005). The POC has a little contribution to the upwelling along the coast since it turns towards northwest to west at 24°S and is found until the water depths of 700 m (Wyrki, 1967). In contrast, the PCC flows northward at much shallower depths due to upwelling processes along to coast. The PCC divert from the coast around 5°S and joins to the westward flowing SEC (Wyrki, 1965). The CPDCC is flowing equatorward beneath the PCUC carrying cold and low salinity Antarctic Intermediate Water (Figure 1.3; Chaigneau et al., 2013; and the references therein). The equatorial subsurface water masses of PCCC and PCUC flow poleward beneath the surface currents at water depths of 100 to 400 m (Mohtadi et al., 2005) and they are fed by subsurface flowing EUC and SSCCs (Montes et al., 2010; Montes et al., 2011), thereby contributing to the coastal upwelling. The PCCC flows southward at 80°W and is strongest near 100 m depth but extends up to 500 m depth. It gets weaker and its transport decreases further south at around 22°S (Wyrki, 1967). The characteristics of the PCUC were documented by in situ measurements (Brockmann et al., 1980; Huyer et al., 1991; Czeschel et al., 2011; Chaigneau et al., 2013), and approximated by modelling studies (Montes et al., 2010; Montes et al., 2011). It originates at around 3-5°S as a shallow water mass and prevails from 50 to 300 m water depths. The PCUC prevails over the shelf and upper continental slope in the northern and central part of the region (Brockmann et al., 1980; Huyer et al., 1991; Czeschel et al., 2011). On its way south, it detaches from the continental slope south of 15°S but remains close to sea floor (Chaigneau et al., 2013).

Intermediate waters such as Antarctic Intermediate Water (AAIW) in the south of ~20°S and North Pacific Intermediate Water (NPIW) in the north of ~20°N are not the major water masses in the Eastern Equatorial Pacific (Fiedler and Talley, 2006). The low salinity ($S < 34.5$) AAIW forms at the Subpolar Front by mixing of cold fresh Sub-Antarctic Mode Water (SAMW) and Polar Front waters (Sloyan and Rintoul, 2001). It spreads northwards up to Equator in the western part of the Pacific Ocean (Tsuchiya and Talley, 1996), whereas offshore Peru and below the Peruvian current system, the AAIW spreads northward arriving until 25-30°S at water depths between 500 and 1300 m (Figure 1.4; Fiedler and Talley, 2006). Below the AAIW, old and oxygen-poor Pacific Deep Water (PDW) extends towards the South (Fuenzalida et al., 2009). The deepest water mass in the area is the northward spreading Antarctic Bottom Water (AABW; Mohtadi et al., 2005).

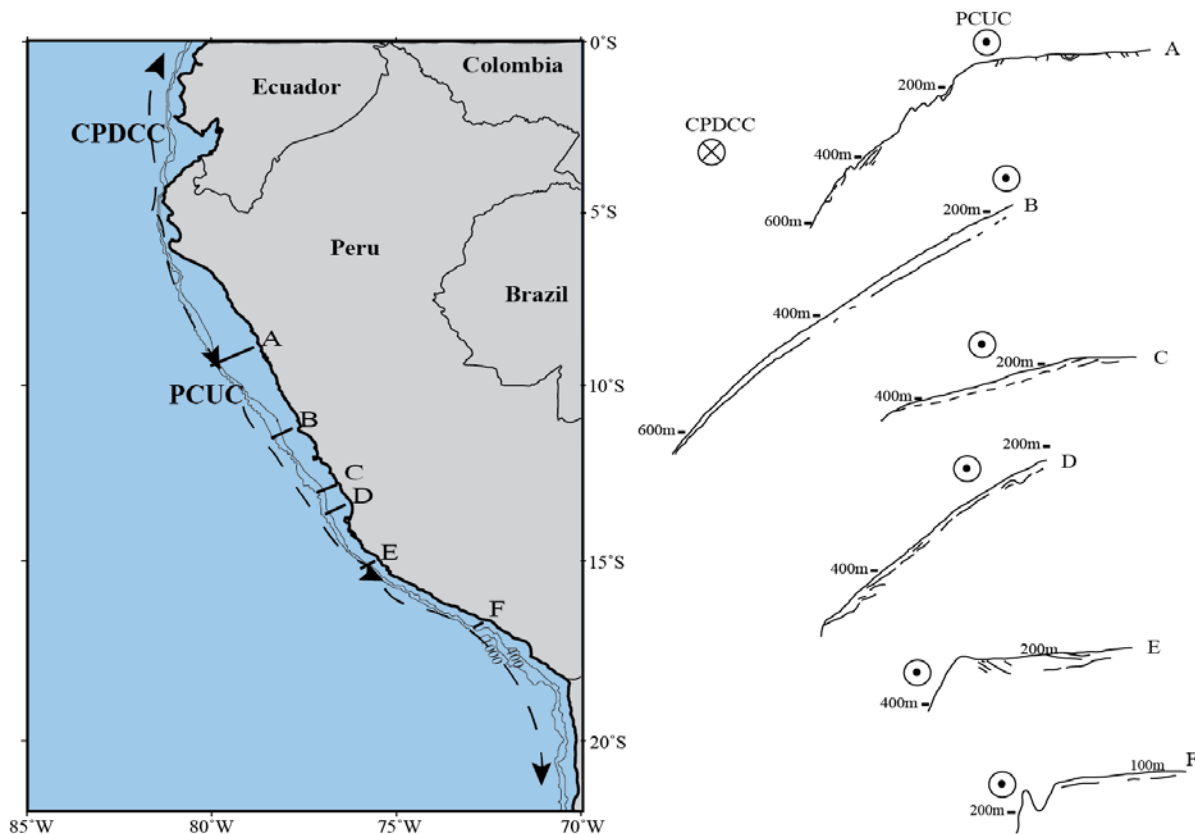


Figure 1.3. The approximate positions of the PCUC and the CPDCC in relation with the sea-floor topography. Sea-floor profiles are modified after Suess et al. (1987), locations of the cores of the currents are after Chaigneau et al. (2013).

1.4.2. The Peruvian OMZ & Upwelling

In the southern part of the EEP, persistent, long shore south-easterly trade winds induce a westward offshore Ekman transport of surface waters. Warm waters accumulate in western Pacific elevating the sea level (Wyrski and Wenzel, 1984) whereas in the area of the EEP, the eastward flowing undercurrents balance the pressure gradient caused by the elevated sea level in the west (Kessler, 2006). They bring cold and nutrient rich water masses and thereby sustain high productivity in the surface waters. Off Peru, these cold and nutrient rich waters rise from 50 to 350 m (mean depth of 130 m; Gunther, 1936) and reduce the surface water temperature by about 3°-4°C (e.g., Resig, 1990). The coasts of Peru and Chile are recognized as the most productive upwelling zone and ecosystem of today's world oceans (Ryther et al., 1971; Pennington et al., 2006). The most intense section of the Peruvian coastal upwelling is observed in the area between 5°S and 15°S reaching up to 100 km offshore and in particularly at 10°S to 15°S where the shelf becomes narrower. The strongest upwelling occurs in distinct cells in this section along the margin (Strub et al., 1998; Echevin et al., 2011; Mollier-Vogel et al., 2012).

Peruvian coastal upwelling is mostly seasonal because trade wind intensity is linked to the position of the Intertropical Convergence Zone (ITCZ), and reaches the maximum strength during southern hemisphere winter (Jun-Aug) (Pennington et al., 2006; Mollier-Vogel et al., 2013).

The whole region is characterized by not only high primary production but also by oxygen depletion in the water column due to decomposition of the organic matter. Sinking organic detritus is entrained by the PCUC, where the decay consumes oxygen in the water column. As oxygen advection is low and the flux of organic matter is high, excess oxygen consumption beneath the thermocline creates an extensive oxygen minimum zone (OMZ). The factors contributing the extreme oxygen deficiency in the EEP were considered as; (1) high production at the surface, (2) a sharp permanent pycnocline which obstructs the ventilation of subsurface water masses, (3) a sluggish deep circulation and thus limited advection of oxygenated deep waters from below the pycnocline (Kamykowski and Zentara, 1990; Helly and Levin, 2004; Fiedler and Talley, 2006). Identification of an oxygen depleted environment and classification of dissolved oxygen levels in these environments have been a matter of confusion and discussion. Kamykowski and Zentara (1990) presented their statistically treated data of dissolved oxygen concentrations in ml/l. Most of the following studies on oxygen minimum zones and oxygen depleted environments used this unit. Helly and Levin (2004) used a threshold value of <0.5 ml/l to estimate the coverage of OMZs in world oceans. The OMZs are also defined for dissolved oxygen concentrations of <20 $\mu\text{mol/kg}$ (Fuenzalida et al., 2009) which is approximately 0.5 ml/l. The present study uses the unit $\mu\text{mol/kg}$ as bottom-water-oxygen (BWO) concentration unit, and will report both values and units when necessary.

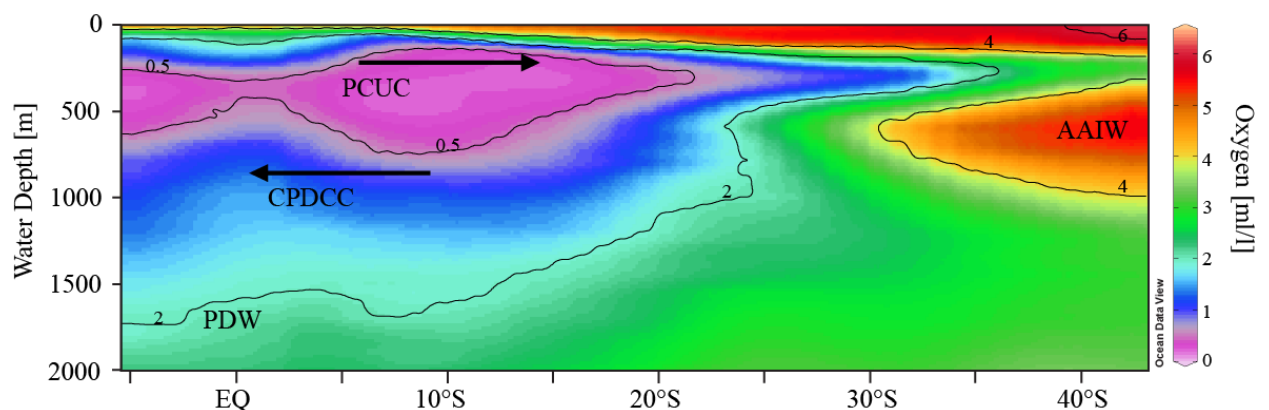


Figure 1.4. Latitude vs depth transect around 80°W showing the dissolved oxygen concentrations ($1 \text{ ml/l} = \sim 45 \mu\text{mol/kg}$; WOD2013 (Boyer et al., 2013)) and the principle water masses of the region (PCUC: Peru-Chile Undercurrent, CPDCC: Chile-Peru Deep Coastal Current, AAIW: Antarctic Intermediate Water and PDW: Pacific Deep Water).

The Peruvian OMZ has been estimated to cover ~34% of the total OMZ area in the world (in definition of hypoxia where dissolved oxygen levels of <0.5 ml/l; <20 $\mu\text{mol/kg}$ prevail; Helly and Levin, 2004). Water masses and currents in the area regulate the thickness of the OMZ. Distinct thinning occurs where the PCUC develop along the coastline whereas lower boundary depth of the OMZ also shows distinct latitudinal variations due to the influence of mid-depth circulation system in the region (Figure 1.4; Helly and Levin, 2004). The upper boundary of the Peruvian OMZ is located at 50-100 m water depth. Strong stratification below a very thin surface mixed layer extending to 50 m water depth limits the ventilation of the OMZ from above (Fuenzalida et al., 2009). The OMZ is around 500 m thick with marked oxygen minimum conditions (e.g., Strub et al., 1998; Fuenzalida et al., 2009). The core of the OMZ is centred off Peru to about 1000 km offshore between 5 and 13°S, where the upper boundary is shallow and the thickness reaches even 700 m (Figure 1.4). Further south towards the Chilean coasts and further north near the Equator, the thickness and the intensity of the OMZ decreases. Its boundaries extend along the Chilean coasts to about 37°S, driven by the southward flow of the PCUC along the continental margin (Fuenzalida et al., 2009). Seasonal or decadal changes in the position of the lower boundary are not expected but upper boundary may show inter-annual shifts of 65 to 100 m by changes in circulation as experienced during the 1997-1998 El Niño event (e.g. Helly and Levin, 2004).

1.4.3. Sediment distribution along the Peruvian margin

Late Quaternary sediments from the continental shelf and slope are predominantly olive green to dark grey green silt and clay. They show laminations within the OMZ whereas around the OMZ foraminifera bearing, bioturbated silty clays are found (Pfannkuche et al., 2011). At some levels coarse-grained sediments prevail which consist of foraminiferal sand (e.g., Oberhansli et al., 1990). South of 10°30'S, sediments from intense upwelling areas and within the OMZ are organic-rich diatom bearing silty clays which are occasionally laminated in places forming a 100 m thick, lens-shaped body on the gentle slope between 11 and 14°S (Krissek et al., 1980; Suess et al., 1987; Wefer et al., 1990; Pfannkuche et al., 2011). Terrigenous silts are found seaward south of 7°S, and grain size tends to decrease seaward as well (Krissek et al., 1980). The composition of the sand fraction is variable due to varying Andean detritus input. Quartz and volcanic glass are abundant. Phosphorites that consist of hard grounds, crusts, nodules, pelletal grains and silt-sized grains (Manheim et al., 1975; Burnett, 1977; Glenn and Arthur, 1988) are abundant along the margin, particularly in Quaternary upwelling deposits (Garrison and Kastner, 1990). Ongoing phosphorite formation coincides with the upper and

lower boundaries of the OMZ (Burnett and Veeh, 1977). Widespread phosphorite hard grounds were also reported on the broad shelf north of 10°30'S (Reinhardt et al., 2002; Arning et al., 2009).

Sediments are typically composed of terrigenous material, organic matter (represented by TOC), carbonate (CaCO₃), phosphorites and biogenic opal (Böning et al., 2004). In general, the southern sediments show lamination and high porosities (93-98%) because they are mainly composed of diatoms. Particulate organic matter (POC) values reach up to 15-20% (Neira et al., 2001; Levin, 2003). At the Peruvian continental margin, the highest organic carbon accumulation has been recorded on the shelf and upper slope at around 15°S as a result of high fluvial discharge by the Pisco River, intense oxygen minimum conditions and high surface water productivity. The shelf between 11 - 14°S is wider and the accumulation rates of organic matter are lower even though the organic carbon concentrations are higher (Reimers and Suess, 1983). Further north offshore Ecuador, coarse calcareous biogenic debris dominates the shelf sediments (Krissek and Scheidegger, 1983). Towards the Chilean coasts, sedimentation rates show a distinct increase with reference to the higher detrital input (Muñoz et al., 2004). Sediments from upper slope do not show a distinct south-north difference in grain size whereas middle or lower slope sediments show a south-to-north fining in grain size due to the increase of seaward terrestrial input and winnowing (Krissek et al., 1980).

1.5. Micropaleontological proxies: benthic foraminifera

The overwhelming majority of modern foraminifera pursue benthic lifestyle and they constitute an extensive part in marine benthic ecosystems (e.g., Gooday, 2003). They are known for their fossil record reflecting environmental changes (e.g., Van der Zwaan et al., 1999; Murray, 2006), such as temperature, surface productivity, bottom and pore water redox conditions etc. A well-documented recent distribution of benthic foraminiferal species and assemblage characteristics like population density and diversity provide background data for an interpretation of past bottom water conditions. Early investigators used benthic foraminifera as paleobathymetric indicators (e.g., Bandy, 1953a;b). Certain species were thought to be present at the same depth all over the world. Further studies showed that benthic foraminifera live not only at the surface of the sediment but also within the first 10 cm of the sediment (Corliss, 1985;1991). In the following years, studies focusing on the microhabitats showed that the faunal distributions and abundances are influenced and determined by the flux and temporal fluctuations of organic matter to the sea floor and the availability of the resources (e.g., oxygen) which result with mobilization of the foraminifera within the sediment (Barmawidjaja et al.,

1992; Loubere et al., 1993; Jorissen et al., 1995). However, later investigations revealed that the tolerance limits vary amongst species and certain species may occur in different sediment depths under conditions as predicted limiting factors (e.g., Sen Gupta and Machain-Castillo, 1993; Bernhard et al., 1997). Using benthic foraminiferal assemblages as proxies for certain environmental parameters is an ongoing debate (Van der Zwaan et al., 1999; Gooday, 2003; Jorissen et al., 2007), however, by investigating the environmental niches which determine the benthic foraminiferal assemblages in certain regions, it is possible to reconstruct the changes in the environmental conditions. With the increasing number of investigations on the living (stained) benthic foraminiferal assemblages, paleo-reconstructions are getting further.

1.5.1. Benthic foraminifera in oxygen depleted habitats

As mentioned earlier, the classification of the oxygen depleted environments, terminology for different oxygen levels and the units used for oxygen concentrations has been under debate (Table 1.1). Furthermore, Jorissen et al. (2007) used the term hypoxic for all the environments where foraminiferal assemblages are potentially influenced without setting a specific value for a threshold oxygen level. In addition to the classification; certain thresholds are reported having negative impacts on marine organisms and ecosystems; oxygen levels <70 $\mu\text{mol/kg}$ for some large macro-organisms (Stramma et al., 2010) and for meiofaunal abundance and diversity (Wetzel et al., 2001), which is defined as hypoxic environment, whereas 50 $\mu\text{mol/kg}$ is reported as an onset for certain organisms and ecosystems which need specific physiological adaptations to abide (Seibel, 2011). Oxygen levels of 22 $\mu\text{mol/kg}$ are used as a threshold for indicating the center of the OMZs (Helly and Levin, 2004; Fuenzalida et al., 2009), and laminated sediments are observed at oxygen levels are 7 $\mu\text{mol/kg}$ where macrofauna is absent (Schönfeld et al., 2015). This study recognizes the above mentioned thresholds and uses the following terms and classification; oxic, dysoxic, microxic and anoxic with ranges of >45 $\mu\text{mol/kg}$, $5-45$ $\mu\text{mol/kg}$, <5 $\mu\text{mol/kg}$ and absence of dissolved oxygen, respectively.

Oxygen depleted environments are usually characterized with high organic matter flux to the sea floor. These two ecological factors, organic flux to sea floor and bottom-and pore-water oxygenation, are known to be the principal factors to control the benthic foraminiferal abundances and microhabitats (e.g., Lutze and Coulbourn, 1984; Corliss and Emerson, 1990; Kaiho, 1994; Loubere, 1994; Alve and Bernhard, 1995; Loubere, 1996; Ohga and Kitazato, 1997; Altenbach et al., 1999; Gooday and Rathburn, 1999; Fontanier et al., 2003; Geslin et al., 2004). According to a proposed conceptual model, the microhabitat depth of endobenthic foraminifera in the sediment is controlled by the availability of food in oligotrophic

environments whereas oxygen concentration in the sediment controls the living depth of the species in eutrophic environments (Barmawidjaja et al., 1992; Jorissen et al., 1995). In most continental margin environments, the oxygen penetration depth within the sediments rarely exceeds 5 cm and vary between mm and first 10 cm (Reimers et al., 1992; Cai and Sayles, 1996). Furthermore, certain deep infaunal species are also observed below the oxygen penetration depths, hence in anoxic sediments (e.g., Corliss and Emerson, 1990; Rathburn and Corliss, 1994; Bernhard and Alve, 1996; Schönfeld, 2001; Koho et al., 2008) indicating that oxygen is not always the limiting factor determining benthic foraminiferal living depths. Consequently, certain species are found to be tolerant to extreme low oxygen levels which suggest that their distributions could be used as indicators of oxygen-depleted conditions (e.g., Sen Gupta and Machain-Castillo, 1993; Bernhard et al., 1997; Kaiho, 1999).

Table 1.1. Classification of different environments and thresholds of bottom-water-oxygen for benthic foraminifera and benthic biota in general.

Reference	BWO range (ml/l)	BWO range ($\mu\text{mol/kg}$)	Classification
Sen Gupta and Machain-Castillo, 1993	2.0-8.0	90-360	oxic
	0.2-2.0	9-90	dysoxic
	0.0-0.2	0-9	suboxic
	0.0	0.0	anoxic
Kaiho, 1994	>1.5	>67.5	oxic
	0.3-1.5	13.5-67.5	suboxic
	0.1-0.3	4.5-13.5	dysoxic
	<0.1	<4.5	anoxic
Bernhard and Sen	>1	>45	oxic
Gupta, 1999;	0.1-1	5-45	dysoxic
Levin, 2003;	<0.5	<5	microxic
Mallon et al., 2012	0.0	0.0	anoxic

The consumption of oxygen is a restrictive factor for the average size of a species in areas with oxygen depleted bottom water conditions (Loubere, 1994). High population densities and a low diversity of benthic foraminifera have been documented by several studies in oxygen depleted environments (Phleger and Soutar, 1973; Sen Gupta and Machain-Castillo, 1993; Bernhard et al., 1997; Jannink et al., 1998; Bernhard and Sen Gupta, 1999; Gooday et al., 2000;

Gooday, 2003; Koho and Piña-Ochoa, 2012; Mallon et al., 2012; Cauille et al., 2014). Absence of predators, such as the epifaunal gastropod *Mitrella permodesta* (Bernhard and Reimers, 1991), and competitors is also advantage for the assemblages in oxygen-depleted environments (Phleger and Soutar, 1973; Neira et al., 2001; Levin et al., 2002; Levin, 2003). There have been several studies which focused on specific benthic foraminiferal response to different oxygen levels. Laboratory experiments were performed (e.g., Moodley et al., 1997; Geslin et al., 2004) or in situ observations were made, which focused on the Arabian Sea and the Indian Ocean (Hermelin and Shimmield, 1990; den Dulk et al., 1998; Jannink et al., 1998; Gooday et al., 2000; Schumacher et al., 2007; Cauille et al., 2014), off Namibia (Leiter and Altenbach, 2010) and the Eastern Pacific Ocean (Smith, 1964; Phleger and Soutar, 1973; Douglas and Heitman, 1979; Mullins et al., 1985; Mackensen and Douglas, 1989; Bernhard et al., 1997; Mallon et al., 2012; Cardich et al., 2015). All these studies depicted a well-defined suite of hypoxia-resistant species. It should be noted that most hypoxia-resistant species are also found in oxygenated environments at deep or intermediate endobenthic habitats (Sen Gupta and Machain-Castillo, 1993; Murray, 2001).

In general, most low-oxygen tolerant foraminifera are calcareous species (Gooday, 2003). They are advantageous in environments with low oxygen and high organic matter as compared to the agglutinated species preferring oxygenated conditions and being less tolerant to hypoxic conditions (Bernhard and Sen Gupta, 1999; Gooday and Rathburn, 1999; Gooday et al., 2000; Levin et al., 2002). Studies also show that thin walled species have advantages in oxygen depleted environments (e.g., *Bolivina* spp., *Globobulimina* spp.; Phleger and Soutar, 1973; Kaiho, 1994). They are often characterized by elongate or flattened morphologies (Gooday, 2003). Another morphological feature is that these thin walled calcareous species generally have higher pore densities and pore-sizes in oxygen-depleted habitats as compared to oxic settings (Kaiho, 1994; Bernhard and Sen Gupta, 1999; Piña-Ochoa et al., 2010; Glock et al., 2011; Kuhnt et al., 2013). The most common species observed in the OMZs worldwide are *Bolivina* species (such as *B. costata*, *B. seminuda*, *B. spissa*), *Globobulimina* species (*G. affinis*, *G. pacifica*), *Nonionella* species (*N. stella*, *N. turgida*), *Bulimina* species (*B. marginata*, *B. exilis*), *Buliminella* species (*B. elegantissima*, *B. tenuata*), *Cassidulina* (*C. delicata*) species, and a few others (Sen Gupta and Machain-Castillo, 1993; Bernhard and Sen Gupta, 1999; Jorissen et al., 2007; Schumacher et al., 2007). Experimental results of Moodley et al. (1997) showed that *Nonionella* and *Stainforthia* species survived longer under anoxic conditions than in oxic settings. Although they did not show reproduction, they seemingly could stand oxygen-depleted environments. Certain agglutinated species such as *Reophax* spp., *Trochammina* spp., *Adercotryma* spp. are

also found in modern OMZs but they are not tolerant to intense oxygen depletion (Gooday, 2003).

1.5.2. Benthic foraminifera of the Eastern Equatorial Pacific OMZs

Several studies documented the benthic foraminiferal distribution off the Eastern Pacific coasts. Most of the works focused on the North American Coasts, in particular California borderland basins (e.g., Uchio, 1960; Douglas and Heitman, 1979; Mullins et al., 1985; Mackensen and Douglas, 1989; Silva et al., 1996; Bernhard et al., 1997; Gooday and Rathburn, 1999; Rathburn et al., 2001). The Peruvian and Chilean fauna was documented by (Bandy and Rodolfo, 1964; Phleger and Soutar, 1973; Khusid, 1974; Ingle et al., 1980; Resig, 1981;1990; Schönfeld and Spiegler, 1995; Figueroa et al., 2005; Morales et al., 2006; Tapia et al., 2008; Cardich et al., 2012; Mallon, 2012; Mallon et al., 2012; Cardich et al., 2015). Some of the studies focused on living benthic foraminifera, but most of them concern dead assemblages. Sediments underneath the Peruvian OMZ support a high population density (Sen Gupta and Machain-Castillo, 1993; Mallon et al., 2012; Cardich et al., 2015, Pérez et al., unpublished). As observed in many oxygen depleted environments, an inverse correlation between diversity and population density was observed at the Peruvian OMZ. Overall, species of the family Bolivinitidae are tolerant to the dyoxic and microxic conditions (Phleger and Soutar, 1973; Khusid, 1974; Manheim et al., 1975; Ingle et al., 1980; Resig, 1981;1990; Heinze and Wefer, 1992; Mallon et al., 2012; Cardich et al., 2015). The most common species observed in the region by all the studies mentioned are; *Bolivina costata*, *B. interjuncta*, *B. spissa*, *B. seminuda*, *B. plicata*, *Globobulimina pacifica* and *Uvigerina peregrina*.

Early studies subdivided the distributions of foraminifera assemblages in relation to water depths (e.g., Resig, 1981), whereas later studies focused on factors like food availability and oxygen concentrations. The assemblages are characterized by low-oxygen tolerant *Bolivina* species (Resig, 1981; Cardich et al., 2015). In particular, *B. costata* is dominating on the mid-to outer shelf and becomes rare below 150 m to about 500 m water depth (Resig, 1990; Cardich et al., 2012; Mallon et al., 2012; Cardich et al., 2015). Mallon et al. (2012) unveiled that not all of the species of the Boivinitidae family are tolerant to oxygen depleted conditions in the same way. Each species has its own tolerance limits to oxygen depletion. For instance, *Bolivina seminuda* is found everywhere whereas *Bolivina costata* is restricted to shallow, upper bathyal of the margin and *Bolivina spissa* are much more abundant outside of the OMZ core, giving an example of “ecological partition” between *B. seminuda* and *B. spissa*. Their occurrence in different depths indicated different oxygen and food demands. Additionally, Glock et al. (2011)

showed that *B. seminuda* is better adapted to oxygen depleted environments as compared to *B. spissa*. General trends indicate that, food availability and increased values of oxygen concentration at the lower OMZ boundary make this environment rich in species. Especially some opportunists are absent within the OMZ, such as *Angulogerina angulosa*, *U. peregrina*, *Bolivinita minuta* (Mallon et al., 2012). The proportions of the agglutinated species also increase with water depth (Resig, 1981; Pérez et al., unpublished) and increasing bottom-water oxygen concentration (Mallon et al., 2012). Common taxa include *Reophax* spp., *Eggerella* spp., *Rhizammina* spp., *Saccamina* spp. and *Trochammina* spp. (Pérez et al., unpublished). High food availability in oxygen depleted conditions creates a less competitive environment so that certain species tolerating these extreme conditions could attain high densities (e.g., Gooday, 2003; Jorissen et al., 2007). It is also known that some species mentioned before, use alternative metabolic pathway in the absence of oxygen (Risgaard-Petersen et al., 2006; Piña-Ochoa et al., 2010; Glock et al., 2012b; Koho and Piña-Ochoa, 2012; Fontanier et al., 2014).

2. METHODOLOGY AND STRATIGRAPHIES OF THE SEDIMENT CORES

The present study focuses on nine sediment cores obtained in 2008 during SFB754 expeditions M77 Leg 1 & 2 aboard *R/V Meteor*. Selection of the core locations was accomplished by sediment-echosounder profiling and bathymetric surveying during the expeditions (Pfannkuche et al., 2011). They were located at continental slope of the Peruvian margin covering an area between 3°S and 18°S from water depths of 270 m to 1300 m (Table 2.1, Figure 2.1 and Figure 2.2). Four of these sediment cores were described earlier and their stratigraphic information were previously published (Mollier-Vogel, 2012; Mollier-Vogel et al., 2013). This chapter reports the stratigraphical information gathered from the remaining five cores which were used in different publications (Schönfeld et al., 2015; Erdem et al., 2016) (Chapter 3).

The sediment cores are stored in cold storage room of GEOMAR Kiel.

The sediment cores were split half, described and preliminary information was gathered on board. Measurements of the sediment lightness (L^*) were done at every sediment core whereas the magnetic susceptibility (SI) measurements were only available for the short gravity cores obtained during M77 Leg 1. For details of the preliminary analyses on the sediment cores which were obtained during the expeditions, see the cruise report (Pfannkuche et al., 2011). The working halves of the sediment cores concerning this study were later sampled in the laboratory with 10 cm resolution up to 20 cc samples and 10 cc parallel samples (except core 47-2; this core was sampled previously by others). The 20 cc sample series were wet-sieved using a 63 μm sieve

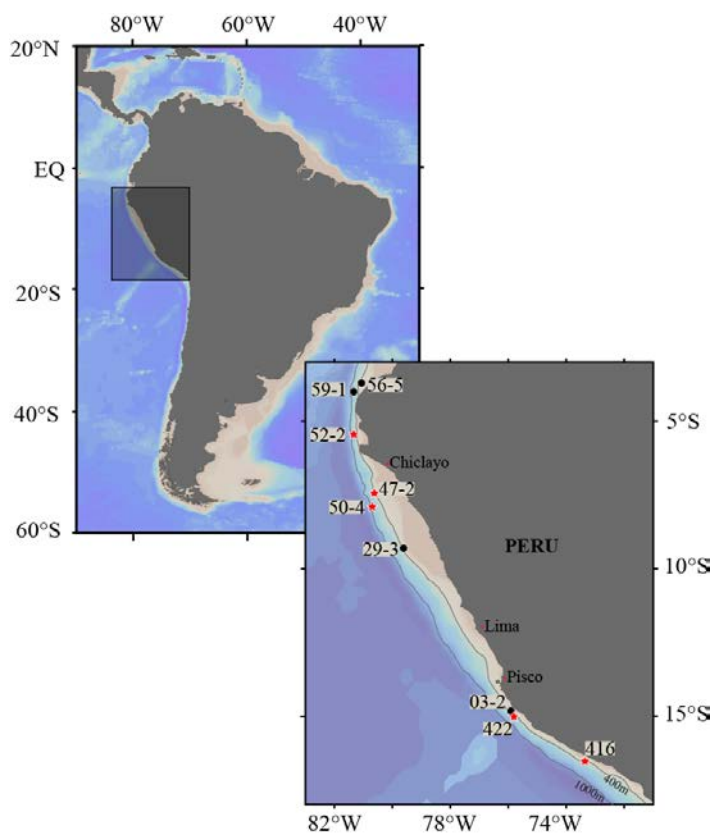


Figure 2.1. Map of the research area: red stars show the locations of the sediment cores which described in the present study for the first time and the black rounds show the core locations from the previous studies. See Figure 2.2 for the core locations in relation with the OMZ.

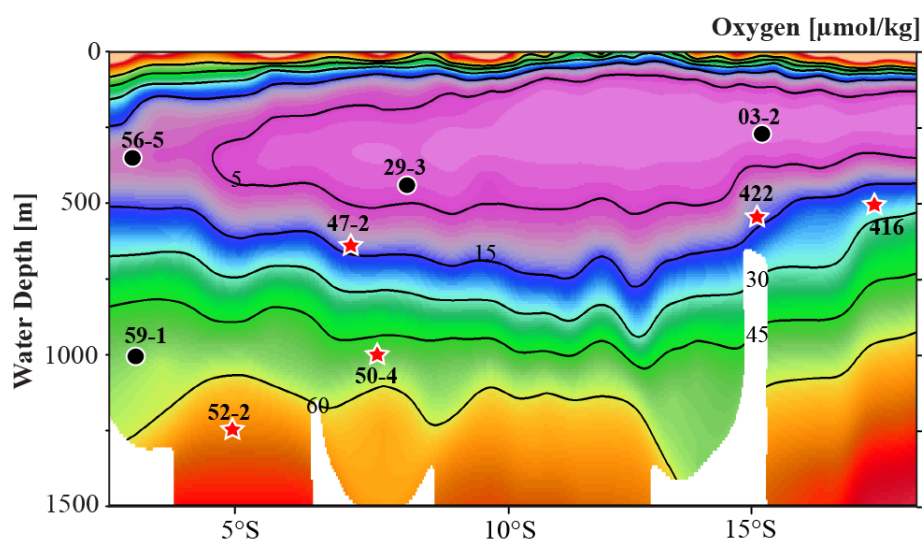


Figure 2.2. Depth vs latitude section showing the dissolved oxygen concentrations and the core locations as in Figure 2.1. Red stars show the locations of the sediment cores which described in the present study for the first time and the black rounds show the core locations from the previous studies. Oxygen data were taken from a CTD compilation after Schönfeld et al. (2015).

Table 2.1. The metadata of the sediment cores used in this study.

Cruise	Core name	Year	Lat (S)	Long (W)	Water depth (m)	Reference
M77/2	056-PC5	2008	03°44.99'	81°07.48'	355	Mollier-Vogel et al., 2013
M77/2	059-PC1	2008	03°57.01'	81°19.23'	997	Mollier-Vogel et al., 2013
M77/2	052-PC2	2008	05°29.01'	81°27.00'	1249	This study
M77/2	047-PC2	2008	07°52.01'	80°31.36'	626	This study
M77/2	050-PC4	2008	08°01.01'	80°30.10'	1013	This study
M77/2	029-PC3	2008	09°17.70'	79°37.11'	433	Mollier-Vogel, 2012
M77/2	003-PC2	2008	15°06.21'	75°41.28'	271	Mollier-Vogel, 2012
M77/1	422-GC7	2008	15°11,39'	75°34,87'	517	This study
M77/1	416-GC4	2008	17°28,13'	71°52,62'	505	This study

and residues were dried in 40°C oven. The sieved dry samples were later used for microfossil, sand-fraction examinations and further analyses such as; isotope analyses, radiocarbon dating. The other series of the 10 cc samples were freeze dried and used for determination of physical properties such as dry bulk density and pore density (physical properties for core M77/2-47-2 were not available). All this information was later used in order compare and correlate the sediment cores and for the calculation of the accumulation rates. Additional to the physical

properties, subsamples of 3 to 20 mg dried samples from cores M77/2-50-4 and 52-2 were used for total nitrogen (TN), total carbon (TC) and organic carbon (TOC) content with a Carbon Erba Element Analyzer (NA1500) at GEOMAR, Kiel. The long-term precision was ± 0.6 % of the measured values as revealed by repeated measurements of two internal carbon standards. Results regarding to total organic carbon were reported in Schönfeld et al. (2015).

2.1. Age models of the sediment cores

Oxygen ($\delta^{18}\text{O}$) and carbon ($\delta^{13}\text{C}$) isotope analyses were accomplished using a Thermo Fisher Scientific 253 Mass Spectrometer coupled to a CARBO KIEL automated carbonate preparation device at GEOMAR, Kiel. For the analysis, three to six specimens of the benthic foraminifera species *Uvigerina peregrina*, *U. striata* and *Globobulimina pacifica* were picked out from the >63 μm residues, according to availability. The results were reported in per mil (‰) relative to the VPDB (Vienna Pee Dee Belemnite) scale and calibrated versus NBS19 (National Bureau of Standards) and to an in-house standard (Solnhofen limestone).

The ^{14}C Accelerator Mass Spectrometer (AMS) radiocarbon datings were performed at Beta Analytic, Inc., Florida, USA. For each dating point, from the >63 μm size fraction 229 to 250 specimens of the planktonic foraminifera species *Neogloboquadrina dutertrei* were picked. We were able to use *N. dutertrei* only in the sediment cores from the northern part of the region while in the southern cores this species was either absent or rare. In samples from the southern cores, from the >63 μm size fraction 33 to 179 specimens of *Planulina limbata* or 5 to 20 g of bulk sediment were used. Sedimentary organic carbon and foraminifera radiocarbon ages revealed a systematic offset of ~ 900 years, which was also observed and reported previously (Mollier-Vogel, 2012). Conventional radiocarbon datings were later calibrated applying the marine calibration set Marine 13 (Reimer, 2013) and using the software Calib 7.0 (Stuiver and Reimer, 1993). Reservoir ages ranging from 89 to 338 years for this region were taken into account according to the marine database (<http://calib.qub.ac.uk/marine/>). Ages are expressed in thousands of years (ka) before 1950 AD (abbreviated as cal ka BP; Table 2.2). The radiocarbon based chronologies for each sediment core were formed by linear interpolating the radiocarbon results. The chronologies of the cores were later supplemented and tuned using AnalySeries software with the Antarctic EPICA $\delta^{18}\text{O}$ reference stack (EPICA Community Members Members, 2006). These results were later compared to the previously published age models and benthic $\delta^{18}\text{O}$ records of the northern cores M77/2-56-5 and 59-1 (Figure 2.3.; Mollier-Vogel et al., 2013; Nürnberg et al., 2015). Core specific information regarding to the age models and reservoir ages are given in details below. Once the age models were complete and sedimentation

rates were calculated, accumulation rates (AR_{bulk} (g/cm² ka)) were calculated following (Van Andel et al., 1975) for each core by using the dry bulk densities gathered from the physical property measurements.

Table 2.2. Age models of the five sediment cores listed in accordance to their location (from north to south).

Core Depth (cm)	Con. age (yrs)	error (yrs)	Correlation	Depth therein (m)	Con. age (yrs)	Cal. Age (cal ka BP)	Material	Remarks
M77/2-052-PC2 (Res. Age ΔR: 102 \pm 175)								
90			059-1	1.48	3490	3.13	<i>N. dutertrei</i>	
229			059-1	4.03	7815	8.09	<i>N. dutertrei</i>	
319			059-1	6.58	10470	11.27	<i>N. dutertrei</i>	
370	12290	50				13.64	<i>N. dutertrei</i>	
550	19320	80				22.68	<i>N. dutertrei</i>	
630	24470	130				28.01	<i>N. dutertrei</i>	
770			EPICA	1181.7		30.56		
880	31880	270				35.25	<i>N. dutertrei</i>	
952			EPICA	1334.2		38.88		
1100	41740	770				44.7	<i>N. dutertrei</i>	
M77/2-047-PC2 (Res. Age ΔR: 186 \pm 49)								
88			EPICA	627		10.39		
111	8150	40				8.44	<i>P. limbata</i>	Discard
111	12455	55				13.72	<i>N. dutertrei</i>	
198	25650	250				28.63	<i>N. dutertrei</i>	Discard
218	25190	130				28.62	<i>N. dutertrei</i>	
248			EPICA	1243		34.11		
283			EPICA	1348		39.60		
323			EPICA	1501		48.61		
M77/2-050-PC4 (Res. Age ΔR: 186 \pm 49)								
10	10380	40				11.19	<i>N. dutertrei</i>	
40			EPICA	683		11.61		
80	12800	70				14.13	<i>N. dutertrei</i>	
190	14480	60				16.83	<i>N. dutertrei</i>	

Chapter 2: Methodology and stratigraphies of the sediment cores

250	15370	60			17.98	<i>N. dutertrei</i>	
350	17690	70			20.62	<i>N. dutertrei</i>	
450	18750	70			22.01	<i>N. dutertrei</i>	
550	20330	90			23.72	<i>N. dutertrei</i>	
824			EPICA	1114	26.97		
1010	25680	130			29.12	<i>N. dutertrei</i>	
1190	29030	170			32.39	<i>N. dutertrei</i>	
1302			EPICA	1245	34.11		
1461			EPICA	1288	36.57		
1745			EPICA	1370	40.86		
M77/2-422-GC7 (Res. Age ΔR: 338 \pm 186)							
31.5	21950	90			25.55	Sediment	
77	22300	90			25.84	Sediment	
122	25510	120			28.80	Sediment	
145			EPICA	1151	29.48		
154			EPICA	1160	29.79		
168	27320	140			30.83	Sediment	
212	27610	140			30.99	Sediment	
257	28200	150			31.29	Sediment	
275			EPICA	1181	31.52		
307	19350	70			22.50	Sediment	Discard
M77/2-416-GC4 (Res. Age ΔR: 338 \pm 186)							
20	15900	60			18.41	<i>P. limbata</i>	
35			406	16	16320	18.83	<i>P. limbata</i>
45			406	23	16600	19.14	<i>P. limbata</i>
60	16910	70			19.49	<i>P. limbata</i>	
100	17690	80				<i>P. limbata</i>	Discard
110	17560	80			20.29	<i>P. limbata</i>	
160	18080	90			20.92	<i>P. limbata</i>	
210	18610	80			21.62	<i>P. limbata</i>	
230	18970	80			22.09	<i>P. limbata</i>	
245	19370	90			22.52	<i>P. limbata</i>	
250	19550	100			22.68	<i>P. limbata</i>	
290	18930	90				<i>P. limbata</i>	Discard

310	21050	130	24.42	<i>P. limbata</i>
345	22560	120	26.05	<i>P. limbata</i>

2.2. Core specific information

Core M77/2-052-PC2

The M77/2-052-PC2 is a long piston core and here referred as 52-2. It was collected from the northern part of the region and from 1249 m water depths. The sediment core is composed of homogeneous olive green grey mud with no significant change in sedimentological characteristics (Figure 2.5). The weight percentages of $>63 \mu\text{m}$ determinations and information on sediment surface lightness (L^*) showed a change around 5 m core depth, indicating higher porosity, less sandy and darker material for the topmost 5 m. For the $\delta^{18}\text{O}$ and $\delta^{13}\text{C}$ measurements benthic foraminifera *Uvigerina peregrina* were picked. Benthic $\delta^{18}\text{O}$ values ranged between 3.083 and 4.755 (Figure 2.3), whereas benthic $\delta^{13}\text{C}$ values ranged between -1.115 and -0.037 (Figure 2.4). Radiocarbon dating of this core was done by 5 dating points using the planktonic foraminifera *Neogloboquadrina dutertrei*. This species were rare at the first 3 m of the core, so we were unable to date the core for these depths. We recognized a good correlation between $\delta^{18}\text{O}$ curves of the core 52-2 and 59-1, therefore the age model was accomplished by correlation to core 59-1 for the Holocene part and tuned by correlation to EPICA ice-core for the later periods (Figure 2.3). It covers whole period of 40 ka without gaps and disturbances in the downcore record. Sedimentation rates for the last 25 ka ranged between 11 and 28 cm ka^{-1} (Figure 2.6). Total nitrogen (TN), total carbon (TC) and total organic carbon (TOC, C_{org}) measurements were accomplished with 10 cm resolution for the first 700 m of the core 52-2. The CaCO_3 (%) values were calculated using the values TC (%) and TOC (%). Total organic carbon values ranged between 1 and 3 % showing a distinct slight increase starting from 390 cm (~14 cal ka BP), whereas CaCO_3 values ranged between 1 and 7 %, showing similar trend with $>63 \mu\text{m}$ (weight %) of this core. A distinct drop was observed between core depths of 450 cm and 500 cm (17 and 20 cal ka BP). Total nitrogen percentages (TN (%)) were in accordance with TC (%). The accumulation rates of N (AR_N) and C_{org} ($\text{AR}_{C_{\text{org}}}$) were calculated accordingly.

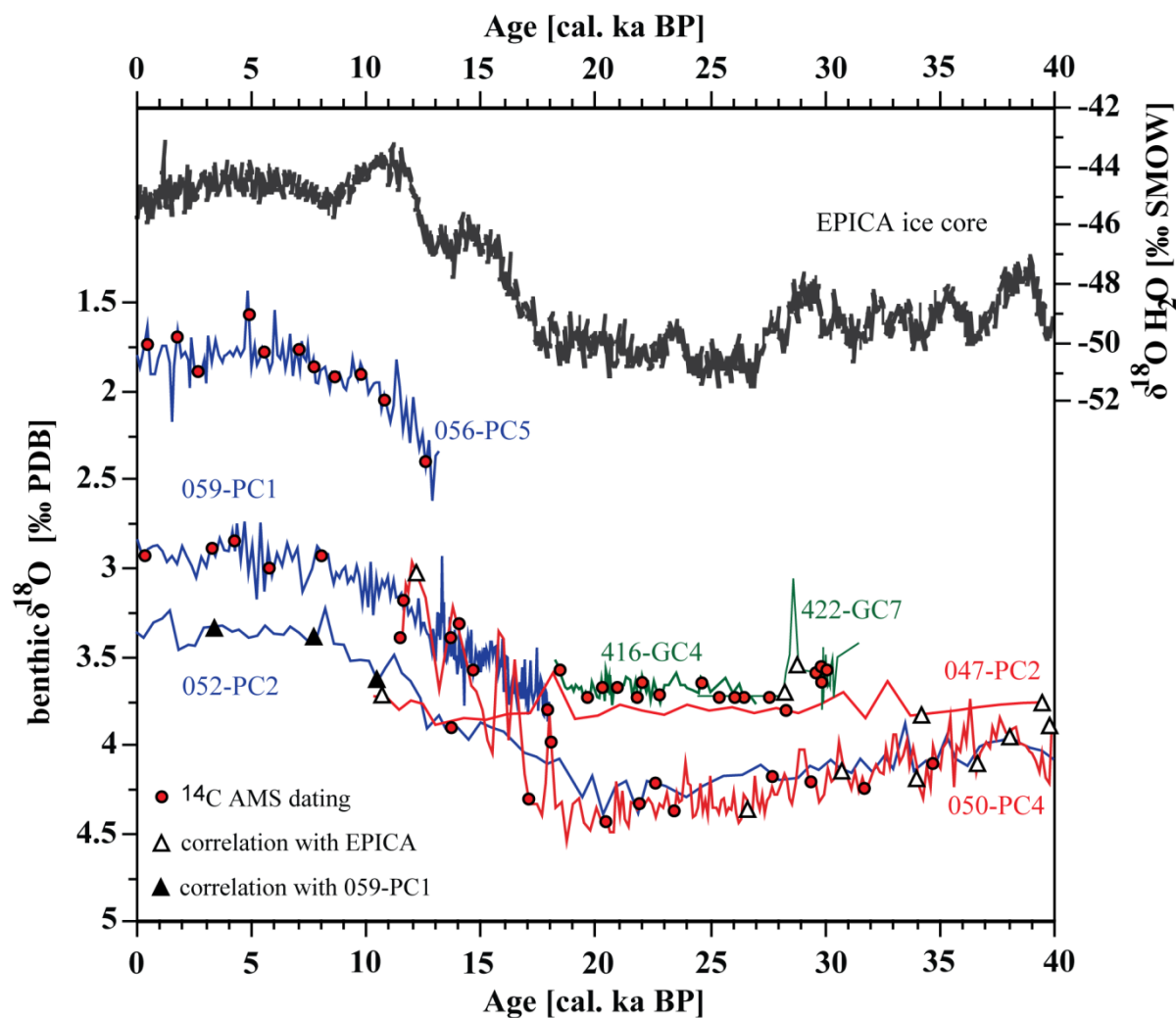


Figure 2.3. Benthic $\delta^{18}\text{O}$ isotope curves of the sediment cores with age control points. Graphs are depicted in different colours regarding to the core locations; blue for the northern cores, red for the central and green for the southern cores.

Core M77/2-050-PC4

The M77/2-050-PC4 is a long piston core and is here referred as 50-4. It was collected from the central part of the region and from 1013 m water depths. The sediment core is composed of olive green to olive green grey homogeneous mud bearing foraminifera throughout the core. There are some changes in the sediment colour and some laminas are also observed but these are not continuous and distinct differences. The $>63\ \mu\text{m}$ weight % values showed a similar change to core 52-2 around 2 m core depth. Lightness (L^*) did not show such a similarity (Figure 2.5). For the $\delta^{18}\text{O}$ and $\delta^{13}\text{C}$ measurements of the core 50-4, benthic foraminifera species *Uvigerina peregrina* and *Globobulimina pacifica* (only for the first 4 m of the core, not shown here) were used. Benthic $\delta^{18}\text{O}$ values ranged between 2.896 and 4.655 (Figure 2.3), whereas benthic $\delta^{13}\text{C}$ values ranged between -3.679 and -0.117 (Figure 2.4).

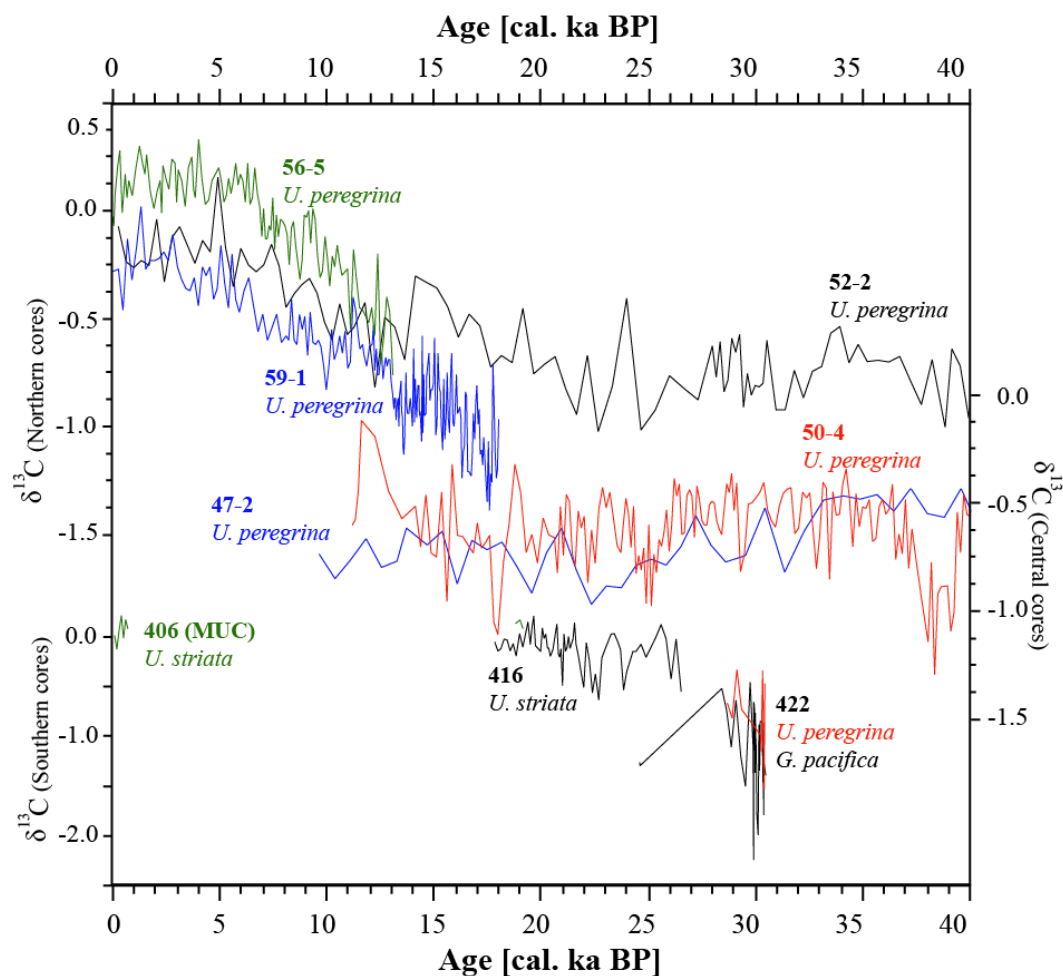


Figure 2.4. Benthic $\delta^{13}\text{C}$ isotope curves of the sediment cores indicating the species used for the measurements. Graphs are depicted according to the sediment core locations as in Figure 2.2. Note that the scale bar for the southern cores is different from the others.

Radiocarbon dating of this core was done by 9 dating points using the planktonic foraminifera species *N. dutertrei*. The age model was improved with correlation and tuning to EPICA ice core (Figure 2.7). It revealed a hiatus in downcore record for the first 11 ka. Irregular values in the isotope values from the first meters of this might indicate that the ongoing bottom-water activities starting already before 11 ka (see chapter 3). Sedimentation rates for the period between 11 and 25 ka ranged between 18 and 85 cm ka^{-1} (Figure 2.7). Total nitrogen (TN), total carbon (TC) and total organic carbon (TOC, C_{org}) measurements were accomplished with 20 cm resolution of the core 50-4. The CaCO_3 (%) values were calculated using the values TC (%) and TOC (%). TOC values ranged between 2 and 5 % showing a distinct increase starting from 180cm (16.5 cal ka BP). The CaCO_3 values ranged between 5 and 20 %, showing similar trend with $>63 \mu\text{m}$ (weight %) of the core. The Total nitrogen (TN %) values were in accordance with TC (%). The accumulation rates of N (AR_N) and C_{org} (AR_{Corg}) were calculated accordingly.

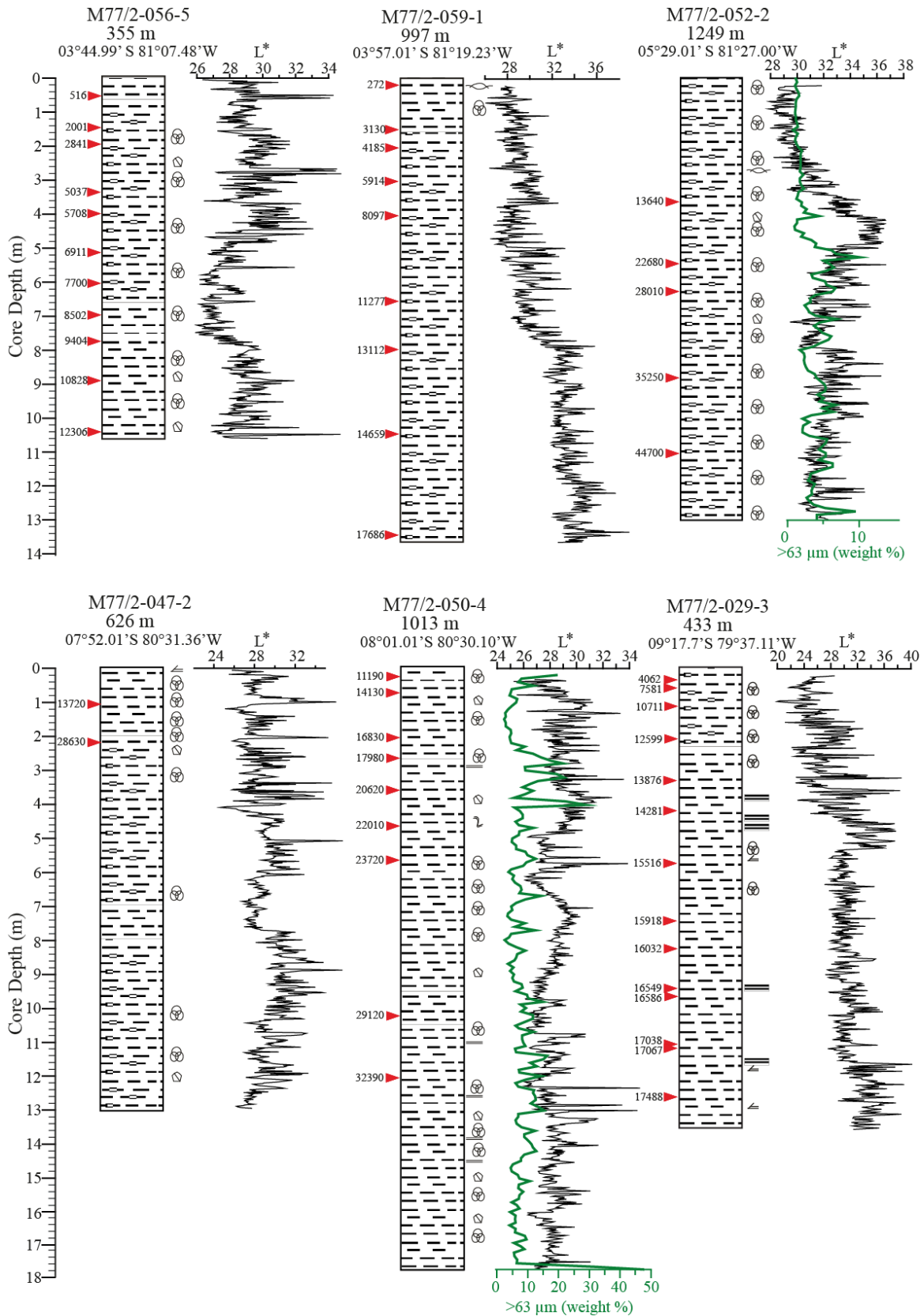


Figure 2.5. See next page for description of the figure and details.

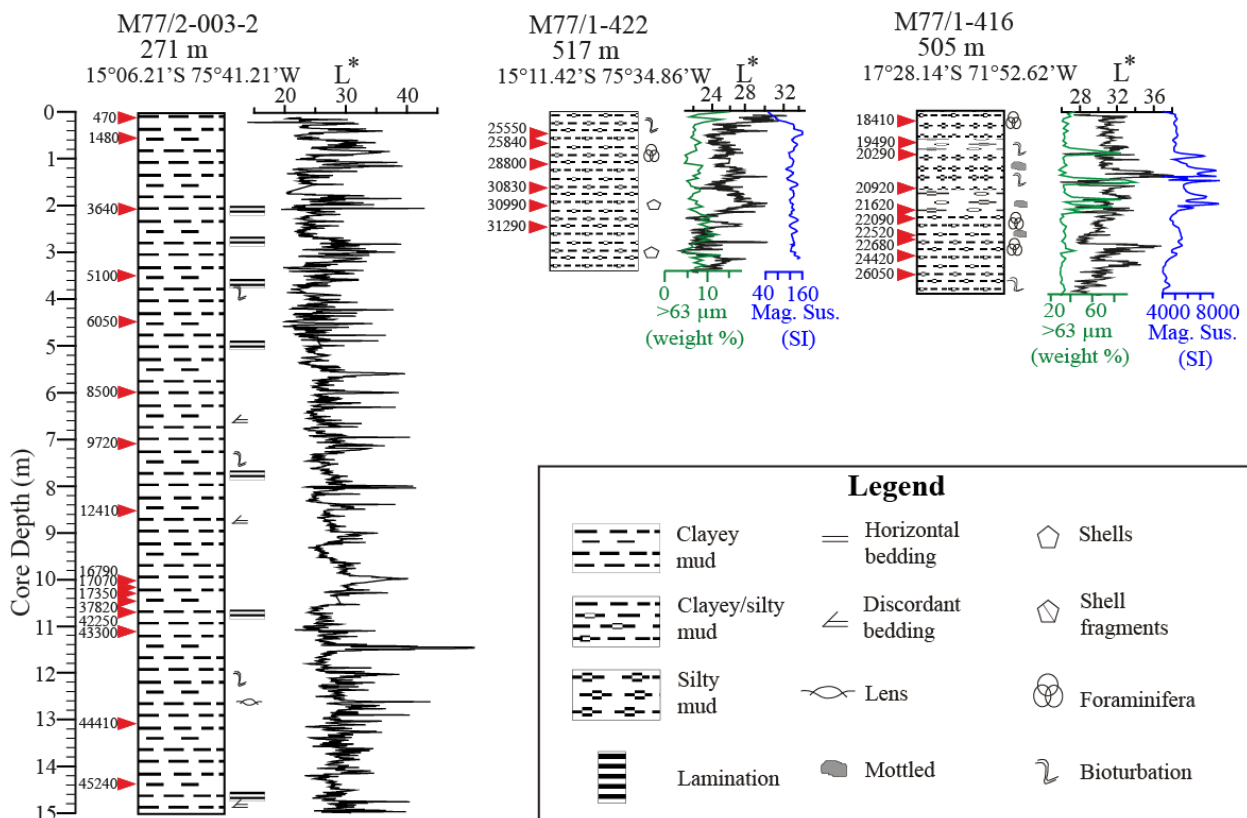


Figure 2.5. *continued* Core stratigraphies showing the sedimentological features and information on lightness (L*) measured and described aboard *R/V Meteor*; Magnetic Susceptibility (SI) were measured only at the gravity cores from southern part of the region during the M77 Leg 1 (Pfannkuche et al., 2011). Red triangles indicate the ¹⁴C dating points with calibrated ages (cal yr BP; see Table 2.1 for the references of the age models). Additional information of the weight percentage (weight %) of >63 μm material is available only at 4 sediment cores.

Core M77/2-047-PC2

The M77/2-47-PC2 is a long piston core and here referred as 47-2. The sediment core was collected from the central part of the region and from 626 m water depths. Most of the core is composed of dark olive green grey to olive green grey homogeneous mud. Discontinuity and slumps were reported at the first centimetres of the core. There are some banded and laminated layers also reported in the core description (Figure 2.5). Lightness (L*) indicated fluctuations throughout the core. Physical properties of this core were not available. For the $\delta^{18}\text{O}$ and $\delta^{13}\text{C}$ measurements benthic foraminifera species *U. peregrina* and planktonic species *N. dutertrei* (data not presented here) were used. Benthic $\delta^{18}\text{O}$ values ranged between 3.584 and 4.121 (Figure 2.3) and benthic $\delta^{13}\text{C}$ values ranged between -1.034 and -0.389 (Figure 2.4). Radiocarbon dating of this core was done by 2 dating points using the planktonic foraminifera

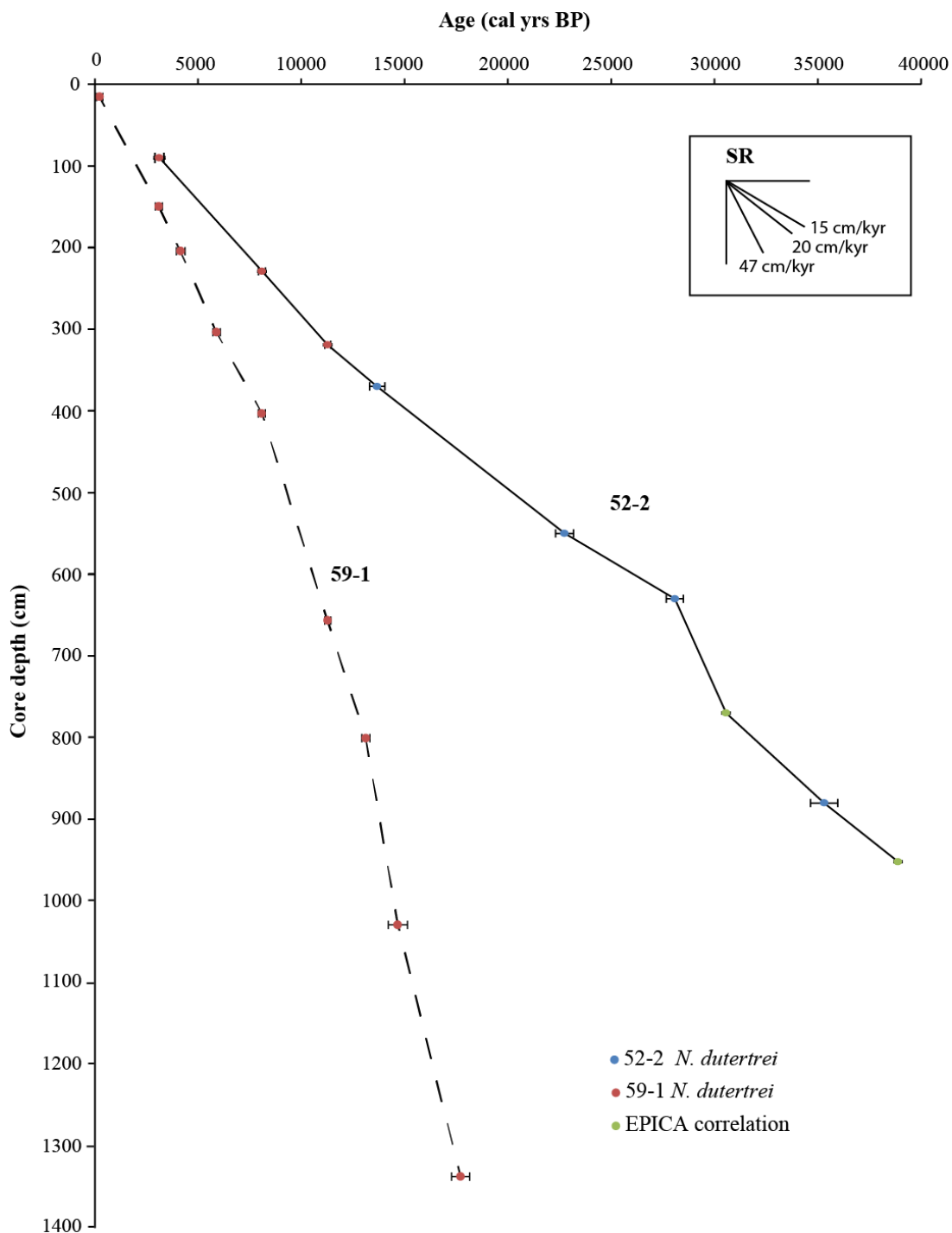


Figure 2.6. The age vs core depth (cm) relationships for the core 52-2 showing the linear interpolation applied to the radiocarbon datings. The age uncertainties (2 sigma) were shown as error bars. For comparison the same information of the core 59-1 is plotted together and shown as dashed line (values directly taken from Mollier-Vogel et al., 2013). Sedimentation rates (SR) were calculated for each and presented as slopes of three different intervals within the interpolation line.

species *N. dutertrei*. The age model was done mostly according to correlation with the EPICA ice core and with these 2 dating points (Figure 2.8). Two dating points were discarded and sediments concerning the Holocene period were apparently eroded. For comparison two additional dating were done at a short core (Multicorer MUC) 47-3 which was obtained from the same location. AMS dating results for the 47-3 (MUC) also revealed that mixing and reworking of the Holocene sediments at this sampling location. Sedimentation rates also did not exceed 7.5cm ka^{-1} due to active reworking and erosion in these region and water depths (see Chapter 3 for further info). Overall, the results from this core should be taken into consideration with caution.

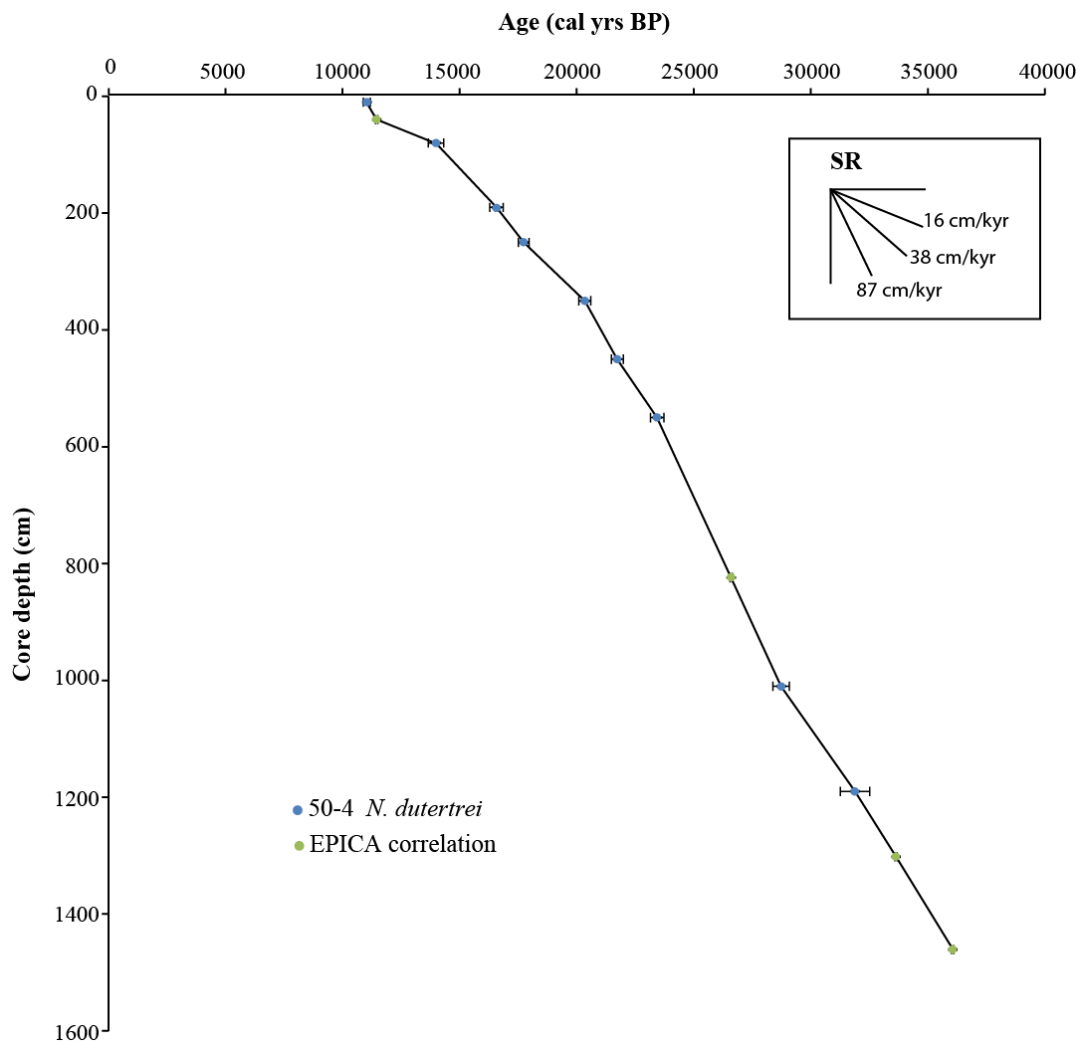


Figure 2.7. The age vs core depth (cm) relationships for the core 50-4 showing the linear interpolation applied to the radiocarbon datings. The age uncertainties (2 sigma) were shown as error bars. Sedimentation rates (SR) were calculated for each and presented as slopes of three different intervals within the interpolation line.

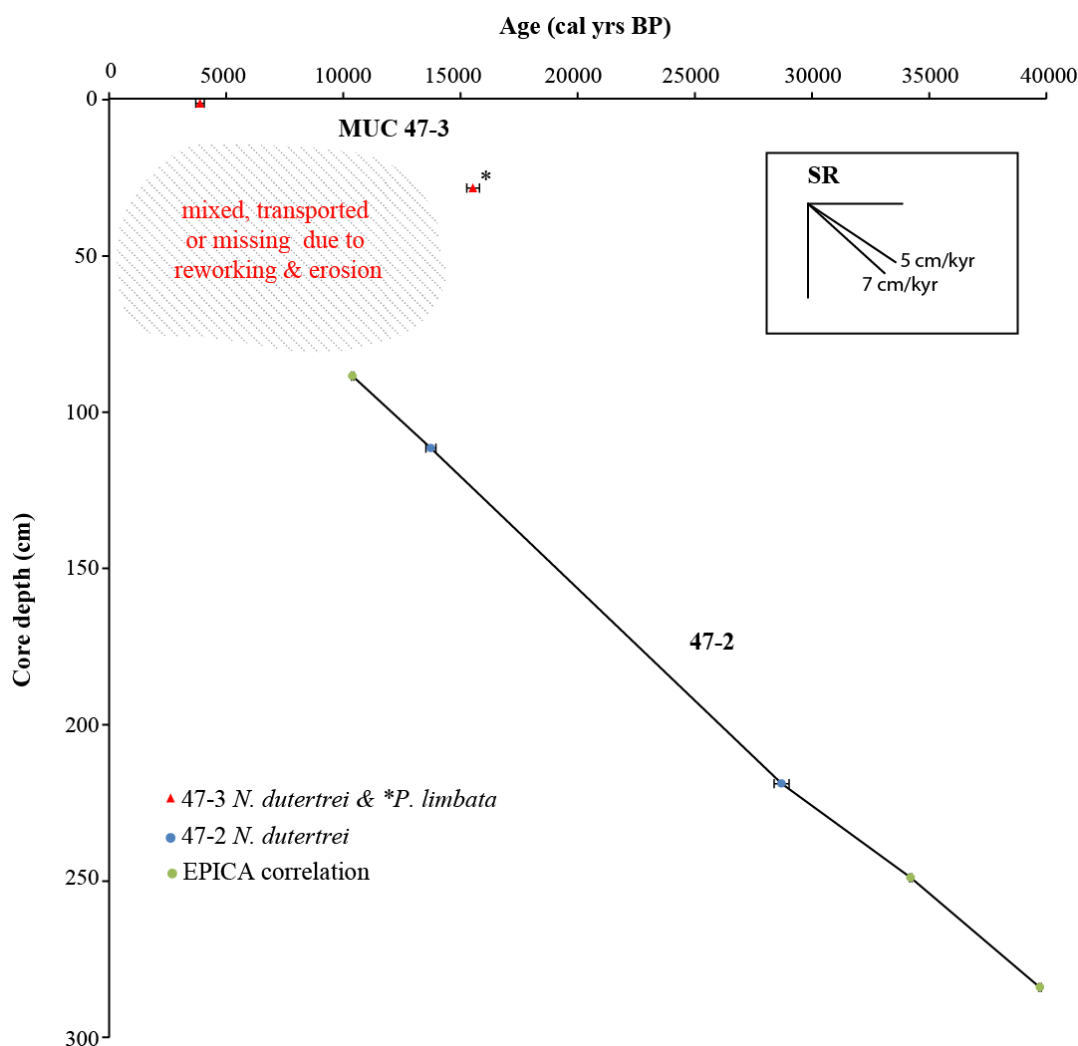


Figure 2.8. The age vs core depth (cm) relationships for the core 47-2 showing the linear interpolation applied to the radiocarbon datings. The age uncertainties (2 sigma) were shown as error bars. For comparison and in order to understand the surface processes, the radiocarbon datings from the MUC 47-3 were included. The Holocene section of the core 47-2 is missing or the material corresponding time interval has been mixing. Sedimentation rates (SR) were calculated for each and presented as slopes of three different intervals within the interpolation line.

Core M77/1-422-GC7

The M77/1-422-GC7 is a short gravity core and here is referred as 422. The sediment core was collected from the southern part of the region and from 517 m water depths during M77 Leg 1. The core is composed of dark olive green bioturbated mud. No distinct changes in the sedimentary structure were observed. The weight percentages of $>63 \mu\text{m}$ material (weight %) values did not show distinct changes (Figure 2.5). For the $\delta^{18}\text{O}$ and $\delta^{13}\text{C}$ measurements endobenthic species *Uvigerina peregrina*, *U. striata* (not shown here) and *Globobulimina*

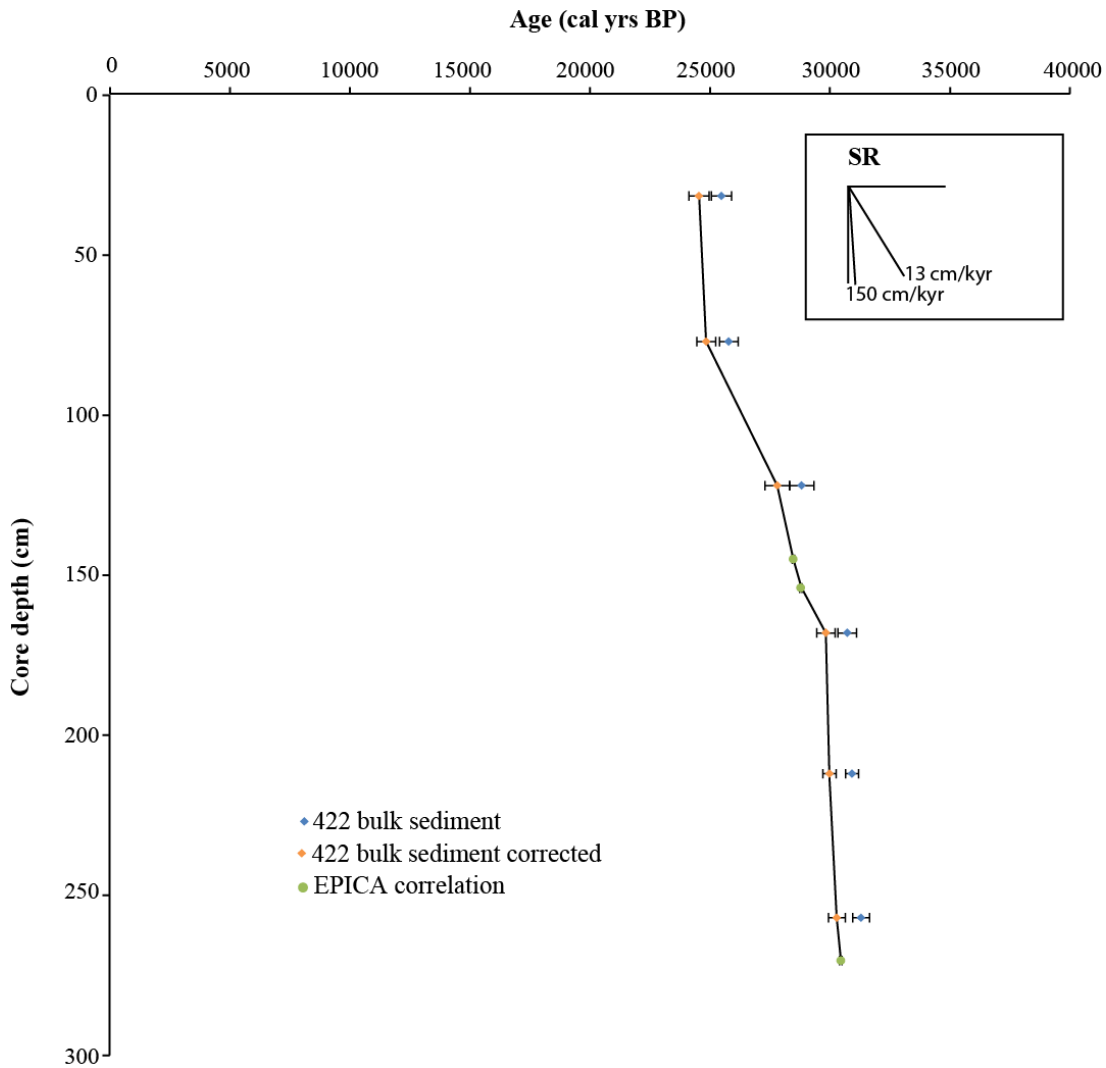


Figure 2.9. The age vs core depth (cm) relationships for the core 422 showing the linear interpolation applied to the radiocarbon datings (corrected ages of this core). The age uncertainties (2 sigma) were shown as error bars. Sedimentation rates (SR) were calculated for each and presented as slopes of three different intervals within the interpolation line.

pacifica were used. Benthic $\delta^{18}\text{O}$ values ranged between 3.053 and 3.755 (Figure 2.3), and benthic $\delta^{13}\text{C}$ values ranged between -2.314 and -0.327 (Figure 2.4). Radiocarbon datings of this core were done at 6 dating points using the bulk sediments since the planktonic species were rare or absent and single species based benthic foraminifera dating was not also possible. Age correction of 970 years was applied because the offset observed between carbonate and sediment radiocarbon datings from the region. As mentioned earlier it was reported by Mollier-Vogel (2012) and was also observed at another close-by short core (MUC406 same location of 416). The age model was improved and tuned by correlation with the EPICA ice core (Figure 2.9). This core revealed a hiatus for the first 24 ka. It is not involved further in the benthic

foraminiferal investigations. The irregular values observed at the first centimetres in both oxygen and carbon isotopes analyses might be results of reworking of the sediments which later led to erosion in the region. Sedimentation rates during the period between 24 to 30 ka showed values up to 150 cm ka⁻¹.

Core M77/1-416-GC4

The M77/1-416-GC4 is a short gravity core and here is referred as 416. It was obtained from the southern part of the region and from 505 m water depths during the M77 Leg 1. The sediments of this core were composed of olive green grey bioturbated mud with intercalated sandy layers. Magnetic susceptibility values showed increases at core depths between 0.7 and 2 m (Figure 2.5). The weight percentages of the >63 µm material (weight %) values showed similar trends as magnetic susceptibility. Endobenthic species *Uvigerina peregrina* and *U. striata* were picked for the δ¹⁸O and δ¹³C measurements. The distribution of the *U. striata* was continuous and *U. peregrina* was measured as a supplementary. Here, results from the *U. striata* measurements are presented together with the results obtained from the MUC 406 from the same sampling location. Benthic δ¹⁸O values ranged between 3.516 and 3.874 (Figure 2.3), and benthic δ¹³C values ranged between -0.555 and 0.202 (Figure 2.4). Radiocarbon dating of this core was done by 10 dating points using the benthic species *Planulina limbata*. The age model was improved by correlating with a short core MUC 406 (Figure 2.10). An offset of 970 years between bulk sediment radiocarbon and carbonate radiocarbon was observed at this short core. Sedimentation rates high values up to 80 cm ka⁻¹ around 20 cal ka BP. The hiatus was observed best at these two cores. The MUC 406 revealed a gap within the first centimetres whereas in the gravity core 416, the whole Holocene period is missing.

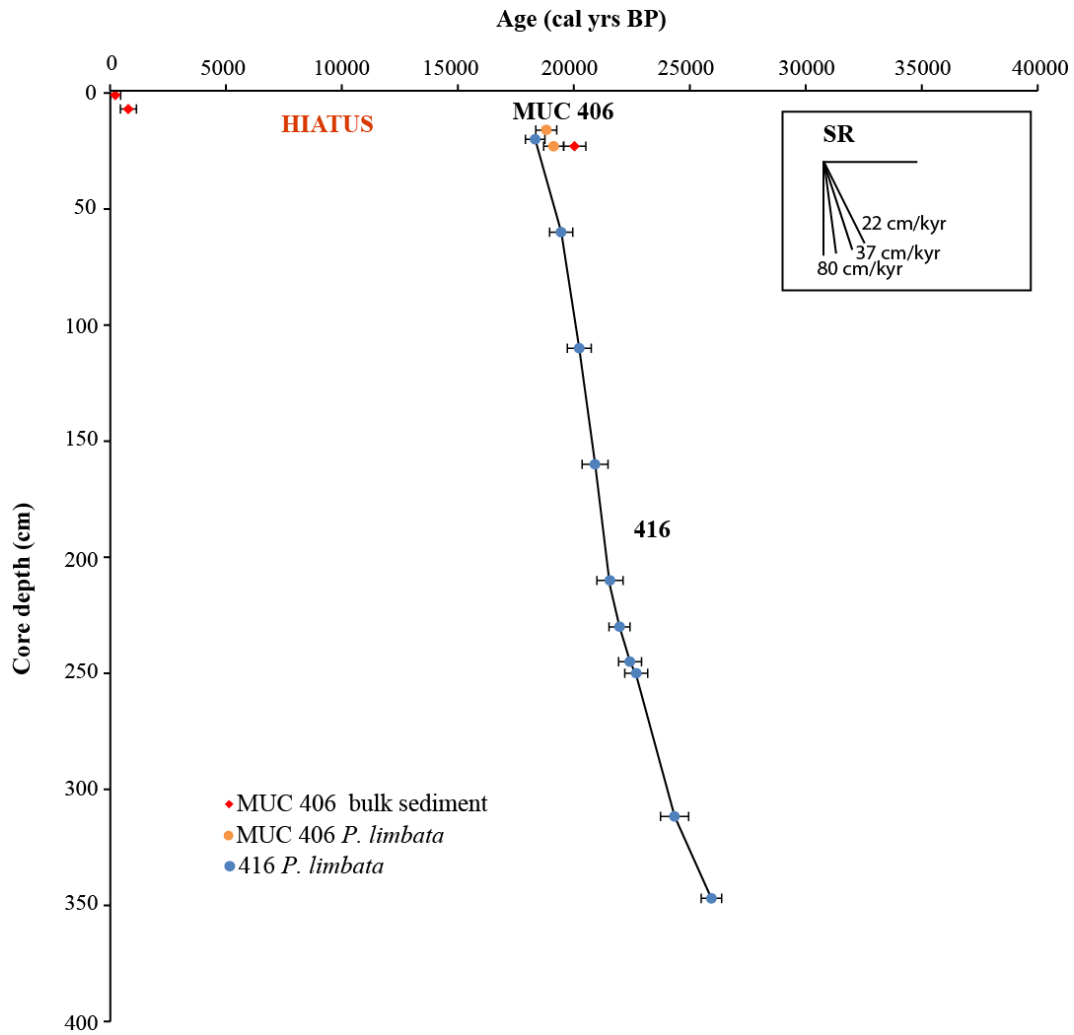


Figure 2.10. The age vs core depth (cm) relationships for the core 416 showing the linear interpolation applied to the radiocarbon datings. It is supplemented with the radiocarbon datings from the MUC 406 from the same location. Different materials dated at this short core revealed an offset of 970 years between bulk sediment and foraminifera radiocarbon ages. Hiatus is observed within the MUC 406. The age uncertainties (2 sigma) were shown as error bars. Sedimentation rates (SR) were calculated for each and presented as slopes of three different intervals within the interpolation line.

3. PERUVIAN SEDIMENTS AS RECORDERS OF AN EVOLVING HIATUS FOR THE LAST 22 THOUSAND YEARS

**Zeynep Erdem^a, Joachim Schönfeld^a, Nicolaas Glock^a, Marcus Dengler^a, Thomas Mosch^a,
Stefan Sommer^a, Judith Elger^{a,b}, Anton Eisenhauer^a**

a) GEOMAR Helmholtz Centre for Ocean Research Kiel, Wischhofstr. 1-3, 24148, Kiel, Germany.

b) Institute for Geosciences, Christian-Albrechts-Universität zu Kiel, Otto-Hahn-Platz 1, 24118 Kiel, Germany.

Published manuscript:

Erdem et al., 2016, Peruvian sediments as recorders of an evolving hiatus for the last 22 thousand years, *Quaternary Science Reviews*, 137, 1-14, doi:0.1016/j.quascirev.2016.01.029.

Abstract

The Peruvian continental margin is characterized by the presence of one of the strongest and most distinct Oxygen Minimum Zones (OMZs) in today's oceans. Therefore, it has long been in the focus of oceanographic and geological investigations. Observations indicate that OMZs are expanding in relation with currently changing climate. To advance understanding of the temporal evolution of OMZs and climate change, complete paleoceanographic and paleoclimatological reconstructions are needed. However, the development of paleoenvironmental scenarios for the period since the Last Glacial Maximum at this region was hampered by a ubiquitous hiatus and short-term interruptions of the stratigraphical record. In the present study, we combined the stratigraphical information from 31 sediment cores from the Peruvian margin located between 3 to 18°S and water depths of 90 to 1300 m within and below today's OMZ, in order to determine the extent of the hiatus and assess the responsible mechanisms. A widespread unconformity and related erosional features, omission surfaces and phosphorites, were observed in sediment cores from the area south of 7°S, depicting a prograding feature on the continental slope from south to north during the deglaciation. Combining recent oceanographic and sedimentological observations, it is inferred that, tide-topography interaction and resulting non-linear internal waves (NLIWs) shape the slope by erosion, carry sediments upslope or downslope and leave widespread phosphoritic lag sediments, while the Peru Chile Undercurrent (PCUC) transports the resuspended sediments southward causing non-deposition. This exceptional sedimentary regime makes the Peruvian margin a modern analogue for such environments. Overall, our compilation of downcore records showed that enhanced bottom currents due to tide-topography interaction were progressively evolving and affected a wider area with the onset of the last deglaciation. Elevated tidal amplitudes and variability of mid-depth water masses (i.e.; density changes) and hydrodynamics in relation with changing climate were potential reasons of this evolving feature of erosion and reworking. Additionally, erosion and non-deposition was observed widest and even was encountered on the continental shelf during the early Holocene, potentially indicating a strong phase of the PCUC mirroring today's El Niño-like conditions.

Keywords: internal waves, Peruvian OMZ, hiatus, phosphorites, deglaciation, poleward undercurrent

3.1. Introduction

Sediments from the Peruvian margin have been of interest for environmental reconstructions of high productivity areas and OMZs (e.g., Oberhansli et al., 1990; Schrader, 1992; Rein et al., 2005). Short or long periods of non-deposition were observed in most of the sediment cores from continental shelf and slope off Peru. These gaps in the record impeded the reconstructions of Late Pleistocene and Holocene paleoenvironmental conditions (Reimers and Suess, 1983; Froelich et al., 1988; Biebow, 1996; Skilbeck and Fink, 2006; Salvattecchi et al., 2016) Salvattecchi, 2013). It has been suggested that the main reason of erosional intervals and hiatuses was the poleward flowing undercurrent (Reimers and Suess, 1983; Suess et al., 1987; Reinhardt et al., 2002) and the references therein). Recently, it was found that non-linear internal waves (NLIWs) breaking at the continental slope were affecting the sedimentation on Peruvian continental margin (Mosch et al., 2012). In fact, these waves have been suggested as important hydrodynamic energy source shaping the continental slope morphology, deposition and erosion of sediments (Cacchione et al., 2002; Pomar et al., 2012; Lamb, 2014). Previous works on the hiatus and erosional features concentrated on shelf and upper slope sediments off Peru and did not consider deposits from the middle or lower slope in the region. The present paper presents a compilation of sediment core and surface sediment studies (Table 3.1) including results from new cores recovered from greater depths with the aim to understand the development of erosion in space and time and to elucidate what has driven the development of non-deposition since the Last Glacial Maximum (LGM).

3.2. Regional setting

The continental shelf and slope off Peru (Fig. 3.1) is characterized by one of the most pronounced oxygen minimum zones (OMZ) in today's world oceans (e.g., Fuenzalida et al., 2009). It is a tectonically active margin with a narrow continental shelf extending down to about 600 m water depth in places (Krissek et al., 1980; Strub et al., 1998). The northernmost area is characterized by marginal gulfs which are under influence of major rivers (Krissek and Scheidegger, 1983). The shelf between 7°S and 10°30'S is broad (~30 km) and the continental slope is steep with a pronounced shelf break (Reimers and Suess, 1983; Suess et al., 1987; Reinhardt et al., 2002). The shelf between 11 and 14°S is narrow (~15 km) and deeper compared with the north. The transition from shelf to slope is less pronounced (Reimers and Suess, 1983). South of 15°S, the continental shelf is narrower (<5 km) and the continental slope steepens again towards the Chilean margin (Krissek et al., 1980).

Table 3.1. Publications used as source for this compilation and review.

Information	Publications (Author, Year)
Continental shelf and slope morphology, Recent sediment distribution and characteristics as overview	Krissek et al. (1980); Krissek and Scheidegger (1983); Reimers and Suess (1983); Suess et al. (1987)
Recent sediment distribution and characteristics from certain areas and transects	Koide and Goldber (1982), Henrichs and Farrington (1984), Kim and Burnett (1988), McCaffrey et al. (1990), Arthur et al. (1998), Levin et al. (2002), Böning et al. (2004), Muñoz et al. (2004), Gutiérrez et al. (2006), Sifeddine et al. (2008), Scholz et al. (2011), Mosch et al. (2012), Dale et al. (2015).
Phosphorite formation offshore Peru, phosphogenesis, phosphorite characteristics, their surface and downcore distributions	Veeh et al. (1973), Manheim et al. (1975), Burnett and Veeh (1977), Burnett (1980); Burnett et al. (1982), Froelich et al. (1988), Glenn and Arthur (1988), Garrison and Kastner (1990), Arning et al. (2009), Noffke et al. (2012).
Stratigraphical information; sediment cores, age models, dating points, sediment structures	Reimers and Suess (1983), Biebow (1996)Reimers and Suess (1983), Biebow (1996), Wolf (2002), Rein (2004), Agnihotri et al. (2006), Skilbeck and Fink (2006), Chazen et al. (2009), Pfannkuche et al. (2011), Mollier-Vogel (2012); Mollier-Vogel et al. (2013), Salvattecì (2013), Salvattecì et al. (2016).

3.2.1. Physical Oceanography

The Peruvian OMZ is maintained by the combination of a sluggish oceanic circulation and high primary productivity in the surface mixed layer, leading to elevated organic matter export and enhanced consumption of dissolved oxygen (e.g., Wyrski, 1962). Highest productivity is observed at the continental margin between 5 and 15°S (e.g., Echevin et al., 2008). The major current system in the research area is Peru Current System (Gunther, 1936; Huyer et al., 1991; Strub et al., 1998), which is shaped by the topography of the continental margin. The Peru Current System is composed of the Peru-Chile Countercurrent (PCCC), the Peru-Chile Undercurrent (PCUC; or the Peruvian Undercurrent (PUC)), deep equatorward Chile-Peru Deep Coastal Current (CPDCC), and surface Peru Coastal Current (PCC). The subsurface currents PCCC and PCUC are fed by eastward equatorial subsurface currents (Montes et al., 2010;

Czeschel et al., 2011). While the PCCC prevails 100-300 km offshore (Strub et al., 1995), the PCUC flows poleward above the continental slope and the outer shelf (Fig. 3.1; Strub et al., 1998; Chaigneau et al., 2013). The CPDCC is flowing equatorward beneath the PCUC carrying cold and low salinity Antarctic Intermediate Water (Chaigneau et al., 2013; and the references therein). The characteristics of the PCUC were documented by in situ measurements (Brockmann et al., 1980; Huyer et al., 1991; Czeschel et al., 2011; Chaigneau et al., 2013), and invoked by numerical modelling studies (Montes et al., 2010; Montes et al., 2011). It originates at around 3-5°S as a shallow water mass and prevails from 50 to 300 m water depths. The PCUC has a well-defined core between 50 and 200 m and flows with average velocities of 5-15 cm s⁻¹ (Chaigneau et al., 2013). The current prevails over the shelf and upper continental slope in the northern and central part of the region (Brockmann et al., 1980; Huyer et al., 1991; Czeschel et al., 2011). On its way south, the current deepens, in accordance with potential vorticity conservation. It detaches from the continental slope south of 15°S but remains close to sea floor (Chaigneau et al., 2013). During ENSO phases and concomitant changes of equatorial subsurface currents, the PCUC shows pronounced variability. The current settles at greater depths and weakens during La Niña periods, whereas it flows at shallower depths and intensifies during El Niño periods (Shaffer, 1982; Huyer et al., 1991; Hill et al., 1998; Montes et al., 2011). Velocities of up to 30 cm s⁻¹ were recorded between 9°S and 14°S in March 2010 which corresponds to El Niño period (Chaigneau et al., 2013).

Beside the deep currents, highly energetic baroclinic or NLIWs may exert an influence on the sediment distribution in relation to changes in sea floor topography. These waves are generated by tide-topography interaction and by internal wave reflection at the continental slope (e.g., Lamb, 2014)). They are associated with strongly elevated near-bottom velocities and thus elevated bottom shear stress and near-bottom turbulence that can be high enough to inhibit sediment deposition and even erode the sediment surface (e.g., Cacchione et al., 2002; Pomar et al., 2012). Furthermore, shoaling NLIW can form boluses that advect sediments and dense fluid upslope (e.g., Hosegood and van Haren, 2004; Bogucki et al., 2005; Martini et al., 2013; Bourgault et al., 2014). These waves are preferentially generated at topographic slopes classified as 'critical slopes', where the continental slope exhibits the same angle to the horizontal as the path of energy propagation of internal tides or waves (e.g., Cacchione et al., 2002; Lamb, 2014). Additionally, these sites are subject to internal wave breaking, enhanced mixing, and dissipation (e.g., Gayen and Sarkar, 2011; Lamb, 2014). Numerical simulations suggest that at critical slopes, the magnitude of the near-bottom velocities and the energy transfer to the internal wave is predominantly controlled by the strength of the incident barotropic tide and the horizontal

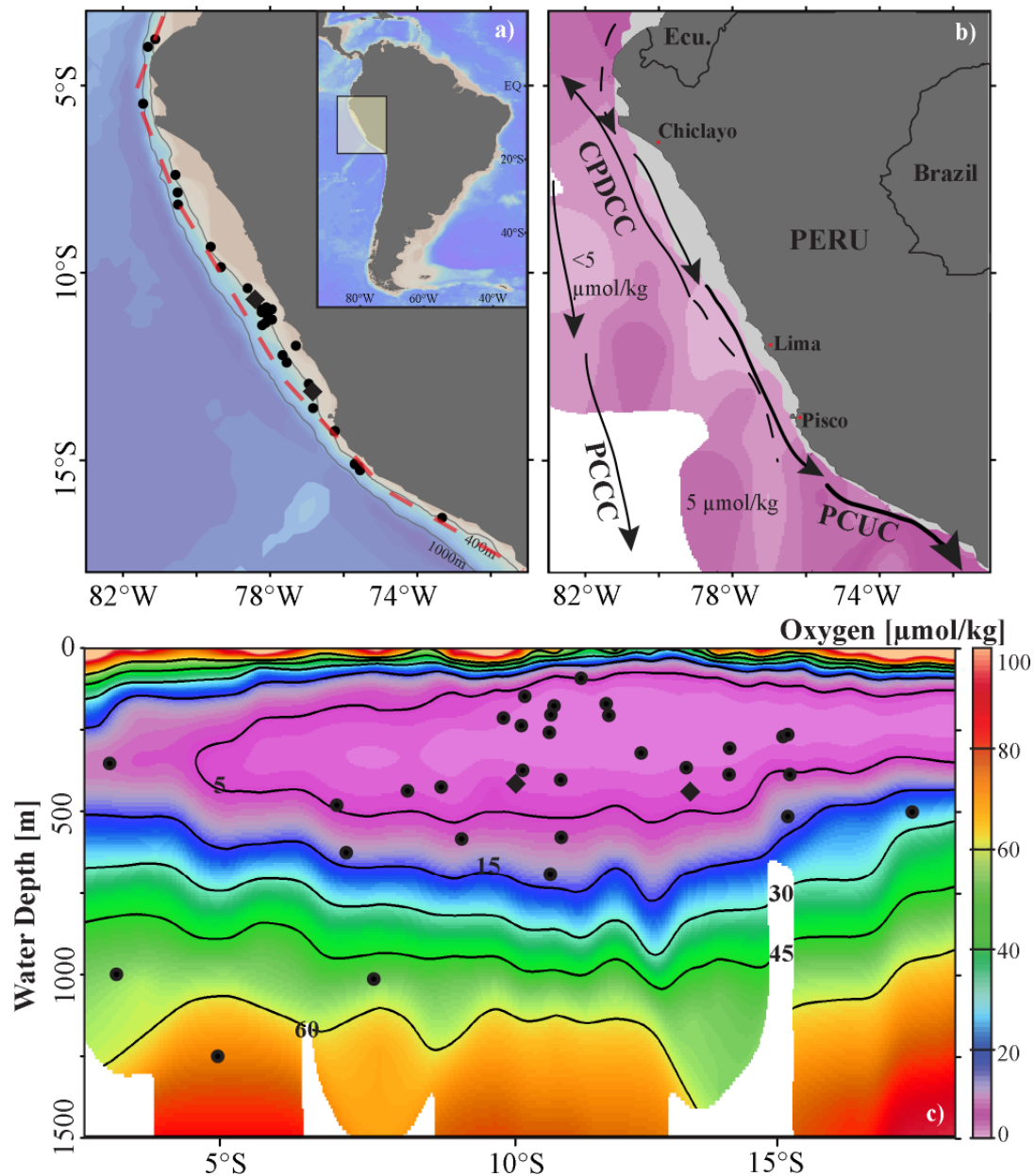


Figure 3.1. Maps of research area (a) showing the locations of 33 sediment cores along the shelf off Peru (round: cores with age models; diamonds: cores without age models) and red dashed line indicates approximate position of the transect shown in (c); (b) 400 m water depth hydrodynamics showing the approximate positions of the poleward flowing currents (Note that 400 m is the estimated deepest point PCUC impinges the sea floor, modified after Czeschel et al., 2011 and Chaigneau et al., 2013); (PCCC: Peru-Chile Countercurrent, PCUC: Peru-Chile Undercurrent and CPDCC: Chile-Peru Deep Coastal Current), and mean oxygen concentration as indicated in (c); Latitude vs depth section of dissolved oxygen concentrations along the shelf and core locations projected on the section. Oxygen data used after Schönfeld et al., (2015). Colour scale bars show the same values for both (b) and (c); prepared using Ocean Data View software.

extent of the critical slope (e.g., Gayen and Sakar, 2012). On the continental slope of Peru, extended critical slope regions were found close to 11°S between 500-730 m water depths (Mosch et al., 2012) and surface expressions of NLIW travelling onshore have been detected by satellite imagery (Jackson, 2007).

3.2.2. Sediments and topography of Peruvian margin

Sediments of the Peruvian margin show differences from north to south and shelf to slope in accordance with the seafloor topography, position of upwelling centres, boundaries of the OMZ, and bottom current dynamics (Krissek et al., 1980; Reimers and Suess, 1983). There is currently no sedimentation at the pronounced shelf breaks in the north of 10°30'S and south of 15°S (Reimers and Suess, 1983; Suess et al., 1987). Shelf and upper slope sediments within the OMZ are organic rich diatom bearing silty clays which are occasionally laminated in places, south of 10°30'S. Organic rich muds form a 100 m thick, lens-shaped body on the gentle slope between 11 and 14°S (Krissek et al., 1980; Suess et al., 1987). Foraminiferal sands and silty clays were found outside the OMZ. Slumps, erosional surfaces and phosphorites in various forms are common features in the area. Phosphorites were recorded in Peruvian margin sediments as old as the middle Miocene, but they are particularly abundant in Quaternary upwelling deposits (Garrison and Kastner, 1990). Youngest phosphorite formations coincide with the upper and lower boundaries of the OMZ (Burnett and Veeh, 1977). They consist of hard grounds, crusts, nodules, pelletal grains and silt-sized grains (Veeh et al., 1973; Burnett, 1977; Glenn and Arthur, 1988; Garrison and Kastner, 1990). Widespread phosphorite hard grounds were found in particular on the broad shelf in the north of 10°30'S (Reinhardt et al., 2002; Arning et al., 2009). Phosphorite nodules of various sizes were also reported from sediment cores (Garrison and Kastner, 1990; Pfannkuche et al., 2011).

The architecture of young sedimentary systems was revealed by hydroacoustic and seismic surveys on the shelf and upper slope (Reinhardt et al., 2002; Pfannkuche et al., 2011). They found features of sediment re-deposition and erosion, such as mud waves (Fig. 3.2) and phosphorite hard grounds, between 250-400 m water depths. In water depths of 500-750 m at 11°S the acoustic data revealed other erosional features (Fig. 3.2). The morphological step in 650 m water depth could be a headwall with landslide deposits beneath. Truncated wavy reflectors of varying thickness and high amplitude reflection in between occur at about 700 m depth. They are typical for an erosional channel with an infill drift. In these areas, the sea floor is occasionally covered by phosphorite nodules and hard grounds (Mosch et al., 2012). Similar phosphorite

formations from the same depth range were found around 12°S and 13°S (Arthur et al., 1998; Levin et al., 2002).

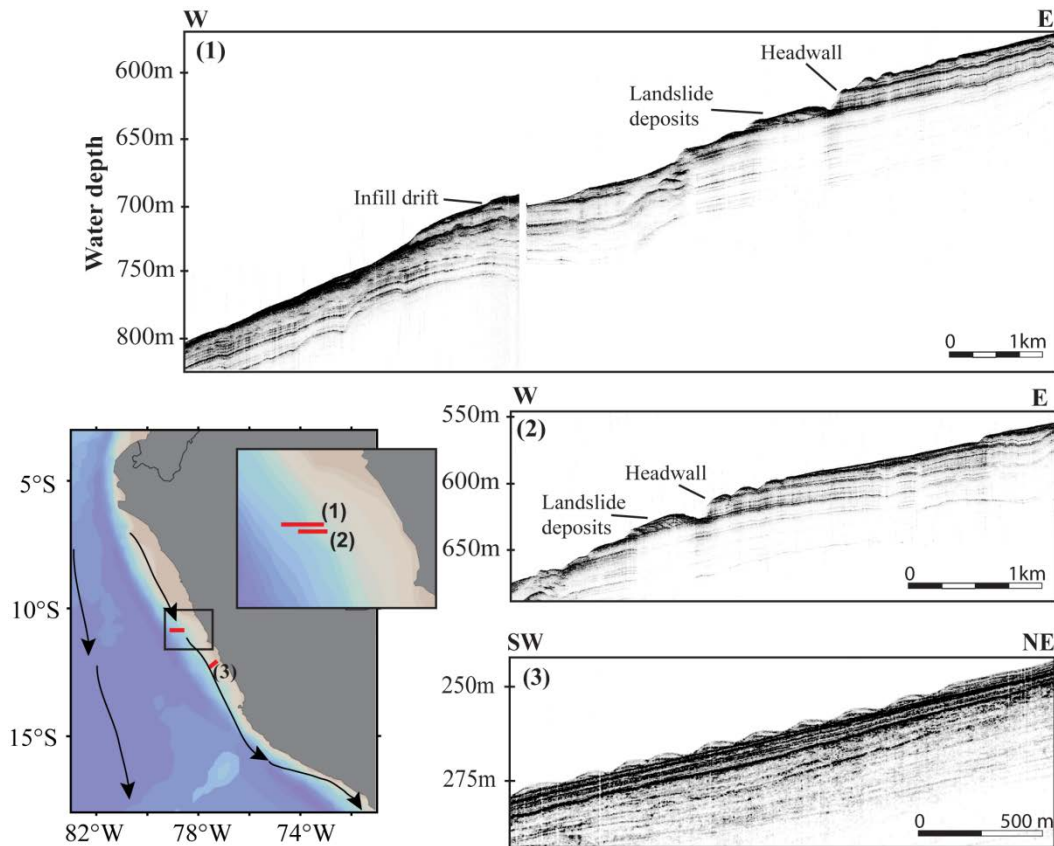


Figure 3.2. Parasound profiles obtained during M77 cruise Leg 1. Profiles 1 and 2 are two parallel from 11°S showing the eroded young sediments in the region. This depth interval is covered by phosphorite nodules and hard grounds (Mosch et al., 2012). Profile 3 is from 12°S showing mud waves created by the near-bottom current activity.

3.3. Material and Methods

3.3.1. Chronostratigraphy

Sediment cores were located at the continental slope between the water depths of 90 to 1300 m and latitudes of 3-18°S within and below today's OMZ (Fig. 3.1). Nine of the cores were recovered during R/V Meteor cruises M77/1 and M77/2 in 2008 (Pfannkuche et al., 2011). Information of the remaining cores was taken from the literature (Table 3.2). We considered visual core descriptions and physical properties of the cores from which chronostratigraphic information was available. Age models from previously published M77/2 cores were adopted following Mollier-Vogel, 2012 and Mollier-Vogel et al., 2013. Otherwise, conventional radiocarbon datings from previous studies and own ^{14}C Accelerator Mass Spectrometer (AMS) datings were calibrated using the software Calib 7.0 (Stuiver and Reimer, 1993) and applying the

marine calibration set Marine13 (Reimer, 2013). Reservoir age corrections were done according to the marine database (<http://calib.qub.ac.uk/marine/>) ranging from 89 to 338 years for this region. The radiocarbon-based chronologies were supplemented with benthic oxygen isotope curves correlated to stacked standard records (e.g., Lisiecki and Raymo, 2005) or Antarctic ice cores (EPICA Community Members, 2006). All ages are expressed in thousands of years (ka) before 1950 AD (abbreviated as cal ka BP). Average sedimentation rates of each core were calculated. Recent sedimentation rates were constrained by ^{210}Pb activity profiles (Koide and Goldber, 1982; Reimers and Suess, 1983; Kim and Burnett, 1988; McCaffrey et al., 1990; Gutiérrez et al., 2009; Scholz et al., 2011; Mosch et al., 2012; Dale et al., 2015).

New cores from M77/1 and M77/2 were opened and described aboard R/V Meteor (Pfannkuche et al., 2011). Cores showing distinct slumps and erosional surfaces were not sampled for further studies. Intervals of these structures were noted as a geological event. From the other, seemingly undisturbed cores, two parallel sets of volume defined samples were taken using cut-off syringes at 5 cm and 10 cm intervals. The first set of samples was freeze-dried and weighed for determining the physical properties. The second set of samples was wet sieved immediately on a 63 μm sieve. The remaining $>63 \mu\text{m}$ fraction of the samples was dried at 50 $^{\circ}\text{C}$, weighed and stored for further analysis. Stable oxygen isotope ($\delta^{18}\text{O}$) measurements of the cores were done with 3 to 6 individuals of benthic foraminiferal species *Uvigerina peregrina*, *Uvigerina striata* or *Globobulimina pacifica* according to availability. The tests of single species were crushed. Isotopic measurements were done with a Thermo Scientific MAT253 mass spectrometer equipped with an automated CARBO Kiel IV carbonate preparation device at GEOMAR, Kiel. Isotope values were reported in per mil (‰) relative to the VPDB (Vienna Pee Dee Belemnite) scale and calibrated versus NBS 19 (National Bureau of Standards) as well as to an in-house standard (Solnhofen limestone). Long-term analytical accuracy (1-sigma) for $\delta^{18}\text{O}$ and $\delta^{13}\text{C}$ was better than 0.06 ‰ and 0.03 ‰ on the VPDB scale. AMS radiocarbon datings were performed at Beta Analytic, Florida, USA. For each dating, 229 to 250 specimens of planktonic foraminiferal species *Neogloboquadrina dutertrei* were picked from the size fraction $>63 \mu\text{m}$. In samples which did not contain enough *N. dutertrei*, 33 to 179 specimens of *Planulina limbata* or 5 to 20 g of bulk sediment were used for radiocarbon dating. A systematic offset between sedimentary organic carbon and planktonic foraminiferal ages of ~900 years was observed supporting previous observations from the region (Mollier-Vogel, 2012).

Table 3.2. Metadata of sediment cores used in this study.

Cruise	Core Name	Year	Location		Water Depth (m)	Reference
			S	W		
M77/2	056-PC5	2008	03°44.99'	81°07.48'	355	Mollier-Vogel et al., 2013
M77/2	059-PC1	2008	03°57.01'	81°19.23'	997	Mollier-Vogel et al., 2013
M77/2	052-PC2	2008	05°29.01'	81°27.00'	1249	This study
RC-23-06	GS-1s	1982	07°38.2'	80°33.8'	480	Froelich et al., 1988
M77/2	047-PC2	2008	07°52.01'	80°31.36'	626	This study
M77/2	050-PC4	2008	08°01.01'	80°30.10'	1013	This study
ODP Leg201	1227B	2002	08°59.44'	79°57.35'	440	Skilbeck and Fink, 2006
M77/2	029-PC3	2008	09°17.70'	79°37.11'	433	Mollier-Vogel, 2012
SO147	41SL	2000	09°51'	79°20'	587	Wolf, 2002
RC-23-06	28BX-2	1982	10°22.7'	78°31.1'	216	Froelich et al., 1988
SO78	158-3	1992	10°55.33'	78°06.23'	237	Biebow, 1996
ODP Leg201	1229E	2002	10°58.56'	77°57.46'	152	Skilbeck and Fink, 2006
SO78	159-3	1992	10°58.79'	78°13.80'	373	Biebow, 1996
SO78	175-1	1992	11°03.12'	78°13.75'	695	Biebow, 1996
ODP Leg201	1228B	2002	11°03.85'	78°04.66'	262	Skilbeck and Fink, 2006
SO78	173-4	1992	11°05.64'	78°01.35'	204	Biebow, 1996
R/V Wecoma	7706-40	1977	11°15'	77°57'	186	Reimers and Suess, 1983
R/V Wecoma	7706-41	1977	11°20'	78°07'	411	Reimers and Suess, 1983
R/V Wecoma	7706-44	1977	11°24'	78°13'	580	Reimers and Suess, 1983
SO147	4SL	2000	11°56'	77°18'	96	Wolf, 2002
SO147	106KL	2000	12°03'	77°39.8'	184	Wolf, 2002; Rein et al., 2004

RC-23-06	GS-6	1982	12°05.1'	77°40'	203	Froelich et al., 1988
R/V Wecoma	7706-04	1977	12°58'	76°57'	325	Reimers and Suess, 1983
R/V Wecoma	7706-37	1977	13°37'	76°50'	370	Reimers and Suess, 1983
Galathea 3	G10	2007	14°13.81'	76°14.35'	312	Salvatecci et al., 2016
Galathea 3	G14	2007	14°14.12'	76°15.30'	390	Salvatecci et al., 2016
M77/2	003-PC2	2008	15°06.21'	75°41.28'	271	Mollier-Vogel, 2012
M77/1	422-GC7	2008	15°11.39'	75°34.87'	517	This study
MW87-08	PC-2	1987	15°15'	75°58'	270	Agnihotri et al., 2006 Chazen et al., 2009
RC-23-06	310BX-3	1982	15°16.9'	75°23.9'	387	Froelich et al., 1988
M77/1	416-GC4	2008	17°28.13'	71°52.62'	505	This study

Once chronostratigraphy of the cores was accomplished, the following specific time intervals were chosen for further work: Recent (0-500 yr BP), late Holocene (LH; 3-5 cal ka BP), early Holocene (EH; 8-10 cal ka BP), Bølling/Allerød (BA; 13-14.5 cal ka BP), Heinrich-Stadial 1 (HS1; 15-17.5 cal ka BP) and Last Glacial Maximum (LGM; 20-22 cal ka BP). We used the term “Recent” for the time period covering the last 500 years to be able to compare surface sediment distribution with other periods in downcore records. Lithological characteristics, sedimentation rates, sedimentary structures such as laminations, bandings, slump folds, hard grounds, sand-rich intervals, and discordant beddings were noted and combined for the corresponding time windows.

3.3.2. Determination of critical slope areas

Topographic boundaries accelerate an energy cascade from large-scale open ocean tides to high-mode baroclinic tides of short vertical wave length or NLIWs (e.g., Gerkema and Zimmerman, 1995). The magnitude of this energy conversion is controlled by the continental slope topography (α) and the slope of the linear internal tide energy propagation ($\tan(\beta)$).

$$\tan(\beta) = ((\sigma^2 - f^2) / (N^2 - \sigma^2))^{1/2}, \quad (1)$$

where σ is the frequency of the internal tides, f is Coriolis parameter and N is buoyancy frequency. Topographic slopes are classified as transmissive (subcritical; $\alpha < \beta$), critical ($\alpha \approx \beta$)

or reflective (supercritical; $\alpha > \beta$) (Fig. 3.3; Holloway, 1985; Cacchione et al., 2002). Critical slope areas were evaluated following Schafstall et al. (2010) and Mosch et al. (2012). Multibeam bathymetric data in combination with conductivity-temperature–depth (CTD) profiles were obtained on four zonal transects (8°S, 10°S, 11°S and 12°S) along the continental slope during M77 cruises in 2008. Multibeam surveys were conducted using the shipboard echosounder system (EM 120) and post-processing of the data was performed using MB System 5.1.1 (Caress and Chayes, 2001). Buoyancy frequency (N),

$$N = ((g/\rho_0)*(d\rho/dz) - g^2/c^2)^{1/2}, \quad (2)$$

where g is the earth gravity acceleration, ρ_0 is the potential density, c is the speed of sound, and $d\rho/dz$ is the vertical density gradient, was calculated from the CTD data using the adiabatic levelling method (Fofonoff, 1985). Evaluation of the slope of internal tide energy propagation (eq. 1) was accomplished by using N averaged in the depth range between 100 and 200 m above sea floor to exclude the bottom boundary layer following Mosch et al. (2012).

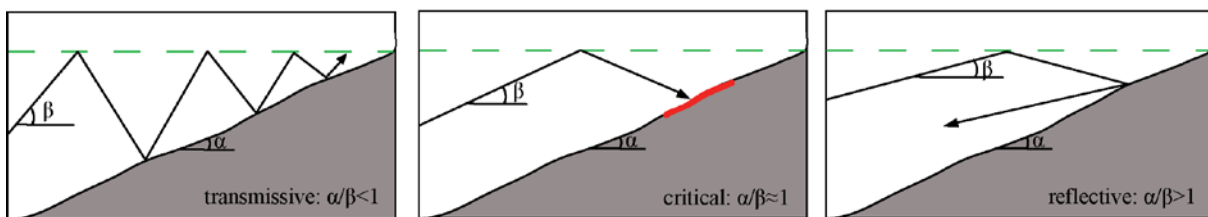
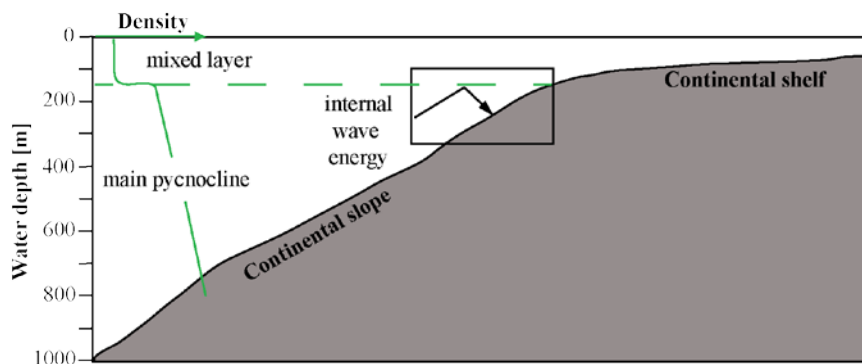


Figure 3.3. The behaviour of propagating internal wave energy (modified after Cacchione et al., 2002). In critical conditions, energy is trapped and impinges the sea floor. Red area indicates intensified bottom current velocities. Increase in upslope bottom current velocities are also observed in transmissive conditions.

3.4. Results

3.4.1. General facies distribution

Recent sediments of the last 500 years mark distinct differences between north and south of 10°30'S, such as texture, grain size, organic carbon values, or the abundance of foraminifera and diatoms. Downcore records of the last 22 ka showed significant changes between sediment cores recovered from north and south of 7°S. In general, sediments from north of 7°S consisted of planktonic foraminifera bearing silty clays showing no lamination. The sedimentation rates were relatively high (28–125 cm ka⁻¹) without abrupt changes downcore (Table 3.3). These cores represent a complete record since the LGM showing neither distinct lithological changes nor erosional features. South of 7°S, however most of the sediment cores showed unconformities, erosional surfaces or slumps and distinct changes in lithology. Sedimentation rates varied from 6 to 345 cm ka⁻¹. Planktonic foraminifera were less abundant in cores towards the south where diatoms became dominant.

Table 3.3. Average sedimentation rates (cm ka⁻¹) on the continental shelf and upper slope offshore Peru. Recent values were taken from literature and indicated as intervals. Downcore values are calculated for the specific time intervals according to the ¹⁴C datings in corresponding sediment cores. H = “Hiatus”.

	Recent 0-500 yrs BP	LH 3-5 ka BP	EH 8-10 ka BP	BA 13-14.5 ka BP	HS1 15-17.5 ka BP	LGM 20-22 ka BP
3-7°S Shelf		64	100			
3-7°S Slope		28-55	28-80	21-129	20-102	20
7-10°S <600 m		H and 6	H and 21	131 and H	157-345	38
7-10°S >600 m	70	H	H	7-16	7-44	7-72
11-12°S <350 m	40-450	9-71	H	3-17	3-6	4 and H
11-12°S >350 m	11-100	11 and H	H and 12	11-32	33 and H	H
12-15°S <350 m	310-610	46-105	55-87	18-99	9-36	H
12-15°S >350 m	160-320	H	H	H and 53	35	22
17-18°S Slope		H	H	H	H	66 nd H

3.4.2. Sediments of the time windows: Recent, late and early Holocene, BA, HSI and LGM

Recent (0-500 yr BP) sediments of the Peruvian continental shelf and upper slope are characterized by two main units. These are foraminifera bearing calcareous muds between 5 and 10°S and between 15 and 17°S above 250 m water depth, and diatom bearing organic rich muds between 10 and 15°S and above 500 m water depth (Fig. 3.4). The highest Recent sedimentation rates of up to 600 cm ka⁻¹ were observed in the centre of OMZ between 12 and 15°S (Table 3.3). Lamination and bands are not ubiquitous. They show a patchy occurrence between 12 and 14°S at water depths of 100 to 250 m. Bacterial mats are common on sediment surfaces at around 15°S and between water depths of 100 to 600 m. At greater depths on the continental slope and further north of the mud lens, foraminifera bearing muds with sand-rich intervals and phosphorite layers were observed. Below and southwards outside of the OMZ, greenish grey silty clays are accumulating.

During the late Holocene (3-5 cal ka BP), non-deposition was observed in a wide area in all of the cores recovered from south of 7°S and below 300 m water depth. Cores from shallower depths between 12 and 15°S consisted of laminated, dark greenish grey clays and silty clays (Fig. 3.4). They showed slump folds and discordant bedding planes. Sediment cores from the shelf and upper slope at 11°S consisted of diatomaceous mud with both sandy and laminated intervals. Distinct lithological changes, slump folds and discordant beddings were dated to have originated around 4 to 6 cal ka BP. In the region south of 7°S, sedimentation rates strongly varied (Table 3.3). Sediments from north of 7°S consisted of hemipelagic olive green grey silty clays with abundant planktonic foraminifera. A distinct lithological change from olive green-grey silty clay to dark olive green-grey clay in one northern core (M77/2-059-PC1) was dated at 3 cal ka BP. The sedimentation rates were around 60 cm ka⁻¹ on the shelf and upper slope and 30 cm ka⁻¹ at greater depths.

The widest extension of the hiatus was observed during the early Holocene (8-10 cal ka BP). In fact, majority of the cores recovered from south of 7°S contained no sediments from this period. Only seven cores retrieved from above 400 m water depth between 12 to 15°S showed bands and laminations with sedimentation rates ranging from 55 to 87 cm ka⁻¹. Slump folds were also observed in these southern, shallow cores. Discordant bedding was dated to 9 ka BP in one core (M77/2-003-PC2) at 15°S. Shelf and slope at 11°S exhibited major erosional features during this period. Slump folds, phosphorite sand layers, concretions and hard grounds were found in almost all cores from this latitude. There is currently only one core (7706-44) from 580 m water depth, which shows non-laminated silty clays with a sedimentation rate of 22 cm ka⁻¹.

Foraminifera bearing olive green grey silty clays were found north of 7°S and showed no major lithological change during this period (Fig. 3.4). Sedimentation rates ranged from 28 to 99 cm ka⁻¹ from slope to shelf in the north.

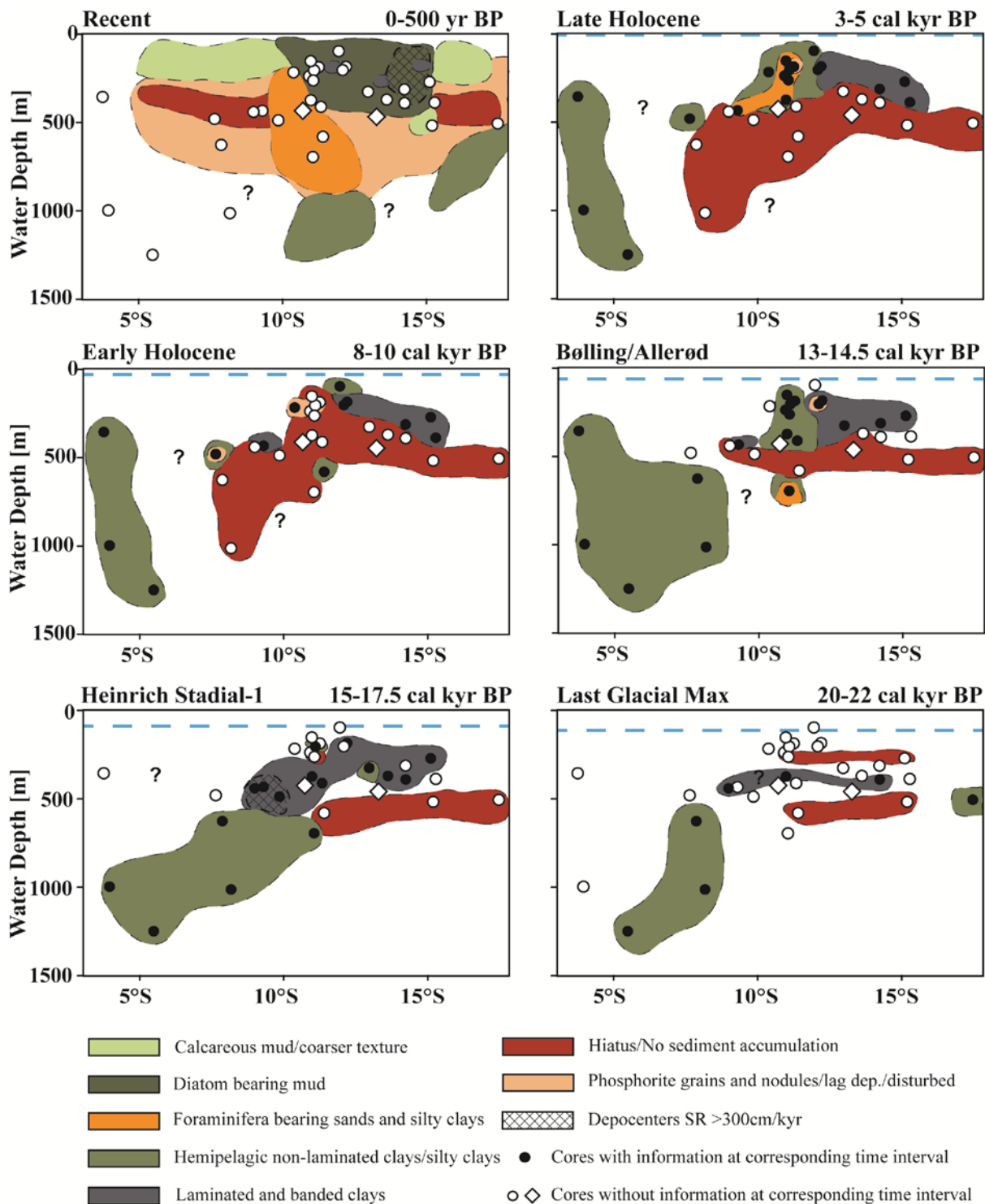


Figure 3.4. Sediment characteristics in specific time intervals in latitude vs depth section as in Figure 3.1, (c). Blue dashed lines indicate the approximate sea level in corresponding time interval.

During the Bølling/Allerød (13-14.5 cal ka BP), the extent of the hiatus was confined to south of 8°S and around 500 m depth. One core (SO78-175-1) recovered from 11°S and 700 m depth showed non-laminated silty clays with sand intervals during this time interval. Shallower depths around 11°S showed diatomaceous hemipelagic mud and low sedimentation rates ranging from 3 to 8 cm ka⁻¹. Upper slope and shelf sediments showed laminations south of 11°S (Fig. 3.4). Around 12-14 cal ka BP, either a distinct lithological change or discordant bedding was observed in almost all of the upper slope cores from south of 8°S. However, the cores north of 8°S showed bioturbated foraminifera bearing olive green to grey muds with low sedimentation rates (7-21 cm ka⁻¹) in deeper water depths and higher rates (~102 cm ka⁻¹) around 600 m at 3°S.

During Heinrich Stadial 1 (15-17.5 cal ka BP) only three cores from south of 10°S and below 500 m showed a hiatus. Sediments of shallower depths at 11°S showed sandy layers, shell lags, and erosional surfaces. Laminations were observed widest in this period (Fig. 3.4) with highest sedimentation rates (200-350 cm ka⁻¹) between 8 and 10°S and above 500 m. Below 500 m depth and north of 11°S, sediments consisted of non-laminated green to grey silty clays with abundant planktonic foraminifera.

Only 13 sediment cores were long enough to retrieve sediments from the LGM (20-22 cal ka BP). The southernmost core (M77/1-416-GC4) consisted of bioturbated greenish grey silty clay. Four cores recovered from the continental shelf and slope between 10°S and 15°S showed a hiatus. Two of them were from around 250 m and the other two were from around 500 m water depth. Upper slope sediments between 250 and 500 m showed diatomaceous oozes with laminations (Fig. 3.4). The sedimentation rates ranged from 4 to 66 cm ka⁻¹ at the south of 7°S. Northern cores consisted of non-laminated, foraminifera bearing olive green to grey silty clays with sedimentation rates ranging from 7 to 72 cm ka⁻¹ (Table 3.3).

3.4.3. Distribution of phosphorites

Different types of phosphorites in various sizes were found in Recent sediments at the Peruvian continental margin from the shelf to about 1000 m water depth (Fig. 3.4). Considering the classification of Garrison and Kastner (1990), the most common type is D-phosphorite. They are well-cemented, dark coloured and found in forms of nodules, gravels and hard grounds. These phosphorites were observed in shelf and upper slope sediments. In particular, they were abundant around and north of 11°S between 200 to 600 m water depths and around 15°S between 100 to 600 m water depths. Few centimetre thick crusts and hard grounds were reported from the shelf in the northern part of the region. Occasional or irregular phosphorite grains and nodules were also found around 5°S on the slope. With minor exceptions, the rest of the

phosphorites indicated in Figure 3.4; Recent are F and/or P-phosphorites. F-phosphorites are light coloured small sized nodules that were observed within the diatomaceous oozes. P-phosphorites are phosphatic sands which were found often in a mixture of coated grains and fish debris. These sands were observed between 7°S and 10°S on the upper slope. Some surface sediments from 15°S around 200 m water depths also contained phosphorite grains and nodules with abundant fish debris.

All of the above mentioned phosphorite types were also observed in sediment cores. Since they were considered as lag deposits (Veeh et al., 1973; Oberhansli et al., 1990) and representing periods of non-deposition or erosion (e.g., Garrison and Kastner, 1990), most of the phosphorite-bearing cores were not used in paleoclimate studies. The age models are less constrained so that the time intervals of phosphorite formation are not well known. Five sediment cores out of 31 with an advanced chronostratigraphy showed concretions and hard grounds (D-phosphorites) in the early Holocene (Fig. 3.4). Phosphorite layers were observed in other M77 cores, which were not considered in this study, from around 400 to 600 m water depths between 10°45'S to 17°S (Pfanckuche et al., 2011). In particular, at M77/2-026-PC1 from 11°S and 424 m, phosphorite nodules and crusts were observed forming meter-thick layers. Another core, from ODP Site 686 Leg 112, from 14°S and 446 m water depth showed various layers of phosphorites in the Holocene part (Garrison and Kastner, 1990; core locations as diamonds in Fig.3.1; see Appendix). These records provide corroborating evidence that the sporadic early Holocene phosphorites formed a band of occurrences between 400 and 600 m depth.

3.4.4. Near critical slope areas

The ratio between the continental slope angle (α) and the angle of internal tide energy propagation to the horizontal (β) was calculated for the four zonal transects along 8°S, 10°S, 11°S and 12°S, from 100 to 1300 m water depths (Fig. 3.5). The 11°S data previously published by Mosch et al. (2012) but are included here for the sake of completeness. The ratios showed that critical slope regions occur frequently between 500 m and 1000 m. Near-critical slope areas are indicated by values between 0.7 and 1.3. They particularly occur around 300 m, between 500-600 m and 800-900 m at the 8°S transect, between 200-300 m and depths >700 m at 10°S, at 500 m and between 600-750 m at 11°S, and between 500-600 m, around 700 m and between 800-1050 m at 12°S. The near-critical slope region at 11°S in a water depth between 600 and 750 m corresponds to the erosional surface observed in seismic profiles (Fig. 3.2) and phosphorite

hard grounds. The cross-slope extent of the near-critical slope regions are between 5 km and 20 km, larger than typically found in the ocean.

When the slope is reflective, as indicated by values of $\alpha/\beta > 1$ for the northern transects 8°S and 10°S from 600 m to 800 m depth and from 350 m to 550 m depth respectively, the onshore propagating internal tides are reflected back offshore. In the southern transects at 11°S and 12°S however, the internal wave energy is reflected onto the continental slope and accumulates in shallower water depths indicated by values of $\alpha/\beta < 1$. A particularly noteworthy feature in the transects at and southern of 10°S is the near-constant distribution of the ratios in the depth range between about 500 and 1000 m exhibiting near-critical or slightly lower values.

3.5. Discussion

Sediment cores off Peru have distinct interruptions and disturbances in their downcore record reflecting the region's sedimentary and oceanographic dynamics. The information gathered within this study shows that, except during the early Holocene, the main erosion is restricted to an area below today's 400 m water depth. In particular south of 7°S, non-deposition and erosional surfaces are common features, whereas in the north, the sedimentary record is not interrupted. Here, the sediment composition and structures showed differences as compared to the south. The topography and hydrodynamics differed as well, probably in relation with the upwelling centres or due to the effect of fluvial discharge (Mollier-Vogel et al., 2013). Most likely, the northern margin of Peru acts as topographic barrier and keeps the area as two separate sedimentary basins.

The PCUC has been attributed to have an erosive effect on upper slope sediments in previous studies (Reimers and Suess, 1983; Suess et al., 1987; Arthur et al., 1998; Reinhardt et al., 2002; Junium et al., 2015). It was thought to be the main cause of the low sedimentation rates, non-deposition and erosion on the shelf and upper continental slope above 400 m water depth south of 7°S. Considering the average velocities of the PCUC as known today, additional oceanographic processes causing elevated near-bottom velocities are required to drive non-deposition and erosion. Furthermore, erosional features are also found in greater water depths where the PCUC is not present (Fig. 3.2). Since the information on sediment distribution for water depths >700 m is limited, eroded sediment structures from these depths are not always well documented. However, the hiatus found at >700 m depths, and in particular around 8°S below 800 m, can be explained by enhanced near-bottom velocities due to highly baroclinic or NLIWs that result from tide-topography interaction at near-critical continental slopes (Fig. 3.5).

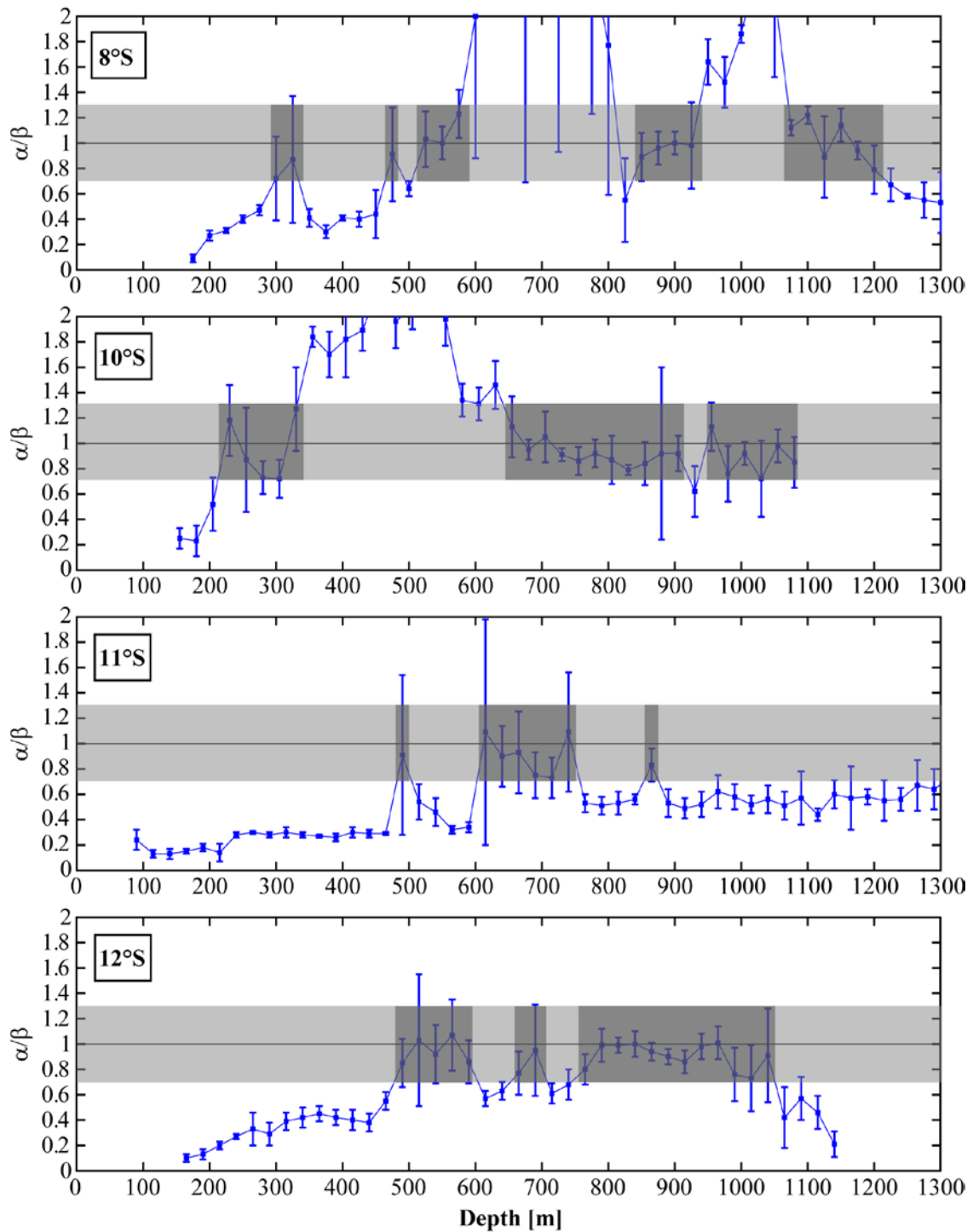


Figure 3.5. Critical slope calculations vs water depth profiles for four transects from north to south. Dark grey shaded areas indicate near-critical slopes where NLIWs are erosive; α is the continental slope; β is the angle of the energy propagation of the internal wave to the horizontal. Note that 11°S measurements are from the same transect as in seismic profile (1) in Fig. 3.2.

The internal waves can inhibit sediment deposition, resuspend and transport sediments through the generation of NLIWs from tides incident on near-critical slopes (Hosegood and van Haren, 2004; Bogucki et al., 2005; Martini et al., 2013; Bourgault et al., 2014). As a consequence, they

may play an important role in shaping our continental slope system by transporting sediments upslope or downslope (Cacchione et al., 2002; Puig et al., 2004; Klymak et al., 2011; Pomar et al., 2012; Shanmugam, 2013; Lamb, 2014). According to the critical slope analysis from the four zonal transects offshore Peru, near-critical slopes of elevated cross-slope extent frequently occur between 500 and 1000 m (Fig. 3.5). Furthermore, shipboard and moored velocity observations at the continental slope and shelf at 12°S (Sommer et al., 2014) as well as satellite imagery (Jackson, 2007) have captured energetic non-linear wave trains propagating toward the coast that likely originate from tide-topography interaction at near-critical slopes. As a result of this process, sediments are kept in suspension above sea floor (Arthur et al., 1998; on site observations during SFB754 cruises) or carried upslope where PCUC transports them further south. Non-deposition found in greater water depths in the north is probably result of such process as NLIWs carry the sediments upslope over the shelf and the PCUC sweeps them away. This sweeping away and southward transport of sediments from the northern broad shelf was documented in previous studies (Reimers and Suess, 1983; Suess et al., 1987). The southward transport is probably the reason of high sedimentation rates up to 600 cm ka⁻¹ observed around 15°S along the shelf above 350 m depth (Table 3.3; Fig. 3.4). Whereas in greater water depths, exceptionally low sediment (11 cm ka⁻¹) and mass accumulation rates were recently determined at the lower OMZ boundary at about 400 m depth along a transect between 12°S and 13°S (Dale et al., 2015) where the continental slope is critical. The authors argue that sediment winnowing at 11°S and 12°S due to internal waves likely affect sedimentation rates determined in their study. The erosive effect of NLIWs were found between 600-750 m water depths around 11°S (Fig. 3.2; Mosch et al., 2012); 500-600 m around 12°S and 400-700 m around 13°30'S (Arthur et al., 1998). Arthur et al. (1998) documented velocity measurements and surface sediments from 70 m to 1000 m water depths at two transects (12°S and 13°30'S), and reported poleward flow between 500 and 700 m depth. According to recent long-term observations of the PCUC velocity structure a poleward current is not present at these water depths (Chaigneau et al., 2013).

3.5.1. Phosphorites as erosion indicators

The presence of phosphorites has been associated with high organic rich matter input, changing redox conditions and elevated bottom currents, thus, low sedimentation rates. Once the bottom currents resuspend sediment particles from the sea floor, heavier phosphorite grains accumulate and concentrate into greater phosphorite formations (Baker and Burnett, 1988; Föllmi, 1996). Such authigenic phosphorite formations and beds have been widely documented in fossil records since the Cretaceous (e.g., Kennedy and Garrison, 1975; Soudry et al., 2006;

Föllmi et al., 2015). These phosphorite beds were recognized in close relation with unconformities and erosional features, thus used as indicators of major paleoenvironmental and paleoclimatological changes (Föllmi et al., 2015). Almost all of the studies considering the formation of Peruvian phosphorites pointed out the relation between phosphorite formation and winnowing, non-deposition or low sedimentation rates in conjunction with low oxygen values (e.g., Veeh et al., 1973; Manheim et al., 1975; Burnett, 1977; Garrison and Kastner, 1990; Oberhänsli et al., 1990; Arning et al., 2009). The ongoing formation of hard grounds on the shelf around 10°S is considered to result from a combination of the latest low stand and the jet like structure of PCUC in that area (Garrison and Kastner, 1990; Reinhardt et al., 2002; Arning et al., 2009). Phosphorite crusts and nodules are currently occurring at around and south of 11°S between water depths of 100-400 m and 500-750 m as a result of enhanced near-bottom velocities (Arthur et al., 1998; Levin et al., 2002; Mosch et al., 2012) and excess phosphate concentrations close to sediment-water interface (Froelich et al., 1988; Noffke et al., 2012). In situ benthic flux measurements from 11°S indicated that benthic P release is the highest among all OMZs in the world (Noffke et al., 2012). This high release is due to dissolution of Fe-oxides, organic matter degradation and microbial matt occurrences on the shelf. P release at greater depths within the OMZ was attributed to organic matter degradation. Besides all these factors decomposition of fish debris was assumed to contribute to this high release. In particular at >300 m water depths where high P fluxes correspond to lower organic carbon: P ratios were thought to be a result of authigenic phosphorite formation (Noffke et al., 2012).

Phosphorites were found in almost all the sediment cores obtained from the south of 10°S. As mentioned before, the absence of adequate age models limits the reconstruction of phosphorite formation periods in downcore records. Biebow (1996) used the intervals of hard grounds as a correlation point between cores and recorded that they correspond to the early Holocene (6-8 ka BP) indicating a hiatus on the shelf. Two cores (M77/2-026-1 & 686A) with fairly precise age models showed thick layers of phosphorite nodule and crusts with upwards increasing abundance towards the Recent period. This pattern makes it difficult to tackle a single hiatus but rather points to an evolution of widespread erosion and winnowing along the upper slope. One common feature these two cores show is that phosphorite layers overlie laminated sediments probably corresponding to the HS1 period, in which laminated sediments showed maximum extent (Appendix). Burnett (1980) also pointed out the possibility of a relationship of phosphorite formation with changing climatic conditions because phosphorite formations enhanced during interglacial periods. Since phosphorite formations coincide with high bottom water activities and episodic oxygenation events (e.g., Garrison and Kastner, 1990), it is likely

that winnowing and reworking intensified in combination with rising sea level and increasing bottom water oxygenation after the HS1 (Jaccard and Galbraith, 2012; Moffitt et al., 2015).

3.5.2. Evolving sedimentary dynamics at the Peruvian margin

The data presented above revealed a progressively northward extension of non-deposition during the last deglaciation. Information on LGM sediments is limited to a few records. The data showed two erosional bands at different depths indicating probably two different erosive areas. The upper band might be due to coastal erosion and lag sediment formation at low sea level at that time. The lower band indicates the bottom water activity and most probably the effect of NLIWs. This bipartitioning is exclusively found on the upper slope or at the shelf break during LGM and HS1. The laminations that found widest on the shelf and upper slope during HS1 indicate both, a quiet hydrodynamic environment and disoxic bottom waters. Bottom-dwelling macrofauna is absent at oxygen levels $<5 \mu\text{mol kg}^{-1}$ (Schönfeld et al., 2015). These conditions facilitate the preservation of laminations. High surface primary production (Pedersen, 1983; Pedersen et al., 1988) and expansion of the OMZ (Hendy and Pedersen, 2006; Jaccard and Galbraith, 2012; Moffitt et al., 2015; Salvattecchi et al., 2016) was reported for the period 14-19 ka BP to have prevailed in the Eastern Equatorial Pacific. Highest sedimentation rates during HS1 were found around 9°S and 500 m water depth (Table 3.3). In contrast, sedimentation rates were relatively low in greater water depths, possibly indicating NLIWs carrying the sediments upslope. The less pronounced or absent PCUC around 9°S would not impede sedimentation at shallower depths. After HS1, laminated sediments are restricted to a mud lens between $11\text{-}14^{\circ}\text{S}$. This restricted occurrence is probably due to the topography difference between north and south of $10^{\circ}30'\text{S}$ and the invigorating PCUC which limits the sedimentation in the north over the shelf. The progressively decreasing sedimentation rates, northward extending hiatus, decrease in coverage by laminated sediments, and the increased occurrence of phosphorites suggest that the erosive influence of the NLIWs and sediment displacement by the PCUC increased during BA and following periods. While detailed potential causes of NLIW intensification during this period are discussed in the next section, compelling evidence suggested stronger El Niño-like conditions in the Eastern Equatorial Pacific since 17-18 ka BP (e.g., Moy et al., 2002; Keefer et al., 2003; Rein et al., 2005; Koutavas and Joanides, 2012; Carré et al., 2014). A higher frequency of extreme El Niño-like climatic events may trigger stronger bottom currents, affecting wider areas with progressive sea level rise.

The widest distributed hiatus and erosional features were found during the early Holocene. The erosion observed in shelf sediments, in particular at shallow depths around 11°S ,

could be explained by an intense and strong phase of near-bottom currents. All the cores from this transect showed slumps, non-deposition or phosphorite crusts, and hard grounds as seen today on the shelf further to the north. One possibility is that the current was intense, strong and extensive on the shelf during that time creating the same phosphorite pavement as in the north today. Most of the studies reported a hiatus or non-depositional intervals between 6-10 ka BP (Suess et al., 1987) and 6-8 ka BP (Biebow, 1996). Some studies indicated weaker El-Niño conditions having prevailed during the period of 6-8 ka BP but suggested stronger El Niño before 8 ka BP (Keefer et al., 2003; Rein et al., 2005; Carré et al., 2014). Given the climatic-oceanographic linkage, enhanced El Niño would have triggered conditions developing an extended hiatus during EH (8-10 ka BP). Whether upwelling was intensified or not during this period is a matter of discussion and apparently hampered by the lack of reliable sedimentary archives. Common agreement is that climate and oceanographic conditions were extreme and different from earlier time intervals (e.g., Suess et al., 1987; Rein et al., 2005; Carré et al., 2014). After 6 cal ka BP, the conditions over the shelf around 11°S became calmer in terms of less erosion but laminations were still sparse. This implies that bottom waters were better ventilated in the region. Sandy intervals indicate that high-energy conditions were still prevailing on the shelf but not as strong as during the early Holocene. Reimers and Suess (1983) suggested that the current became detached from the sea floor around 6 ka BP and sedimentation resumed. There is an abrupt change in climatic conditions of the region documented by intensifying ENSO conditions and abundance of extreme climate events after 6 ka BP (Rodbell, 1999; Andrus et al., 2002; Chazen et al., 2009; Ehlert et al., 2013). Such conditions would allow both, sedimentation and erosion alternating on very short time scales.

3.5.3. Potential effects of mid-depth hydrodynamic change

Non-depositional features and low sedimentation rates are observed today where the continental slope is critical and near-critical marking the erosive effect of the NLIWs. Compilation of downcore records indicated extended erosion, on the shelf and upper slope, but also at greater depths. This supports the idea that these waves are much more effective and erosive than the PCUC in particular on the slope. The northward prograding hiatus is therefore most likely a result of intensified NLIWs. An intensified PCUC may have had a supporting influence. The strength of near-bottom currents due to NLIW and thus their erosional potential predominately depends on the horizontal extent of critical slopes which is controlled by stratification and the amplitudes of the barotropic tides and internal waves impinging the continental slope. State of the art global numerical simulations of the evolution of barotropic

tides since the LGM suggest that the amplitudes of the semidiurnal and diurnal tides were significantly larger than today (Thomas and Sündermann, 1999; Egbert et al., 2004; Wilmes and Green, 2014). Wilmes and Green (2014) showed that in the semidiurnal tidal energy dissipation was increased by a factor of two in the southern Pacific during the LGM and subsequent deglaciation. This suggests that tide-topography interaction was significantly enhanced during the LGM and deglaciation, and gradually decreased towards today's levels and provides an explanation for the hiatus observed in sediment records.

Due to the steepness of the continental slope off Peru, near-critical regions are more extensive compared to other regions from where near-critical slopes were reported (Cacchione et al., 2002; Hosegood and van Haren, 2004; Carter et al., 2005; Schafstall et al., 2010; Klymak et al., 2011; Martini et al., 2013). As NLIWs shape the continental slope and shelf breaks, these regions extend in area while they winnow and re-deposit the sediments until new regions become critical (Cacchione et al., 2002). It thus can be assumed that sediment reworking has been significant in the past and this process has been active thousands of years. Additionally, NLIW formation depends mainly on stratification and thus the density gradient in the water column. Climatically induced changes of water mass properties in the ocean causing changes of the oceans' stratification during the last deglaciation might have favoured the formation of the NLIWs causing an extension of sediment reworking. Current knowledge about the water mass distribution since LGM and absence of data for offshore Peru (e.g., reconstructed paleo-density values) limits further constraints on possible density changes and its influence on mid-depth dynamics. Overall, sedimentary information proved that changes in mid-depth hydrodynamics have been playing an important role for sediment distribution on the Peruvian margin, resulting in an extending hiatus with the onset of the last deglaciation.

3.6. Conclusions

Paleoceanographic reconstructions at the Peruvian continental margin are hampered by gaps and hiatus found in sedimentary records as a result of strong erosional processes. Combination of sedimentary information gathered from surface sediment distribution and sediment cores with observational analyses of modern oceanography showed that complex hydrodynamics of the region have been playing an important role on erosion as well as sediment distribution since the LGM. Thus, the Peruvian margin is a good example for a current-dominated sedimentary regime in terms of NLIWs impact on erosion and ongoing phosphorite formations.

By determination of critical slopes, we identified regions where the NLIWs are formed, erode and shape the continental slope today. These critical slopes are so far the widest in range reported. Within these areas NLIWs keep sediment particles in suspension above the seafloor and displace them upwards or downwards the continental slope. The resuspended particles are further carried southward along the continental slope and shelf by the PCUC as it intensifies. This process results in low sedimentation rates, non-deposition and erosion around and south of 7°S, whereas a depocenter forms on the shelf and upper slope at around 15°S. Modern phosphorite occurrences and the absence or patchiness of laminations in the region are also indicators of active winnowing and reworking.

The widespread hiatus that has evolved since the LGM extended on the continental shelf and slope south of 7°S. This evolving feature of erosion and non-deposition that has been observed on the continental slope agrees with the evolution of the barotropic tide amplitude known from model studies. It suggests enhanced tide-topography interaction and intensified NLIWs with the onset of the deglaciation as compared to today. Various forms of phosphorites were also observed in much wider areas during the Holocene, particularly on the continental shelf, supporting the hypothesis of intensified reworking in the region. Additionally, the early Holocene (8-10 ka BP) was the only period where the hiatus was actually encountered on the continental shelf. This leads to the conclusion that during the early Holocene, the bottom currents were stronger which potentially indicates more frequent El Niño-like conditions.

Acknowledgements

This work was funded by Deutsche Forschungsgemeinschaft (DFG) through SFB 754 “Climate–Biogeochemistry Interactions in the Tropical Ocean”. We would like to thank captain and crew of M77 Leg 1 & 2 cruises and Dirk Nürnberg, Christian dos Santos Ferreira for operating the Parasound system and providing data. We would like to thank to Martin Frank during data compilation from various literature, Silke Voigt for valuable comments and Kristin Doering for feedbacks during preparation of this paper. We would also like to thank the Editor Collin M. Wallace and an anonymous reviewer for their constructive comments.

4. DOWNCORE BENTHIC FORAMINIFERAL DISTRIBUTIONS FROM THE PERUVIAN MARGIN FOR THE LAST 22,000 YEARS

This chapter describes downcore distributions of the common calcareous benthic foraminifera from five sediment cores obtained from the Peruvian Margin. The sediment cores were recovered during the M77 cruises Leg 1 and Leg 2 in 2008. Detailed information regarding to the sediment cores can be found in Chapter 2. Concerning the foraminifera study, the working halves of the cores were sampled with 10 cm resolution 10 to 20 cc sediment samples. The samples were wet-sieved on a 63 μm screen immediately after sampling (except for cores 47-2 and 59-1 which were sampled previously by others) and residues were dried in 40°C oven. After completion of the age models of the sediment cores (see Chapter 2), we focused on specific time intervals with 300 to 500 years resolution and worked with the sieved dry samples corresponding to these time intervals (Figure 4.1.). The samples were later split with an Otto microsplitter in order to attain similar total numbers of specimens, which is around 300 per sample (Murray, 2006). From the split material, the foraminifera were dry picked, collected in Plummer cell slides, sorted by species, fixed with glue and counted. Statistical analyses (e.g., Fisher α and Shannon_H diversity index, dominance; see Appendix) are applied using the software PAleontological STatistics (PAST) Version 3.11. Common species were imaged with a CamScan 44/EDX scanning electron microscope and a Keyence VHX-700 FD digital camera at the Institute for Geosciences, Kiel University. The following references were followed for the taxonomy of the involved species; Natland (1950), Cushman and McCulloch (1955), Barker (1960), Uchio (1960), Smith (1964), Boltovskoy and Theyer (1970), Coulbourn (1980), Ingle et al. (1980), Resig (1981;1990), Whittaker (1988), Loeblich and Tappan (1988), Figueroa et al. (2005), Mallon (2012), Ellis and Messina Catalogues.

4.1. General trends

In total of 190 species were identified in all the sediment cores. The taxonomical reference list, optical microscope and SEM images of the common species and their downcore distribution details (species protocols) for each sediment core can be found in Appendix. Three of the all species belong to the group of the agglutinated species which were observed only in the deep cores (59-1, 52-2 and 50-4). The most abundant species with relative abundance (%) more than 5 % constitutes at least 70 % of whole benthic foraminiferal assemblages in the samples. This percentage drops to 60 % in the samples at cores 59-1 and 52-2 where the Fisher α diversity indicates relatively higher values as well. In total 36 species were observed within the group of

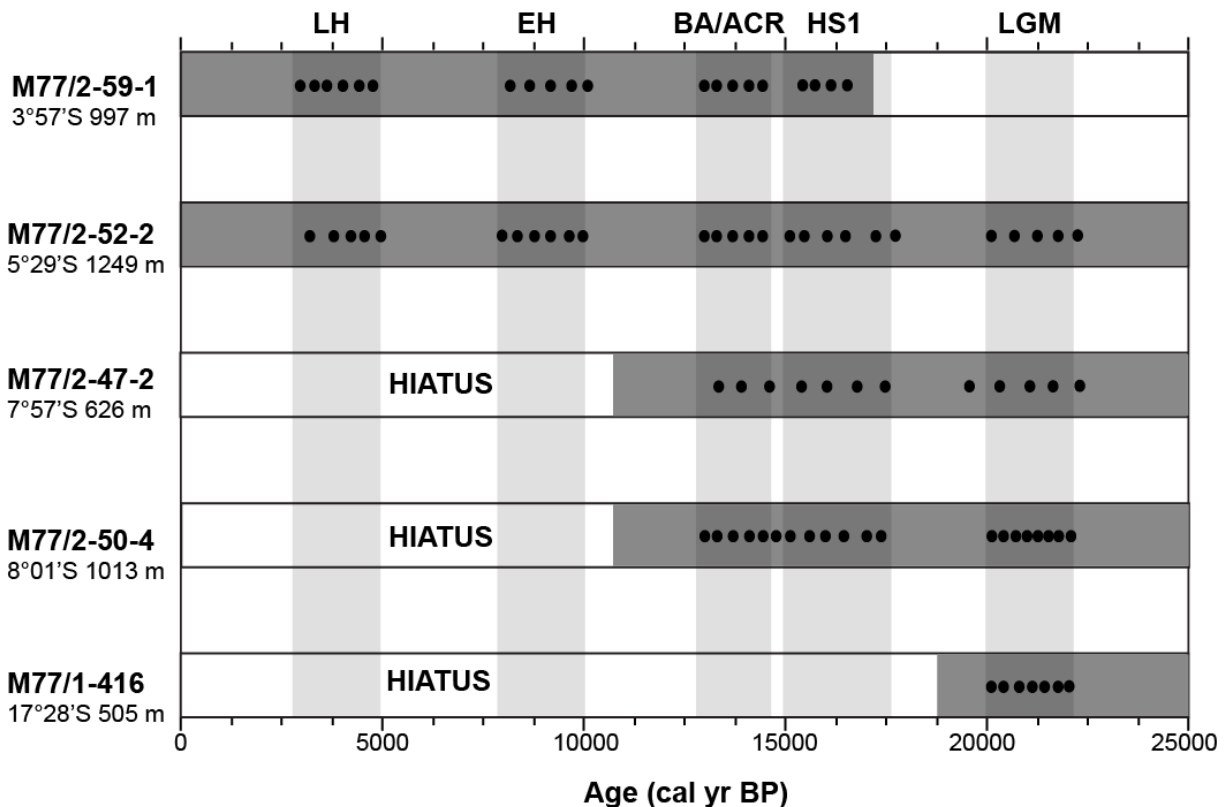


Figure 4.1. Schematic description of the focused time intervals and samples considered regarding to the benthic foraminifera study at each core.

>5 % in the sediment samples. The most common species observed in all cores are *Bolivinita minuta*, *Cassidulina delicata* and *Epistominella exigua*.

Core M77/2-59-1

Twenty samples were investigated and in total of 161 species were identified at this core. The Fisher α diversity index indicates highest ranges within the five cores. The downcore benthic foraminiferal distributions reveals a distinct change at core depth 843 cm which corresponds to the end of the period Bølling Allerød / Antarctic Cold Reversal; 13.5 cal ka BP (Figure 4.2). The most abundant species is *Bolivinita minuta* which indicates an increasing trend after this interval in the core reaching up to 30 % in the late Holocene. *Cassidulina delicata* occurs more than 5 % throughout the core with increasing percentages up to 20 % during the Holocene periods whereas *Epistominella exigua* reaches percentages of 25 % during the Termination I. The overall trends and appearances of *Bolivina* species shows significant differences compared to other cores. Common Peruvian margin species such as *Bolivina seminuda*, *B. costata* or *B. spissa* are observed in low numbers, whereas *B. pacifica* indicates slightly increased percentages in accordance with *E. exigua* during the BA/ACR. The small species *Anomalinoidea minimus* are observed with percentages around and more than 5 % only at

this core. This species was observed and described in the Mediterranean Sea (Vismara Schilling and Parisi, 1981). Its size does not exceed 150 μm therefore it is potentially disregarded when the $>150 \mu\text{m}$ size fraction is considered. In the sediment samples, this species is observed only at

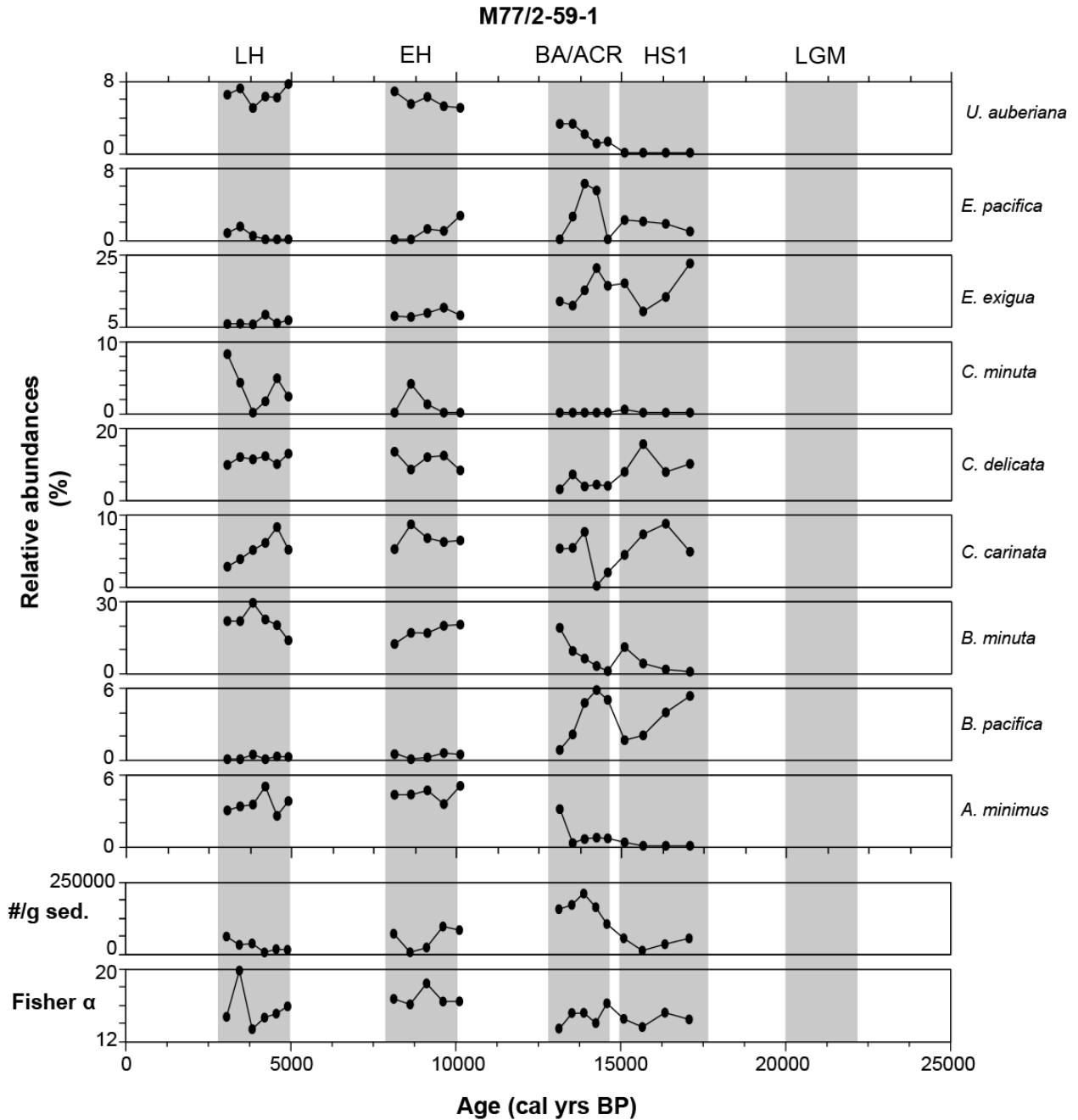


Figure 4.2. The downcore distributions of the most abundant species observed in the core 59-1 together with Fisher α diversity index and abundance (specimen per gram sediment; #/g sed) calculated for each sample.

the northern cores 59-1, 52-2 and few specimens are also observed in the core 47-2. Its distribution in the Mediterranean Sea was reported as in co-occurrence with *Epistominella exigua* and *Alabaminella weddellensis* (= *Eponides pussillus* of Schmiedl et al. (2003)) and in

association with the sapropels suggesting “a high recolonization potential of deep-sea areas following anoxic periods” (Schmiedl et al., 2003) and the references therein. In the open oceans these small opportunistic species were reported as indicators of enhanced phyto-detritus input to the sea floor (e.g., Gooday and Lamshead, 1989; Gooday, 2003). In the core 59-1, *Anomalinoidea minimus* co-occurs with *Alabaminella weddellensis*, *Bolivinita minuta* and *Uvigerina auberiana*. The decreasing trend of the *Epistominella exigua* while these species shows increasing trends might be related to their low tolerance to the low oxygenation in the bottom waters during the deglaciation whereas *E. exigua* is potentially much more tolerant to low oxygen concentrations and benefits from less competitive environment. High productivity and low bottom water oxygen conditions during the deglaciation was reported for the EEP (e.g., Pedersen, 1983; Hendy and Pedersen, 2006) which supports this idea.

Core M77/2-52-2

In total of 170 species identified within 27 samples from this sediment core. Fisher α diversity index shows a fluctuating trend throughout the core with high values during the LGM and at the beginning of the BA/ACR (Figure 4.3). Diversity is observed lowest during the HS1 and the late Holocene. Abundance calculations indicate anti-correlating fluctuations to diversity where minimum values are observed during the LGM. Increasing abundance and decreasing diversity might be indication of deoxygenation during the time periods of BA/ACR and the Holocene (particularly the LH). The overall most dominant species are *Bolivina costata*, *Epistominella exigua*, *Cassidulina delicata* and *Bolivinita minuta*. The relative abundance of the *Bolivina costata* shows a distinct increase in the Holocene with percentages reaching up to 43 % at the end of the early Holocene where Fisher α and abundance show anti-correlation. *Bolivina spissa* shows a similar increasing trend in the corresponding time intervals but with much less proportions (2 – 8 %). *Epistominella exigua* shows highest abundances at the onset of the HS1 which is followed by gradually decreasing trend during the deglaciation. This decreasing trend shows correlation with dominance and anti-correlation with the Fisher α diversity. The abundances of *Cassidulina delicata* distribution indicates fluctuations throughout the core with percentages ranging from 5 to 21 % with highest values during the late Holocene. *Bolivinita minuta* shows increased abundances (10 – 20 %) only at two samples (350 cm and 360 cm) during the end of the BA/ACR period start of the Younger Dryas (12.7 – 13.1 cal ka BP). This distinct increase in the abundance of *B. minuta* is observed in core 59-1 as well which corresponds to the same time period. Its relative abundance continues increasing during the

Holocene in core 59-1 whereas in core 52-2 the overall assemblage is dominated by *Bolivina costata* during the Holocene.

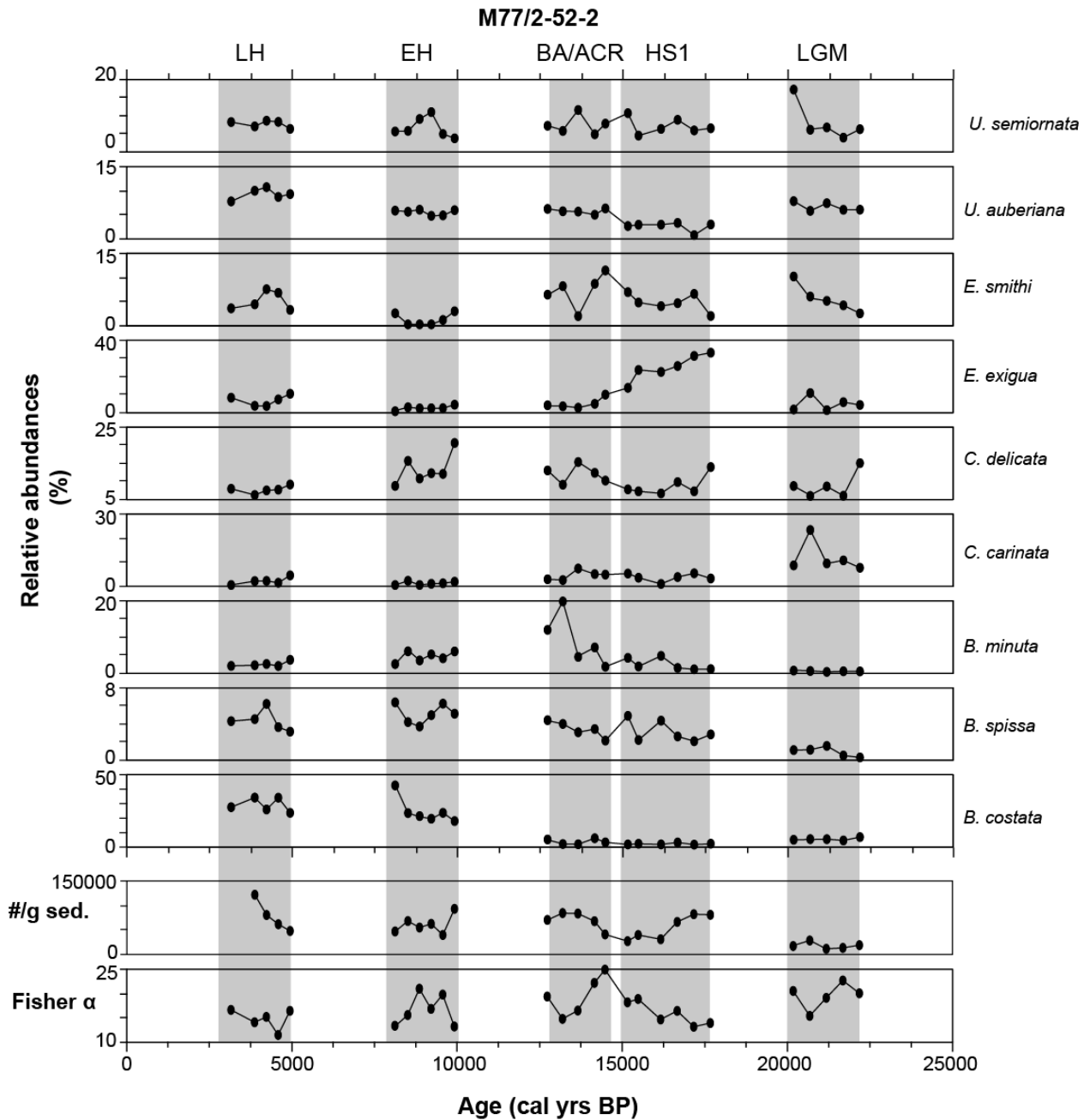


Figure 4.3. The downcore distributions of the most abundant species observed in the core 52-2 together with Fisher α diversity index and abundance (specimen per gram sediment; #/g sed) calculated for each sample.

Core M77/2-50-4

The information from the Holocene is missing in this core due to erosion in the region. Benthic foraminiferal investigations are accomplished in 20 samples and in total of 138 species

are identified. Overall, 17 species are observed with relative abundances > 5 % and they constitute more than 70 % within the whole assemblage observed in each sample (except three samples from the LGM interval). Fisher α diversity and abundance show anti-correlation in the investigated time intervals (Figure 4.4). Diversity is observed in higher values during the LGM (still low compared to the northern core 59-1 and 50-4) which is followed by gradually

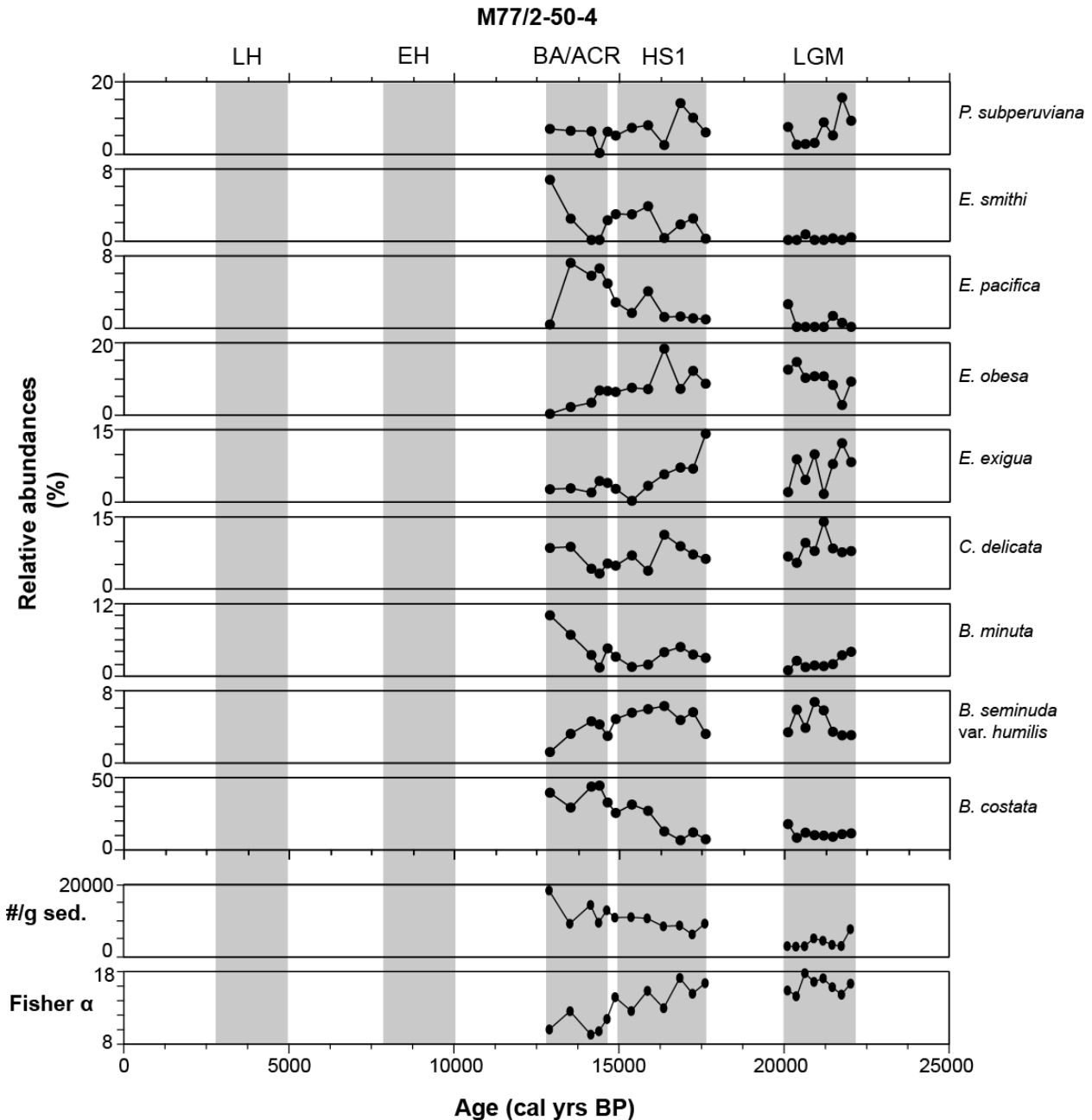


Figure 4.4. The downcore distributions of the most abundant species observed in the core 50-4 together with Fisher α diversity index and abundance (specimen per gram sediment; #/g sed) calculated for each sample.

Chapter 4: Downcore benthic foraminiferal distributions from the Peruvian Margin for the last 22,000 years

decreasing trend during the Termination I. This trend shows correlation with the relative abundance changes of *Bolivina costata*, which is overall the most abundant species observed in this core. Its relative abundances within the assemblages reach up to 50 % during the BA/ACR. The decreasing diversity and simultaneously increasing abundance trend might be indication of decreasing oxygen levels during the Termination I in the core location. The distribution of *Epistominella exigua* indicates fluctuating trend during the LGM as if it is pointing out the fluxes of high detritus input to the sea floor in these intervals. Its trend during the deglaciation shows similarities to its distribution in core 52-2 although with much less percentages. Its maximum percentages are around 15 % during the onset of the HS1 and decreases to < 5 % in the BA/ACR. Meanwhile *Bolivinita minuta* occur with percentages < 5 % during the LGM and HS1 and distinctly starts to increase at the end of the BA/ACR which is similar to its distributional pattern in the northern cores. Overall, besides *Bolivina costata*, species which belong to genus *Epistominella* dominate the assemblages in this core.

Core M77/2-47-2

Similar to core 50-4, the information regarding to the Holocene period is missing in this core and additionally due to low sedimentation rates the sampling resolution is around 500 years (Figure 4.1). In total of 12 samples are investigated and 87 species are identified. Overall trends of the abundant species do not reveal distinct changes from LGM to end of the Termination I whereas both Fisher α diversity and abundance indicate a slightly decreasing values during the Termination I compared to the LGM (Figure 4.5). In total of nine species show abundance more than 5 % in this core and they constitute at least 70 % of the whole assemblages in each sample. The most abundant species is *Bolivina costata* with proportions ranging between 15 and 30 %. It is followed by *Epistominella obesa* and *Cassidulina delicata* with percentages fluctuating around 10 %. Neither *Epistominella exigua* nor *Bolivinita minuta* shows significant high percentages in this core as they do in the northern cores.

Core M77/1-416

Due to erosion, it is only possible to investigate the LGM in this core, in which seven samples are analysed and in total of 61 species are identified. Within the 61 species, 12 species are observed with > 5 % abundances in different samples (Figure 4.6). Diversity and abundance show similar fluctuating trends. In two different samples, 140 cm and 180 cm, *Buliminella elegantissima* and *Nonionella auris* show high relative abundances around 21 % and 9-15 %, respectively. They are absent in other samples and their occurrences are known to be limited to

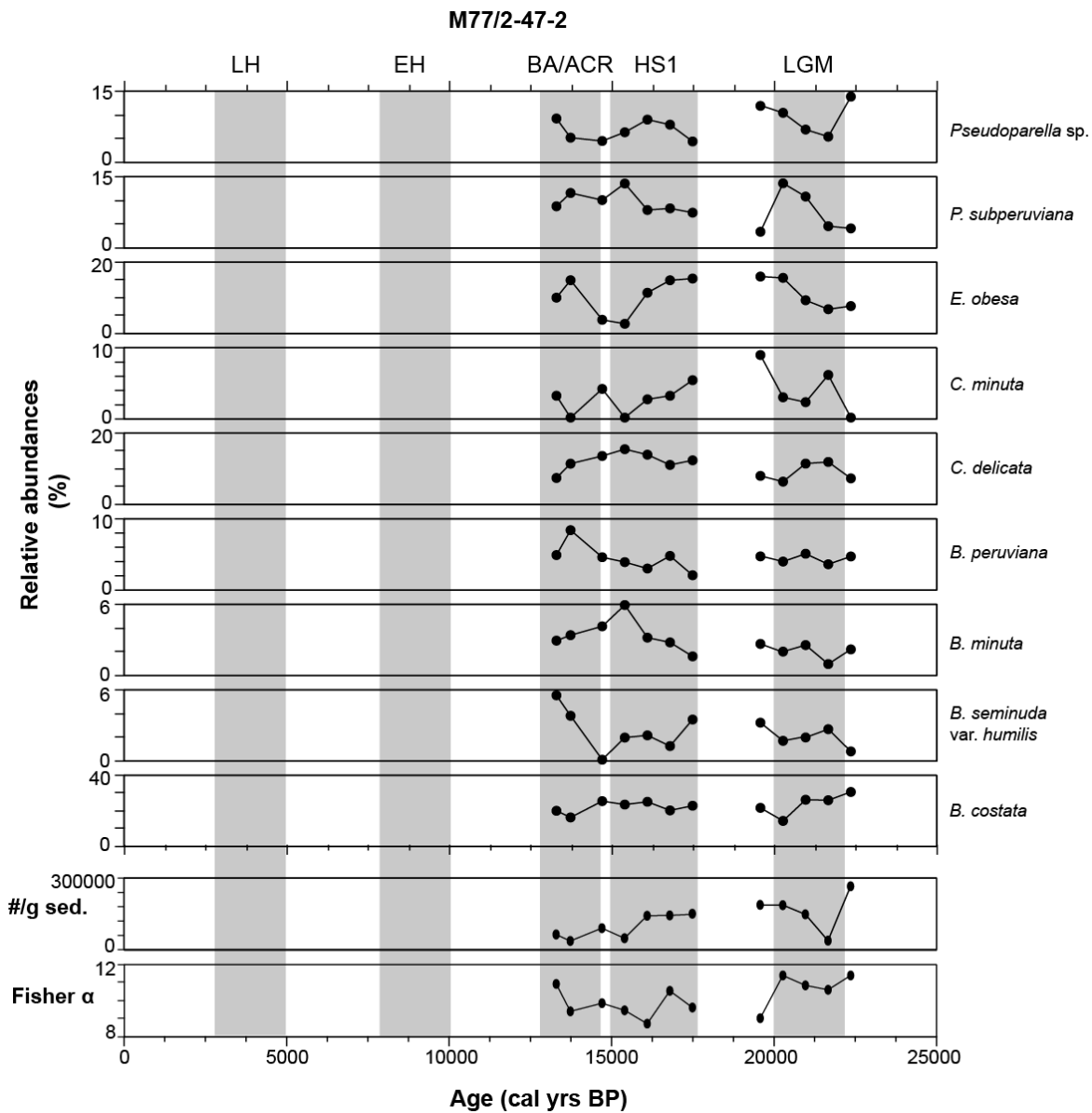


Figure 4.5. The downcore distributions of the most abundant species observed in the core 47-2 together with Fisher α diversity index and abundance (specimen per gram sediment; #/g sed) calculated for each sample.

the shelf (e.g., Ingle et al., 1980; Resig, 1990; Mallon, 2012). Comparing their relative abundances with the sedimentological information and physical properties measured at this core reveal the downward transportation occurrences in the core location (Figure 4.7). High values of magnetic susceptibility (SI) and the $> 63 \mu\text{m}$ (weight %) at the same core depths together with increasing abundances of *B. elegantissima* and *N. auris* are indicators of the downslope transportation. *Epistominella pacifica* and *E. afueraensis* show high abundances in this core. The distribution *Cassidulina auka* reveal an increasing trend whereas the *Bolivina seminuda* var. *humilis* is decreasing which might be an indication of changing bottom-water conditions.

Chapter 4: Downcore benthic foraminiferal distributions from the Peruvian Margin for the last 22,000 years

Comparing the LGM information from all cores (except core 59-1) shows that this core is the least diverse in terms of benthic foraminiferal distributions. The species indicate regional differences as well. For instance *Bolivina costata* is limited to a few specimens in one sample but *Cassidulina auka* is one of the most abundant species whereas in the northern cores it is observed as rare.

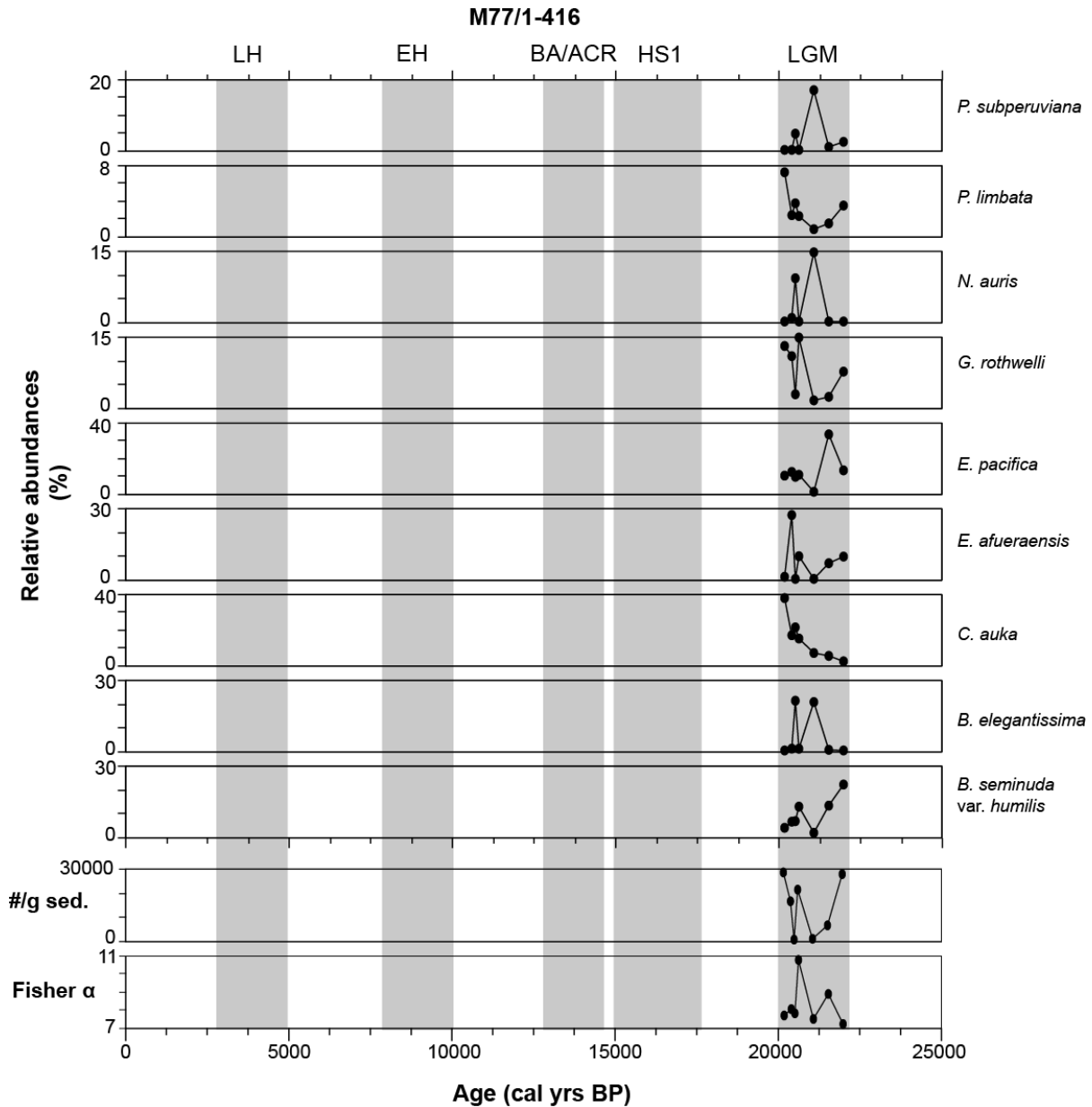


Figure 4.6. The downcore distributions of the most abundant species observed in the core 416 together with Fisher α diversity index and abundance (specimen per gram sediment; #/g sed) calculated for each sample.

4.2. The most abundant species and their indications

In overall distributional patterns, *Bolivina costata* is one of the most abundant species observed but its occurrence is limited to the sediment cores between 5°S and 8°S and water depths of 620 m to 1250 m (Figure 4.8). Not much is known about the ecology of *Bolivina costata*, as well as its distribution in the global oceans. Offshore Peru, previous observations reported its tolerance to oxygen minimum conditions (Khusid, 1974; Mallon et al., 2012) and even to sulfidic pore waters (Cardich et al., 2012; Cardich et al., 2015). Its distribution is thought to be limited to the continental shelf offshore Peru and is used as a proxy for sea-level fluctuations (Resig, 1990). The observations on the living (rose-Bengal stained) benthic foraminifera from the region indicate that they are found also in deeper parts of the Peruvian margin (Mallon, 2012). Another record from the region used this species (together with *B. seminuda* and *Nonionella auris* as an indicator of enhanced upwelling and productivity periods (Heinze and Wefer, 1992). Its distribution in core 50-4 indicated an increasing trend from 10 % to 45 % during the Termination I whereas in the deeper core 52-2 from 5°S revealed similar changes but in later period during the Holocene (Figure 4.8). Considering its distributions within the living assemblages (Mallon et al., 2012; Cardich et al., 2015), this species could be used as indicator for

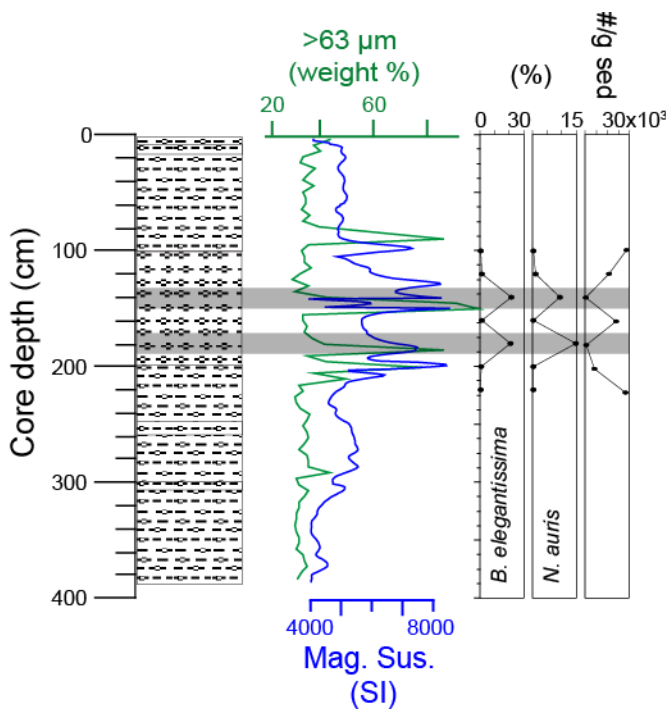


Figure 4.7. Visual description of core M77/1-416 with magnetic susceptibility (SI) measurements and < 63 µm (weight %) information. Relative abundances of given species are potentially in relation with the downslope transported material.

Epistominella exigua is a well known indicator of high phyto-detritus input and surface water productivity (Gooday, 1988; Gooday and Lambshead, 1989; Gooday, 1993; Smart et al., 1994). It is absent in cores from 8°S 626 m and 17°S 505 m and its abundances show relative increases during the Termination I in the northern cores but with different magnitudes. *Epistominella exigua* shows high abundances

oxygen depleted conditions which suggests gradually increasing deoxygenation in and expanding OMZ with the onset of Termination I in the north.

in core 52-2 during the HS1 and it is followed by a distinct decreasing trend toward the end of the deglaciation whereas in the northernmost core 59-1, its relative abundance indicates fluctuations but always stays around similar values during the whole deglaciation (Figure 4.8). The southern core within these three cores, 50-4, does not reveal similar values. This suggests that different surface water processes have been taking place above these core locations. The northern part of the 5°S might have been under influence of the Equatorial system. The significant drop in the occurrence of the *E. exigua* in the core 52-2 and its continuous occurrence in core 59-1 could be interpreted as northward shift of the upwelling cell and subsequent high surface productivity during the deglaciation. Furthermore, the anti-correlation trend which is observed between *Bolivinita minuta* and *Epistominella exigua* is rather interesting. The ecology of *B. minuta* is not known much, but the other *Bolivinita* species are observed as in association with sustained organic matter input (Sarkar and Gupta, 2014; and the references therein). The living benthic foraminiferal information from the shelf indicated that it is one of the common species of the OMZ setting and tolerant to low bottom oxygen conditions but not found as abundant as *Bolivina costata* for instance in the OMZ core (Mallon et al., 2012). Its slightly increasing trend at the end of the BA/ACR period is observed in all cores from the northern part of the region and could be related to Younger Dryas which is often not observed in the Southern Hemisphere records. Additionally, this slight increase is also in accordance with the distributional pattern of *Anomalinoidea minimus* in core 59-1, which might be an indication of short-term ventilation of intermediate depths during this time period.

Cassidulina delicata is one of the common species of upper- middle bathyal assemblages (500-1000 m) offshore Peru and Chile (Ingle et al., 1980; Resig, 1981) and offshore California (Bandy, 1953a; Zalesny, 1959; Uchio, 1960). It occurs dominantly together with *Epistominella pacifica*, *E. smithi*, *Bolivinita minuta*. Additionally, off Chile, Ingle et al. (1980) related this diverse assemblage with the occurrence of the AAIW. It is also reported as one of the low oxygen tolerant species (Douglas and Heitman, 1979; Sen Gupta and Machain-Castillo, 1993). In the sediment samples, *C. delicata* is one of the most abundant species and our findings agree with the previous observations. Except core 416, in all cores it is observed with percentages more than 5 % without indicating distinct changes throughout the cores, seemingly not influenced by environmental factors as other species did.

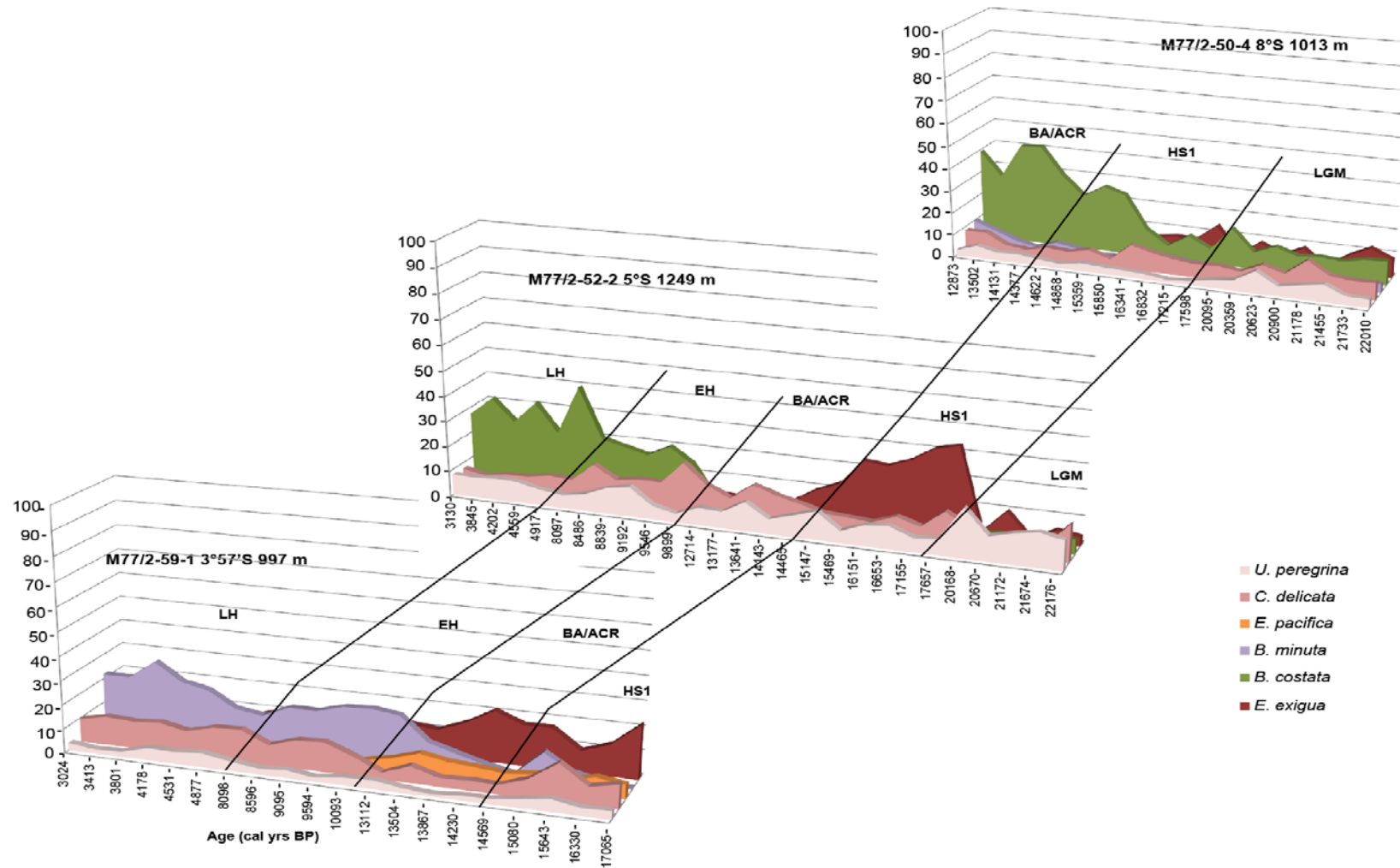


Figure 4.8. Comparison of downcore distributions of the most abundant species in three northern cores.

**5. BOTTOM-WATER DEOXYGENATION AT THE PERUVIAN MARGIN
DURING THE LAST DEGLACIATION RECORDED BY BENTHIC
FORAMINIFERA**

Zeynep Erdem^a, Joachim Schönfeld^a, Anthony E. Rathburn^b, Maria-Elena Pérez^c, Jorge Cardich^d, Nicolaas Glock^a, Kristin Doering^{a,e}

a) GEOMAR Helmholtz Centre for Ocean Research Kiel, Wischhofstr. 1-3, 24148, Kiel, Germany.

b) Indiana State University, Science Building 159, Terre Haute, Indiana 47809, USA

c) Natural History Museum, Department of Palaeontology, London, UK

d) Instituto del Mar del Perú (IMARPE), Av. Gamarra y Gral. Valle, Chucuito, Callao 01, Peru

e) Institute for Geosciences, Christian-Albrechts-Universität zu Kiel, Otto-Hahn-Platz 1, 24118 Kiel, Germany.

Abstract

Deciphering the dynamics of dissolved oxygen in the mid-depth ocean during the last deglaciation is essential to understand the currently expanding oxygen minimum zones (OMZs) in relation with the Global Warming. Many paleo-proxy records from the Eastern Pacific Ocean indicate an extension of oxygen depleted conditions during the deglaciation but the deoxygenation has not been quantified to date. Being one of the largest OMZs in the world's oceans, the Peruvian OMZ is a key area to monitor such changes in bottom-water oxygenation in relation to changing climatic conditions. A multiple regression analysis was applied to a joint dataset of living (rose Bengal stained) calcareous benthic foraminiferal distributions from the Peruvian continental margin, and bottom-water oxygen (BWO) concentrations during sampling periods were used as dependant variable. The correlation was significant ($R^2 = 0.959$; $p < 0.05$) indicating that the foraminiferal assemblages are rather governed by oxygen availability than by the deposition of particulate organic matter. We applied this transfer function to four sediment cores from the northern part of the Peruvian OMZ between 3°S and 8°S and 600 m to 1250 m water depths; thereby recording the changes in the lower boundary of the Peruvian OMZ. Each core displayed a similar trend of decreasing BWO levels since the Last Glacial Maximum (LGM). Even though the estimated BWO concentrations were relatively low compared to modern values, the overall change from the Last Glacial Maximum to the Holocene was reckoned to 25 $\mu\text{mol/kg}$. The deoxygenation trend was time-transgressive, commenced at the southern core, and gradually spread to deeper waters and to the northernmost core location. This pattern indicates a gradual northward expansion of the OMZ during the last deglaciation which was most probably governed by changes in the dynamics of the subsurface and intermediate waters.

5.1. Introduction

The Oxygen Minimum Zones (OMZs) occur where intense upwelling and high primary productivity result in elevated oxygen consumption within the water column in combination with sluggish ventilation (Wyrski, 1962; Helly and Levin, 2004; Fuenzalida et al., 2009). In today's world oceans, the most pronounced OMZs with oxygen concentrations $< 20 \mu\text{mol/kg}$ are observed offshore northwest and southwest Africa, in the Arabian Sea and the Bay of Bengal in the Indian Ocean, and along the continental margin of the Eastern Pacific at low latitudes (Helly and Levin, 2004; Paulmier and Ruiz-Pino, 2009). These zones also exhibited an expanding trend during last decades in which the global oceans change to warmer conditions (Stramma et al., 2008; Stramma et al., 2010). In this respect, paleoceanographic reconstructions of the bottom-

Chapter 5: Bottom-water deoxygenation at the Peruvian Margin during the last Deglaciation recorded by benthic foraminifera

water oxygenation during the last Deglaciation are a valuable approach to understand the dynamics of the OMZs during changing climatic conditions (e.g. Jaccard and Galbraith, 2012; Moffitt et al., 2015; Praetorius et al., 2015). The Eastern Equatorial Pacific (EEP) has been in focus of various paleoceanographic studies to unravel the dynamics of the surface productivity and bottom-water oxygenation (BWO; Heinze and Wefer, 1992; Cannariato and Kennett, 1999; Hendy and Pedersen, 2006; Moffitt et al., 2014; Scholz et al., 2014; Salvattecchi et al., 2016). The region is characterized by a strong and shallow OMZ maintained at intermediate water depths as a result of enhanced upwelling (Pennington et al., 2006). All the above mentioned attempts used similar proxies such as sedimentary textures (laminations), productivity proxies (Corg, $\delta^{15}\text{N}$, biogenic opal), redox sensitive elements (e.g., U, Mo, Cd, V, Mn) and benthic foraminiferal distributions (e.g., Jaccard et al., 2014; Moffitt et al., 2015). The studies indicated that cold, glacial periods were generally associated with contracted OMZ whereas warm or interglacial periods were associated with an expansion of the OMZ. However, the number of approaches for BWO reconstructions for the Peruvian margin is limited to a few, and the records are mostly from sediment cores recovered from shallower than 400 m water depths (Heinze and Wefer, 1992; Scholz et al., 2014; Moffitt et al., 2015; Salvattecchi et al., 2016). Besides, only a couple of these approaches attempted to quantify the decrease in BWO so far. In a review, Schönfeld et al. (2015) demonstrated that laminated sediments of the Peruvian margin indicated oxygen concentrations $<7 \mu\text{mol/kg}$ and accumulation rates of the organic carbon could be used as a quantification method for concentration of $>10 \mu\text{mol/kg}$, depending on other parameters. A recent study focusing on the Peruvian margin used redox sensitive elements (Fe, Mo, U) and found a 5 to 10 $\mu\text{mol/kg}$ decrease from glacial to interglacial periods in the centre of the OMZ at depths (Scholz et al., 2014). Because of the lack of complete records from the continental slope off Peru (Reimers and Suess, 1983; Erdem et al., 2016) and the limited applicability of some of the redox proxies (laminated sediments, Mo, U) to sediments accumulated under higher oxygenated conditions, paleo-oxygen reconstructions were not possible at the lower suboxic/oxic boundary of the Peruvian OMZ to date. However, benthic foraminiferal fauna were structured with oxygenation at these depths (Mallon et al., 2012). Following this motivation, the present study aimed to reconstruct paleo-oxygen conditions since the Last Glacial Maximum (LGM) by using benthic foraminiferal distributions in sediment cores from the Peruvian OMZ between 600 and 1250 m water depth. We compiled all available information on living (rose Bengal stained) benthic foraminiferal distributions along the Peruvian margin as calibration dataset to investigate the following questions: 1) did the Peruvian OMZ structure show differences in terms of vertical and horizontal extension since the LGM? 2) if there are such differences, as indicated by other

records from the EEP, can we actually quantify these changes in BWO concentrations by using the information of the living faunas? 3) if so, how much did the BWO levels change since the LGM?

5.1.1. Benthic foraminifera as oxygen proxy

Certain benthic foraminiferal species and assemblages have been suggested as proxies for bottom-water oxygenation, in particular for low-oxic to anoxic conditions (e.g., Sen Gupta and Machain-Castillo, 1993; Kaiho, 1994; Alve and Bernhard, 1995; Bernhard et al., 1997; Baas et al., 1998; Nordberg et al., 2000; Schmiedl et al., 2003; Leiter and Altenbach, 2010). Since the OMZs occur where a high input of particulate organic matter prevails, these species also flourish under elevated food availability. Therefore, applications of certain species to reconstruct ancient BWO concentrations were often challenged by the TROX-model (Barmawidjaja et al., 1992; Jorissen et al., 1995). This conceptual model explains the vertical microhabitat structure of benthic foraminifera within the sediments by both, the availability of the organic matter and dissolved oxygen (Van der Zwaan et al., 1999). However, a growing number of publications reporting the living (stained) benthic foraminiferal distributions and the prevailing environmental conditions showed some features in common (Phleger and Soutar, 1973; Mackensen and Douglas, 1989; Sen Gupta and Machain-Castillo, 1993; Bernhard et al., 1997; den Dulk et al., 1998; Jannink et al., 1998; Levin et al., 2002; Schumacher et al., 2007; Cardich et al., 2012; Mallon et al., 2012; Caille et al., 2014; Cardich et al., 2015). First, benthic foraminiferal faunas are characterized by a low diversity and high population density in oxygen-depleted environments, 2) most but not all living specimens were found dwelling in the first one or two cm of the surface sediments, 3) species with a thin, porous test wall (e.g. Bolivinids) are more advantageous as compared to agglutinated and porcelaneous species. Additionally, the pore densities of the tests were recognised as indicators of low bottom and pore-water redox conditions (Kaiho, 1994; Glock et al., 2011; Kuhnt et al., 2013). A comparison of different OMZ settings showed that certain assemblages and distributions indeed could be used to identify the changes of the OMZ structures provided certain threshold values are considered: microoxic conditions $<5 \mu\text{mol/kg}$, dysoxic conditions $5\text{-}45 \mu\text{mol/kg}$, oxic conditions $>45 \mu\text{mol/kg}$. In particular, an extreme low BWO (ca. $2 \mu\text{mol/kg}$) tolerant group was found within the OMZ core, a transitional group was recorded around the lower boundary of the OMZ, and a much more cosmopolitan and diverse group was observed outside the OMZ (Table 5.1; Schumacher et al., 2007; Mallon et al., 2012; Caille et al., 2014).

Table 5.1. Common species considered in this study and reported from different oxygen depleted environments.

Species	Ecology
<i>Bolivina costata</i>	Characteristic species of the Peruvian margin particularly on the shelf (Resig, 1981;1990; Cardich et al., 2012); tolerant to low BWO <5 $\mu\text{mol/kg}$ (Khusid, 1974; Resig, 1981; Mallon et al., 2012) even to sulfidic pore-waters (Cardich et al., 2015); used as a proxy for enhanced upwelling during interglacial periods (Heinze and Wefer, 1992).
<i>Bolivina seminuda</i>	Dominant in different OMZs (Phleger and Soutar, 1973; Hermelin and Shimmield, 1990; Bernhard et al., 1997; Ohga and Kitazato, 1997; Gooday et al., 2000; Cardich et al., 2012; Cauille et al., 2014); tolerant to extreme low BWO <2.5 $\mu\text{mol/kg}$ (Mallon et al., 2012; Cardich et al., 2015); able to use nitrate for respiration (Pina-Ochoa et al., 2010); better adapted to low BWO levels compared to other <i>Bolivina</i> species e.g., <i>B. spissa</i> (Glock et al., 2011); suggested as dysoxic indicator (Kaiho, 1994), used as a proxy for enhanced upwelling during interglacial periods (Heinze and Wefer, 1992).
<i>Bolivina spissa</i>	Common in the OMZs in the Pacific Ocean (Douglas and Heitman, 1979; Ingle et al., 1980; Mackensen and Douglas, 1989; Nomaki et al., 2006; Glud et al., 2009; Fontanier et al., 2014); indicates intermediate hypoxic conditions/lower boundary of the OMZ core (Mullins et al., 1985; Mallon et al., 2012), potentially able to use nitrate for respiration (Glock et al., 2011); suggested as dysoxic indicator (Kaiho, 1994); used as a proxy for suboxic conditions (Cannariato and Kennett, 1999) and for intermediate hypoxia (Moffitt et al., 2014).
<i>Bolivinita minuta</i>	Common in the OMZ of the Gulf of Panama (Golik and Phleger, 1977); mostly at the lower boundary/outside the core of the OMZ offshore Peru-Chile (Ingle et al., 1980; Mallon et al., 2012). Other <i>Bolivinita</i> species are associated with sustained organic matter flux (Sarkar and Gupta, 2014; and the references therein).
<i>Bulimina exilis</i>	Dominant in different OMZs (Smith, 1964; Douglas and Heitman, 1979; Bernhard et al., 1997; den Dulk et al., 1998; Jannink et al., 1998; Cauille et al., 2014; Cardich et al., 2015); associated with fresh organic matter input (Caralp, 1989); suggested as dysoxic indicator (Kaiho, 1994); used as a proxy for dysoxic conditions (Cannariato and Kennett, 1999) and severe hypoxia (McKay et al., 2015);

Chapter 5: Bottom-water deoxygenation at the Peruvian Margin during the last Deglaciation recorded by benthic foraminifera

	Praetorius et al., 2015).
<i>Cassidulina delicata</i>	Common in the Eastern Pacific OMZs at the lower continental slope (Uchio, 1960; Ingle et al., 1980), and under intermediate BWO concentrations, lowest observed is 4.5 $\mu\text{mol/kg}$ (Golik and Phleger, 1977; Douglas and Heitman, 1979; Resig, 1981; Mackensen and Douglas, 1989; Kaiho, 1994).
<i>Epistominella exigua</i>	Cosmopolitan, typical in the deep sea environment, opportunistic, associated with pulsed supply of phytodetritus (Gooday, 1988; Gooday, 1993; Smart et al., 1994) and elevated BWO (Schmiedl et al., 1997; Gupta and Thomas, 2003; Jannink et al., 1998); reported as one of the dominant species along the Peru-Chile margin (Ingle et al., 1980; Resig, 1981).
<i>Epistominella pacifica</i>	Dominant offshore Peru and California at dysoxic and suboxic conditions (Khusid, 1974; Douglas and Heitman, 1979; Mackensen and Douglas, 1989); suboxic to oxic conditions in the Gulf of Panama (Golik and Phleger, 1977).
<i>Hoeglundina elegans</i>	Reported as common in areas with variable organic matter input and elevated BWO (Gooday, 2003; and the references therein; Sarkar and Gupta, 2014); also observed in dysoxic sediments (lowest BWO measured 9 $\mu\text{mol/kg}$; Douglas and Heitman, 1979; Mackensen and Douglas, 1989); indicator of elevated oxygenation (Geslin et al., 2004).
<i>Prygo murrhyna</i>	Suggested as oxic indicator (Kaiho, 1994); associated with low to moderate flux of organic matter and moderate BWO (Gooday, 2003; Sarkar and Gupta, 2014). Generally, large <i>Miliolids</i> are reported being restricted to higher BWO concentrations (in Arabian Sea >16 $\mu\text{mol/kg}$; Caille et al., 2014) and suggested as a proxy for rapid ventilation of oxygen-depleted environments (den Dulk et al., 2000).
<i>Uvigerina peregrina</i>	Cosmopolitan (Gooday and Jorissen, 2012), associated with high organic matter input (Altenbach et al., 1999; Schönfeld and Altenbach, 2005); common in dysoxic sediments of different OMZs (Smith, 1964; Ingle et al., 1980; Ohga and Kitazato, 1997), particularly outside the OMZ core and at the OMZ lower boundary (Jannink et al., 1998; Mallon et al., 2012).

5.1.2. Regional setting

The Peruvian OMZ is one of the most pronounced OMZs in the world (Figure 5.1; Paulmier and Ruiz-Pino, 2009), covering the Peruvian continental shelf and upper slope, with its thickest part between 5°S and 15°S and 50 to 750 m water depths (Figure 5.2; Fuenzalida et al., 2009). The intensity of the OMZ is dependent on the low ventilation of advected intermediate waters, diapycnal mixing, and the extremely high primary productivity in the surface waters (Karstensen et al., 2008; Brandt et al., 2015). The productivity is regulated by the wind-driven upwelling of cold, nutrient-rich, and oxygen-poor waters from intermediate depths (e.g., Pennington et al., 2006). The main source of these upwelled waters is the Peru-Chile Under-

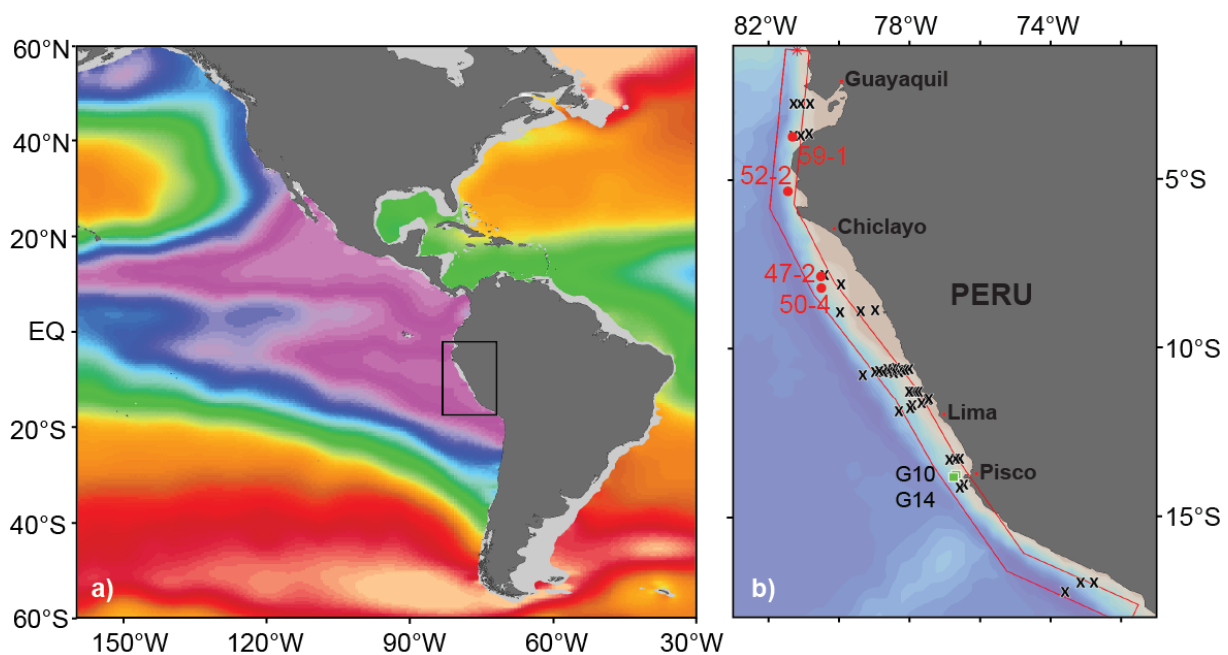


Figure 5.1. Location map of the study area (square in panel a) in the Eastern Equatorial Pacific and structure of the OMZ at 400 m water depths. The purple area indicates dissolved oxygen values <0.5 ml/l to <20 $\mu\text{mol/kg}$; World Ocean Database 2013 (Boyer et al., 2013)). b: detail map of the study area showing the locations of the surface samples (x), the sediment cores (red circles) and stacked record of two cores (green squares) from (Salvatteci et al., 2016). See Figure 5.2 for the sample locations in relation with water depth and the OMZ intensity.

current (PCUC). It originates around 3-5°S and flows southward between 50 and 300 m water depths (Montes et al., 2010; Chaigneau et al., 2013). The PCUC is fed by the Equatorial Undercurrent (EUC) and Southern Subsurface Countercurrents (SSCCs; Montes et al., 2010). Below the PCUC, northward flowing Chile-Peru Deep Coastal Current (CPDCC) carries the cold Antarctic Intermediate Waters as a thin layer (AAIW; Chaigneau et al., 2013). The AAIW is not one of the major water masses offshore Peru (Fiedler and Talley, 2006), it forms at the Subpolar

Front and reaches until 25-30°S at water depths between 500 and 1300 m (Sloyan and Rintoul, 2001; Fiedler and Talley, 2006).

5.2. Materials and Methods

5.2.1. Sediment cores

Four sediment cores were considered in this study (M77/2-47-2; 50-4; 52-2 and 59-1). They have been collected during expedition M77 Leg 2 with *R/V Meteor* in 2008 from the continental slope between 3°S and 9°S and water depths of 600 m and 1250 m around the lower boundary of today's OMZ (Figure 5.1 and Figure 5.2). The age model of the core M77/2-59-1 (3°57'S 997 m) has been established by Mollier-Vogel et al. (2013). Age models of the other cores were previously described elsewhere (Erdem et al., 2016). Organic carbon accumulation rates (AR_{Corg}) and $\delta^{15}\text{N}$ data of core 59-1 were taken from (Mollier-Vogel, 2012), AR_{Corg} of cores 50-4 and 52-2 were reported already by (Schönfeld et al., 2015) while the record of core 52-2 has recently been revised and extended to 20 ka. For this study, we focused on the following time intervals with 300 to 500 years resolution at each core (see Appendix): the late Holocene (LH; 3-5 cal ka BP), the early Holocene (EH; 8-10 cal ka BP); the Bølling Allerød/Antarctic Cold Reversal (BA/ACR; 13-14.5 cal ka BP), the Heinrich Stadial-1 (HS1; 15-17.5 cal ka BP) and the Last Glacial Maximum (LGM; 20-22 cal ka BP). For benthic foraminiferal analyses, 10 to 20 cc sediment samples were wet sieved on a 63 μm screen immediately after they were taken, and the residues were dried at 40°C. They were later split with an Otto microsplitter when needed, in order to attain similar total numbers of specimens, which is around 300 per sample (Murray, 2006). The foraminifera were dry picked, collected in Plummer cell slides, sorted by species, fixed with glue and counted. Common species were imaged with a CamScan 44/EDX scanning electron microscope and a Keyence VHX-700 FD digital camera at the Institute for Geosciences, Kiel University.

5.2.2. Surface samples and living benthic foraminifera

Information on the living (stained) benthic foraminifera was compiled from three independent datasets. They comprise 45 locations from the Peruvian continental shelf and slope from water depths of 48 to 2092 m between 1°45'S and 17°28'S (Figure 5.2, Table 5.2). Four of the samples from a transect around 12°30'S were collected in December – January 1998 during Panorama Expedition, Leg 3a, with *R/V Melville*. The faunal inventory at these stations has not been published previously. Information regarding to eight surface sediment samples were collected from the continental shelf and uppermost slope around 12°S and 14°S during different

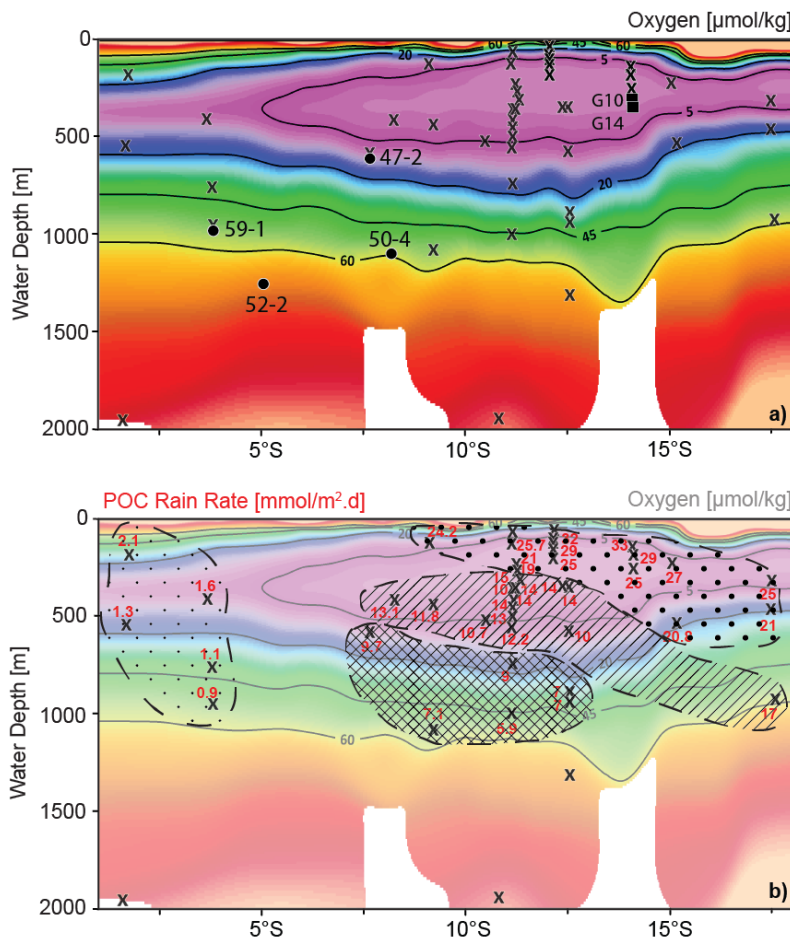


Figure 5. 2. Depth vs latitude profile of the dissolved oxygen concentrations measured during the M77 Leg & 2 expeditions (red line in Figure 1, b show the position of this profile; CTD data compilation after Schönfeld et al., 2015); a) shows the location of the surface samples (x), the sediment cores (circles and core names) and two cores of the stacked record (green squares) from Salvattecchi et al. (2016), b) show the oxygen conditions and particulate organic carbon rain rates (RRPOC) calculated for each surface sample (Dale et al., 2015). Rain rates are grouped indicating different values (<5, 5-10, 10-20 and >20 $\text{mmol/m}^2\text{d}$), see text for details.

monitoring expeditions in August and April 2009, 2010 and 2011. For the present study, averaged values are used for these eight stations (for details see Cardich et al., 2015). The remaining 33 surface samples were collected in October to December in 2008 during *R/V Meteor* expeditions M77 Leg 1 & 2 with a multicorer and tubes of 10 cm inner diameter (Mallon, 2012; Mallon et al., 2012). Census data were based on the information from the topmost layer, mostly the 0 to 10 mm interval. Some samples from the M77 cruise covered different depth intervals within the first 10 mm. The size fractions of >63 μm were always considered. In case of fractionated subsamples, we combined the values of different fractions considering the volumes and splits reported for each subsample. Based on the work of Mallon (2012), differences in taxonomic concepts for some species were discussed among the co-authors involved, and a consensus has been achieved, which is applied

Chapter 5: Bottom-water deoxygenation at the Peruvian Margin during the last Deglaciation recorded by benthic foraminifera

Data reduction: consideration of taphonomy

After compilation of the dataset was accomplished, the inventory of living benthic foraminiferal species was compared with that from the sediment cores. As expected, the agglutinated species in the sediment cores did not resemble those in the surface samples. Only single specimens of three species were found in some samples of core 50-4 and 52-2. The agglutinated species have lower preservation potential in the sediment record because their organic cement is decomposed during early diagenesis and changing redox conditions in the sediment (Schröder, 1988; Mackensen et al., 1990). Following this reason, only species with calcareous tests were taken into account for further investigation. The percentages were recalculated for the total calcareous assemblage. Even though agglutinated species were not involved in our downcore application, they are well known for their low tolerance to oxygen minimum conditions (Bernhard and Sen Gupta, 1999; Gooday and Rathburn, 1999; Gooday et al., 2000; Levin et al., 2002; Mallon et al., 2012). Therefore, we considered their abundances separately and the proportions of agglutinated species in living faunas were noted down to be used for a comparison of the results.

Environmental data

Bottom water oxygen (BWO) concentrations were measured at the time of sampling and reported to vary between 0.9 and 100.4 $\mu\text{mol/kg}$ (Table 2). Bottom water conditions from the *R/V Melville* stations around 12°30'S were previously reported (Levin et al., 2002). The second dataset of eight stations reported BWO concentrations for each expedition (Cardich et al., 2015). For the purpose of this study, we considered the averaged values. The BWO of the *R/V Meteor* M77 stations were taken from Mallon et al. (2012) and from a synoptic compilation of all CTD hydrocasts from this area taken during expeditions in the framework of the SFB 745 Collaborative Research Centre (Schönfeld et al., 2015). Rain rates of particulate organic carbon (RRPOC; $\text{mmol/m}^2\text{d}$) for six of the stations (indicated as bold in Table 2), were taken directly from (Dale et al., 2015). The other rates were estimated by using curves and equations provided for water depths between 100 and 1000 m (Martin et al., 1987; Dale et al., 2015). Different primary productivity values were used for the RRPOC calculations considering the latitudinal differences of the sampling locations. For the region around 11-12°S, values reported in Supplementary information of Dale et al. (2015) were used since the observations were done close to sampling period of Mallon et al. (2012). For the region around and south of 15°S, values reported in Martin et al. (1987) were considered. For the northern part of the region, estimations from (Pennington et al., 2006) were used.

Chapter 5: Bottom-water deoxygenation at the Peruvian Margin during the last Deglaciation recorded by benthic foraminifera

Table 5.2. Metadata of surface samples from the living benthic foraminifera dataset. Particulate organic carbon rain rates (RRPOC) of six stations, indicated as bold, were taken from Dale et al. (2015), others were calculated (see text for details). Bottom water oxygen (BWO) concentrations were taken from reference publications.

Sample	Location (Lat – Long)	Water depth (m)	BWO ($\mu\text{mol/kg}$)	RRPOC ($\text{mmol/m}^2\cdot\text{d}$)	Reference
776	1°45.14' 82°37.47'	2092	100.4	N.A.	Mallon, 2012
767	1°53.49' 81°11.75'	526	19	1.3	Mallon, 2012
772	1°57.01' 81°07.23'	207	30.8	2.1	Mallon, 2012
744	3°45.01' 81°07.29'	350	6.8	1.6	Mallon, 2012
757	3°51.01' 81°15.49'	700	40	1.1	Mallon, 2012
753	3°56.95' 81°19.16'	995	54	0.9	Mallon, 2012
723	7°52.01' 80°31.36'	627	8.2	9.7	Mallon, 2012
716	7°59.99' 80°20.51'	359	2.5	13.1	Mallon, 2012
694	9°02.97' 79°26.88'	115	1.9	24.2	Mallon, 2012
692	9°17.70' 79°37.11'	437	2.9	11.8	Mallon, 2012
684	9°17.69' 79°53.86'	1105	56.6	7.1	Mallon, 2012
553	10°26.38' 78°54.7'	521	4.8	10.7	Mallon, 2012
669	10°53.22' 78°46.38'	1923	98.4	N.A.	Mallon, 2012
516	10°59.00' 78°21.00'	511	4.8	13	Mallon, 2012
549	10°59.81' 78°31.26'	1004	44.8	5.9	Mallon, 2012
540	11°00.01' 77°47.41'	79	5.3	15.3	Mallon, 2012
470	11°00.00' 77°56.61'	145	3.3	25.7	Mallon, 2012
449	11°00.00' 78°09.97'	319	2.3	13.5	Mallon, 2012
473	11°00.03' 78°09.95'	316	2.3	9.8	Mallon, 2012
482	11°00.02' 78°14.17'	375	2.3	14	Mallon, 2012
456	11°00.01' 78°19.23'	465	3.8	13.7	Mallon, 2012
487	11°00.00' 78°23.17'	579	8.6	12.2	Mallon, 2012
459	11°00.02' 78°25.6'	697	15.7	9	Mallon, 2012
676	11°05.01' 78°00.91'	211	2	21	Mallon, 2012
583	11°06.86' 78°03.11'	248	2.1	19.2	Mallon, 2012
582	11°09.70' 78°04.93'	291	2.3	17.6	Mallon, 2012
C1	12°01.90' 77°13.07'	48	10	N.A.	Cardich et al., 2015
C2	12°02.76' 77°17.27'	94	5.8	N.A.	Cardich et al., 2015
C3	12°02.34' 77°22.53'	117	4.8	32.4	Cardich et al., 2015
C4	12°02.93' 77°29.01'	143	6.1	29.1	Cardich et al., 2015

Chapter 5: Bottom-water deoxygenation at the Peruvian Margin during the last Deglaciation recorded by benthic foraminifera

C5	12°02.22' 77°39.07'	175	6.1	26.1	Cardich et al., 2015
616	12°22.69' 77°29.06'	302	2.2	8	Mallon, 2012
Site305	12°22.70' 77°29.10'	305	0.9	14	Levin et al., 2002
Site562	12°32.5' 77°29.6'	562	11.6	10	Levin et al., 2002
622	12°32.74' 77°34.73'	823	27.7	7	Mallon, 2012
Site830	12°32.8' 77°34.8'	830	37.5	7	Levin et al., 2002
Site1210	12°40.3' 77°38.5'	1210	79.5	N.A.	Levin et al., 2002
P1	14°01.20' 76°18.78'	120	1.8	33.2	Cardich et al., 2015
P2	14°04.32' 76°25.20'	180	1.6	29.2	Cardich et al., 2015
P3	14°07.50' 76°30.54'	300	2.7	24.8	Cardich et al., 2015
635	15°04.75' 75°44.00'	214	2.4	27.6	Mallon, 2012
421	15°11.39' 75°34.81'	522	13.8	20.8	Mallon, 2012
403	17°26.00' 71°51.41'	298	2.5	24.8	Mallon, 2012
406	17°28.01' 71°52.40'	492	25.3	21.1	Mallon, 2012
410	17°38.40' 71°58.23'	918	58	17	Mallon, 2012

5.2.3. Statistical analyses

We standardized the data matrix by calculating the proportions of the involved calcareous species referring to the total calcareous species of each sample. Percentages were preferred instead of individuals per cm³ since this information would create an inconsistency when applied to surface sediment samples and to fossil abundances in the same manner. Once living benthic foraminifera percentages were calculated and environmental information corresponding to each sample was compiled, three different “approach datasets” were created in order to test the consistency of the planned downcore application. These three approaches bore some differences in terms of the index species involved (Table 5.3). In this way, it was possible to compare the specific-single-species impact. Approach 1 (shown as red) involved the species showing at least four occurrences with percentages more than 5 % in the living foraminifera dataset. In total 18 species were considered. For Approach 2 (shown as blue) the common species observed both in the surface samples and in the sediment samples were listed. From those the species found at the sediment cores and with at least four occurrences in the surface samples were considered. This “blue” dataset comprised 25 species. Considering the differences between the surface sample and sediment core locations, we focused on surface sediment samples taken from >250 m water depth for Approach 3 (shown as green). Again, only species with at least four occurrences in the living benthic foraminifera dataset were involved. They were in total 25 species from 31 surface

samples instead of 45. After determining the “red, blue and green” subsets, we performed statistical tests to observe whether there is any significant difference between the datasets and to see the relation of the species and their distributions with environmental variables.

All statistical analyses were performed with the software PAleontological STatistics (PAST) Version 3.11. *Q*-mode hierarchical cluster analyses were applied using the Unweighted Pair Group Method (UPGMA) based on Bray-Curtis similarity matrix. After determination of the clusters, Canonical Correspondence Analysis (CCA) was performed to the same datasets to see the relation between the species, stations and environmental variables (BWO and RRPOC). Additionally, multiple regression analysis was applied to each subset in order to assess their significance and to evaluate the reliability of the approaches.

5.3. Results and Discussion

5.3.1. Living benthic foraminiferal distributions

The dataset of living calcareous benthic foraminifera from the Peruvian margin comprised 45 surface sediment samples and 130 different calcareous species. As previously mentioned, the agglutinated species were not considered in this dataset due to their low preservation potential in the sedimentary record. However, their relative abundances were taken into consideration. When the oxic ($>45 \mu\text{mol/kg}$), dysoxic ($5-45 \mu\text{mol/kg}$), and microoxic ($<5 \mu\text{mol/kg}$) classification was applied to this dataset, 19 samples were classified as microoxic, another 19 samples were classified as dysoxic and the remaining 7 samples were classified as oxic. In case the prevailing BWO increased, the diversity of calcareous species and the total relative abundance of the agglutinated species increased as well (Appendix). A marked increase in the proportion of agglutinated species was observed at stations with BWO higher than $15 \mu\text{mol/kg}$, and a further increase was recorded around $40 \mu\text{mol/kg}$. These data are in good agreement with previous observations on the low tolerance of agglutinant species to oxygen depleted conditions ($<0-20 \text{ ml/l} = \sim 9 \mu\text{mol/kg}$; Gooday et al., 2000). One important detail worth to mention is that the proportion of the agglutinated taxa was more than 50 % in samples with BWO $>45 \mu\text{mol/kg}$. This implies that these five “oxic” stations did not represent the total calcareous taxa very well; neither do they in the approach subsets that we statistically analysed.

Considering the criteria used for the approach datasets of this study, the most important living calcareous taxa comprised 36 species and 12 out of them were involved in all of the approach datasets (Table 3). The living taxa were dominated by Bolivinids (Appendix). The majority of the surface samples were from within or around the OMZ (Figure 5.2) and *Bolivina*

Chapter 5: Bottom-water deoxygenation at the Peruvian Margin during the last Deglaciation recorded by benthic foraminifera

Table 5.3. List of the living benthic foraminifera species which were considered in the different approach datasets, regression coefficients and 1-sigma errors that were calculated with multiple regression analyses. All regression analyses are significant (p values <0.05). See Appendix for full genus names.

	Approach 1		Approach 2		Approach 3	
	BWO Coef.	1 σ	BWO Coef.	1 σ	BWO Coef.	1 σ
<i>Species / Constant</i>	21.325	7.087	30.093	5.5298	23.991	5.2742
<i>A. angulosa</i>					2.3709	0.4738
<i>B. alata</i>			-0.6583	0.80348	-0.57931	0.36142
<i>B. costata</i>	-0.20944	0.14987	-0.30812	0.14756	-0.32112	0.10048
<i>B. interjuncta</i>	-0.28655	0.17956	-0.57092	0.12556	-0.41784	0.074338
<i>B. pacifica</i>			-0.57023	1.3856		
<i>B. plicata</i>	-0.39277	0.52553	-0.43193	0.42926	-0.077149	0.16386
<i>B. seminuda</i>	-0.1975	0.099158	-0.30205	0.074345	-0.27122	0.049582
<i>B. serrata</i>			-4.5609	1.9667		
<i>B. spissa</i>	0.18364	0.17501	-0.076629	0.11732	0.12441	0.091249
<i>B. minuta</i>	-1.3877	0.43934	-1.9364	0.30427	-1.6215	0.52109
<i>B. elegantissima</i>	-0.2416	1.2262	-0.28727	0.99319	0.38907	0.52084
<i>B. exilis</i>	-0.18043	0.18401	-0.22745	0.14861		
<i>C. carmenensis</i>	-0.17558	0.31649			-0.29534	0.17532
<i>C. inflatus</i>			-1.6916	1.1584		
<i>C. crassa</i>	-0.35733	0.71058	-1.004	0.82	-1.522	0.36606
<i>C. delicata</i>	-0.098228	0.31241	0.43673	0.20474	0.40221	0.19924
<i>C. wuellerstorfi</i>	1.5296	0.83344			-0.12206	0.22286
<i>E. exigua</i>			1.3701	0.51006		
<i>E. obesa</i>			1.3373	0.98225	0.21016	0.3179
<i>E. pacifica</i>	-0.27803	0.34774	0.30041	0.16043	0.4065	0.12589
<i>F. fusiformis</i>			-0.75753	1.316	-0.25894	0.46955
<i>G. multilocula</i>					0.85235	0.37673
<i>G. neosoldanii</i>					-1.2914	1.2104
<i>G. soldanii</i>					0.2868	0.85655
<i>H. elegans</i>	1.5134	0.26535	1.4367	0.19109	1.5354	0.097211
<i>M. barleeaanum</i>	2.9271	1.6312				
<i>N. auris</i>			-0.041668	0.30373		
<i>N. stella</i>			-0.16539	0.36564		
<i>P. subperuviana</i>			-0.080764	0.55753	0.13922	0.4372
<i>P. subcarinata</i>					6.9754	2.0292
<i>P. murrhyna</i>	1.9746	0.67697			0.9889	0.6668
<i>Q. seminulum</i>			1.9289	0.7274		
<i>U. auberiana</i>			3.8804	2.8275		
<i>U. peregrina</i>	0.3974	0.31793	0.83565	0.16777	0.43753	0.15454
<i>V. glabra</i>	-0.20836	0.95048				
<i>V. oblonga</i>					0.27899	1.3998

species are known for their high-tolerance to hypoxic even anoxic conditions (Table 5.1; Mullins et al., 1985; Schumacher et al., 2007; Pina-Ochoa et al., 2010; Glock et al., 2011; Mallon et al., 2012; Cardich et al., 2015). The most dominant species was *Bolivina seminuda* with percentages reaching up to 90 % in the centre of the OMZ at microoxic stations. It was followed by *Bolivina costata*, *B. interjuncta*, *B. spissa* and *Bolivinita minuta* with increasing BWO concentrations. At samples with BWO of more than 7-8 $\mu\text{mol/kg}$, the percentages of *B. seminuda* decreased distinctly. At higher BWO >15 $\mu\text{mol/kg}$, *Uvigerina peregrina* became the most dominant species. The proportions of *other calcareous* species also increased markedly. *Pyrgo murrhyna* and *Melonis barleeaanum* were observed only at stations with BWO above 45 $\mu\text{mol/kg}$.

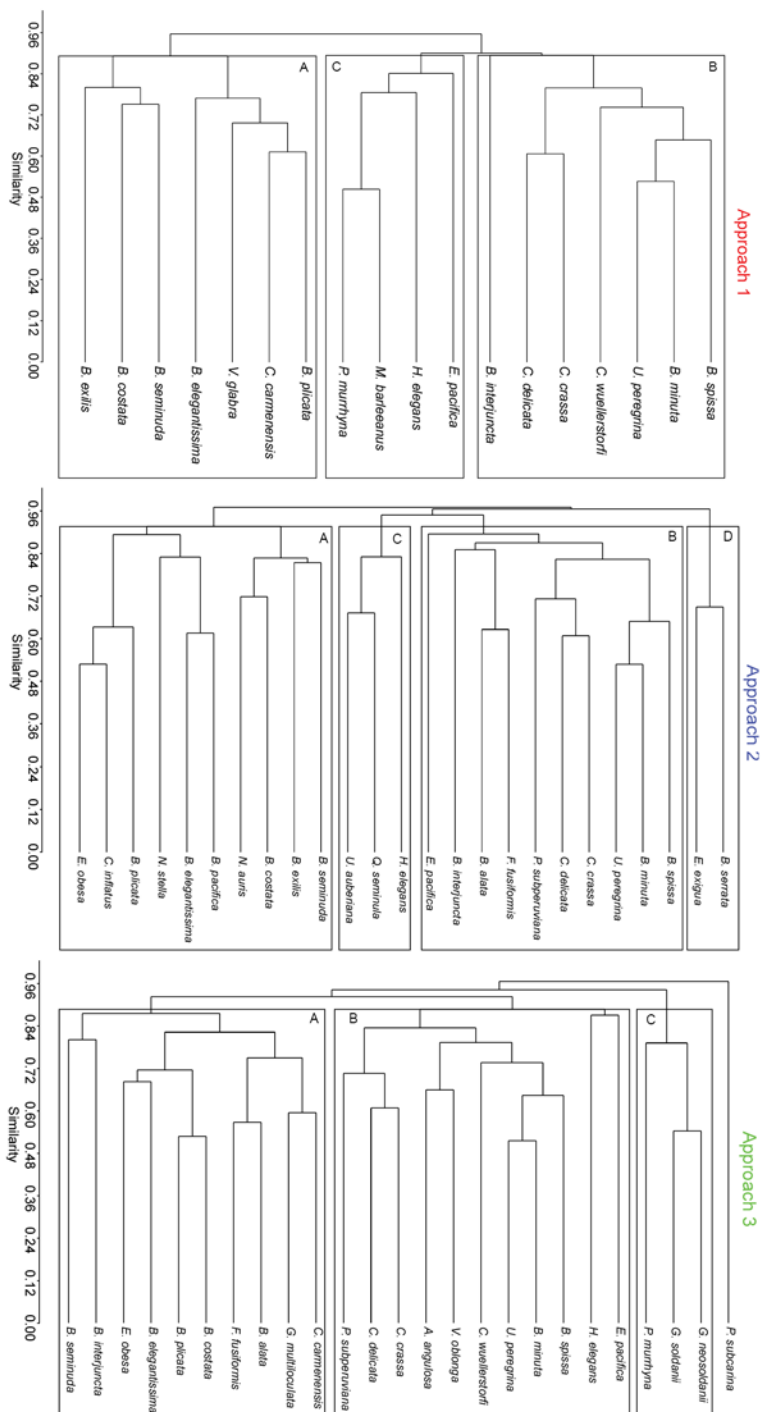
The low BWO and high RRPOC values did not show an eye-catching covariance as expected. Furthermore, distinct threshold values in RRPOC in relation to benthic foraminiferal distributions were not recognised. *Bolivina seminuda* distributions can be taken as an example; it was abundant at samples with extreme-low oxygen and high rain rates but was not specifically abundant at samples with higher oxygen concentrations and high rain rates.

5.3.2. Results and interpretation of statistical analyses

Clusters and ecological indications

Q-mode cluster analyses revealed similar clusters for every approach. There were small differences observed within the clusters due to the different index species involved in the approach datasets. Approach 2 formed 4 clusters whereas Approach 1 and 3 formed 3 clusters (Figure 5.3). The 4th cluster (D) consisted of *Epistominella exigua* and *Bolivina serrata*. Both species were observed with percentages more 5 % in one sample and with much less percentages in few more samples. Therefore, they were not involved in Approaches 1 and 3 and their distribution should be considered with caution while interpreting the results. Within the 12 index species that were involved in all the approach datasets, *Bolivina costata*, *B. plicata*, *B. seminuda* and *Buliminella elegantissima* were observed always in the same cluster (A), while *Bolivina spissa*, *Bolivinita minuta*, *Cassidulina crassa*, *C. delicata* and *Uvigerina peregrina* were always observed in cluster B. Cluster C was the smallest cluster in numbers and it consisted of species such as *Hoeglundina elegans* (observed in cluster B in Approach 3), *Pyrgo murrhyna*, *Melonis barleeaanum* and *Quinqueloculina seminulum*. Cluster C species were generally observed in samples with higher percentages of agglutinated species and *other calcareous*. Therefore, species that group in cluster C are much less in number compared to other cluster species. Considering the ecological indications of the above mentioned species (see Table 5.1), Cluster A likely

Chapter 5: Bottom-water deoxygenation at the Peruvian Margin during the last Deglaciation recorded by benthic foraminifera



represent the shelf environment on the Peruvian margin under microoxic conditions, so the OMZ core, Cluster B represent a transitional community which is adapted to broader environmental variations including increasing water depths, BWO concentrations (dysoxic conditions) and potentially a different organic carbon input. Cluster C represent mostly Miliolid species which are known to be not tolerant to low oxygen conditions, hence oxic conditions. Similar trends of such different assemblages in relation with changing BWO and organic matter were also observed in the OMZ of the Arabian Sea (Jannink et al., 1998; Cauille et al., 2014). Even though there are different species involved in the groups representing the OMZ core, around the boundary of the OMZ and outside of the OMZ, the transitional appearance of these

Figure 5.3. Q-mode cluster analyses applied to each groups from low diversity - high density to more diverse and cosmopolitan assemblages indicate certain similarities.

Comparison of living taxa in different OMZ settings additionally revealed that each OMZ has its kind of own characteristic assemblages. The most abundant species are not observed in such abundances in another OMZ indicating that they adapt the conditions in these regions and are not observed with similar numbers in another similar environment. For

example, *Bolivina dilatata* is common in the Arabian OMZ (Jannink et al., 1998) and *Bolivina costata* is dominant in the Peruvian OMZ (Cardich et al., 2012; Mallon et al., 2012; Cardich et al., 2015). This somehow “trapped” occurrence of this community might be due to the structure and the shape of these OMZ settings, prevailing since thousands of years, and the strong adaptation of these assemblages to these conditions during a long time. Similar assumptions were made for the OMZ core assemblages in the Northern Arabian Sea (Jannink et al., 1998). Therefore, expecting to find the same specific species within the same BWO range in different OMZs is potentially misleading. Although there are not many frequent species observed in different OMZs, *Bolivina seminuda* and *Bulimina exilis* are within the few common abundant species (Table 5.1; Bernhard et al., 1997; den Dulk et al., 1998; Cardich et al., 2015). Increased percentages of these two species actually could be used as extreme-low BWO indicator in downcore records (e.g., McKay et al., 2015; Praetorius et al., 2015). Additionally, total numbers of the Miliolids could be oxic condition indicators as previously suggested (den Dulk et al., 2000) but this approach would not produce sensible results outside OMZ settings. Accordingly, comparisons of relative abundances of these low-oxygen tolerant and not-tolerant species in fossil record might be indeed used in determining the suboxic – oxic transitions.

CCA and regression analyses

The Canonical Correspondence Analysis (CCA) for each approach dataset indicated that BWO and RRPOC did not show a distinct correlation (in Figure 5.2). Within the 12 index species which were included in all approach datasets, *Uvigerina peregrina*, *Hoeglundina elegans* and *Epistominella pacifica* showed positive correlations with BWO whereas *Bolivina plicata* showed negative correlations in all the tests for approaches. *Bolivina seminuda* and *Buliminella elegantissima* showed positive correlation with RRPOC, whereas *Bolivina spissa* and *Bolivinita minuta* showed negative correlations in all approaches. It is important to note that *B. seminuda* and *B. spissa* are reacting to environmental variables such different as shown both in clusters and CCA results. *Bolivina seminuda* represent the OMZ core whereas *B. spissa* distributions followed the OMZ boundary. On the other hand, *Bolivina costata* and *B. interjuncta* showed either negative correlation with BWO or positive correlation with RRPOC.

The multiple regression analyses for each dataset revealed similar results as observed in the analyses mentioned above. Additionally this analysis was used to quantify similarities and correlations; therefore the results of the multiple regression analyses were later used for the comparison of the approaches. Tests on dependent variables were significant for all of the 3 approaches (p value >0.05) except for RRPOC in Approach 3. In the results for each approach,

BWO values showed better correlations of estimated vs. measured BWO with the involved species ($R^2 = 0.883$; 0.959 ; 0.998 respectively) than estimated vs. calculated or measured RRPOC ($R^2 = 0.701$; 0.785 ; 0.905 (note that $p > 0.05$) respectively) (Figure 5.4). These results showed that this joint dataset of living benthic foraminiferal distributions could be used to reconstruct the past-BWO levels in the Peruvian OMZ setting. Consequently; we generated three separate equations to quantify BWO concentrations by using the regression coefficients for each index species in each approach (Table 5.3). These equations were later applied to the sediment core samples of the corresponding time intervals individually. The errors were calculated according to the standard errors reported as results of regression analyses (Table 5.3). The results of different approaches were later compared to each other and modern day conditions (Figure 5.5). We did not apply the same procedure to reconstruct the RRPOC in downcore record because the results of the regression analyses did not show a significant correlation as BWO estimations did. In addition, three sediment cores were recovered around or deeper than 1000 m which was the maximum depth for any reliable RRPOC calculations.

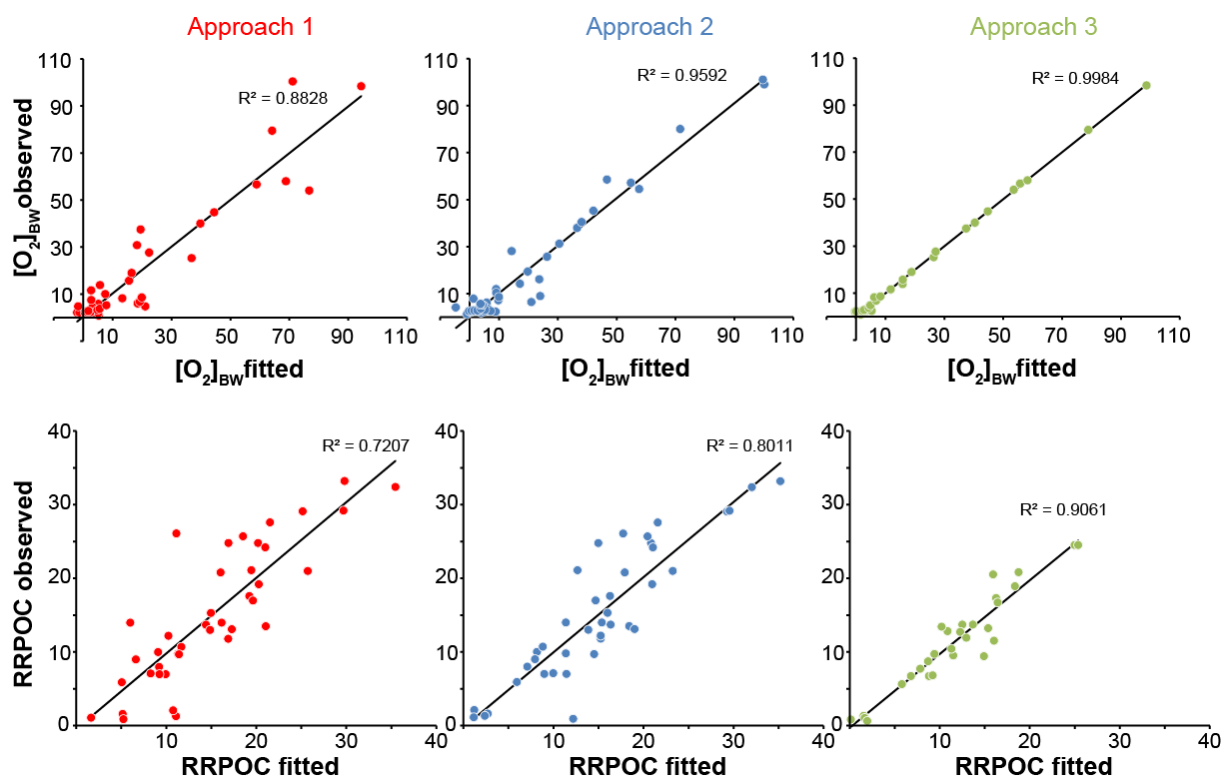


Figure 5.4. Graphs showing the regression results applied to the living benthic foraminifera dataset for each approach for bottom water oxygen and rain rates.

5.3.3. Quantification of BWO concentrations: downcore records

Erosion, reworking and high energetic bottom conditions prevail at the continental slope of the Peruvian margin. The Holocene from cores 47-2 and 50-4 were missing (Erdem et al., 2016), and, due to the high sedimentation rates, core 59-1 covers only the time intervals late Holocene (LH), early Holocene (EH), Bølling Allerød/Antarctic Cold Reversal (BA/ACR), and Heinrich Stadial-1 (HS1). Consequently, it was only possible to compare the time intervals the HS1 and the BA/ACR in all of the sediment cores. Here, we present the results of each core separately in order from south to north with regards to their on the continental slope and water depths.

Core M77/2-47-2

This core was retrieved from 07°52'S and 626 m water depths, and the prevailing BWO at this location was 8.2 $\mu\text{mol/kg}$ during the time of sampling. The sedimentation rates did not exceed 7.5 cm/ka; therefore sample spacing was higher as compared to the other cores. The time intervals, the BA/ACR, the HS1 and the LGM, were covered by 12 samples in total. In terms of benthic foraminiferal assemblages, this core showed the lowest overall species richness (in total 87 species) and the overall abundances (number of individuals per gram sediment ($\#/g_{\text{sed}}$)) were highest among the four cores (Chapter 4, Appendix). Additionally, agglutinated species were absent and single specimens of *Quinqueloculina seminulum* and *Melonis barleeaanum* were observed in few samples only. When the paleo-oxygen was estimated for this core, the results showed similar fluctuations over time, even though distinct differences were observed between the different approaches (Figure 5.5). Estimated BWO of Approach 1 ranged between 5 \pm 9 $\mu\text{mol/kg}$ and 13 \pm 7 $\mu\text{mol/kg}$ with lowest values observed around 15 cal ka BP. When compared to the modern conditions of 8.2 $\mu\text{mol/kg}$; these estimated values are still in an acceptable range if one assumes that the BWO did not profoundly change during LGM and the deglaciation at the core location. Considering the Approach 2, most of the involved species were present with low abundances not exceeding 1 %. Their contribution to estimated concentrations was expected to be low even though some of them had relatively high regression coefficients (Table 5.3). The estimated BWO were highest with Approach 2, ranging between 22 \pm 11 $\mu\text{mol/kg}$ and 47 \pm 17 $\mu\text{mol/kg}$ with lowest concentrations again around 15 cal ka BP. Approach 3 estimates ranged between 16 \pm 7 $\mu\text{mol/kg}$ and 23 \pm 9 $\mu\text{mol/kg}$, with lowest concentrations around 22 cal ka BP. The overall absence of the agglutinated species together with scarcity of the oxic species in the core suggests that the prevailing BWO were rarely above 45 $\mu\text{mol/kg}$. Therefore; Approach 2 seemed to be the least applicable approach for the core 47-2. According to the results of the

Chapter 5: Bottom-water deoxygenation at the Peruvian Margin during the last Deglaciation recorded by benthic foraminifera

Approaches 1 and 3 together with other indications, core 47-2 represented an environment in which the prevailing BWO were always low (dysoxic conditions) with maximum changes around 5 to 10 $\mu\text{mol/kg}$ during the time intervals analysed.

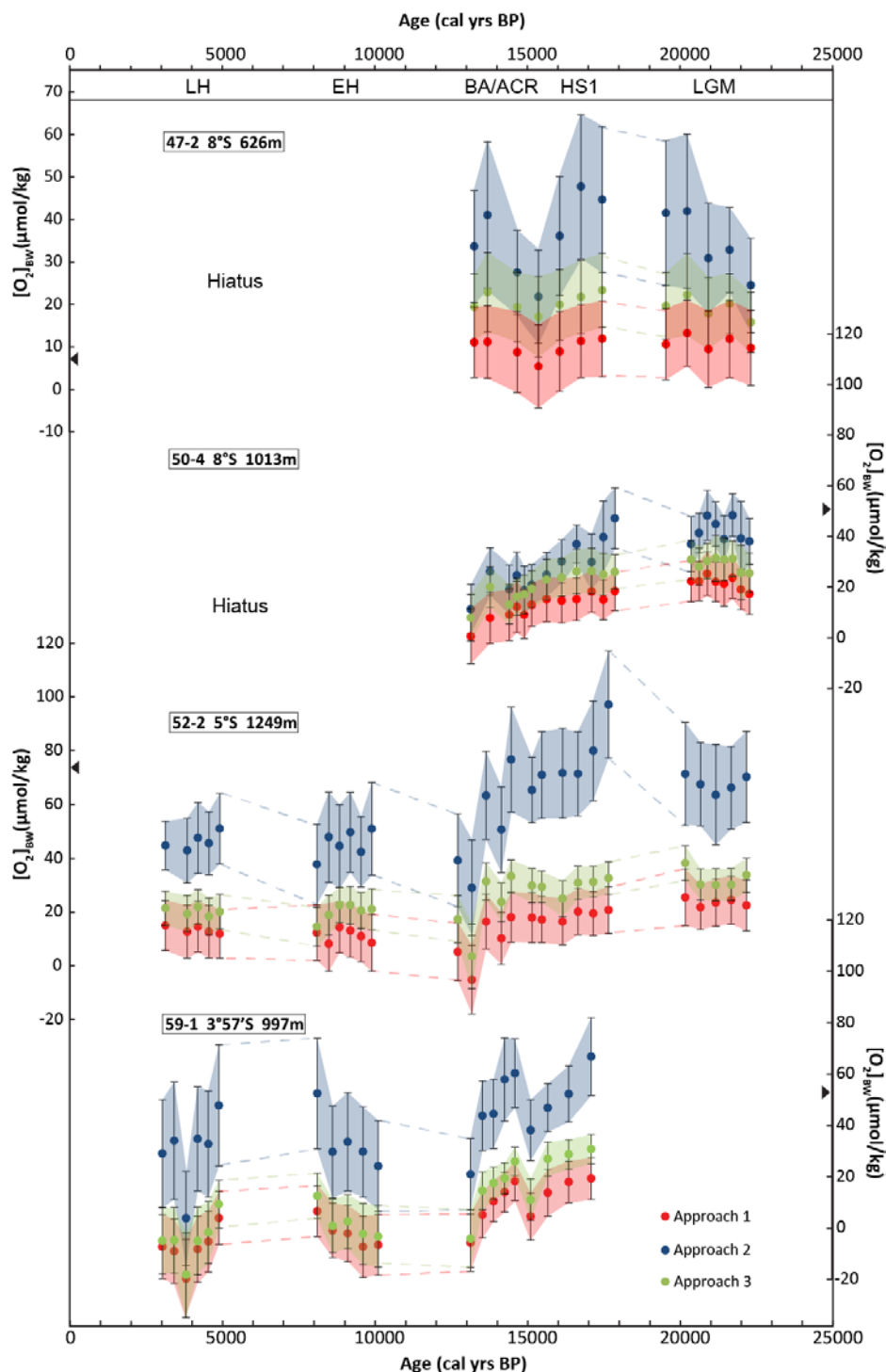


Figure 5.5. Comparison of the estimated BWO concentrations as results of three different approaches applied to four sediment cores from south to north and shallow to deep regarding to their location on the continental slope and the OMZ. Black triangles indicate the modern BWO measured during sampling in 2008.

Chapter 5: Bottom-water deoxygenation at the Peruvian Margin during the last Deglaciation recorded by benthic foraminifera

Core M77/2-50-4

Core 50-4 was collected from 8°S and 1013 m water depth and the prevailing BWO was 52 $\mu\text{mol/kg}$ during retrieval. In total, 20 samples were analysed covering the time intervals BA/ACR, HS1 and LGM. Not less than 138 benthic foraminiferal species were identified in samples from this core. Within these species, only one was agglutinated and occurred as single specimen in samples from the early HS1 and LGM. Oxic-condition species (*Pyrgo* spp., *Quinqueloculina* spp.) were scarce in the same samples but totally absent in samples from the BA/ACR period. The most abundant species was *Bolivina costata*, reaching up to 44 % during this period. As a result of the Approach 1 the estimated concentrations ranged from 13 to 21 $\mu\text{mol/kg}$ during the LGM, varied between 11 and 14 $\mu\text{mol/kg}$ during the HS1 and between -3 and 9 $\mu\text{mol/kg}$ during the BA/ACR. Obviously, a result of negative BWO is an artefact. Approach 2 estimates ranged from 33 to 44 $\mu\text{mol/kg}$ during the LGM, between 21 and 44 during HS1 and varied between 7 and 22 $\mu\text{mol/kg}$ during the BA/ACR. The results of the Approach 3 indicated similar trends as compared to the other approaches. The estimates for the LGM varied between 22 and 27 $\mu\text{mol/kg}$, between 19 and 22 $\mu\text{mol/kg}$ during HS1, and between 4 and 16 $\mu\text{mol/kg}$ during the BA/ACR. Errors of each approach were around 9 $\mu\text{mol/kg}$. Comparing to the conditions prevailing at the core location today, the estimated concentrations were generally lower than anticipated. Since the Holocene was missing in this core, we cannot assess the BWO change after the deglaciation. Disappearance of *Prygo murrhyna* and the agglutinated species after HS1, and the increasing abundance of *B. costata* during the same time interval indicated that bottom-water conditions successively became dysoxic starting from the HS1. Considering the appearances of *P. murrhyna*, the results of Approach 2 seemed to be the applicable approach for this core. Note that *P. murrhyna* was not included in the Approach 2 dataset and has been observed living at the time of sampling only at stations with BWO >45 $\mu\text{mol/kg}$. When the average concentrations of Approach 2 for each time interval were considered as reliable, the estimates revealed a 22 $\mu\text{mol/kg}$ drop in BWO during the early part of the deglaciation (Figure 5.5).

Core M77/2-52-2

The core 52-2 was collected from 5°S and a water depth of 1249 m. The BWO were measured as 74 $\mu\text{mol/kg}$ at the core location during the expedition. It is the only core which spans all time intervals considered in this study. In total, 27 samples were analysed and 170 species were identified in which 3 of them were agglutinated. Both, the agglutinated and the Miliolids were scarce but present in all of the time intervals investigated. Among the most

abundant species, *Bolivina costata* showed an increasing trend from 4 % in the LGM to up to 42 % in the Holocene. A similar trend was observed in core 50-4 but during different time intervals. *Bolivina costata* showed elevated proportions in core 50-4 starting at the onset of the BA/ACR, whereas in the core 52-2, a distinct increase was recognised during the EH. *Cassidulina delicata* showed ranges between 8 % and 20 % with highest proportions during the EH. *Epistominella exigua* showed its highest proportions of up to 33 % during HS1, probably indicating an enhanced phytodetritus input to the sea floor at that time. Their abundance pattern may potentially mislead the interpretation of the BWO quantification approach revealing the highest values at the onset of HS1. As mentioned above, *E. exigua* was overall not very frequent in the surface sediment samples, and was therefore not included in Approach 1 and 3 datasets.

The estimated BWO of Approach 1 indicated stable condition during the LGM with values ranging from 22 to 25 $\mu\text{mol/kg}$, which was followed by a decreasing trend from 21 to 16 $\mu\text{mol/kg}$ during HS1 and from 18 to -5 $\mu\text{mol/kg}$ during the BA/ACR. After the deglaciation, the fluctuations got weaker indicating more-or-less stable conditions and values ranging from 8 to 14 $\mu\text{mol/kg}$ during the EH and 12 to 15 $\mu\text{mol/kg}$ during the LH. The errors were around 9 $\mu\text{mol/kg}$ for this approach. In Approach 2, BWO estimates during the LGM varied between 64 and 71 $\mu\text{mol/kg}$, between 65 and 97 $\mu\text{mol/kg}$ during HS1 which was followed with a significant drop during the BA/ACR from 77 to 29 $\mu\text{mol/kg}$. As observed in Approach 1, during the EH and LH estimated concentrations did not reveal distinct changes and ranged between 38 and 51 $\mu\text{mol/kg}$ and between 43 and 51 $\mu\text{mol/kg}$, respectively. The standard errors were with 15 $\mu\text{mol/kg}$, which are markedly higher than in Approach 1 estimates. The estimated BWO of Approach 3 showed ranges from 30 to 38 $\mu\text{mol/kg}$ during the LGM, varied between 25 and 33 $\mu\text{mol/kg}$ during HS1, between 4 and 33 $\mu\text{mol/kg}$ during the BA/ACR. Similar to other approaches, The Holocene did not indicate significant increase or decrease. The estimates ranged between 15 and 23 $\mu\text{mol/kg}$ during the EH and between 18 and 22 $\mu\text{mol/kg}$ during the LH. The errors of this approach results were around 7 $\mu\text{mol/kg}$. Estimated concentrations below zero were obviously artefacts of the method. Overall, concentrations estimated as results of Approach 1 and 3 were too low with maximums below 40 $\mu\text{mol/kg}$, whereas the present day observations indicated values around 70 $\mu\text{mol/kg}$. Generally, higher BWO levels than present day values were anticipated in the downcore. The presence of *P. murrhyna* and the agglutinated species throughout the core also suggested that the prevailing BWO levels have been around and more than 40-45 $\mu\text{mol/kg}$ during the considered time intervals. Accordingly, the Approach 2 yielded the most reliable estimates as it was for core 50-4. When the average concentrations for each interval were considered, a drop in BWO of up to 25 $\mu\text{mol/kg}$ may have taken place during the deglaciation. Concentrations

slightly increased thereafter and did not change very much during the early and late Holocene (Figure 5.5).

Core M77/2-59-1

The core was recovered from the northernmost part of the study area, at 3°57'S and 997 m water depths, and the BWO were measured as 54 $\mu\text{mol/kg}$ during the sampling. The core location has been under the influence of major riverine input. The sedimentation rates throughout the core were with 50 and 170 cm/ka rather high as compared to the other cores (Mollier-Vogel et al., 2013). Because of these high sedimentation rates, the LGM was not retrieved by this core. In total 20 samples were analysed covering the corresponding time intervals and 161 species were identified. Agglutinated species were scarce but present as well as the Miliolids. They were more frequent in samples from the lower part of the core, older than 9 cal ka. The most dominant species throughout the core was *Bolivinita minuta* with percentages showing a distinct increase from 9 % to 19 % during the BA/ACR and later reaching up to 25% during the late Holocene (see Chapter 4). It is followed by *Cassidulina delicata* with proportions around 4 % during the BA/ACR and around 10 % during the Holocene. *Epistominella exigua* showed similar trends in this core reaching up to 30 %, not only during the HS1, as in core 52-2, but also during the BA/ACR, indicating an enhanced organic matter flux to the sea floor. We did not observe such a distinct increase in the southern core 50-4 during the same period where the maximum proportions were around 10 % during the early LGM and the HS1. This pattern probably mirrors enhanced productivity in the EEP as it was observed in various records (Pedersen, 1983; Pedersen et al., 1988; Hendy and Pedersen, 2006) . The influence of productivity from the Peruvian upwelling to the South is considered to be of minor importance. The latitude of 5°S is seemingly a boundary where differences in productivity were observed between various Peruvian margin cores to the North and South, including core 52-2 (K. Doering, Kiel, pers. comm.). Considering the BWO quantification approaches, the estimated BWO as results of Approach 1, in particular for the Holocene time intervals, were below zero. Accordingly, we cannot take the results of Approach 1 at face value. The Approach 2, the BWO estimates ranged between 38 and 67 $\mu\text{mol/kg}$ during HS1, between 21 and 61 $\mu\text{mol/kg}$ during the BA/ACR, between 24 and 53 $\mu\text{mol/kg}$ during the EH and between 4 and 48 $\mu\text{mol/kg}$ during the LH, with errors around 15 $\mu\text{mol/kg}$. Similar to Approach 1, the estimated BWO values fall below zero in the late Holocene. Highest BWO estimates were observed during HS1 which did not exceed 31 $\mu\text{mol/kg}$. Considering the modern conditions and the presence of the Miliolids, in particular *Prygo murrhyna*, Approach 2 estimates are deemed to be closest to reliability as they were for

cores 50-4 and 52-2 as well. The average BWO from the results of the Approach 2 were calculated for each interval of core 59-1, and the difference between the HS1 and the EH was 17 $\mu\text{mol/kg}$ drop in BWO.

5.3.4. Comparison with other proxies and records from the EEP

The BWO estimates of the three different approaches indicated offsets and were generally lower than anticipated, though their overall trends showed similarities. The records revealed a distinct decrease in BWO during the deglaciation in all of the cores from the lower OMZ oxic-suboxic boundary. As discussed in the previous chapter, the results of Approach 2 were closest to modern conditions and to other paleo-oxygenation indicator species provided they are available for the same core. For a further interpretation and comparisons with other proxy-records from the region, we primarily focused on the results of Approach 2 (Figure 5.6). Three cores did not cover all the time intervals considered, limiting the spatial comparison of BWO differences between the LGM and the Holocene. Nevertheless when the records were stacked, the estimates showed a decreasing trend starting from the LGM, a distinct drop during the deglaciation with fluctuations from the HS1 to the BA/ACR, and a slight increase followed by relatively stable concentrations during the Holocene. None-the-less, the Holocene concentrations were still lower than those of the LGM. This trend is consistent with the results reported in recent reviews of bottom-water deoxygenation during the deglaciation in the Eastern Pacific Ocean (Jaccard and Galbraith, 2012; Moffitt et al., 2015). Both reviews consider results from different proxies (e.g., lamination, $\delta^{15}\text{N}$, redox sensitive elements) which are known to indicate oxygen depleted conditions obtained from sediment cores from above 500 m water depths offshore Peru.

Comparing the differences between our cores studied, the decrease from HS1 to the BA/ACR was 15 $\mu\text{mol/kg}$ in core 50-4, 25 $\mu\text{mol/kg}$ at core 52-2 and only 5 $\mu\text{mol/kg}$ in core 59-1. The difference between the BA/ACR and the early Holocene BWO was around 7 $\mu\text{mol/kg}$ at core 52-2 and around 12 $\mu\text{mol/kg}$ at core 59-1. It has to be noted that the standard error is 15 $\mu\text{mol/kg}$ in both cores implying a rather minute change if at all. None-the-less, the overall decrease was the largest in the deepest core implying that the absolute changes at the lower boundary were larger than in the centre of the OMZ. This might be a reason why the approaches did not reveal such distinct changes in the core 47-2. Another quantification approach by comparison of Fe and Mo/U in core M77/2-24-5 from the upslope (210 m water depths) offshore Peru at 11°S reported a drop of 5 to 10 $\mu\text{mol/l}$ during the deglaciation (Scholz et al., 2014) corroborating our estimates. Once the OMZ has intensified during the deglaciation, it is

Chapter 5: Bottom-water deoxygenation at the Peruvian Margin during the last Deglaciation recorded by benthic foraminifera

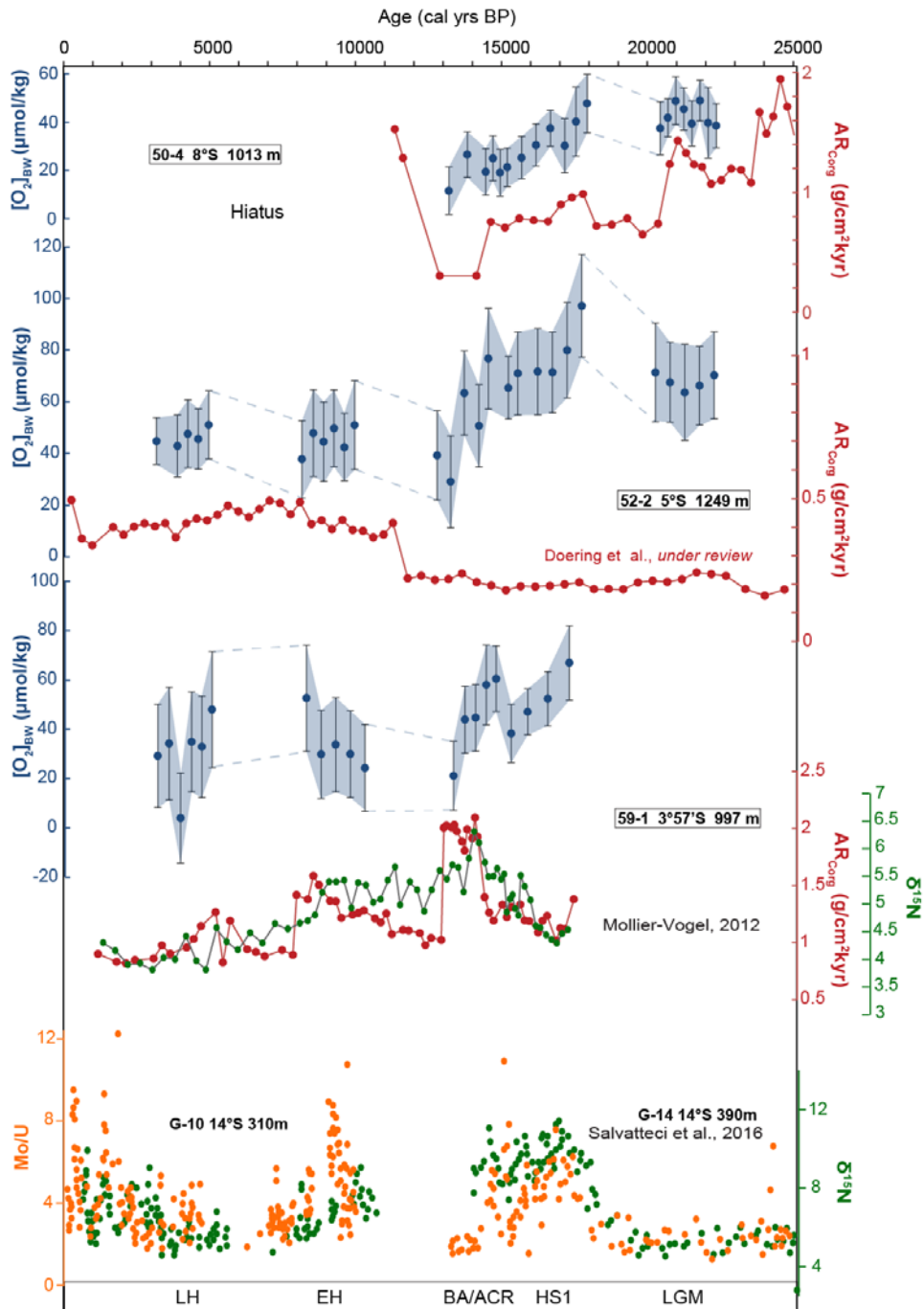


Figure 5.6. Comparison of BWO estimated concentrations of Approach 2 with other proxy-records for productivity and redox conditions from the same cores and another stacked record of two neighbouring sediment cores from the southern part of the region.

conceivable that the decrease in BWO was stronger at the lower boundary of the OMZ than on the top. Furthermore, differences and delays were observed in the timings of the distinct decreases between the different cores. In the southern core 50-4, the most distinct decrease started already with the onset of the HS1 whereas the decreasing trend did not commence before the end of this period in the slightly deeper core 52-2. The amount of the BWO decrease from

HS1 to the BA/ACR was around 15 to 25 $\mu\text{mol/kg}$ in the cores 50-4 and 52-2, whereas it was only 5 $\mu\text{mol/kg}$ in the northern core. At this core, the values raised later by 11 $\mu\text{mol/kg}$ in the BA/ACR to the Holocene transition whereas the decrease was only around 6 $\mu\text{mol/kg}$ in the core 52-2. This indicated a south to north time-transgressive and decreasing trend in BWO.

Other productivity and redox proxies from the region revealed similar trends (Figure 5.6). Laminated sediments indicating BWO of $<7 \mu\text{mol/kg}$ (e.g., Schönfeld et al., 2015) were observed widest in extent during the HS1, in particular at the continental shelf and upper slope between 10 and 18°S (Erdem et al., 2016). Stacked records from the Peruvian margin at 14°S revealed a correlation between enhanced productivity, as indicated by increased $\delta^{15}\text{N}$ values, and elevated bottom-water redox conditions as indicated by increasing Mo/U values within the laminated sediments during the HS1 period (Salvatteci et al., 2016). A similar increasing trend in $\delta^{15}\text{N}$ values from core 59-1 started not earlier than at onset of the BA/ACR, thereby correlating with the organic carbon accumulation rates and the increase in the proportion of *Epistominella exigua* between 13 cal ka BP and 15.6 cal ka BP (Chapter 4; Appendix). Although C-org accumulation rates from core 52-2 did not reveal such trends, *E. exigua* showed a similar increase indicating enhanced productivity during HS1 which apparently followed later by decreasing BWO of up to 25 $\mu\text{mol/kg}$. These data suggested that bottom-water deoxygenation did not always co-occur with enhanced surface productivity. The facultative discrepancy might be a corroborating evidence that other parameters than primary productivity were influencing the oxygen dynamics in the Peruvian OMZ as they do today; for instance ventilation of intermediate waters or changes in the hydrodynamics (Karstensen et al., 2008; Brandt et al., 2015). However, it should be kept in mind that the Peruvian margin potentially represents a much more complex structure in terms of productivity as it is mirrored in biogenic opal and $\delta^{30}\text{Si}$ records (Doering et al., 2016). The same caution should be applied to our *E. exigua* records. The species was observed in the northern cores but not in the core 50-4 situated much closer to the main upwelling area. Although the productivity signatures in the sediments showed variations among the different cores, the BWO calculations always showed similar trends. This might be indication of different dynamics in the surface waters than in intermediate waters which needs further investigation. Even though our estimated BWO concentrations were lower than anticipated, the quantification approach is consistent in terms of absolute changes and coherent with other proxies. Finally, our data and the comparison with other proxies indicated an expansion of the northern part of the Peruvian OMZ in terms of thickness and wideness during the last deglaciation with a decrease in BWO of 25 $\mu\text{mol/kg}$ drop at its lower boundary.

5.4. Summary and Conclusions

Using of benthic foraminiferal assemblages as bottom water oxygenation proxy has been under debate since the oxygen-deficiency indicator species can be found in many other environments as well. When certain thresholds are applied, for instance microxic (<5 $\mu\text{mol/kg}$), dysoxic (5-45 $\mu\text{mol/kg}$), oxic (>45 $\mu\text{mol/kg}$), similar assemblages were found in different oxygen minimum zone settings world-wide, even though they are composed of different species. Future genetic barcoding will reveal whether this variability indicates a confined regional distribution for specific species (Pawlowski and Holzmann, 2014), or whether these species are just morphological variations of the same genotypes, hence displaying a global biogeographical pattern of subspecies (Schönfeld, 2006). In any case, species-specific approaches should be applied to sediment core records only once living benthic foraminiferal distributions from the same region are available as reference data sets for proxy calibration.

Three different datasets of living (rose Bengal stained) benthic foraminiferal distribution from the continental shelf and slope off Peru obtained in different studies and by different investigators could successfully be merged and a taxonomic consensus was reached. The faunal distribution data were accomplished with bottom-water-oxygen (BWO) concentrations measured during the sampling periods. The application of the statistical analyses (cluster analyses, CCA and multivariate multiple regression) to this dataset revealed the dominant assemblages and their relation with the environmental variables. Certain species and assemblages showed a much better correlation with BWO concentrations than with rain rates of particulate organic carbon (RRPOC). Application of a multiple regression analysis with BWO as dependant variable indicated that the foraminiferal assemblages are rather governed by oxygen availability than by the deposition of particulate organic matter. The correlation with BWO was significant ($R^2 = 0.959$; $p < 0.05$), therefore we applied the transfer function to four different sediment cores taken from the lower boundary of the Peruvian Oxygen Minimum Zone (OMZ) in order to quantify the BWO. When compared to the prevailing bottom-water conditions at core locations today, our estimates were generally lower than anticipated. Therefore, we took the absolute changes during specific time intervals into consideration. The data revealed a drop in BWO of 25 $\mu\text{mol/kg}$ at the lower boundary of the OMZ during the last deglaciation. The decrease was largest at the deepest core site whereas differences were not significant closer to the centre of the OMZ. This pattern points to either a reduced lateral advection of oxygen by mid-depth currents from the North, or a reduced diapycnal mixing by less strong internal waves.

Chapter 5: Bottom-water deoxygenation at the Peruvian Margin during the last Deglaciation recorded by benthic foraminifera

A comparison with other productivity indicators and redox proxies from the region revealed that deoxygenation of the bottom waters did not always co-occur with the enhanced productivity above the core site. Downcore benthic foraminiferal distributions indicated a gradual decrease in BWO levels since the Last Glacial Maximum (LGM). We observed marked latitudinal differences north and south of 5°S in primary productivity as indicated by increased abundances of *Epistominella exigua*, whereas the oxygenation reconstructions showed a gradual decrease from south to north during the corresponding time intervals. Decrease in BWO levels started with the onset of Heinrich Stadial 1. This was observed at the southernmost core, and it was followed by a distinct drop during the deglaciation in all other cores. Later, a slight increase was observed in the northern cores during the Holocene. This general trend is in line with previous paleo-oxygenation proxy records from the Eastern Pacific Ocean, supporting credibility to the benthic foraminiferal approach.

Acknowledgement

We would like to thank the crew and captain of R/V Meteor during the cruises M77 legs 1 and 2, Bettina Domeyer for the organic carbon measurements, Elfi Mollier-Vogel and Phillipe Martinez for collaboration, Wolfgang Kuhnt and his group for helping with the real colour pictures and Sebastian Meyer and his team for providing the SEM images, Renato Salvatecci for collaboration and helpful discussions. This work was funded by Deutsche Forschungsgemeinschaft (DFG) through SFB 754 “Climate–Biogeochemistry Interactions in the Tropical Ocean” and the French program CNRS-INSU-IMAGO (project COMICS to Ph. Martinez) which funded the additional analyses of core 59-1.

6. SUMMARY AND OUTLOOK

6.1. Summary

The present study took part in the second phase of the collaborative research centre SFB754 with the aim of reconstructing the bottom-water-oxygenation (BWO) by using the benthic foraminiferal assemblages for the last 22,000 years offshore Peru. The main focus was to develop a quantification method, which relied on the living benthic (rose-Bengal stained) foraminiferal faunas from the region and to apply the ecological data to sediment cores from the Peruvian margin.

The Peruvian margin is characterized by a persistent and pronounced OMZ as result of strong upwelling, enhanced surface productivity and sluggish ventilation of the subsurface waters. The understanding of relationships between these processes with the changing climatic conditions, e.g., during the glacial-interglacial transitions, is essential. Many paleoceanographic investigations from the Eastern Equatorial Pacific (EEP) reported indications of an extensive deoxygenation during the last deglaciation period. Therefore, the structure of the Peruvian OMZ potentially experienced spatio-temporal changes since the Last Glacial. With this motivation, the present study primarily focused on the sediment cores from the lower boundary of Oxygen Minimum Zone (OMZ) in addition to previously studied cores that were investigated during the first of phase of the project. During the first phase of SFB 754 the main goal was to investigate the processes in the OMZ core. Therefore, those cores were mainly from within the OMZ. For the benthic foraminiferal approach, we needed sediment cores where changes of bottom-water oxygenation were profoundly recorded. Consequently, five new sediment cores from the mid continental slope and lower oxic-suboxic boundary of the OMZ between 5°S and 18°S were chosen for this study. The stratigraphic descriptions and age models of these cores were reported in Chapter 2. For the sake of completeness, the stratigraphic information from the first phase of the SFB754 (Mollier-Vogel, 2012) are also included in this chapter. In addition to the stratigraphic information, measurements of total organic carbon and total nitrogen were accomplished from two sediment cores (cores 50-4 and 52-2) as part of this study and were reported in a different publication (Schönfeld et al., 2015) and are parts of this study as documented in Chapter 2 and Chapter 5.

The sediment cores revealed a ubiquitous hiatus that started in the southernmost part of the region already during the late Pleistocene, whereas the hiatus was absent in the sediment cores in the northern part of 7°S. The northern core 52-2 is the only complete record within the

five sediment cores considered for this study. The hiatus observed in the downcore record indicated also an evolving trend from south to north with the onset of the Termination I, which led us to question the reasons behind it. Gaps in the sedimentary record from the Peruvian continental shelf and slope are common features for the Peruvian margin. Therefore, most of the paleo-reconstructions from the region are limited in extent and scattered. In order to gain further insights, we investigated 22 sediment core descriptions and visualized the extent of the gaps observed in the sedimentary records. We focused on the sedimentary characteristics in the time intervals late Holocene (LH; 3-5 cal ka BP), early Holocene (EH; 8-10 cal ka BP), Bølling Ållerød/Antarctic Cold Reversal (BA/ACR; 13-14.5 cal ka BP), Heinrich Stadial-1 (HS1; 15-17.5 cal ka BP) and Last Glacial Maximum (LGM; 20-22 cal ka BP) and compared these intervals with the Recent (0-500 yrs BP) sedimentary distribution and prevailing hydrodynamics along the margin. Comparison of the time periods revealed a northward extension and an evolving hiatus since the LGM. The maximum spatial extent of the laminated sediments was recorded during the HS1. The maximum extent of the hiatus was observed during the EH, which was the only period when widespread erosion took place along the continental shelf and not only at the slope as recorded during the other periods. This brought up the conclusion that the poleward undercurrent (PCUC) could not be the only erosive feature as postulated in earlier studies. Further investigation included determinations of the critical slopes at four transects from the Peruvian margin which revealed enhanced bottom-water activities due to the high tide-topography interactions and the formation of non-linear internal waves (NLIWs). These waves were also reported in other studies of ancient rock sequences in terms of transported sediments and turbidite sections. Chapter 3, for the first time, presents a modern analogue in which such an environment and ongoing processes could be investigated. Additionally, the regions which are classified as critical slopes, where the tide-topography interaction is highest, are so far widest in area at present. Their occurrence is dependent on the density gradient within the water column. The evolving hiatus might be an indication of the intensification of the NLIW formations and their interaction with the sea floor during the deglaciation. This is in accordance with global models that indicated larger amplitudes of the tides during the LGM and the subsequent deglaciation in the South Pacific Ocean. Potential changes in the mid-depth hydrodynamics and water masses during the last deglaciation are also conceivable, which needs further investigation. The increasing influence of the Equatorial subsurface waters in the region (e.g., Nürnberg et al., 2015), the PCUC along the shelf, starting already during the BA/ACR and would limit the presence of laminated sediments and impede the sedimentation on the continental shelf.

As most of the sediment cores from the southern part of the region were non-continuous, we focused on four sediment cores from between 3°S and 9°S and water depths of 600 m and 1250 m to investigate the northern extension of the Peruvian OMZ. We were also able to compare the benthic foraminiferal assemblages during the LGM with those in the southernmost core 416. Chapter 4 summarizes the main findings; the distribution of the most abundant species during the corresponding time intervals from five sediment cores. The taxonomic notes and species documented by real colour optical microscope and SEM images were reported. Overall distributional patterns indicated assemblage similarities on genus level but showed some differences in species level. The most common species observed in all the sediment cores from the north is *Bolivinita minuta*, followed by *Cassidulina delicata* and *Epistominella exigua*. *Epistominella exigua* is known to be an indicator of high productivity, a pulsed or high flux of phyto-detritus to the sea floor. This species was observed mostly in the northernmost cores during the Termination I but not with similar abundances in the cores south of 5°S, potentially indicating differences in surface water dynamics between these two areas. For instance, the recent in situ observations from the region indicated that the poleward flowing PCUC originates at these latitudes (between 3-5°S) as a surface current and it gets deeper during its path to the south which later contributes to the upwelling (Chaigneau et al., 2013). Such differences in the surface water masses and dynamics are potentially influential in the benthic foraminiferal response, as observed in the variations of *E. exigua* distributions.

A comprehensive dataset of living (stained) calcareous benthic foraminiferal faunas was used for the purpose of bottom-water oxygen (BWO) quantification of fossil assemblages in corresponding time intervals. The compilation comprised existing datasets from Mallon (2012), Cardich et al. (2012 and 2015), Levin (2002) and Pérez et al (*unpublished*). A multiple regression analysis was applied to these data of living calcareous benthic foraminifera where the bottom water oxygen (BWO), that were measured during sampling periods, were used as a dependant variable. The correlation was significant ($R^2 = 0.959$; $p < 0.05$) therefore we applied this method to the benthic foraminiferal assemblages collected from the sediment cores. Even though, the estimated oxygen concentrations were lower than anticipated as compared to the present day values, the overall trends and fluctuations observed in the cores showed similarities and were consistent with previous reports from the region. Because of the missing time intervals in different cores, it was only possible to compare the Termination I in full detail. The calculations revealed a decrease in the BWO levels from the LGM to the Holocene of ca. 25 $\mu\text{mol/kg}$. The overall magnitude of the decrease in estimated BWO concentrations was highest in the deepest core and lowest in the shallowest core. This was likely because of the extending the

lens-shaped OMZ. Once the OMZ has intensified during the deglaciation, it is conceivable that the decrease in BWO was stronger at the lower boundary of the OMZ than in shallower depths. The Holocene was investigated at the two northern cores only, and it indicated a slight increase in BWO levels ($\sim 10 \mu\text{mol/kg}$) since the BA/ACR. There was no distinct difference between the early and late Holocene. Overall fluctuating trend observed in the estimated BWO concentrations from the LGM to the late Holocene is in accordance with previous records using different proxy-approaches. They also indicate enhanced deoxygenation during the Termination I and slight increase in the BWO levels during the Holocene. In the sediment cores from the north, this trend revealed a time-transgressive pattern indicating a gradual expansion in the shape of the OMZ with the onset of the Termination I. Moreover, the bottom-water deoxygenation apparently was not always coupled with high primary production since the comparison with the other proxies from the region and from the same cores revealed different implications. The distributional pattern of *Epistominella exigua* could be given as such an example. This implied that the export production was not the main driver of the oxygenation of the intermediate waters in the region. The intensification of subsurface currents or any similar changes in the mid-depth dynamics would have had an impact on the ventilation of the OMZ. For instance, the oxygen-rich Antarctic Intermediate Water (AAIW) is thought to be extending far in the north during the deglaciation compared to its modern distribution (Marchitto et al., 2007). The presence of oxygen rich intermediate waters of southern origin might be an explanation for a decoupling of the surface productivity and oxygenation of the intermediate waters which in accordance with the observations from further south (Muratli et al., 2009). The changes of the tide-topography interactions also could be in relation with these modifications of the intermediate water masses.

Besides hosting a persistent OMZ and representing a high energetic environment, the Peruvian margin is one of the places in the world where ongoing phosphatization is observed. Phosphorites are one of the major sedimentary features in the area and actually could be used as bottom-water oxygenation proxy and also for decoding the erosion and the hiatus since they occur where the boundaries of the OMZ meet with high energetic bottom water conditions. Furthermore, the role of the NLIWs in sedimentation should not be neglected in terms of sediment remobilization along the Peruvian shelf and slope.

6.2. Outlook

Comparing the other proxy records and sedimentary features observed in different sediment cores from the region, the Peruvian margin revealed a really complex system. Unfortunately, the ongoing bottom-water turbulences and their erosional signature left in the

downcore record limit our interpretations since the LGM. Another limiting factor for the paleo-oxygen reconstruction is the applicability of different proxies to the same sediment cores. Well-known extreme low oxygen proxies, such as redox sensitive elements and laminations, are not applicable outside the OMZ core where the benthic foraminiferal quantification approach was applied. Consequently, other proxies, such as productivity indicators (e.g., ARCOrg_{bulk}, biogenic opal, $\delta^{30}\text{Si}$, $\delta^{15}\text{N}$), were also used in order to see the relationships between the bottom water deoxygenation and the export production. However, these processes were not always coupled during different time intervals and also showed latitudinal and regional differences. Even though, application of multi-proxy approaches (including the element/Ca measurements of benthic foraminifera shells (e.g., Glock et al., 2012a; Koho et al., 2015) and the pore densities of certain species (Glock et al., 2011; Glock et al., 2012b) to the existing sediment cores and information would extend our knowledge about the deoxygenation and its relation with the export production in the region. During the third phase of the SFB754, another quantification approach by using molybdenum isotopes (e.g., Siebert et al., 2003; Siebert et al., 2006) is to be applied to the sediment cores from the region which will potentially corroborate the information gained from benthic foraminifera. Moreover, the present study focused on specific time intervals therefore the benthic foraminiferal information did not cover the mid-Holocene (5-8 ka BP) in which the observed variations have been a matter of discussion. Apparently, the investigations of this period are hampered due to the erosion in the southern part of the region but in the northern sediment cores (cores 59-1 and 52-2) offer an alternative. Various records indicated changes in the SSTs, in the upwelling intensity and in the ENSO phases during this period. Therefore, comparison of the BWO levels using the benthic foraminiferal quantification method with other proxies from the region would help to elucidate this interesting period.

This study also showed that the gaps in the sedimentary record could be something worthwhile to investigate in order to understand the changing conditions over time. Sediment cores with omission surfaces are often discarded because of the inconsistency of data or simply the discontinuity of the record. The expanding and evolving hiatus from the Peruvian margin revealed potential changes in mid-depth hydrodynamics which might be related to changes in the water masses at depths. As discussed earlier, the potential differentiations of the subsurface and intermediate water masses could also be explanation of the decoupling of the primary productivity, N – loss and deoxygenation in the region, which needs further investigations. The variations or changes of the subsurface water dynamics could be investigated through various proxies as it was done for the northernmost part of the region (Nürnberg et al., 2015). Investigations using different proxies in order to decipher the pelagic – benthic (de)coupling on

Chapter 6: Summary and Outlook

the existing information and cores would improve our understanding of this complex system, in this case for the last deglaciation. A recent similar approach was done in north east Atlantic coastal upwelling system (McKay et al., 2014) pointing out once more that the benthic foraminiferal response to the prevailing conditions in both bottom and surface water is essential in the understating of such complex systems.

REFERENCES

- Agnihotri, R., Altabet, M.A., Herbert, T., 2006. Influence of marine denitrification on atmospheric N₂O variability during the Holocene. *Geophysical Research Letters* 33, L13704, 1-5.
- Altenbach, A.V., Pflaumann, U., Schiebel, R., Thies, A., Timm, S., Trauth, M., 1999. Scaling percentages and distributional patterns of benthic foraminifera with flux rates of organic carbon. *The Journal of Foraminiferal Research* 29, 173-185.
- Alve, E., Bernhard, J.M., 1995. Vertical migratory response of benthic foraminifera to controlled oxygen concentrations in an experimental mesocosm. *Marine Ecology Progress Series*, 116, 137-151.
- Andrus, C.F., Crowe, D.E., Sandweiss, D.H., Reitz, E.J., Romanek, C.S., 2002. Otolith delta ¹⁸O record of mid-Holocene sea surface temperatures in Peru. *Science* 295, 1508-1511.
- Arning, E.T., Lückge, A., Breuer, C., Gussone, N., Birgel, D., Peckmann, J., 2009. Genesis of phosphorite crusts off Peru. *Marine Geology* 262, 68-81.
- Arthur, M.A., Dean, W.E., Laarkamp, K., 1998. Organic carbon accumulation and preservation surface sediments of the Peru margin. *Chemical Geology* 152, 273-286.
- Baas, J.H., Schönfeld, J., Zahn, R., 1998. Mid-depth oxygen drawdown during Heinrich events: evidence from benthic foraminiferal community structure, trace-fossil tiering, and benthic δ¹³C at the Portuguese Margin. *Marine Geology* 152, 25-55.
- Baker, K.B., Burnett, W.C., 1988. Distribution, texture and composition of modern phosphate pellets in Peru shelf muds. *Marine Geology* 80, 195-213.
- Bandy, O.L., 1953a. Ecology and Paleocology of some California foraminifera Part I. The Frequency distribution of recent foraminifera off California. *Journal of Paleontology* 27, 161-185.
- Bandy, O.L., 1953b. Ecology and Paleocology of some California foraminifera Part II. Foraminiferal evidence of subsidence rates in the Ventura Basin. *Journal of Paleontology* 27, 200-203.
- Bandy, O.L., Rodolfo, K.S., 1964. Distribution of foraminifera and sediments, Peru-Chile Trench area. *Deep-Sea Research* 11, 817 - 837.
- Barker, R.W., 1960. Taxonomic notes on the species figured by H.B.Brady in his report on the foraminifera dredged by H.M.S. Challenger during the years 1873-1876. Society of Economic Paleontologists and Mineralogists Tulsa, Oklahoma, USA.
- Barmawidjaja, D.J., Jorissen, F.J., Puskaric, S., Van der Zwaan, G.J., 1992. Microhabitat selection by benthic foraminifera in the northern Adriatic Sea. *Journal of Foraminiferal Research* 22, 297-317.
- Bernhard, J.M., Alve, E., 1996. Survival, ATP pool, and ultrastructural characterization of benthic foraminifera from Drammensfjord (Norway): response to anoxia. *Marine Micropaleontology* 28, 5-17.

References

- Bernhard, J.M., Gupta, B.K.S., Borne, P.F., 1997. Benthic foraminiferal proxy to estimate dysoxic bottom-water oxygen concentrations; Santa Barbara Basin, US Pacific continental margin. *The Journal of Foraminiferal Research* 27, 301 - 310.
- Bernhard, J.M., Reimers, C.E., 1991. Benthic foraminiferal populations related to anoxia: Santa Barbara Basin. *Biogeochemistry* 15, 127-149.
- Bernhard, J.M., Sen Gupta, B.K., 1999. Foraminifera of oxygen-depleted environments, *Modern foraminifera*. Springer, pp. 201-216.
- Biebow, N., 1996. Dinoflagellatenzysten als Indikatoren der spat-undpostglazialen Entwicklung des Auftriebsgeschehens vor Peru, GEOMAR report 57, *Paleoceanography*. Christian Albrechts Universität zu Kiel, Kiel, p. 100.
- Bogucki, D., Redekopp, L.G., Barth, J., 2005. Internal solitary waves in the Coastal Mixing and Optics 1996 experiment: multimodal structure and resuspension. *Journal of Geophysical Research* 110:C02024.
- Bourgault, D., Morsilli, M., Richards, C., Neumeier, U., Kelley, D.E., 2014. Sediment resuspension and nepheloid layers induced by long internal solitary waves shoaling orthogonally on uniform slopes. *Continental Shelf Research* 72, 21-33.
- Boyer, T.P., Antonov, J.I., Baranova, O.K., Coleman, C., Garcia, H.E., Grodsky, A., Johnson, D.R., Locarnini, R.A., Mishonov, A.V., O'Brien, T.D., Paver, C.R., Reagan, J.R., Seidov, D., Smolyar, I.V., Zweng, M.M., 2013. *World Ocean Database 2013*, NOAA Atlas NESDIS 72, in: Levitus, S. (Ed.). National Oceanographic Data Center Ocean Climate Laboratory.
- Böning, P., Brumsack, H.-J., Böttcher, M.E., Schnetger, B., Kriete, C., Kallmeyer, J., Borchers, S.L., 2004. Geochemistry of Peruvian near-surface sediments. *Geochimica et Cosmochimica Acta* 68, 4429-4451.
- Brandt, P., Bange, H.W., Banyte, D., Dengler, M., Didwischus, S.-H., Fischer, T., Greatbatch, R.J., Hahn, J., Kanzow, T., Karstensen, J., Körtzinger, A., Krahnemann, G., Schmidtko, S., Stramma, L., Tanhua, T., Visbeck, M., 2015. On the role of circulation and mixing in the ventilation of oxygen minimum zones with a focus on the eastern tropical North Atlantic. *Biogeosciences* 12, 489-512.
- Brockmann, C., Fahrbach, E., Huyer, A., Smith, R.L., 1980. The poleward undercurrent along the Peru coast: 5 to 15°S. *Deep Sea Research Part A. Oceanographic Research Papers* 27, 847-856.
- Burnett, W.C., 1977. Geochemistry and origin of phosphorite deposits from off Peru and Chile. *Geological Society of America Bulletin* 88, 813.
- Burnett, W.C., 1980. Apatite-glaucinite associations off Peru and Chile: palaeo-oceanographic implications. *Journal of Geological Society* 137, 757-764.
- Burnett, W.C., Beers, M.J., Roe, K.K., 1982. Growth rates of phosphate nodules from the continental margin off Peru. *Science* 215, 1616-1618.

References

- Burnett, W.C., Veeh, H.H., 1977. Uranium-series disequilibrium studies in pbosphorite nodules from the west coast of South America. *Geochimica et Cosmochimica Acta* 41, 755-764.
- Cacchione, D.A., Pratson, L.F., Ogston, A.S., 2002. The shaping of continental slopes by internal tides. *Science* 296, 724-727.
- Cai, W.-J., Sayles, F.L., 1996. Oxygen penetration depths and fluxes in marine sediments *Marine Chemistry* 52, 123-131.
- Cannariato, K.G., Kennett, J.P., 1999. Climatically related millennial-scale fluctuations in strength of California margin oxygen-minimum zone during the past 60 k.y. *Geology* 27, 975-978.
- Caralp, M.H., 1989. Abundance of *Bulimina exilis* and *Melonis barleeanum*: Relationship to the quality of marine organic matter. *Geo-Marine Letters* 9, 37-43.
- Cardich, J., Gutiérrez, D., Romero, D., Pérez, A., Quipúzcoa, L., Marquina, R., Yupanqui, W., Solís, J., Carhuapoma, W., Sifeddine, A., Rathburn, A., 2015. Calcareous benthic foraminifera from the upper central Peruvian margin: control of the assemblage by pore water redox and sedimentary organic matter. *Marine Ecology Progress Series* 535, 63-87.
- Cardich, J., Morales, M., Quipúzcoa, L., Sifeddine, A., Gutiérrez, D., 2012. Benthic Foraminiferal Communities and Microhabitat Selection on the Continental Shelf Off Central Peru, in: al., A.e. (Ed.), *Anoxia: Evidence for Eukaryote Survival and Paleontological Strategies*, Springer, pp. 323-340.
- Caress, D.W., Chayes, D.N., 2001. Improved management of large swath mapping data sets in MB System Version 5, *EOS Trans. Fall Meet.* 47
- Carré, M., Sachs, J.P., Purca, S., Schauer, A.J., Braconnot, P., Falcón, R.A., Julien, M., Lavallée, D., 2014. Holocene history of ENSO variance and asymmetry in the eastern tropical Pacific. *Science* 345, 1045-1048.
- Carter, G.S., Gregg, M.C., Lien, R.-C., 2005. Internal waves, solitary-like waves, and mixing on the Monterey Bay shelf. *Continental Shelf Research* 25, 1499-1520.
- Caulle, C., Koho, K.A., Mojtahid, M., Reichart, G.J., Jorissen, F.J., 2014. Live (Rose Bengal stained) foraminiferal faunas from the northern Arabian Sea: faunal succession within and below the OMZ. *Biogeosciences* 11, 1155-1175.
- Chaigneau, A., Dominguez, N., Eldin, G., Vasquez, L., Flores, R., Grados, C., Echevin, V., 2013. Near-coastal circulation in the Northern Humboldt Current System from shipboard ADCP data. *Journal of Geophysical Research: Oceans* 118, 5251-5266.
- Chazen, C.R., Altabet, M.A., Herbert, T.D., 2009. Abrupt mid-Holocene onset of centennial-scale climate variability on the Peru-Chile Margin. *Geophysical Research Letters* 36, L18704, 1-5.
- Corliss, B.H., 1985. Microhabitats of benthic foraminifera within deep sea sediments. *Nature* 314, 435-438.
- Corliss, B.H., 1991. Morphology and microhabitat preferences of benthic foram from the northwest Atlantic Ocean. *Marine Micropaleontology* 17, 195-236.

References

- Corliss, B.H., Emerson, S., 1990. Distribution of Rose Bengal stained deep sea benthic foram from Nova Scotian continental margin and Gulf of Maine. *Deep Sea Research* 37, 381-400.
- Coulbourn, W.T., 1980. Relationship between the distribution of foraminifera and geologic structures of the Arica bight, South America. *Journal of Paleontology* 54, 696-718.
- Czeschel, R., Stramma, L., Schwarzkopf, F.U., Giese, B.S., Funk, A., Karstensen, J., 2011. Middepth circulation of the eastern tropical South Pacific and its link to the oxygen minimum zone. *Journal of Geophysical Research* 116, C01015, 1-13.
- Dale, A.W., Sommer, S., Lomnitz, U., Montes, I., Treude, T., Liebetrau, V., Gier, J., Hensen, C., Dengler, M., Stolpovsky, K., Bryant, L.D., Wallmann, K., 2015. Organic carbon production, mineralisation and preservation on the Peruvian margin. *Biogeosciences* 12, 1537-1559.
- den Dulk, M., Reichart, G.-J., Heyst, S.V., Zachariasse, W.J., Zwaan, G.J.V.d., 2000. Benthic foraminifera as proxies of organic matter flux and bottom water oxygenation? A case history from the northern Arabian Sea. *Palaeogeography, Palaeoclimatology, Palaeoecology* 161, 337-359.
- den Dulk, M., Reichart, G.-J., Memon, G.M., Roelofs, E.M.P., Zachariasse, W.J., Zwaan, G.J.V.d., 1998. Benthic foraminiferal response to variations in surface water productivity and oxygenation in the northern Arabian Sea. *Marine Micropaleontology* 35, 43-66.
- Doering, K., Ehlert, C., Grasse, P., Crosta, X., Fleury, S., Frank, M., Schneider, R., 2016. Differences between mono-generic and mixed diatom silicon isotope compositions trace present and past nutrient utilisation off Peru. *Geochimica et Cosmochimica Acta*, 177, 30-47.
- Douglas, R.G., Heitman, H.L., 1979. Slope and basin benthic foraminifera of the California Borderland. *Society of Economic Paleontologists and Mineralogists* 27, 231-246.
- Echevin, V., Aumont, A., Ledesma, J., Flores, G., 2008. The seasonal cycle of surface chlorophyll in the Peruvian upwelling system: A modelling study. *Progress in Oceanography* 79, 167-176.
- Echevin, V., Colas, F., Chaigneau, A., Penven, P., 2011. Sensitivity of the Northern Humboldt Current System nearshore modeled circulation to initial and boundary conditions. *Journal of Geophysical Research* 116, C07002, 1-16.
- Egbert, G.D., Ray, R.D., Bills, B.G., 2004. Numerical modeling of the global semidiurnal tide in the present day and in the last glacial maximum. *Journal of Geophysical Research* 109, 2156-2202.
- Ehlert, C., Grasse, P., Frank, M., 2013. Changes in silicate utilisation and upwelling intensity off Peru since the Last Glacial Maximum – insights from silicon and neodymium isotopes. *Quaternary Science Reviews* 72, 18-35.
- EPICA Community Members, 2006. One-to-one coupling of glacial climate variability in Greenland and Antarctica. *Nature* 444, 195-198.

References

- Erdem, Z., Schönfeld, J., Glock, N., Dengler, M., Mosch, T., Sommer, S., Elger, J., Eisenhauer, A., 2016. Peruvian sediments as recorders of an evolving hiatus for the last 22 thousand years. *Quaternary Science Reviews* 137, 1-14.
- Fiedler, P.C., Talley, L.D., 2006. Hydrography of the eastern tropical Pacific: A review. *Progress in Oceanography* 69, 143-180.
- Figueroa, S., Marchant, M., Giglio, S., Ramirez, M., 2005. Foraminiferos bentonicos rotalinidos del centro sur de Chile (36°S-44°S). *Gayana* 69, 329-363.
- Fofonoff, N.P., 1985. Physical properties of seawater: a new salinity scale and equation of state for seawater. *Journal of geophysical Research-oceans* 90, 3332-3342.
- Föllmi, K.B., 1996. The phosphorus cycle, phosphogenesis and marine phosphate-rich deposits. *Earth Sciences Review* 40, 55-124.
- Föllmi, K.B., Hofmann, H., Chiaradia, M., de Kaenel, E., Frijia, G., Parente, M., 2015. Miocene phosphate-rich sediments in Salento (southern Italy). *Sedimentary Geology* 327, 55-71.
- Fontanier, C., Duros, P., Toyofuku, T., Oguri, K., Koho, K.A., Buscail, R., Grémare, A., Radakovitch, O., Deflandre, B., Nooijer, L.J.D., Bichon, S., Goubet, S., Ivanovsky, A., Chabaud, G., Menniti, C., Reichart, G.-J., Kitazato, H., 2014. Living (stained) deep-sea foraminifera off Hachinohe (NE Japan, western Pacific): environmental interplay in oxygen-depleted ecosystems *Journal of Foraminiferal Research* 44, 281-299.
- Fontanier, C., Jorissen, F.J., Chaillou, G., David, C., Anschutz, P., Lafon, V., 2003. Seasonal and interannual variability of benthic foraminiferal faunas at 550m depth in the Bay of Biscay. *Deep Sea Research Part I: Oceanographic Research Papers* 50, 457-494.
- Froelich, P.N., Arthur, M.A., Burnett, W.C., Deakin, M., Hensley, V., Jahnke, R., Kaul, L., Kim, K.-H., Roe, K., Soutar, A., Vathakanon, C., 1988. Early diagenesis of organic matter in Peru continental margin sediments: Phosphorite precipitation. *Marine Geology* 80, 309-343.
- Fuenzalida, R., Schneider, W., Garcés-Vargas, J., Bravo, L., Lange, C., 2009. Vertical and horizontal extension of the oxygen minimum zone in the eastern South Pacific Ocean. *Deep Sea Research Part II: Topical Studies in Oceanography* 56, 992-1003.
- Garrison, R.E., Kastner, M., 1990. Phosphatic sediments and rocks recovered from the Peru margin during ODP Leg 112, in: Suess, E., Von Huene, R., al., e. (Eds.), *Proceedings of the Ocean Drilling Program: Scientific Results*. Ocean Drilling Program, College Station, TX, pp. 111-134.
- Gayen, B., Sarkar, S., 2011. Direct and large-eddy simulations of internal tide generation at a near-critical slope. *Journal of Fluid Mechanics* 681, 48-79.
- Gerkema, T., Zimmerman, J.T.F., 1995. Generation of nonlinear internal tides and solitary waves. *Journal of Physical Oceanography* 25, 1081-1094.
- Geslin, E., Heinz, P., Jorissen, F., Hemleben, C., 2004. Migratory responses of deep-sea benthic foraminifera to variable oxygen conditions: laboratory investigations. *Marine Micropaleontology* 53, 227-243.

References

- Glenn, C.R., Arthur, M.A., 1988. Petrology and major element geochemistry of Peru margin phosphorites and associated diagenetic minerals: authigenesis in modern organic-rich sediments. *Marine Geology* 80, 231-267.
- Glock, N., 2011. Benthic foraminifera as geochemical and micropaleontological proxies for redox conditions in the Peruvian oxygen minimum zone. Christian-Albrechts-Universität zu Kiel, Kiel, p. 121.
- Glock, N., Eisenhauer, A., Liebetrau, V., Wiedenbeck, M., Hensen, C., Nehrke, G., 2012a. EMP and SIMS studies on Mn/Ca and Fe/Ca systematics in benthic foraminifera from the Peruvian OMZ: a contribution to the identification of potential redox proxies and the impact of cleaning protocols. *Biogeosciences* 9, 341-359.
- Glock, N., Eisenhauer, A., Milker, Y., Liebetrau, V., Schönfeld, J., Mallon, J., Sommer, S., Hensen, C., 2011. Environmental Influences on the Pore Density of *Bolivina spissa* (Cushman). *The Journal of Foraminiferal Research* 41, 22-32.
- Glock, N., Schönfeld, J., Mallon, J., 2012b. Functionality of pores in benthic foraminifera and bottom water oxygen, in: al., A.e. (Ed.), *Anoxia. Evidence for Eukaryote Survival and Paleontological Strategies*, Springer, pp. 537-552.
- Glud, R.N., Thamdrup, B., Stahl, H., Wenzhoefer, F., Glud, A., Nomaki, H., Oguri, K., Revsbech, N.P., Kitazato, H., 2009. Nitrogen cycling in a deep ocean margin sediment (Sagami Bay, Japan). *Limnol. Oceanogr* 54, 723-734.
- Golik, A., Phleger, F.B., 1977. Benthonic foraminifera from the Gulf of Panama. *The Journal of Foraminiferal Research* 7, 83-99.
- Gooday, A.J., 1988. A response by benthic Foraminifera to the deposition of phytodetritus in the deep sea. *Nature* 332, 70-73.
- Gooday, A.J., 1993. Deep-sea benthic foraminiferal species which exploit phytodetritus: characteristic features and controls on distribution. *Marine Micropaleontology* 22, 187-205.
- Gooday, A.J., 2003. Benthic foraminifera (Protista) as tools in deep-water palaeoceanography: environmental influences on faunal characteristics. *Advances in Marine Biology* 46, 1-90.
- Gooday, A.J., Bernhard, J.M., Levin, L.A., Suhr, S.B., 2000. Foraminifera in the Arabian Sea oxygen minimum zone and other oxygen-deficient settings: taxonomic composition, diversity, and relation to metazoan faunas. *Deep-Sea Research II* 47, 25-54.
- Gooday, A.J., Jorissen, F.J., 2012. Benthic Foraminiferal Biogeography: Controls on Global Distribution Patterns in Deep-Water Settings. *Annual Review of Marine Science* 4, 237-262.
- Gooday, A.J., Lambshead, P.J.D., 1989. Influence of seasonally deposited phytodetritus on benthic foraminiferal populations in the bathyal northeast Atlantic: the species response *Marine Ecology Progress Series* 58, 53-67.

References

- Gooday, A.J., Rathburn, A.E., 1999. Temporal variability in living deep-sea benthic foraminifera: a review. *Earth-Science Reviews* 46, 187-212.
- Gunther, E.R., 1936. A report on oceanographical investigations in Peru coastal current. *Discovery reports* 13, 107-276.
- Gupta, A.K., Thomas, E., 2003. Initiation of Northern Hemisphere glaciation and strengthening of the northeast Indian monsoon: Ocean Drilling Program Site 758, eastern equatorial Indian Ocean. *Geology* 31, 47-50.
- Gutiérrez, D., Sifeddine, A., Field, D., Ortlieb, L., Vargas, G., Chávez, F.P., Velazco, F., Ferreira, V., Tapia, P., Salvattecí, R., Boucher H., Morales, M.C., Valdés, J., Reyss, J.L., Campusano, A., Boussafir M., Mandeng-Yogo, M., García, M., Baumgartner T., 2009. Rapid reorganization in ocean biogeochemistry off Peru towards the end of the Little Ice Age. *Biogeosciences* 6, 835-848.
- Gutiérrez, D., Sifeddine, A., Reyss, J.L., Vargas, G., Velazco, F., Salvattecí, R., Ferreira, V., Ortlieb, L., Field, D., T., B., M., B., H., B., Valdés, J., Marinovic, L., Soler, P., Tapia, P., 2006. Anoxic sediments off Central Peru record interannual to multidecadal changes of climate and upwelling ecosystem during the last two centuries. *Advances Geoscience* 6, 119-125.
- Heinze, P.-M., Wefer, G., 1992. The history of coastal upwelling off Peru (11°S, ODP Leg 112, Site 680B) over the past 650 000 years, *Geological Society Special Publications*. Geological Society, London, pp. 451-462.
- Helly, J.J., Levin, L.A., 2004. Global distribution of naturally occurring marine hypoxia on continental margins. *Deep Sea Research Part I: Oceanographic Research Papers* 51, 1159-1168.
- Hendy, I.L., Pedersen, T.F., 2006. Oxygen minimum zone expansion in the eastern tropical North Pacific during deglaciation. *Geophysical Research Letters* 33, L20602, 1-5.
- Henrichs, S.M., Farrington, J.W., 1984. Peru upwelling region sediments near 15°S. 1. Remineralization and accumulation of organic matter. *Limnol. Oceanogr* 29, 1-19.
- Hermelin, J.O.R., Shimmield, G.B., 1990. The importance of the oxygen minimum zone and sediment geochemistry in the distribution of Recent benthic foraminifera in the northwest Indian Ocean. *Marine Geology* 91, 1-29.
- Hill, A.E., Hickey, B.M., Shillington, F.A., Strub, P.T., Brink, K.H., Barton, E.D., Thomas, A.C., 1998. Eastern ocean boundaries Coastal segment (E), in: Robinson, A.R., Brink, K.H. (Eds.), *The Sea*, pp. 29-67.
- Holloway, P.E., 1985. A comparison of semidiurnal internal tides from different bathymetric locations on the Australian north-west shelf. *Journal of Physical Oceanography* 15, 240-251.
- Hosegood, P., van Haren, H., 2004. Near-bed solibores over the continental slope in the Faeroe-Shetland Channel. *Deep Sea Research Part II: Topical Studies in Oceanography* 51, 2943-2971.

References

- Huyer, A., Knoll, M., Paluszkiwicz, T., Smith, R.L., 1991. The Peru Undercurrent: a study in variability. *Deep Sea Research Part A. Oceanographic Research Papers* 38, S247-S271.
- Ingle, J.C., Keller, G., Kolpack, R.L., 1980. Benthic foraminiferal biofacies, sediments and water masses of the southern Peru-Chile Trench area, southeastern Pacific Ocean. *Micropaleontology* 26, 113-150.
- Jaccard, S.L., Galbraith, E.D., 2012. Large climate-driven changes of oceanic oxygen concentrations during the last deglaciation. *Nature Geoscience* 5, 151-156.
- Jaccard, S.L., Galbraith, E.D., Froelicher, T.L., Gruber, N., 2014. Ocean (De)oxygenation across the last deglaciation. *Oceanography* 27, 26 - 35.
- Jackson, C., 2007. Internal wave detection using the Moderate Resolution Imaging Spectroradiometer (MODIS). *Journal of Geophysical Research* 112, C11012, 1-13.
- Jannink, N.T., Zachariasse, W.J., Zwaan, G.J.V.d., 1998. Living (Rose Bengal stained) benthic foraminifera from the Pakistan continental margin (northern Arabian Sea). *Deep Sea Research Part I: Oceanographic Research Papers* 45, 1483-1513.
- Jorissen, F.J., Fontanier, C., Thomas, E., 2007. Chapter Seven Paleooceanographical Proxies Based on Deep-Sea Benthic Foraminiferal Assemblage Characteristics. 1, 263-325.
- Jorissen, F.J., Stigter, H.C.d., Widmark, J.G.V., 1995. A conceptual model explaining benthic foraminiferal microhabitats. *Marine Micropaleontology* 26, 3-15.
- Junium, C.K., Arthur, M.A., Freeman, K.H., 2015. Compound-specific $\delta^{15}\text{N}$ and chlorin preservation in surface sediments of the Peru Margin with implications for ancient bulk $\delta^{15}\text{N}$ records. *Geochimica et Cosmochimica Acta* 160, 306-318.
- Kaiho, K., 1994. Benthic foraminiferal dissolved-oxygen index and dissolved-oxygen levels in the modern ocean. *Geology* 22, 719-722.
- Kaiho, K., 1999. Effect of organic carbon flux and dissolved oxygen on the benthic foraminiferal oxygen index (BFOI). *Marine Micropaleontology* 37, 67-76.
- Kamykowski, D., Zentara, S.-J., 1990. Hypoxia in the world ocean as recorded in the historical data set. *Deep-Sea Research* 37, 1861-1874.
- Karnauskas, K.B., Murtugudde, R., Busalacchi, A.J., 2007. The Effect of the Galápagos Islands on the Equatorial Pacific Cold Tongue. *Journal of Physical Oceanography* 37, 1266-1281.
- Karstensen, J., Stramma, L., Visbeck, M., 2008. Oxygen minimum zones in the eastern tropical Atlantic and Pacific oceans. *Progress in Oceanography* 77, 331-350.
- Keefer, D.K., Moseley, M.E., deFrance, S.D., 2003. A 38 000-year record of floods and debris flows in the Ilo region of southern Peru and its relation to El Niño events and great earthquakes. *Palaeogeography, Palaeoclimatology, Palaeoecology* 194, 41-77.
- Kennedy, W.J., Garrison, R.E., 1975. Morphology and genesis of nodular phosphates in the Cenomanian Glauconitic Marl of South-East England. *Lethaia* 8, 339-360.

References

- Kessler, W.S., 2006. The circulation of the eastern tropical Pacific: A review. *Progress in Oceanography* 69, 181-217.
- Khusid, T.A., 1974. Distribution of benthic foraminifers off west coast of South America. *Oceanology-USSR* 14, 900-904.
- Kim, K.H., Burnett, W.C., 1988. Accumulation and biological mixing of Peru margin sediments. *Marine Geology* 80, 181-194.
- Klymak, J.M., Alford, M.H., Pinkel, R., Lien, R.C., Yang, Y.J., Tang, T.Y., 2011. The breaking and scattering of the internal tide on a continental slope. *Journal of Physical Oceanography* 41, 926-945.
- Koho, K.A., de Nooijer, L.J., Reichart, G.J., 2015. Combining benthic foraminiferal ecology and shell Mn/Ca to deconvolve past bottom water oxygenation and paleoproductivity. *Geochimica et Cosmochimica Acta* 165, 294-306.
- Koho, K.A., García, R., de Stigter, H.C., Epping, E., Koning, E., Kouwenhoven, T.J., van der Zwaan, G.J., 2008. Sedimentary labile organic carbon and pore water redox control on species distribution of benthic foraminifera: A case study from Lisbon–Setúbal Canyon (southern Portugal). *Progress in Oceanography* 79, 55-82.
- Koho, K.A., Piña-Ochoa, E., 2012. Benthic foraminifera: inhabitants of low-oxygen environments, in: Al., A.V.A.e. (Ed.), *Anoxia Evidence for Eukaryote Survival and Paleontological Strategies*. Springer, pp. 251-285.
- Koide, M., Goldber, E.D., 1982. Transuranic nuclides in two coastal marine sediments off Peru. *Earth and Planetary Science Letters* 57, 263-277.
- Koutavas, A., Joanides, S., 2012. El Niño-Southern Oscillation extrema in the Holocene and Last Glacial Maximum. *Paleoceanography* 27, PA4208, 1-15.
- Krissek, L.A., Scheidegger, K.F., 1983. Environmental controls on sediments texture and composition in low oxygen zones off Peru and Oregon, in: Tiede, J., Suess, E. (Eds.), *Coastal upwelling, Pt. B, its sediment record*, pp. 163-180.
- Krissek, L.A., Scheidegger, K.F., Kulm, L.D., 1980. Surface sediments of the Peru-Chile continental margin and the Nazca plate. *Geological Society of America Bulletin* 91, 321.
- Kuhnt, T., Friedrich, O., Schmiedl, G., Milker, Y., Mackensen, A., Lückge, A., 2013. Relationship between pore density in benthic foraminifera and bottom-water oxygen content. *Deep Sea Research Part I: Oceanographic Research Papers* 76, 85-95.
- Lamb, K.G., 2014. Internal Wave Breaking and Dissipation Mechanisms on the Continental Slope/Shelf. *Annual Review of Fluid Mechanics* 46, 231-254.
- Leiter, C., Altenbach, A.V., 2010. Benthic Foraminifera From The Diatomaceous Mud Belt Off Namibia: Characteristic Species For Severe Anoxia. *Palaeontologia Electronica* 13, 1-19.
- Levin, L., Gutiérrez, D., Rathburn, A., Neira, C., Sellanes, J., Munoz, P., Gallardo, V., Salamanca, M., 2002. Benthic processes on the Peru margin: a transect across the oxygen minimum zone during the 1997-98 El Niño. *Progress in Oceanography* 53, 1-27.

References

- Levin, L.A., 2003. Oxygen Minimum Zone Benthos: Adaptation and Community Response to Hypoxia, in: Gibson, R.N., Atkinson, R.J.A. (Eds.), *Oceanography and Marine Biology: An Annual Review*. Taylor & Francis London, pp. 1-45.
- Lisiecki, L.E., Raymo, M.E., 2005. A Pliocene-Pleistocene stack of 57 globally distributed benthic $\delta^{18}\text{O}$ records. *Paleoceanography* 20, PA1003, 1-17.
- Loeblich, A.R., Tappan, H., 1988. *Foraminiferal Genera and Their Classification*. Van Nostrand Reinhold, New York.
- Loubere, P., 1994. Quantitative estimation of surface ocean productivity and bottom water oxygen concentration using benthic foraminifera. *Paleoceanography* 9, 723-735.
- Loubere, P., 1996. Surface ocean productivity and bottom water oxygen signals in deep water benthic foraminiferal assemblages. *Marine Micropaleontology* 28, 247-261.
- Loubere, P., Gary, A., Lagoe, M., 1993. Sea-bed biogeochemistry and benthic foraminiferal bathymetric zonation on the slope of the N.W. Gulf of Mexico. *Palaios* 8, 439-449.
- Lutze, G.F., Coulbourn, W.T., 1984. Recent benthic foraminifera from the continental margin of northwest Africa: Community structure and distribution. *Marine Micropaleontology* 8, 361-401.
- Mackensen, A., Douglas, R.G., 1989. Down-core distribution of live and dead deep-water benthic foraminifera in box cores from the Weddell Sea and the California continental borderland. *Deep Sea Research Part A. Oceanographic Research Papers* 36, 879-900.
- Mackensen, A., Grobe, H., Kuhn, G., Fütterer, D.K., 1990. Benthic foraminiferal assemblages from the eastern Weddell Sea between 68 and 73°S: Distribution, ecology and fossilization potential. *Marine Micropaleontology* 16, 241-283.
- Mallon, J., 2012. Benthic foraminifera of the Peruvian and Ecuadorian continental margin. *Christian-Albrechts-Universität zu Kiel*, Kiel, p. 279.
- Mallon, J., Glock, N., Schönfeld, J., 2012. The response of benthic foraminifera to low-oxygen conditions of the Peruvian oxygen minimum zone, in: al., A.V.A.e. (Ed.), *Anoxia: Evidence for Eukaryote Survival and Paleontological Strategies*. Springer, pp. 305-321.
- Manheim, F., Rowe, G.T., Jipa, D., 1975. Marine Phosphorite Formation off Peru. *Journal of Sedimentary Petrology* 45, 243-251.
- Marchitto, T.M., Lehman, S.J., Ortiz, J., Fluck, J., Van Geen, A., 2007. Marine radiocarbon evidence for the mechanism of deglacial atmospheric CO_2 rise. *Science* 316, 1456-1459.
- Martin, J.H., Knauer, G.A., Karl, D.M., Broenkow, W.W., 1987. VERTEX: carbon cycling in the northeast Pacific. *Deep Sea Research* 34, 267-283.
- Martini, K.I., Alford, M.H., Kunze, E., Kelly, S.M., Nash, J.D., 2013. Internal Bores and Breaking Internal Tides on the Oregon Continental Slope. *Journal of Physical Oceanography* 43, 120-139.
- McCaffrey, M.A., Farrington, J.W., Repera, D.J., 1990. The organic geochemistry of Peru margin surface sediments: I. A comparison of the C37 alkenone and historical El Niño records. *Geochimica et Cosmochimica Acta* 54, 1671-1682.

References

- McKay, C.L., Filipsson, H.L., Romero, O.E., Stuut, J.-B.W., Donner, B., 2014. Pelagic-benthic coupling within an upwelling system of the subtropical northeast Atlantic over the last 35 ka BP. *Quaternary Science Reviews* 106, 299-315.
- McKay, C.L., Groeneveld, J., Filipsson, H.L., Gallego-Torres, D., Whitehouse, M.J., Toyofuku, T., Romero, O.E., 2015. A comparison of benthic foraminiferal Mn / Ca and sedimentary Mn / Al as proxies of relative bottom-water oxygenation in the low-latitude NE Atlantic upwelling system. *Biogeosciences* 12, 5415-5428.
- Moffitt, S.E., Hill, T.M., Ohkushi, K., Kennett, J.P., Behl, R.J., 2014. Vertical oxygen minimum zone oscillations since 20 ka in Santa Barbara Basin: A benthic foraminiferal community perspective. *Paleoceanography* 29, 44-57.
- Moffitt, S.E., Moffitt, R.A., Sauthoff, W., Davis, C.V., Hewett, K., Hill, T.M., 2015. Paleoceanographic Insights on Recent Oxygen Minimum Zone Expansion: Lessons for Modern Oceanography. *PLoS ONE* 10, 1-44.
- Mohtadi, M., Hebbeln, D., Marchant, M., 2005. Upwelling and productivity along the Peru–Chile Current derived from faunal and isotopic compositions of planktic foraminifera in surface sediments. *Marine Geology* 216, 107-126.
- Mollier-Vogel, E., 2012. Peruvian Oxygen Minimum Zone dynamics during the last 18000 years. *Christian-Albrechts-Universität zu Kiel, Kiel*, p. 160.
- Mollier-Vogel, E., Leduc, G., Bösch, T., Martinez, P., Schneider, R.R., 2013. Rainfall response to orbital and millennial forcing in northern Peru over the last 18 ka. *Quaternary Science Reviews* 76, 29-38.
- Mollier-Vogel, E., Ryabenko, E., Martinez, P., Wallace, D., Altabet, M.A., Schneider, R., 2012. Nitrogen isotope gradients off Peru and Ecuador related to upwelling, productivity, nutrient uptake and oxygen deficiency. *Deep Sea Research Part I: Oceanographic Research Papers* 70, 14-25.
- Montes, I., Colas, F., Capet, X., Schneider, W., 2010. On the pathways of the equatorial subsurface currents in the eastern equatorial Pacific and their contributions to the Peru-Chile Undercurrent. *Journal of Geophysical Research* 115.
- Montes, I., Schneider, W., Colas, F., Blanke, B., Echevin, V., 2011. Subsurface connections in the eastern tropical Pacific during La Niña 1999–2001 and El Niño 2002–2003. *Journal of Geophysical Research* 116.
- Moodley, L., Zwaan, G.J.v.d., Herman, P.M.J., Kemper, L., Breugel, P.v., 1997. Differential response of benthic meiofauna to anoxia with special reference to Foraminifera (Protista: Sarcodina). *Marine Ecology Progress Series* 158, 151-163.
- Morales, M., Field, D., Mayor Pastor, S., Gutierrez, D., Sifeddine, A., Ortlieb, L., Ferreira, V., Salvatelli, R., Velasco, F., 2006. Variations in Foraminifera over the last 460 years from laminated sediments off the coast of Peru. *Boletín de la Sociedad Geológica del Perú* 101, 5-18.
- Mosch, T., Sommer, S., Dengler, M., Noffke, A., Bohlen, L., Pfannkuche, O., Liebetrau, V., Wallmann, K., 2012. Factors influencing the distribution of epibenthic megafauna across

References

- the Peruvian oxygen minimum zone. *Deep Sea Research Part I: Oceanographic Research Papers* 68, 123-135.
- Moy, C.M., Seltzer, G.O., Rodbell, D.T., Anderson, D.M., 2002. Variability of El Niño/Southern Oscillation activity at millennial timescales during the Holocene epoch. *Nature* 420, 162-165.
- Mullins, H.T., Thompson, J.B., McDougall, K., Vercoutere, T.L., 1985. Oxygen-minimum zone edge effects: evidence from the central California coastal upwelling system. *Geology* 13, 491-494.
- Muñoz, P., Lange, C.B., Gutiérrez, D., Hebbeln, D., Salamanca, M.A., Dezileau, L., Reyss, J.L., Benninger, L.K., 2004. Recent sedimentation and mass accumulation rates based on ²¹⁰Pb along the Peru–Chile continental margin. *Deep Sea Research Part II: Topical Studies in Oceanography* 51, 2523-2541.
- Muratli, J.M., Chase, Z., Mix, A.C., McManus, J., 2009. Increased glacial-age ventilation of the Chilean margin by Antarctic Intermediate Water. *Nature Geoscience* 3, 23-26.
- Murray, J.W., 2001. The niche of benthic foraminifera, critical thresholds and proxies. *Marine Micropaleontology* 41, 1-7.
- Murray, J.W., 2006. *Ecology and applications of benthic foraminifera*. Cambridge University Press.
- Natland, M.L., 1950. Report on the Pleistocene and Pliocene Foraminifera, 1940 E.W. Scripps Cruise to the Gulf of California. The Geological Society of America, New York, USA, p. 55.
- Neira, C., Sellanes, J., Levin, L.A., Arntz, W.E., 2001. Meiofaunal distributions on the Peru margin: relationship to oxygen and organic matter availability. *Deep-Sea Research II* 48, 2453–2472.
- Noffke, A., Hensen, C., Sommer, S., Scholz, F., Bohlen, L., Mosch, T., Graco, M., Wallmann, K., 2012. Benthic iron and phosphorus fluxes across the Peruvian oxygen minimum zone. *Limnology and Oceanography* 57, 851-867.
- Nomaki, H., Heinz, P., Nakatsuka, T., Shimanaga, M., Ohkouchi, N., Ogawa, N.O., Kogure, K., Ikemoto, E., Kitazato, H., 2006. Different ingestion patterns of ¹³C-labeled bacteria and algae by deep-sea benthic foraminifera. *Marine Ecology Progress Series* 310, 95-108.
- Nordberg, K., Gustafsson, M., Krantz, A.-L., 2000. Decreasing oxygen concentrations in the Gullmar Fjord, Sweden, as confirmed by benthic foraminifera, and the possible association with NAO. *Journal of Marine Systems* 23, 303-316.
- Nürnberg, D., Bösch, T., Doering, K., Mollier-Vogel, E., Raddatz, J., Schneider, R., 2015. Sea surface and subsurface circulation dynamics off equatorial Peru during the last~ 17 kyr. *Paleoceanography* 30, 984-999.
- Oberhansli, H., Heinze, P., Diester-Haass, L., Wefer, G., 1990. Upwelling off Peru during the last 430,000 yr and its relationship to the bottom-water environment, as deduced from coarse grain-size distributions and analyses of benthic foraminifera at holes 679D, 680B,

References

- and 681B, Leg 112, in: Suess, E., von Huene, R., al., e. (Eds.), Proceedings of the Ocean Drilling Program: Scientific results. Ocean Drilling Program, College Station, TX, pp. 369-390.
- Ohga, T., Kitazato, H., 1997. Seasonal changes in bathyal foraminiferal populations in response to the flux of organic matter (Sagami Bay, Japan). *Terra Nova* 9, 33-37.
- Paulmier, A., Ruiz-Pino, D., 2009. Oxygen minimum zones (OMZs) in the modern ocean. *Progress in Oceanography* 80, 113-128.
- Pawlowski, J., Holzmann, M., 2014. A plea for DNA barcoding of foraminifera. *The Journal of Foraminiferal Research* 44, 62-67.
- Pedersen, T.F., 1983. Increased productivity in the eastern equatorial Pacific during the last glacial maximum (19,000 to 14,000 yr B.P). *Geology* 11, 16-19.
- Pedersen, T.F., Pickering, M., Vogel, J.S., Southon, J.N., Nelson, D.E., 1988. The response of benthic foraminifera to productivity cycles in the eastern equatorial Pacific: Faunal and geochemical constraints on glacial bottom water oxygen levels. *Paleoceanography* 3, 157-168.
- Pennington, J.T., Mahoney, K.L., Kuwahara, V.S., Kolber, D.D., Calienes, R., Chavez, F.P., 2006. Primary production in the eastern tropical Pacific: A review. *Progress in Oceanography* 69, 285-317.
- Pfannkuche, O., Frank, M., Schneider, R., Stramma, L., 2011. Climate-biogeochemistry interactions in the tropical ocean of the SE-American oxygen minimum zone Cruise No. 77, Leg 1-4 October 22 2008 – February 18, 2009 Talcahuano (Chile) – Callao (Peru) – Colon (Panama), METEOR-Berichte 11-2. Institut für Meereskunde der Universität Hamburg.
- Phleger, F.B., Soutar, A., 1973. Production of benthic foraminifera in three east Pacific oxygen minima. *Micropaleontology*, 19, 1, 110-115.
- Piña-Ochoa, E., Hogslund, S., Geslin, E., Cedhagen, T., Revsbech, N.P., Nielsen, L.P., Schweizer, M., Jorissen, F., Rysgaard, S., Risgaard-Petersen, N., 2010. Widespread occurrence of nitrate storage and denitrification among Foraminifera and Gromiida. *Proc Natl Acad Sci U S A* 107, 1148-1153.
- Pomar, L., Morsilli, M., Hallock, P., Bádenas, B., 2012. Internal waves, an under-explored source of turbulence events in the sedimentary record. *Earth-Science Reviews* 111, 56-81.
- Praetorius, S.K., Mix, A.C., Walczak, M.H., Wolhowe, M.D., Addison, J.A., Prah, F.G., 2015. North Pacific deglacial hypoxic events linked to abrupt ocean warming. *Nature* 527, 362-366.
- Puig, P., Palanques A., Guillén, J., Khatib, M.E., 2004. Role of internal waves in the generation of nepheloid layers on the northwestern Alboran slope: implications for continental margin shaping. *Journal of Geophysical Research-Oceans* , C09011.

References

- Rathburn, A.E., Corliss, B.H., 1994. The ecology of living (stained) deep-sea benthic foraminifera from the Sulu Sea. *Paleoceanography* 9, 87-150.
- Rathburn, A.E., Perez, M.E., Lange, C.B., 2001. Benthic-pelagic coupling in The Southern California bight: Relationships between sinking organic material, diatoms and benthic foraminifera. *Marine Micropaleontology* 43, 261-271.
- Reimer, J., Bard, E., Bayliss, A., Beck, J.W., Blackwell, P.G., Ramsey, C.B., Buck, C.E., Cheng, H., Edwards, R.L., Friedrich, M., Grootes, P.M., Guilderson, T.P., Haflidason, H., Hajdas, I., Hatté, C., Heaton, T.J., Hoffmann, D.L., Hogg, A.G., Hughen, K.A., Kaiser, K.F., Kromer, B., Manning, S.W., Niu, M., Reimer, R.W., Richards, D.A., Scott, E.M., Southon, J.R., Staff, R.A., Turney, C.S.M. and van der Plicht, J., 2013. INTCAL13 and Marine radiocarbon age calibration curves 0-50,000 years cal BP. *Radiocarbon* 55, 1869–1887.
- Reimers, C.E., Jahnke, R.A., McCorkle, D.C., 1992. Carbon fluxes and burial rates over the continental slope and rise off central California with implications for the global carbon cycle *Global Biogeochemical Cycles* 6, 199-224.
- Reimers, C.E., Suess, E., 1983. Spatial and temporal patterns of organic matter accumulation on the Peru continental margin, in: Tiede, J., Suess, E. (Eds.), *Coastal upwelling, Pt. B, its sediment record*, pp. 311 - 336.
- Rein, B., 2004. A major Holocene ENSO anomaly during the Medieval period. *Geophysical Research Letters* 31, L17211, 1-4.
- Rein, B., Lückge, A., Reinhardt, L., Sirocko, F., Wolf, A., Dullo, W.-C., 2005. El Niño variability off Peru during the last 20,000 years. *Paleoceanography* 20, PA4003, 1-17.
- Reinhardt, L., Kudrass, H.-R., Lückge, A., Wiedicke, M., Wunderlich, J., Wendt, G., 2002. High-resolution sediment echosounding off Peru: Late Quaternary depositional sequences and sedimentary structures of a current-dominated shelf. *Marine Geophysical Researches* 23, 335-351.
- Resig, J.M., 1981. Biogeography of benthic foraminifera of the northern Nazca plate and adjacent continental margin. *Geological society of America Memoir* 154, 619-644.
- Resig, J.M., 1990. Benthic foraminiferal stratigraphy and paleoenvironments off Peru leg 112, in: Suess, E., Von Huene, R., al., e. (Eds.), *Proceedings of the Ocean Drilling Program, Scientific Results*. Ocean Drilling Program, College Station, TX, pp. 263-296.
- Risgaard-Petersen, N., Langezaal, A.M., Ingvarsen, S., Schmid, M.C., Jetten, M.S., Op den Camp, H.J., Derksen, J.W., Pina-Ochoa, E., Eriksson, S.P., Nielsen, L.P., Revsbech, N.P., Cedhagen, T., van der Zwaan, G.J., 2006. Evidence for complete denitrification in a benthic foraminifer. *Nature* 443, 93-96.
- Rodbell, D.T., 1999. An 15,000-Year Record of El Niño-Driven Alluviation in Southwestern Ecuador. *Science* 283, 516-520.
- Ryther, J.H., Menzel, D.W., Hulbert, E.M., Lorenzen, C.J., Corwin, N., 1971. The production and utilization of organic matter in the Peru coastal current. *Investigacion Pesquera* 35, 43-60.

References

- Salvatteci, R., 2013. Multi-decadal to millennial scale variability in Oxygen Minimum Zone intensity, export production and pelagic fish abundances from marine laminated sediments off Pisco, Peru during the last 25000 years. *l'Université Pierre et Marie Curie, France*, p. 258.
- Salvatteci, R., Gutierrez, D., Sifeddine, A., Ortlieb, L., Druffel, E., Boussafir, M., Schneider, R., 2016. Centennial to millennial-scale changes in oxygenation and productivity in the Eastern Tropical South Pacific during the last 25,000 years. *Quaternary Science Reviews* 131, 102-117.
- Sarkar, S., Gupta, A.K., 2014. Late Quaternary productivity changes in the equatorial Indian Ocean (ODP Hole 716A). *Palaeogeography, Palaeoclimatology, Palaeoecology* 397, 7-19.
- Schafstall, J., Dengler, M., Brandt, P., Bange, H., 2010. Tidel-induced mixing and diapycnal nutrient fluxes in the Mauritanian upwelling region. *Journal of geophysical Research-oceans* 115, C10014.
- Schmiedl, G., Mackensen, A., Müller, P.J., 1997. Recent benthic foraminifera from the eastern South Atlantic Ocean: dependence on food supply and water masses. *Marine Micropaleontology* 32, 249-287.
- Schmiedl, G., Mitschke, A., Beck, S., Emeis, K.-C., Hemleben, C., Schulz, H., Sperling, M., Weldeab, S., 2003. Benthic foraminiferal record of ecosystem variability in the eastern Mediterranean Sea during times of sapropel S5 and S6 deposition. *Palaeogeography, Palaeoclimatology, Palaeoecology* 190, 139-164.
- Scholz, F., Hensen, C., Noffke, A., Rohde, A., Liebetrau, V., Wallmann, K., 2011. Early diagenesis of redox-sensitive trace metals in the Peru upwelling area – response to ENSO-related oxygen fluctuations in the water column. *Geochimica et Cosmochimica Acta* 75, 7257-7276.
- Scholz, F., McManus, J., Mix, A.C., Hensen, C., Schneider, R.R., 2014. The impact of ocean deoxygenation on iron release from continental margin sediments. *Nature Geoscience* 7, 433-437.
- Schönfeld, J., 2001. Benthic foraminifera and pore-water oxygen profiles: a re-assessment of species boundary conditions at the western Iberian Margin *Journal of Foraminiferal Research* 31, 86-107.
- Schönfeld, J., 2006. Taxonomy and distribution of the *Uvigerina peregrina* plexus in the tropical to northeastern Atlantic. *The Journal of Foraminiferal Research* 36, 355-367.
- Schönfeld, J., Altenbach, A.V., 2005. Late Glacial to Recent distribution pattern of deep-water *Uvigerina* species in the north-eastern Atlantic. *Marine Micropaleontology* 57, 1-24.
- Schönfeld, J., Kuhnt, W., Erdem, Z., Flögel, S., Glock, N., Aquit, M., Frank, M., Holbourn, A., 2015. Records of past mid-depth ventilation: Cretaceous ocean anoxic event 2 vs. Recent oxygen minimum zones. *Biogeosciences* 12, 1169-1189.

References

- Schönfeld, J., Spiegler, D., 1995. Benthic foraminiferal biostratigraphy of Site 861, Chile triple junction, Southeastern Pacific, in: Lewis, S.D., Behrmann, J.H., Musgrave, R.J., Cande, S.C. (Eds.), *Proceedings of the Ocean Drilling Program, Scientific Results*, pp. 213-221.
- Schrader, H., 1992. Coastal upwelling and atmospheric CO₂ changes over the last 400,000 years: Peru. *Marine Geology* 107, 239-248.
- Schröder, C.J., 1988. Subsurface Preservation of Agglutinated Foraminifera in the Northwest Atlantic Ocean. *Abh. Geol. B.-A.* 41, 325-336.
- Schumacher, S., Jorissen, F.J., Dissard, D., Larkin, K.E., Gooday, A.J., 2007. Live (Rose Bengal stained) and dead benthic foraminifera from the oxygen minimum zone of the Pakistan continental margin (Arabian Sea). *Marine Micropaleontology* 62, 45-73.
- Seibel, B.A., 2011. Critical oxygen levels and metabolic suppression in oceanic oxygen minimum zones *Journal of Experimental Biology* 214, 326-336.
- Sen Gupta, B.K., Machain-Castillo, M.L., 1993. Benthic foraminifera in oxygen-poor habitats. *Marine Micropaleontology* 20, 183 - 201.
- Shaffer, G., 1982. On the upwelling circulation over the wide shelf off Peru: 1.Circulation. *Journal of Marine Research* 40, 293-314.
- Shanmugam, G., 2013. Comment on “Internal waves, an under-explored source of turbulence events in the sedimentary record” by L. Pomar, M. Morsilli, P. Hallock, and B. Bádenas [*Earth-Science Reviews*, 111 (2012), 56–81]. *Earth-Science Reviews* 116, 195-205.
- Siebert, C., McManus, J., Bice, A., Poulson, R.L., Berelson, W.M., 2006. Molybdenum isotope signatures in continental margin marine sediments. *Earth and Planetary Science Letters* 241, 723-733.
- Siebert, C., Nägler, T.F., von Blackenburg, F., Kramers, J.D., 2003. Molybdenum isotope records as a potential new proxy for paleoceanography *Earth and Planetary Science Letters* 211, 159-171.
- Sifeddine, A., Gutiérrez, D., Ortlieb, L., Boucher, H., Velazco, F., Field, D., Vargas, G., Boussafir, M., Salvattecchi, R., Ferreira, V., García, M., Valdés, J., Caquineau, S., Mandeng Yogo, M., Cetin, F., Solis, J., Soler, P., Baumgartner, T., 2008. Laminated sediments from the central Peruvian continental slope: A 500 year record of upwelling system productivity, terrestrial runoff and redox conditions. *Progress in Oceanography* 79, 190-197.
- Silva, K.A., Corliss, B.H., Rathburn, A.E., Thunell, R.C., 1996. Temporal variation in benthic foraminifera in the San Pedro Basin (California Borderland). *Journal of Foraminifera research* 26, 71-93.
- Skilbeck, C.G., Fink, D., 2006. Data Report: Radiocarbon dating and sedimentation rates for Holocene-Upper Pleistocene sediments, Eastern Equatorial Pacific and Peru continental margin, in: Jørgensen, B.B., D'Hondt, S.L., Müller, D.J. (Eds.), *Proceedings of the Ocean Drilling Program, Scientific Results*, pp. 1-15.

References

- Sloyan, B.M., Rintoul, S.R., 2001. Circulation, renewal, and modification of Antarctic mode and intermediate water*. *Journal of Physical Oceanography* 31, 1005-1030.
- Smart, C.W., King, S.C., Gooday, A.J., Murray, J.W., Thomas, E., 1994. A benthic foraminiferal proxy of pulsed organic matter paleofluxes. *Marine Micropaleontology* 23, 89-99.
- Smith, P.B., 1964. Ecology of benthonic species. Geological Survey Professional Paper, Washington.
- Sommer, S., Dengler, M., Treude, T., 2014. Benthic element cycling, fluxes and transport of solutes across the benthic boundary layer in the Peruvian oxygen minimum zone, (SFB754) – Cruise No. M92 – January 05 – February 03, 2013 – Callao (Peru) – Callao (Peru), Meteor-Berichte, M92, DFG-Senatskommission für Ozeanographie, p. 55.
- Soudry, D., Glenn, C.R., Nathan, Y., Segal, I., Vonderhaar, D., 2006. Evolution of Tethyan phosphogenesis along the northern edges of the Arabian–African shield during the Cretaceous–Eocene as deduced from temporal variations of Ca and Nd isotopes and rates of P accumulation. *Earth-Sea Rev.* 78, 27-57.
- Stramma, L., Johnson, G.C., Firing, E., Schmidtko, S., 2010. Eastern Pacific oxygen minimum zones: Supply paths and multidecadal changes. *Journal of Geophysical Research* 115, C09011, 1-12.
- Stramma, L., Johnson, G.C., Sprintall, J., Mohrholz, V., 2008. Expanding Oxygen-Minimum Zones in the Tropical Oceans. *Science* 320, 655-658.
- Strub, P.T., Mesias, J.M., James, C., 1995. Altimeter observations of the Peru-Chile countercurrent. *Geophysical research letters* 22, 211-214.
- Strub, P.T., Mesías, J.M., Montecino, V., Rutllant, J., Salinas, S., 1998. Coastal ocean circulation off western South America, in: Robinson, A.R., Brink, K.H. (Eds.), *The Sea*. J. Wiley and Sons, New York, pp. 273-314.
- Stuiver, M., Reimer, P.J., 1993. Extended ¹⁴C data base and revised Calib 3.0 ¹⁴C age calibration program. *Radiocarbon* 35, 215-230.
- Suess, E., Kulm, L.D., Killingley, J.S., 1987. Coastal upwelling and a history of organic-rich mudstone deposition off Peru, in: Brooks, J., Fleet, A.J. (Eds.), *Marine Petroleum Source Rocks*. Geological Society, pp. 181-196.
- Tapia, R., Lange, C.B., Marchant, M., 2008. Living (stained) calcareous benthic foraminifera from recent sediments off Concepción, central-southern Chile (~36° S). *Revista Chilena de Historia Natural* 81, 403-416.
- Thomas, M., Sündermann, J., 1999. Tides and tidal torques of the world since the last Glacial Maximum. *Journal of geophysical Research-oceans* 104, 3159-2184.
- Tsuchiya, M., Talley, L.D., 1996. Water-property distributions along an eastern Pacific hydrographic section at 135°W. *Journal of Marine Research* 54, 541-564.
- Uchio, T., 1960. Ecology of living benthonic Foraminifera from the San Diego, California area. *Cushman Foundation Foraminifera Research Special Publications* 5, 1-72.

References

- Van Andel, T.H., Heath, G.R., Moore, T.C., 1975. Cenozoic history and paleoceanography of the central equatorial Pacific. Geol. Soc. Am. Mem 143.
- Van der Zwaan, G.J., Duijnste, I.A.P., Jannink, N.T., den Dulk, M., Kouwenhoven, T.J., 1999. Benthic foraminifers: proxies or problems? A review of paleoecological concepts. Earth-Science Reviews 46, 213-236.
- Veeh, H.H., Burnett, W.C., Soutar, A., 1973. Contemporary phosphorites on the continental margin of Peru. Science 181, 844-845.
- Vismara Schilling, A., Parisi, E., 1981. *Anomalinoidea minimus*, a new benthic foraminiferal species from Pleistocene and Holocene deep sea deposits of the Mediterranean Sea. Riv. Ital. Pal. Stratigr. 87, 284-286.
- Wefer, G., Heinze, P., Suess, E., 1990. Stratigraphy and sedimentation rates from oxygen isotope composition, organic carbon content, and grain size distribution at the Peru upwelling region: Holes 680B and 686B, in: Suess, E., von Huene, R., al., e. (Eds.), Proceedings of the Ocean Drilling Program: Scientific Results. Ocean Drilling Program, College Station, TX, pp. 355-367.
- Wetzel, M.A., Fleeger, J.W., Powers, S.P., 2001. Effects of hypoxia and anoxia on meiofauna: a review with new data from the Gulf of Mexico. Coast. Est. Stud. 58, 165-184.
- Whittaker, J., 1988. Benthic Cenozoic Foraminifera from Ecuador. British Museum (Natural History), London.
- Wilmes, S.B., Green, J.A.M., 2014. The evolution of tides and tidal dissipation over the past 21,000 years. Journal of geophysical Research-oceans 119, 4083-4100.
- Wolf, A., 2002. Zeitliche Variationen im peruanischen Küstenauftrieb seit dem Letzten Glazialen Maximum – Steuerung durch globale Klimadynamik. University of Kiel, Kiel, p. 88.
- Wyrski, K., 1962. The oxygen minima in relation to ocean circulation. Deep Sea Research 9, 11-23.
- Wyrski, K., 1965. Surface currents of the eastern tropical Pacific Ocean. Inter-American Trop. Tuna Comm. Bulletin 4, 271-304.
- Wyrski, K., 1967. Circulation and Water Masses in the Eastern Equatorial Pacific Ocean. International Journal of Oceanology and Limnology 1, 117-147.
- Wyrski, K., Wenzel, J., 1984. Possible gyre-gyre interaction in the Pacific Ocean. Nature 309, 538-540.
- Zalesny, E.R., 1959. Foraminiferal Ecology of Santa Monica Bay, California. Micropaleontology 5, 101-126.

APPENDIX

- 1) Tables for downcore data of the sediment cores
- 2) Supplementary information of Chapter 3
- 3) Benthic foraminifera taxonomy reference list including plates 1-7
- 4) Tables for downcore benthic foraminifera distributions; species protocols
- 5) Supplementary information of Chapter 5

Appendix 1: Downcore data of the sediment cores

Core M77/2-52-2

Depth [cm]	Age [yrs]	>63 μm [w %]	$\delta^{13}\text{C}$ [‰]	$\delta^{18}\text{O}$ [‰]	AR_{bulk} [g/cm ² /ka]	Corg [%]	CaCO_3 [%]	TN [%]
10	271	1.176	-0.07	3.266	16.92	2.918	1.779	0.369
20	629	1.308	-0.24	3.305	13.59	2.644	1.975	0.331
30	986	1.076	-0.26	3.178	13.66	2.460	2.946	0.318
40	1343	1.228	-0.23	3.15	13.90			
50	1701	1.522	-0.25	3.083	14.44	2.766	1.450	0.332
60	2058	1.597	-0.04	3.408	14.37	2.591	1.992	0.322
70	2415	1.226	-0.33	3.364	14.61	2.740	1.000	0.320
80	2773	1.157	-0.12	3.372	14.96	2.756	2.067	0.335
90	3130	1.101	-0.07	3.226	15.38	2.610	1.967	0.320
110	3487	1.061	-0.24	3.205	15.56	2.655	2.321	0.328
120	3845	1.126	-0.14	3.258	14.80	2.459	2.812	0.305
130	4202	1.167	-0.19	3.239	15.46	2.665	2.421	0.321
140	4559	1.338	0.158	3.307	15.48	2.773	2.521	0.315
150	4917	1.411	-0.17	3.288	15.78	2.676	2.496	0.319
160	5274	0.755	-0.35	3.209	16.49	2.679	2.925	0.323
170	5631	1.435	-0.17	3.27	17.35	2.733	3.021	0.322
180	5989	1.127	-0.25	3.277	16.89	2.691	3.246	0.322
190	6346	1.023	-0.28	3.217	16.96	2.557	3.392	0.308
200	6703	1.205	-0.25	3.264	17.97	2.574	3.837	0.309
210	7061	1.504	-0.15	3.337	19.17	2.565	3.796	0.307
220	7418	2.006	-0.25	3.277	19.38	2.496	3.421	0.299
230	7775	1.761	-0.45	3.063	18.35	2.417	4.192	0.298
240	8097	1.810	-0.38	3.355	20.79	2.342	4.292	0.290
250	8486	1.753	-0.34	3.367	17.61	2.331	4.321	0.271
260	8839	1.757	-0.31	3.496	17.65	2.398	4.312	0.284
270	9192	1.775	-0.38	3.485	17.46	2.247	3.933	0.271
280	9546	1.701	-0.52	3.499	19.01	2.231	3.921	0.267
290	9899	2.171	-0.6	3.661	18.77	2.076	4.229	0.248
300	10252	1.706	-0.43	3.553	17.67	2.188	4.671	0.258
310	10606	1.719	-0.57	3.444	18.44	1.970	4.183	0.232
320	10959	1.876	-0.54	3.599	19.08	1.954	3.625	0.231
330	11277	2.289	-0.43	3.662	21.26	1.946	3.350	0.225
340	11787	1.524	-0.82	3.805	12.24	1.795	4.050	0.215
350	12250	1.433	-0.49	4.048	13.12	1.752	3.117	0.211
360	12714	1.254	-0.54	3.947	12.90	1.662	3.425	0.200
370	13177	1.975	-0.69	4.048	12.78	1.699	3.442	0.203
380	13641	1.864	-0.3	4.039	13.37	1.772	3.308	0.205
390	14143	2.184	-0.33	4.142	12.49	1.658	2.900	0.189
400	14645	2.684	-0.36	4.003	13.05	1.495	2.867	0.174
410	15147	2.225	-0.44	4.043	12.75	1.400	3.017	0.166
420	15649	3.864	-0.59	4.077	13.58	1.419	2.642	0.164
430	16151	1.597	-0.48	4.176	12.66	1.511	2.154	0.177
440	16653	1.308	-0.53	4.246	12.34	1.573	2.187	0.181
450	17155	1.004	-0.72	4.281	12.50	1.593	1.433	0.175
460	17657	2.250	-0.67	4.344	13.81	1.497	2.296	0.167
470	18160	1.898	-0.7	4.301	13.11	1.394	3.267	0.163
480	18662	3.337	-0.45	4.452	14.71	1.243	3.637	0.134
490	19164	4.035	-0.76	4.611	14.59	1.247	3.625	0.134
500	19666	3.803	-0.71	4.437	14.87	1.386	5.617	0.154
510	20168	6.206	-0.68	4.755	15.81	1.339	6.171	0.158
520	20670	6.814	-0.83	4.534	15.97	1.299	6.687	0.148

Appendix 1: Downcore data of the sediment cores

530	21172	10.124	-0.95	4.485	16.68	1.300	6.475	0.139
540	21674	5.094	-0.67	4.744	16.07	1.500	5.821	0.153
550	22176	5.952	-1.03	4.482	15.64	1.504	5.687	0.163
560	22678	6.441	-0.81	4.52	16.03	1.428	4.746	0.158
570	23345	5.357	-0.41	4.615	11.93	1.533	6.112	0.156
580	24011	3.317	-1.02	4.521	10.69	1.493	6.504	0.163
590	24678	3.502	-0.93	4.439	10.86	1.669	6.500	0.179
600	25345	5.246	-0.77	4.435	11.48	1.724	6.492	0.183
610	26011	5.406	-0.82	4.348	11.40	1.772	6.704	0.189
620	26678	6.655	-0.88	4.47	12.05	1.616	7.342	0.180
630	27344	6.290	-0.63	4.454	11.69	1.665	6.708	0.181
640	28011	3.944	-0.77	4.359	11.56	1.774	6.546	0.192
650	28193	3.147	-0.61	4.391	41.68	1.674	5.375	0.169
660	28375	3.213	-0.84	4.304	41.43	1.607	5.329	0.177
670	28558	2.411	-0.79	4.378	40.21	1.596	5.575	0.181
680	28740	2.746	-0.59	4.418	40.93	1.680	5.662	0.189
690	28922	3.064	-0.66	4.298	41.10	1.676	5.929	0.187
700	29104	3.878	-0.57	4.411	43.52	1.683	5.596	0.187

Core M77/2-50-4

Depth [cm]	Age [yrs]	>63 μm [w %]	$\delta^{13}\text{C}$ [‰]	$\delta^{18}\text{O}$ [‰]	AR_{bulk} [g/cm ² /ka]	Corg [%]	CaCO ₃ [%]	TN [%]
10	11186	19.211	-0.601	3.382	0.48			
20	11329	7.950	-0.576	3.038	32.28	4.713	8.292	0.464
30	11471	6.920	-0.437	3.079	35.82			
40	11614	11.824	-0.117	2.896	32.40	3.954	11.417	0.438
50	12243	4.651	-0.191	3.112	6.83			
60	12873	4.379	-0.443	3.679	8.35	3.568	8.029	0.377
70	13502	4.069	-0.572	3.171	8.21			
80	14131	6.465	-0.514	3.508	8.47	3.507	7.075	0.372
90	14377	6.177	-0.703	3.657	22.37			
100	14622	4.695	-0.461	3.687	22.67	3.301	7.983	0.351
110	14868	3.520	-0.731	3.799	24.72			
120	15113	2.510	-0.749	3.989	22.06	3.164	6.004	0.338
130	15359	2.752	-0.449	4.064	23.18			
140	15604	2.217	-0.955	3.322	22.94	3.384	7.017	0.353
150	15850	2.767	-0.320	3.372	19.84			
160	16095	2.738	-0.649	3.982	23.54	3.234	8.242	0.335
170	16341	4.294	-0.655	3.496	25.85			
180	16586	4.584			26.84	2.799	10.325	0.294
190	16832	4.055	-0.731	4.189	26.93			
200	17024	4.263	-0.592	4.381	35.82	2.487	10.421	0.260
210	17215	4.556	-0.708	4.372	37.25			
220	17407	8.985	-0.682	4.371	39.02	2.438	11.733	0.252
230	17598	6.282	-0.649	4.442	38.61			
240	17790	11.549	-1.051	4.255	40.75	2.406	14.712	0.242
250	17981	14.120	-1.109	3.829	43.52			
260	18245	17.405	-0.769	4.395	29.81	2.390	16.562	0.256
270	18509	21.309	-0.595	4.368	30.76			
280	18774	8.967	-0.320	4.602	27.90	2.597	15.900	0.280
290	19038	9.113	-0.446	4.375	29.97			
300	19302	19.210	-0.728	4.342	30.52	2.543	18.204	0.276
310	19566	21.658	-0.645	4.490	32.73			
320	19830	13.280	-0.777	4.533	27.07	2.367	19.817	0.261

Appendix 1: Downcore data of the sediment cores

330	20095	10.993	-0.569	4.394	29.45			
340	20359	8.277	-0.647	4.477	28.37	2.581	14.825	0.274
350	20623	11.674	-0.660	4.491	29.39			
360	20762	8.948	-0.823	4.547	54.33	2.263	15.112	0.249
370	20900	5.359	-0.516	4.552	53.03			
380	21039	22.249	-0.743	4.242	55.17	2.583	14.225	0.246
390	21178	29.005	-0.460	4.444	55.20			
400	21317	5.685	-0.491	4.295	56.76	2.333	13.354	0.257
410	21455	7.414	-0.737	4.466	55.74			
420	21594	8.248	-0.786	4.512	55.10	2.227	14.596	0.247
430	21733	8.277	-0.537	4.366	53.93			
440	21871	5.983	-0.614	4.374	52.95	2.279	13.950	0.249
450	22010	6.965	-0.561	4.415	56.77			
460	22181	11.764	-0.869	4.388	44.62	2.384	13.717	0.263
470	22352	7.183	-0.624	4.371	44.99			
480	22523	7.025	-0.779	4.338	44.25	2.478	12.717	0.275
490	22694	4.904	-0.528	4.380	48.78			
500	22866	4.747	-0.427	4.451	45.13	2.638	11.883	0.277
510	23037	6.208	-0.521	4.374	38.85			
520	23208	6.079	-0.449	4.395	42.62	2.768	12.892	0.311
530	23379	9.074	-0.573	4.303	39.67			
540	23550	9.910	-0.696	4.431	41.69	2.576	12.312	0.289
550	23721	12.471	-0.729	4.434	43.22			
560	23840	9.512	-0.595	4.307	69.36	2.397	12.725	0.270
570	23958	8.479	-0.478	4.360	67.08			
580	24077	4.533	-0.550	4.352	62.52	2.373	10.787	0.268
590	24196	3.725	-0.705	4.122	62.63			
600	24314	5.460	-0.514	4.252	58.51	2.781	10.742	0.310
610	24433	4.846	-0.826	4.264	60.02			
620	24552	5.814	-0.743	4.460	66.18	2.928	11.896	0.306
630	24670	7.595	-0.809	4.446	61.82			
640	24789	7.844	-0.708	4.404	60.01	2.848	13.337	0.304
650	24907	7.235	-0.965	4.255	60.33			
660	25026	14.244	-0.6	4.426	61.79	2.384	14.746	0.268
670	25145	9.077	-0.976	4.349	65.40			
680	25263	6.204	-0.737	4.443	64.10	2.246	12.929	0.254
690	25382	4.558	-0.823	4.205	64.63			
700	25501	4.976	-0.669	4.398	70.21	2.185	13.246	0.246
710	25619	3.504	-0.699	4.399	64.95			
720	25738	3.329	-0.633	4.435	61.83	2.180	12.026	0.250
730	25857	4.601	-0.531	4.348	64.73			
740	25975	8.934	-0.723	4.344	64.05	2.217	13.896	0.248
750	26094	5.755	-0.601	4.428	60.09			
760	26213	12.331	-0.385	4.399	62.18	2.483	12.817	0.272
770	26331	4.494	-0.466	4.405	60.69			
780	26450	3.795	-0.411	4.302	58.93	2.342	11.992	0.258
790	26569	2.338	-0.645	4.433	60.36			
800	26687	3.644	-0.636	4.493	60.49	2.654	11.775	0.290
810	26806	6.145	-0.464	4.465	65.06			
820	26925	9.102	-0.438	4.32	65.27	2.461	12.054	0.267
830	27041	6.420	-0.466	4.355	63.51			
840	27157	6.096	-0.658	4.421	68.56	2.530	11.987	0.267
850	27273	5.575	-0.421	4.438	62.81			
860	27388	3.446	-0.485	4.204	67.88	2.484	11.767	0.267
870	27504	5.161	-0.58	4.35	66.37			

Appendix 1: Downcore data of the sediment cores

880	27620	4.156	-0.601	4.409	61.02	2.500	11.204	0.266
890	27735	5.432	-0.601	4.314	63.83			
900	27851	4.921	-0.509	4.432	67.57	2.340	13.479	0.263
910	27967	5.376	-0.491	4.352	66.29			
920	28082	7.841	-0.498	4.335	70.43	2.384	14.025	0.260
930	28198	8.222	-0.584	4.27	66.81			
940	28313	5.981	-0.621	4.32	68.96	2.520	13.737	0.270
950	28429	9.730	-0.645	4.322	72.09			
960	28545	10.043			64.44	2.455	12.475	0.266
970	28660	14.758	-0.41	4.234	66.28			
980	28776	7.617	-0.451	4.194	67.57	2.526	12.167	0.273
990	28892	9.242	-0.362	4.229	66.16			
1000	29007	7.679	-0.535	4.344	69.30	2.613	12.367	0.284
1010	29123	11.621	-0.406	4.371	64.29			
1020	29304	11.568	-0.817	4.249	42.82	2.386	13.083	0.254
1030	29485	8.854	-0.737	4.041	43.78			
1040	29667	5.970	-0.505	4.045	46.11	2.453	12.433	0.249
1050	29848	7.068	-0.498	4.206	45.83			
1060	30029	11.787			41.86	2.626	11.467	0.263
1070	30210	8.019	-0.449	4.240	44.97			
1080	30392	7.999	-0.404	4.365	41.13	2.442	12.200	0.265
1090	30573	8.479	-0.534	4.317	43.02			
1100	30754	9.153	-0.582	4.162	37.10	2.880	9.875	0.296
1110	30935	5.865	-0.611	4.233	40.17			
1120	31116	6.144	-0.514	4.216	39.93	2.741	11.850	0.287
1130	31298	16.188	-0.455	3.999	37.81			
1140	31479	15.010	-0.435	4.124	42.81	2.380	14.592	0.259
1150	31660	10.671	-0.428	4.216	44.13			
1160	31841	12.810	-0.641	4.286	44.04	2.188	17.008	0.239
1170	32023	7.089	-0.614	4.182	42.00			
1180	32204	7.254	-0.449	4.298	45.35	2.199	14.921	0.235
1190	32385	14.328	-0.475	4.218	42.22			
1200	32539	9.349	-0.452	4.296	50.50	2.809	11.700	0.265
1210	32693	5.913			49.63			
1220	32847	6.888	-0.803	4.167	46.23	2.430	15.054	0.266
1230	33001	12.066	-0.653	4.131	51.06			
1240	33155	11.674	-0.403	4.182	51.96	2.646	12.812	0.245
1250	33309	12.266	-0.430	4.196	52.60			
1260	33463	12.535	-0.852	4.028	50.78	2.260	13.342	0.230
1270	33617	10.899	-0.447	4.149	49.22			
1280	33771	13.328	-0.555	3.956	48.92	2.056	14.479	0.223
1290	33925	15.133	-0.552	3.950	48.80			
1300	34079	6.906	-0.410	4.119	48.12	2.187	13.092	0.231
1310	34234	6.770	-0.341	4.082	50.76			
1320	34388	5.926	-0.473	3.985	49.05	2.078	12.767	0.209
1330	34543	6.324	-0.701	4.145	51.50			
1340	34697	7.937	-0.456	4.036	53.45	2.121	13.758	0.222
1350	34851	12.405	-0.610	4.144	49.88			
1360	35006	8.830	-0.517	4.274	51.47	2.006	15.925	0.226
1370	35160	8.793	-0.524	4.34	51.20			
1380	35315	10.064	-0.484	4.15	47.59	2.230	14.750	0.237
1390	35469	11.005	-0.677	4.271	51.71			
1400	35624	11.675	-0.664	4.019	50.44	2.139	17.862	0.233
1410	35778	12.633	-0.516	4.108	50.24			
1420	35933	8.713	-0.482	4.158	50.68	2.562	9.633	0.227

Appendix 1: Downcore data of the sediment cores

1430	36087	7.715	-0.551	4.038	52.57			
1440	36242	7.685	-0.528	4.002	51.07	1.993	13.346	0.219
1450	36395	4.990	-0.412	3.847	49.93			
1460	36551	4.404	-0.76	4.269	53.64	2.098	14.083	0.234
1470	36702	4.657	-0.643	4.022	51.46			
1480	36853	6.735	-0.735	4.054	49.99	2.141	13.496	0.240
1490	37004	7.124	-0.484	3.91	51.05			
1500	37155	10.628	-0.802	3.996	52.43	1.949	14.621	0.225
1510	37306	7.062	-0.619	3.737	54.60			
1520	37457	6.818	-0.733	4.019	50.63	2.372	11.462	0.257
1530	37609	8.497	-0.839	4.178	49.97			
1540	37760	7.177	-0.949	4.072	50.42	2.672	7.987	0.247
1550	37911	7.066			50.98			
1560	38062	4.669	-1.143	3.997	54.41	2.420	7.875	0.242
1570	38213	6.390	-0.774	4.034	50.57			
1580	38364	7.224	-1.295	3.906	48.37	2.411	7.192	0.246
1590	38515	4.183	-0.92	3.975	47.98			
1600	38666	6.039	-0.887	3.845	49.08	2.784	7.812	0.272
1610	38817	5.795			49.09			
1620	38968	5.945	-0.883	3.946	50.44	2.701	9.592	0.270
1630	39119	4.091	-1.093	3.95	49.97			
1640	39271	5.895	-1.006	3.915	49.95	2.622	8.300	0.264
1650	39422	5.842	-0.542	3.912	52.97			
1660	39573	9.054	-0.728	4.005	53.21	2.670	7.871	0.258
1670	39724	9.501	-0.458	4.006	56.59			
1680	39875	5.341	-0.552	4.02	53.00	2.640	8.392	0.265
1690	40026	7.693	-0.563	4.054	49.41			
1700	40177	8.800	-0.518	4.065	54.53	2.245	8.912	0.277
1710	40328	5.355	-0.47	4.112	53.34			
1720	40479	5.535	-0.589	4.182	53.70	2.307	10.654	0.241
1730	40630	6.535	-0.731	4.069	51.64			
1740	40781	6.290	-0.7	4.219	53.23	3.030	9.892	0.309
1750	40933	31.847	-0.634	4.246	51.69			
1760	41084	47.339	-0.452	3.878	61.10	2.550	8.950	0.255

Appendix 1: Downcore data of the sediment cores

Core M77/1-422

Depth (cm)	Age [yrs]	>63 μm (%)	$\delta^{13}\text{C}$ [‰] <i>Globobulimina pacifica</i>	$\delta^{18}\text{O}$ [‰] <i>Globobulimina pacifica</i>	$\delta^{13}\text{C}$ [‰] <i>Uvigerina peregrina</i>	$\delta^{18}\text{O}$ [‰] <i>Uvigerina peregrina</i>
25	21916	13.603				
30	21950	6.173	-1.271	3.382		
35	21980	4.055	-1.300	3.716		
40	22018	11.816				
45	22057	7.428				
50	22095	5.385				
55	22133	4.998				
60	22171	5.543				
65	22209	5.029				
70	22247	5.050				
75	22285	4.447				
80	22300	8.709				
85	22514	6.772				
90	22871	5.334				
100	23227	5.806				
105	23584	4.264				
110	23941	3.063				
115	24297	3.628				
120	24654	3.450				
125	25011	2.820				
130	25367	7.247				
135	25510	6.804	-0.521	3.718		
140	25628	6.056	-0.739	3.585	-0.668	3.623
145	25825	6.684	-1.112	3.489	-0.817	3.502
150	26612	4.998	-0.642	3.053	-0.327	2.540
155	26808	6.027	-1.200	3.571	-0.728	3.557
160	27005	3.381	-1.508	3.578		
165	27202	4.126	-0.457	3.586		
170	27333	4.353	-1.123	3.645		
175	27366	6.709	-2.250	3.677		
180	27399	6.669	-0.659	3.799		
185	27432	4.948	-0.690	3.671		
190	27465	4.665	-0.773	3.446		
195	27498	3.859	-1.372	3.755		
200	27531	5.921	-0.767	3.647		
205	27564	5.483	-1.023	3.650		
210	27597	7.258	-1.115	3.644		
215	27649	3.983	-1.787	3.489		
220	27715	5.590	-2.000			
225	27780	6.708	-0.889	3.642		
230	27846	9.282	-1.349	3.618		
235	27912	6.741	-0.852	3.659	-0.987	3.489

Appendix 1: Downcore data of the sediment cores

240	27977	9.198	-0.852	3.648	-1.156	3.644
245	28043	6.502	-0.851	3.663		
250	28108	8.693	-0.876	3.546	-0.336	3.634
255	28174	7.996	-1.479	3.543		
260	28226	7.988	-1.126	3.510		
265	28292	10.771	-1.799	3.583	-1.534	3.560
270	28357	6.251	-1.266	3.724		
275	28423	8.972	-1.394	3.497	-0.472	3.493
280	28488	5.797				
285	28554	4.393				
290	28620	4.907				
295	28685	2.359				
300	28751	2.297				
305	28816	11.659		3.421		

Core M77/1-416

Depth [cm]	Age [yrs]	>63 μm [w %]	$\delta^{13}\text{C}$ [‰] <i>Uvigerina striata</i>	$\delta^{18}\text{O}$ [‰] <i>Uvigerina striata</i>	$\delta^{13}\text{C}$ [‰] <i>Uvigerina peregrina</i>	$\delta^{18}\text{O}$ [‰] <i>Uvigerina peregrina</i>
0	18190	16.633	-0.064	3.516		
5	18316	9.679	-0.151	3.544		
10	18443	12.428	-0.127	3.632		
15	18569	5.236	-0.030	3.729		
20	18695	4.184	-0.040	3.748		
25	18798	10.196	-0.149	3.738		
30	18901	7.704	-0.077	3.718		
35	19004	5.474	-0.201	3.761		
40	19108	9.610	0.024	3.708		
45	19211	5.200	-0.111	3.747		
50	19314	6.540	0.015	3.727		
55	19417	6.195	0.143	3.801		
60	19520	4.932	-0.084	3.767		
65	19602	8.192	0.089	3.830		
70	19684	5.329	0.202	3.833		
75	19766	12.061	-0.097	3.689		
85	19848	64.214				
90	19930	7.623	-0.154	3.807		
95	20012	4.975	0.081	3.815		
100	20094	5.899	-0.024	3.672		
105	20176	5.698	0.020	3.746		
110	20258	8.697	-0.122	3.723		
115	20340	4.050	-0.121	3.842		
120	20368	0.951	-0.204	3.583		
125	20395	7.362				
130	20423	1.684	-0.138	3.625		
135	20450	15.283	-0.042	3.778		
140	20478	69.326	0.043	3.693		

Appendix 1: Downcore data of the sediment cores

145	20505	78.826	0.120	3.651		
150	20533	5.402	-0.183	3.728		
155	20560	5.223	-0.213	3.797		
160	20588	6.990	-0.129	3.627		
165	20615	5.859	-0.498	3.874		
170	20730	9.101	0.019	3.717		
175	20844	14.450	-0.152	3.727		
180	20959	64.265	-0.117	3.701		
185	21073	7.113	-0.005	3.709		
190	21188	14.871	-0.123	3.648		
195	21302	55.100				
200	21417	9.695	-0.029	3.671		
205	21531	22.975	0.134	3.805		
210	21646	3.553	-0.081	3.677		
215	21760	5.372	-0.210	3.801		
220	21871	1.693	-0.372	3.809		
225	21983	2.357	-0.518	3.639		
230	22094	4.232	-0.068	3.772		
235	22205	7.863	-0.244	3.711		
240	22305	6.889	-0.570	3.838		
245	22405	5.462	-0.382	3.675		
250	22505	7.265	-0.645	3.861		
255	22865	7.559	-0.219	3.712		
260	23015	5.858	-0.135	3.710		
265	23164	3.549				
270	23314	7.154	0.021	3.615		
275	23463	7.658	0.024	3.658		
280	23613	7.477	-0.048	3.715		
285	23763	16.557	-0.135	3.713		
290	23912	2.779	-0.543	3.734		
295	24062	3.519	-0.360	3.753	-0.272	3.733
300	24211	7.371			0.108	3.850
305	24361	5.921	-0.155	3.778		
310	24510	3.877	-0.155	3.644		
315	24660	3.742	-0.082	3.692	0.084	3.730
320	24929	2.744	-0.214	3.773		
325	25199	2.669			0.038	3.734
330	25468	2.106	-0.008	3.653		
335	25737	2.606	0.116	3.776	0.299	3.738
340	26006	3.774	-0.026	3.706		
345	26276	3.597	-0.432	3.812		
350	26545	2.664	-0.031	3.808	-0.342	3.892
355	26814	5.120	-0.555	3.859	-0.106	3.788
360	27084	5.599			-0.242	3.751
365	27353	6.899			-0.152	3.689
370	27622	4.689			-0.397	3.635

Supplementary information provided for Erdem et al., 2016 which can be downloaded through: [http:// dx.doi.org/10.1016/j.quascirev.2016.01.029](http://dx.doi.org/10.1016/j.quascirev.2016.01.029). Note that Supplementary Table 1 and Figure 1 are given in Chapter 2.

Supplementary Table 2: Age models of the cores from literature.

7706-40 (Res. Age ΔR : 89 ± 8)						
Core Depth (cm)	Con. age (yrs)	error (yrs)	Cal. Age (cal ka BP)	Material	Lab number	Remarks
5	571	82	0.13			
50	967	63	0.50			
95	2611	65	2.17			
145	2980	140	2.64			
165	3640	130	3.46			
215	12114	412	13.69			
7706-41 (Res. Age ΔR : 89 ± 8)						
8	840	100	0.36			
25	10100	250	11.07			
45	10700	270	11.88			
70	12500	340	14.18			
110	14280	420	16.66			
160	15500	550	18.16			
7706-44 (Res. Age ΔR : 89 ± 8)						
25	6270	160	6.64			
60	9000	220	9.63			
95	>34000					discarded
7706-04 (Res. Age ΔR : 89 ± 8)						
46	2950	130	2.59			
90	11800	250	13.16			
141	13820	440	15.98			
175	14980	450	17.60			
7706-37 (Res. Age ΔR : 89 ± 8)						
5	1328	72	0.79			
40	13060	200	14.77			
85	14420	370	16.86			
125	14720	490	17.20			
165	16900	630	19.89			
RC-23-06-GS-1s (Res. Age ΔR : 186 ± 49)						
1	1210	150	0.61	Sediment		
13	2965	270	2.51	Sediment		
18	9245	530	9.80	Sediment		
RC-23-06-28BX-2 (Res. Age ΔR : 238 ± 49)						
3	1005	145	0.36	Sediment		
5	1010	160	0.40	Sediment		
9	3005	190	2.47	Sediment		
12	5535	235	5.64	Sediment		
15	7680	350	7.96	Sediment		
21	9700	380	10.29	Sediment		
RC-23-06-GS=6 (Res. Age ΔR : 89 ± 8)						
1	1450	510	0.95	Sediment		
18	11400	1200	12.76	Sediment		
RC-23-06-310BX-3 (Res. Age ΔR : 338 ± 186)						
13	460	195		Sediment		
23	9400	390	9.79	Sediment		
MW8708-PC2						
70			2.13			Cal. Ages taken directly

Appendix 2: Supplementary information of Chapter 3; Erdem et al., 2016.

101			3.01		
185			4.45		
325			6.10		
415			8.10		
430			7.98		
455			8.10		
545			9.05		
SO78-173-4 (Res. Age ΔR: 89 \pm 8)					
41			0.40		Correlation with SO78 cores
165	2250	50	1.70	<i>B. seminuda</i>	
214			2.56		Correlation with SO78 cores
286	4380	75	3.83	<i>B. seminuda</i>	
295			3.96		Correlation with SO78 cores
365			4.94		Correlation with SO78 cores
440			6.00		Correlation with SO78 cores
444			10.00		Correlation with SO78 cores
463			13.48		Correlation with SO78 cores
494	19700	230	19.15	<i>B. seminuda</i>	
SO78-159-3 (Res. Age ΔR: 89 \pm 8)					
24			0.40		Correlation with SO78 cores
54			1.42		Correlation with SO78 cores
65	3620	60	3.07	<i>B. seminuda</i>	
98			6.00		Correlation with SO78 cores
160	23190	310	22.64	<i>B. seminuda</i>	
SO78-175-1 (Res. Age ΔR: 89 \pm 8)					
45	11140	110	10.59	<i>N. dutertrei</i>	
190	15610	130	15.06	<i>N. dutertrei</i>	
SO78-158-3 (Res. Age ΔR: 89 \pm 8)					
25			0.40		Correlation with SO78 cores
148			1.42		Correlation with SO78 cores
182			1.70		Correlation with SO78 cores
230			2.56		Correlation with SO78 cores
272			3.96		Correlation with SO78 cores
300			4.94		Correlation with SO78 cores
340			6.00		Correlation with SO78 cores
342			10.00		Correlation with SO78 cores
371			13.48		Correlation with SO78 cores
SO147-41SL					
20	17780	130	17.23		KIA
320	19680	160	19.13		KIA
SO147-4SL					
20	655	30	1.11		KIA
144	3720	35	3.17		KIA
804	10080	60	9.53		KIA
820	10370	70	9.82		KIA
980	10920	90	10.37		KIA
SO147-106KL					
8	1000	30	0.28	KIA14768	Wolf, 2002
49.5	1305	25	0.53	KIA13318	Wolf, 2002
79.5	1455	20	0.65	KIA12457	Wolf, 2002
97.2	1595	30	0.69	KIA14769	Wolf, 2002
145.8	2105	30	1.26	KIA14770	Wolf, 2002
229	2490	30	1.59	KIA14771	Rein et al., 2004
279	2745	30	1.88	KIA12456	Rein et al., 2004
335	3500	30	2.78	KIA13321	Rein et al., 2004
368	4060	30	3.47	KIA12458	Rein et al., 2004
388	4305	30	3.83	KIA13323	Rein et al., 2004
399	4430	30	3.96	KIA13324	Rein et al., 2004
409	4635	30	4.24	KIA13325	Rein et al., 2004

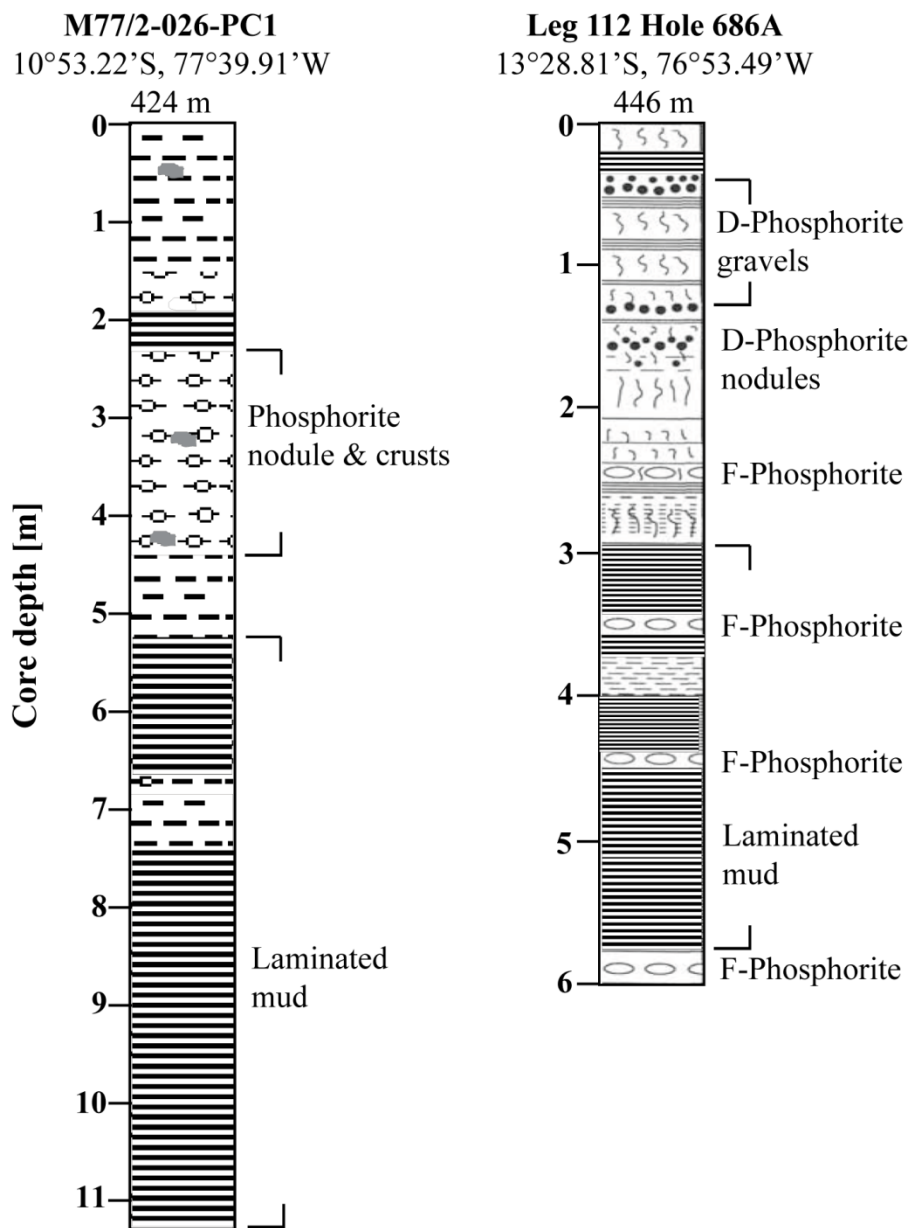
Appendix 2: Supplementary information of Chapter 3; Erdem et al., 2016.

419	4830	30	4.52		KIA13326	Rein et al., 2004
429	4955	30	4.81		KIA13327	Rein et al., 2004
439.4	5660	30	5.60		KIA12459	Rein et al., 2004
449	7810	60	7.83		KIA13328	Rein et al., 2004
469	8375	40	8.39		KIA13329	Rein et al., 2004
479	8750	70	8.93		KIA13330	Rein et al., 2004
489	8835	50	9.00		KIA13331	Rein et al., 2004
499	8740	45	8.93		KIA13332	Rein et al., 2004
509	8840	40	9.00		KIA13333	Rein et al., 2004
519	8780	40	8.98		KIA13334	Rein et al., 2004
529	8905	60	9.03		KIA13335	Rein et al., 2004
540	8815	45	9.00		KIA12117	Rein et al., 2004
549	9085	45	9.40		KIA13336	Rein et al., 2004
559	9245	40	9.49		KIA13337	Rein et al., 2004
569	9240	45	9.47		KIA13338	Rein et al., 2004
579	9320	45	9.53		KIA13339	Rein et al., 2004
589	9310	45	9.53		KIA13340	Rein et al., 2004
599	9440	45	9.55		KIA13341	Rein et al., 2004
609	9615	55	9.91		KIA13342	Rein et al., 2004
619	9470	50	9.60		KIA13343	Rein et al., 2004
629	9585	50	9.89		KIA13344	Rein et al., 2004
639	9740	50	10.15		KIA14772	Rein et al., 2004
645	9795	50	10.19		KIA14773	Rein et al., 2004
659	9815	55	10.21		KIA14774	Rein et al., 2004
809	11090	55	12.10		KIA12116	Rein et al., 2004
950	15180	60	14.63		KIA	Wolf, 2002
964	16700	100	16.15		KIA	Wolf, 2002
IODP Leg201-1227B (Res. Age ΔR: 238 \pm 49)						
26	13956	84	15.89	Sediment	OZG474	
55	13796	78	15.69	Sediment	OZG475	
84	14141	67	16.1	Sediment	OZG105	
259	14528	75	16.55	Sediment	OZG104	
397	15103	107	17.22	Sediment	OZG103	
556	21439	122	21.41	Sediment	OZG106	
IODP Leg201-1229E (Res. Age ΔR: 238 \pm 49)						
20	1331	42	0.65	Sediment	OZG002	
61	1484	35	0.79	Sediment	OZH154	
109	1884	30	1.2	Sediment	OZG108	
139	2313	32	1.65	Sediment	OZH155	
186	2501	49	1.87	Sediment	OZH156	
230	3348	42	2.88	Sediment	OZH157	
IODP Leg201-1228B (Res. Age ΔR: 238 \pm 49)						
20	1142	39	0.52	Sediment	OZG001	
39	1449	50	0.76	Sediment	OZH144	
69	1902	35	1.22	Sediment	OZH145	
94	2134	36	1.44	Sediment	OZH146	
140	2550	36	1.92	Sediment	OZH147	
165	3251	45	2.79	Sediment	OZH148	
190	5151	40	5.23	Sediment	OZG109	
210	9793	50	10.23	Sediment	OZH149	
229	10042	82	10.58	Sediment	OZH150	
242	10648	58	11.36	Sediment	OZG107	
315	42879	760	42.9	Sediment	OZH151	discarded
322	28779	251	28.74	Sediment	OZG472	
322	37446	599	37.45	Sediment	OZH143	
369	44554	935	44.55	Sediment	OZH152	
398	44095	883	44.05	Sediment	OZH153	
399	36156	514	36.16	Sediment	OZG473	discarded
Galathea 3 G14						
9.50	12640	30	13.55	Sediment	S6A-10	
77.50	13465	35	14.68	Sediment	S5A-51	

Appendix 2: Supplementary information of Chapter 3; Erdem et al., 2016.

159	13935	35	15.82	Sediment	S5A-34
221	15330	40	17.58	Sediment	S4A-96
373	17615	50	19.64	Sediment	S2A-49
429.40	19440	70	22.15	Sediment	S1A-5
Galathea 3 G10					
157.70	3395	30	2.96	Sediment	S4B-41
298.70	4845	35	4.83	Sediment	S3B-82
405.30	8345	45	8.32	Sediment	S2B-86
507.90	9800	40	10.07	Sediment	S1B-88

Supplementary Figure 2: Core descriptions showing sediment features of two cores without precise age models.



Taxonomic reference list

Type references are given for each species identified. Angular brackets refer to plates and figures in this thesis.

Alabaminella weddellensis = *Eponides weddellensis* Earland, 1936. [pl. 4, fig. 12 & pl. 6, fig. 24].

Angulogerina angulosa = *Uvigerina angulosa* (Williamson, 1858). [pl. 3, fig. 4].

Angulogerina carinata (Cushman, 1927).

Anomalinoides minimus (Vismara Schilling and Parisi, 1981). [pl. 4, figs. 4-5 & pl. 6, figs. 14, 20].

Bolivina advena (Cushman, 1925).

Bolivina advena Cushman var. *striatella* Cushman, 1925.

Bolivina alata = *Valvulina alata* (Seguenza, 1862). **Note:** This species was denominated as *Bolivina pseudobeyrichi* Cushman and the species name *Bolivina alata* (Seguenza) is considered to have priority. [pl. 2, fig. 10 & pl. 5, fig. 10].

Bolivina albatrossi Cushman, 1922.

Bolivina argentea Cushman 1926. [pl. 2, fig. 5].

Bolivina costata d'Orbigny, 1839. [pl. 1, fig. 1 & pl. 6, fig. 8].

Bolivina doniezi Cushman and Wickenden, 1929.

Bolivina interjuncta = *Bolivina costata* d'Orbigny var. *interjuncta* Cushman, 1926. [pl. 2, fig. 1, pl. 5, fig. 1].

Bolivina interjuncta Cushman var. *bicostata* = *Bolivina costata* d'Orbigny var. *bicostata* Cushman, 1926, illustrated in Cushman, 1937. **Note:** The description and images provided by Uchio (1960) as *Bolivina subargentea* are also similar to what is observed in the sediment samples in this study, but the specimens observed in the sediment cores are too small in size compared to them. The appearance and structure of the costae are the most similar to the *Bolivina interjuncta* Cushman var. *bicostata* Cushman. The costae are not easily recognized because of the small size but they are unquestionably visible at SEM images. [pl. 1, figs., 5-6 & pl. 6, fig. 5].

Bolivina minima Phleger and Parker, 1951.

Bolivina ordinaria Phleger and Parker, 1952. [pl. 1, fig. 2 & pl. 6, fig. 9].

Bolivina pacifica = *Bolivina acerosa* Cushman var. *pacifica* Cushman & McCulloch, 1942. [pl. 1, fig. 10 & pl. 6 fig. 4].

Bolivina plicata d'Orbigny, 1839. [pl. 2, figs. 3-4 & pl. 5, figs. 2-3].

Bolivina quadrata Cushman and McCulloch, 1942.

Bolivina semicostata Cushman, 1911.

Appendix 3: Taxonomy references and Plates

Bolivina seminuda Cushman, 1911. [pl. 1, fig. 4 & pl. 6, fig. 1].

Bolivina seminuda Cushman var. *humilis* Cushman and McCulloch, 1942. **Note:** *Bolivina seminuda* Cushman var. *humilis* showed huge variations in the samples similar to those provided as type figures. [pl. 1, fig. 9 & pl. 6, fig. 3].

Bolivina cf. *seminuda* Cushman var. *humilis* **Note:** This species is similar to type figure 1a in pl. 26 in Cushman and McCulloch, 1942 and it has projections and acute periphery in early chambers similar to *Bolivina minima* but it is not as flat and compressed as *B. minima*. Considering overall appearance, inflated later chambers, structure of the aperture and the appearance of the pores, it is considered as a variation of *B. seminuda* var. *humilis* and could be merged into this group. [pl.1, fig. 3 & pl. 6, fig. 2].

Bolivina serrata = *Bolivina subadvena* Cushman var. *serrata* Natland, 1938.

Bolivina spissa = *Bolivina subadvena* Cushman var. *spissa* Cushman 1926. [pl. 2, fig. 7 & pl. 5, fig. 4].

Bolivina subadvena Cushman 1926. [pl. 2, fig. 2].

Bolivina subaenariensis Cushman, 1922.

Bolivina tongi Cushman var. *filacostata* Cushman and McCulloch, 1942. [pl. 1, fig. 11].

Bolivina tortuosa Brady, 1881 p. 57, illustrated by Brady, 1884.

Bolivina aff. *tortuosa* **Note:** The almost 90° twisted feature and coarse pores of this species are similar features of *Bolivina tortuosa* though the specimens found in the sediment samples are really small in size and they are compressed. [pl. 1, fig. 8 & pl. 6, fig. 7].

Bolivinita minuta = *Bolivina minuta* Natland, 1938 [pl. 1, fig. 7 & pl. 6, fig. 6].

cf. *Buccella peruviana* = *Rotalina peruviana* d'Orbigny, 1839. **Note:** Except the appearance of the aperture, other features are similar to those described in the type reference. *Buccella plana* of McCulloch, 1977 indicated similar features but the appearance of the aperture is different in the specimens of our samples. [pl. 4, figs. 9-10 & pl. 6, figs. 15-17].

Bulimina denudata = *Bulimina pagoda* Cushman var. *denudata* Cushman and Parker, 1938.

Bulimina exilis = *Bulimina elegans* d'Orbigny var. *exilis* Brady, 1884. **Note:** Most of the taxonomical studies from Eastern Pacific denominate this species as *Buliminella tenuata* Cushman or *Bulimina exilis* var. *tenuata* Cushman. The species name *Bulimina exilis* Brady 1884 is considered to have priority though. [pl. 2, figs. 14-15 & pl. 5, figs. 12-13].

Bulimina marginata d'Orbigny 1826.

Bulimina mexicana = *Bulimina inflata* Seguenza var. *mexicana* Cushman, 1922. [pl. 1, fig. 18].

Bulimina pagoda Cushman, 1927. [pl. 1, fig. 19 & pl. 6, fig. 10].

Bulimina rostrata Brady, 1884.

Appendix 3: Taxonomy references and Plates

Bulimina striata d'Orbigny 1826.

Buliminella curta Cushman, 1925. [pl. 1, fig. 12 & pl. 5, fig. 11].

Buliminella curta Cushman var. *basispinata* Stewart and Stewart, 1930. [pl. 2, fig. 16].

Buliminella elegantissima = *Bulimina elegantissima* d'Orbigny, 1839 [pl. 1, fig. 17].

Buliminella tenuata = *Buliminella subfusiformis* var. *tenuata* Cushman, 1927 **Note:** Not *Bulimina tenuata* Cushman. In our samples, this species is small in size, has an aperture with tooth. [pl. 2, fig. 11].

Cancris auriculus = *Nautilus auricula* Fichtel and Moll, 1798.

Cancris carmenensis Natland, 1950.

Cancris inflatus = *Valvulina inflata* d'Orbigny, 1839.

Cassidulina auka Boltovsky and Theyer, 1970 [pl. 4, fig. 11 & pl. 5, fig. 19].

Cassidulina carinata = *Cassidulina laevigata* d'Orbigny var. *carinata* Silvestri, 1896 [pl. 4, fig. 16 & pl. 7, fig. 15].

Cassidulina corbyi Cushman and Hughes, 1925.

Cassidulina crassa d'Orbigny, 1839 [pl. 2, fig. 18 & pl. 5, fig. 18]

Cassidulina delicata Cushman, 1927 **Note:** I followed the suggestion of Uchio (1960) and included *Cassidulina cushmani* Stewart and Stewart, 1930 into the range of variability of this species. [pl. 4, fig. 17 & pl. 5, fig. 17].

Cassidulina depressa Asano and Nakamura, 1937.

Cassidulina laevigata d'Orbigny 1826.

Cassidulina minuta Cushman, 1933. [pl. 4, fig. 15].

Cassidulina pulchella d'Orbigny 1839.

Chilostomella ovoidea Reuss, 1850.

Cibicides aknerianus = *Rotalina akneriana* d'Orbigny, 1846.

Cibicides elmaensis Rau, 1948.

Cibicides floridanus = *Truncatulina floridana* Cushman, 1918.

Cibicides mckannai Galloway and Wissler, 1927 [pl. 7, fig. 2].

Cibicides spiralis Natland, 1938.

Cibicidoides dispars = *Truncatulina dispars* d'Orbigny, 1839.

Cibicidoides mundulus = *Truncatulina mundula* Brady, Parker and Jones, 1888.

Cibicidoides wuellerstorfi = *Anomalina wuellerstorfi* Schwager, 1866 [pl. 7, fig.1].

Dentalina advena = *Nodosaria advena* Cushman, 1923.

Discorbis micens Cushman, 1933.

Discorbis peruvianus = *Rosalina peruviana* d'Orbigny, 1839.

Appendix 3: Taxonomy references and Plates

Dorothia goesii = *Textularia goesii* Cushman, 1911.

Ehrenbergina pupa = *Cassidulina pupa* d'Orbigny, 1839.

Epistominella afueraensis McCulloch, 1977. **Note:** The acute periphery and keeled appearance of the chambers discriminates this species from *Epistominella obesa*. [pl. 3, figs. 8-9 & pl. 6, figs. 21-23].

Epistominella exigua = *Pulvinulina exigua* Brady, 1884. [pl. 4, figs. 2-3 & pl. 6, figs. 18-19].

Epistominella obesa Bandy and Arnal, 1957. **Note:** Bandy and Arnal (1957) described this species as similar to *Pulvinulinella bradyana* Cushman, 1927 but with more inflated chambers. In the sediment samples, it is difficult to distinguish the differences between these two species. Considering the structure of the aperture they are merged in *Epistominella obesa*. [pl. 4, figs. 6-8].

Epistominella pacifica = *Pulvinulinella pacifica* Cushman, 1927. **Note:** This species showed variations such as size, keel type or transparency in our samples. The images provided by Resig (1981) and Coulbourn (1980) as *Epistominella* sp. are similar to those observed in the sediment samples and is included into the range of variability of this species. [pl. 3, figs. 2-3; pl. 4, fig. 1 & pl. 7, figs. 6-8, 13].

Epistominella smithi = *Pulvinulinella smithi* Stewart and Stewart, 1930. [pl. 3, fig. 5 & pl. 7, figs. 3-4].

Eponides pusillus Parr, 1950.

Fissurina alatifundata McCulloch, 1981.

Fissurina alveolata = *Lagena alveolata* Brady, 1884.

Fissurina annectens = *Lagena annectens* Burrows and Holland, 1895. **Note:** Type reference given by Jones, 1895.

Fissurina exculpta = *Lagena exculpta* Brady, 1881, p. 61, illustrated by Brady, 1884.

Fissurina kerguelenensis Parr, 1950.

Fissurina laevigata Reuss, 1850.

Fissurina marginata = *Vermiculum marginatum* Montagu, 1803, illustrated by Walker and Boys, 1784.

Fissurina orbignyana Seguenza, 1862.

Fissurina semimarginata = *Lagena marginata* (Montagu) var. *semimarginata* Reuss, 1870.

Fursenkoina fusiformis = *Bulimina pupoides* d'Orbigny var. *fusiformis* Williamson, 1858 [pl. 1, fig. 15 & pl. 6, fig. 11].

Fursenkoina glabra = *Bulimina patagonica* d'Orbigny var. *glabra* Cushman and Wickenden, 1929 [pl. 1, fig. 16 & pl. 6, fig. 13].

Appendix 3: Taxonomy references and Plates

- Globobulimina affinis* = *Bulimina affinis* d'Orbigny, 1839.
- Globobulimina glabra* Cushman and Parker, 1947.
- Globobulimina hoeglundi* Uchio, 1960.
- Globobulimina ovula* = *Bulimina ovula* d'Orbigny, 1839
- Globobulimina pacifica* Cushman, 1927 [pl. 2, fig. 12 & pl. 5, fig. 16].
- Globocassidulina paratortuosa* = *Cassidulina paratortuosa* Kuwano, 1954.
- Globocassidulina subglobosa* = *Cassidulina subglobosa* Brady, 1881.
- Gyroidina altiformis* = *Gyroidina soldanii* d'Orbigny var. *altiformis* Stewart and Stewart, 1930
- Gyroidina gemma* Bandy, 1953.
- Gyroidina lamarckiana* = *Rotalina lamarckiana* d'Orbigny, 1839.
- Gyroidina neosoldanii* Brotzen, 1936.
- Gyroidina nitidula* = *Rotalia nitidula* Schwager, 1866.
- Gyroidina polia* = *Eponides polius* Phleger and Parker, 1951.
- Gyroidina quinqueloba* Uchio, 1960.
- Gyroidina rothwelli* Natland, 1950. [pl. 3, figs. 10-11 & pl. 7, figs. 9, 14].
- Gyroidina soldanii* d'Orbigny, 1826.
- Gyroidina subtenera* = *Rotalia subtenera* Galloway and Wissler, 1927 [pl. 4, figs, 13-14 & pl. 7, figs, 11-12].
- Hanzawaia bertheloti* = *Rosalina bertheloti* d'Orbigny, 1839.
- Hanzawaia mexicana* Lankford, 1973.
- Hoeglundina elegans* = *Rotalia (Turbinuline) elegans* d'Orbigny, 1826 [pl. 5, fig. 15].
- Lagena amphora* Reuss, 1863.
- Lagena distoma* Parker and Jones, 1864.
- Lagena elongata* = *Miliola elongate* Ehrenberg, 1845.
- Lagena gracillima* = *Amphorina gracillima* Seguenza, 1862.
- Lagena hispidula* Cushman, 1923.
- Lagena laevis* = *Vermiculum laeve* Montagu, 1803.
- Lagena lateralis* Cushman, 1913.
- Lagena meridionalis* = *Lagena gracilis* Williamson var. *meridionalis* Wiesner, 1931.
- Lagena semistriata* = *Lagena striata* (Montagu) var. *semistriata* Williamson, 1848.
- Lagena squamosa* = *Vermiculum squamosum* Montagu, 1803.
- Lagena striata* = *Oolina striata* d'Orbigny, 1839.
- Lagena substriata* Williamson, 1848.
- Lagena sulcata* = *Serpula (Lagena) sulcate* Walker and Jacob, 1798.

Appendix 3: Taxonomy references and Plates

- Lagena sulcata* (Walker and Jacob) var. *peculiaris* Cushman and McCulloch, 1950.
Lagena sulcata (Walker and Jacob) var. *striatopunctata* Parker and Jones, 1865.
Lagena williamsoni Harvey and Bailey, 1854.
Lagenosolenia inflatiperforata McCulloch, 1977.
Laticarinina pauperata = *Pulvinulina repanda* Fitchel and Moll var. *menardii* d'Orbigny subvar. *pauperata* Parker and Jones, 1865.
Lenticulina convergens = *Cristellaria convergens* Bornemann, 1855.
Lenticulina limbosa = *Cristellaria (Robulina) limbosa* Reuss, 1863.
Martinottiella communis = *Clavulina communis* d'Orbigny, 1846.
Martinottiella nodulosa = *Clavulina communis* d'Orbigny var. *nodulosa* Cushman, 1922.
Melonis affinis = *Nonionina affinis* Reuss, 1851.
Melonis barleeaanum = *Nonionina barleeana* Williamson, 1858.
Melonis pompilioides = *Nautilus pompilioides* Fichtel and Moll, 1798.
Nonion commune = *Nonionina communis* d'Orbigny, 1846.
Nonion pizarrensis Berry var. *basispinata* Cushman and Moyer, 1930.
Nonionella cf. auricula Heron-Allen and Earland, 1930.
Nonionella auris = *Valvulina auris* d'Orbigny, 1839.
Nonionella iridea Heron-Allen and Earland, 1932.
Nonionella labradorica = *Nonionina labradorica* Dawson, 1860.
Nonionella miocenica Cushman, 1926.
Nonionella stella = *Nonionella miocenica* Cushman var. *stella* Cushman and Moyer, 1930.
Nonionella turgida = *Rotalina turgida* Williamson, 1858.
Nonionoides grateloupii = *Nonionina grateloupii* d'Orbigny, 1826.
Oolina apiculata Reuss, 1851.
Oolina globosa = *Vermiculum globosum* Montagu, 1803
Oolina truncata = *Lagena truncata* Brady, 1884.
Oridorsalis umbonatus = *Rotalina umbonata* Reuss, 1851. [pl. 7, fig. 10].
Planulina limbata Natland, 1938. [pl. 3, fig. 1 & pl. 7, fig. 5].
Planulina ornata = *Truncatulina ornata* d'Orbigny, 1839.
Praeglobobulimina ovata = *Bulimina ovata* d'Orbigny, 1846.
Praeglobobulimina spinescens = *Bulimina pyrula* d'Orbigny var. *spinescens* Brady, 1884 [pl. 2, fig. 6 & pl. 5, fig. 6].
Pseudoparella subperuviana = *Pulvinulinella subperuviana* Cushman, 1926.

Appendix 3: Taxonomy references and Plates

Pseudoparella sp. **Note:** Small juvenile specimens with large umbilicus. They potentially belong to *Pseudoparella* group but as indicated in the note for *Epistominella obesa*, the differences reported between these two species are difficult to discriminate in our samples.

Pullenia bulloides = *Nonionina bulloides* d'Orbigny, 1846.

Pullenia elegans Cushman and Todd, 1943.

Pullenia quinqueloba = *Nonionina quinqueloba* Reuss, 1851.

Pullenia subcarinata = *Nonionina subcarinata* d'Orbigny, 1839.

Pyrgo depressa = *Biloculina depressa* d'Orbigny, 1826.

Pyrgo lucernula = *Biloculina lucernula* Schwager, 1866.

Pyrgo murrhyna = *Biloculina murrhyna* Schwager, 1866.

Pyrgo serrata = *Biloculina serrata* Bailey, 1861.

Quinqueloculina seminulum = *Serpula seminulum* Linné, 1758.

Quinqueloculina triangularis d'Orbigny, 1846.

Stainforthia complanata = *Virgulina schreibersiana* Czjzek var. *complanata* Egger, 1893. [pl. 2, fig. 9 & pl. 5, fig. 7].

Suggrunda eckisi Natland, 1950. [pl. 1, fig. 13].

Suggrunda porosa Hoffmeister and Berry, 1937. [pl. 1, fig. 14].

Uvigerina cf. *acuelata* d'Orbigny, 1846.

Uvigerina auberiana d'Orbigny, 1839. [pl. 2, fig. 17 & pl. 5, fig. 8].

Uvigerina bifurcata d'Orbigny, 1839.

Uvigerina canariensis d'Orbigny, 1839.

Uvigerina curtica = *Uvigerina pigmea* d'Orbigny var. *curtica* Cushman, 1927.

Uvigerina excellens Todd, 1948.

Uvigerina hispida Schwager, 1866.

Uvigerina peregrina Cushman, 1923. [pl. 2, fig. 13 & pl. 5, fig. 5].

Uvigerina semiornata d'Orbigny, 1846. [pl. 5, fig. 9].

Uvigerina senticosa Cushman, 1927

Uvigerina striata d'Orbigny, 1839. [pl. 3, fig. 6 & pl. 5, fig. 14].

Valvulineria araucana = *Rosalina araucana* d'Orbigny, 1839.

Valvulineria bradyana Fornasini, 1900.

Valvulineria californica Cushman, 1926.

Valvulineria glabra = *Valvulineria vilerdeboana* (d'Orbigny) var. *glabra* Cushman, 1927.

Valvulineria cf. *involuta* Cushman and Dusenbury, 1934.

Valvulineria minuta Parker, 1954.

Appendix 3: Taxonomy references and Plates

Valvulineria cf. olssoni Redmond, 1953.

Valvulineria rugosa = *Rosalina rugosa* d'Orbigny, 1839.

Virgulina apertura Uchio, 1960.

Virgulina bradyi Cushman, 1922.

Virgulina bramlettei Galloway and Morrey, 1929.

Virgulina cornuta Cushman, 1913.

Virgulina pauciloculata Brady, 1884.

Virgulina schreibersiana Czjzek, 1848.

Virgulina seminuda Natland, 1938.

Virgulina spinosa = *Virgulina schreibersiana* Czjzek var. *spinose* Heron-Allen and Earland, 1932.

[pl. 6, fig. 12].

Bibliography of the taxonomic reference list

- Asano, K. and Nakamura, M., 1937. On the Japanese species of Cassidulina. Japanese Jour. Geol. Geogr., Trans. Abstr., Tokyo, Japan, vol. 14, nos. 3-4.
- Bailey, L.W., 1861. Notes on new species of microscopical organisms, chiefly from the Para River, South America, Boston Jour. Nat. Hist., vol. 7, no. 3.
- Bandy, O.L. and Arnal, R.E., 1957. Distribution of recent foraminifera off west coast of Central America. Bull. AAPG, 41, 9, pp. 2037-2053.
- Boltovskoy, E. and Theyer, F., 1970. Foraminiferos recientes de Chile Central. Revista del Museo Argentino de Ciencias Naturales "Bernardino Rivadavia, 2, 9, pp. 280-397.
- Bornemann, J. G., 1855. Die mikroskopische Fauna des Septarienthones von Hermsdorf bei Berlin. Zeitschrift der Deutschen Geologischen Gesellschaft, Berlin, vol. 7, no. 2, pp. 307-371.
- Brady, H.B., 1881. Notes on some of the reticularian Rhizopoda of the Challenger Expedition, Part 3, Quart. Jour. of Micr. Sci., vol. 21, pp. 31-71.
- Brady, H.B., 1884. Report on the Foraminifera dredged by H.M.S. "Challenger" during the years 1873-1876, In: Report on the scientific results of the voyage H.M.S. Challenger during the years 1873-1876, Zoology, vol. 9, 814 pp.
- Brady, H.B., Parker, W.K. and Jones, T.R., 1888. On some foraminifera from the Abrohlos Bank, Zool. Soc. London, Trans., London, vol. 12, pt. 7, no. 1.
- Brotzen, F., 1936. Foraminiferen aus dem schwedischen, untersten Senon von Eriksdal in Schonen. Arsbok Sveriges Geologiska Undersögning, ser. C., no. 396, pp. 206.
- Coulbourn, W.T., 1980. Relationship between the distribution of foraminifera and geologic structures of the Arica Bight, South America, Jour. of Pal., vol. 54, no. 4, pp. 696-718.
- Cushman, J.A., 1911. A monograph of the foraminifera of the North Pacific Ocean, Part 2, Textulariidae. Bull. U. S. Nat. Mus., no. 71, pp.108.
- Cushman, J.A., 1913a. New Textulariidae and other arenaceous Foraminifera from the Philippine Islands and contiguous waters. Proc. U. S. Nat. Mus., vol. 44, pp. 633- 638.
- Cushman, J.A., 1913b. A monograph of the Foraminifera of the North Pacific Ocean, pt 3, Lagenidae, U.S. Nat. Hist. Mus. Bull., no. 71, 125 p.
- Cushman, J.A., 1918. Some Miocene foraminifera of the Coastal Plain of the United States, U.S. Geol. Surv. Bull., Washington D.C., no. 676., pp 73.
- Cushman, J.A., 1922. The Foraminifera of the Atlantic Ocean, Pt. 3, Textulariidae, U.S. Nat. Hist. Mus. Bull., no. 104, 149 pp.
- Cushman, J.A., 1923. The Foraminifera of the Atlantic Ocean, Pt. 4. Lagenidae, U.S. Nat. Hist. Mus. Bull., no. 104, 228 pp.
- Cushman, J.A., 1925. Some Textulariidae from the Miocene of California, Contr. Cushman Lab. Foram. Res., Sharon, Mass., U.S.A, vol. 1, pt. 2, pp. 29-35.

Appendix 3: Taxonomy references and Plates

- Cushman, J.A., 1926a. Some Pliocene Bolivinas from California, Contr. Cushman Lab. Foram. Res., Sharon, Mass., U.S.A, vol. 2, pt. 2, pp. 40-47.
- Cushman, J.A., 1926b. Foraminifera of the typical Monterey of California. Contr. Cushman Lab. Foram. Res., vol. 2, pt. 3, pp. 53-69.
- Cushman, J.A., 1927. Recent Foraminifera from off the West Coast of America, Univ. of California. Scripps Inst. Oceanogr., Bull., Tech. Ser., vol. 1, no. 10, pp. 119-188.
- Cushman, J.A., 1933a. The Foraminifera of the tropical Pacific collections of the "Albatross", 1899-1900. Part 2, Lagenidae to Alveolinidae, U. S. Nat. Mus. Bull., no. 161, pt. 2, 79 pp.
- Cushman, J.A., 1933b. Some new Recent Foraminifera from the Tropical Pacific, Contr. Cushman Lab. Foram. Res., vol. 9, pt. 4, pp. 77-95.
- Cushman, J.A., 1937. A monograph of the subfamily Virguliniinae of the foraminiferal family Buliminidae, Special Publ. No. 9, Cushman Lab. Foram. Res., 228 pp.
- Cushman, J.A. and Dusenbury, jr., A.N., 1934. Eocene Foraminifera of the Poway Conglomerate of California, Contr. Cushman Lab. Foram. Res., vol. 10, pC 3, pp. 51-65.
- Cushman, J.A. and Hughes, D.D., 1925. Some later Tertiary Cassidulinas of California, Contr. Cushman Lab. Foram. Res., vol. 1, no. 1, 99. 11-17.
- Cushman, J.A., and McCulloch, I., 1942. Some Virguliniinae in the collections of the Allan Hancock Foundation, Allan Hancock Pacific Expeditions, vol. 6, no. 4, pp. 179-230.
- Cushman, J.A., and McCulloch, I., 1950. Some Lagenidae in the Collections of the Allan Hancock Foundation, Allan Hancock Pacific Expeditions, vol. 6, no. 6, pp. 295-364.
- Cushman, J.A., and Moyer, D.A., 1930. Some Recent Foraminifera from off San Pedro, California, Contr. Cushman Lab. Foram. Res., vol. 6, pt. 3, pp. 49-62,
- Cushman, J.A. and Parker, F.L., 1938. Notes on some Pliocene and Pleistocene species of *Bulimina* and *Buliminella*, Contr. Cushman Lab. Foram. Res., Sharon, Mass., U.S.A., vol. 14, pt. 3, pp. 53-62.
- Cushman, J.A. and Parker, F. L., 1947. *Bulimina* and related foraminiferal genera. Professional Papers U. S. Geol. Surv., 210-D, pp. 55-176.
- Cushman J.A. and Todd, R., 1943. The genus *Pullenia* and its species, Contr. Cushman Lab. Foram. Res., vol. 19, pt. 1, 23 pp.
- Cushman J.A. and Wickenden, R.T.D., 1929. Recent foraminifera from off Juan Fernandez Islands, U.S. Nat. Mus., Proc., Washington, D.C., U.S.A., no. 2780, vol. 75, art. 9.
- Czjzek, J., 1848. Beitrag zur Kenntnis der fossilen Foraminiferen des Wiener Beckens. Heidinger's Natur. Abhand., Wien, Österreich, vol. 2, no. 1, pp. 137-150.
- Dawson, J.W, 1860. Notice of Tertiary fossils from Labrador, Marine, etc., and remarks on the climate of Canada in the newer Pliocene or Pleistocene record, Canadian Nat. Geol., Montreal, vol. 5.
- d'Orbigny, A.D., 1826. Tableau méthodique de la classe des Céphalopodes, Ann. Sci. Nat. Paris. serie 1, vol. 7, p. 245-315.

Appendix 3: Taxonomy references and Plates

- d'Orbigny, A.D., 1839. Voyage dans l'Amérique méridionale - Foraminifères, vol. 5, pt. 5, 86 pp, Levrault, Strasbourg, France.
- d'Orbigny, A.D., 1846. Foreminifères fossiles du Bassin Tertiaire de Vienne (Autriche), Gide et Compe, Paris, 312 pp.
- Earland, A., 1936. Foraminifera; Part IV - Additional records from the Weddell Sea sector from material obtained by the S.Y. 'Scotia', Discovery Repts. Cambridge, vol. 13, 76 pp.
- Egger, J. G., 1893. Foraminiferen aus Meeresgrundproben, gelothet von 1874 bis 1876 S. M. Sch. Gazelle. Abhandlungen der Bayrischen Akademie der Wissenschaften, München, Math.-Physik. Cl., vol. 18, no. 2, pp. 266-311.
- Ehrenberg, C.G., 1845. Das kleinste organische Leben an mehreren bisher nicht untersuchen Erdpunkten; Mikroskopische Lebensformen von Portugal und Spanien, Süd-Afrika, Hinter-Indien, Japan und Kurdistan, K. Preuss. Akad. Wiss. Berlin, Ber.
- Fichtel, L. von and Moll, J.P.C. von, 1798. Testacea Microscopica alia que minuta ex generibus Argonauta et Nautilus, ad natura pictura et descripta (Mikroskopische und andere kleine Schaltiere aus den geschlectern Argonaute und Schiffer), Camesina, Wien.
- Fornasini, C., 1900. Intorno ad alcuni esemplari di foraminiferi Adriatici. R. Accad. Sci. Ist. Bologna, ser. 5, tomo 8.
- Galloway, J.J. and Morrey, M., 1929. A Lower Tertiary foraminiferal fauna from Manta, Ecuador. Bull. Am. Pal., vol. 15, 56 pp.
- Galloway, J.J. and Wissler, S.G., 1927. Pleistocene foraminifera from the Lomita Quarry, Palos Verdes Hills, California, Jour. of Pal., 1, pp. 35-87.
- Harvey, W.H. and Bailey, J.W., 1854. New species of Diatomaceae, collected by the U.S. Exploring Expedition, under the command of Capt. Wikes, U.S., N. Acad. Nat. Sci. Philadelphia, Proc., vol. 6.
- Heron-Allen, E. and Earland, A., 1930. The foraminifera of the Plymouth district, pt. 1, J. roy. Micr. Soc., London.
- Heron-Allen, E. and Earland, A., 1932. Foraminifera, part I – The ice-free area of the Falkland Islands and adjacent seas. Discovery Reports, vol. 4, pp. 291-460.
- Hoffmeister, W.S. and Berry, C. T., 1937. A new genus of Foraminifera from the Miocene of Venezuela and Trinidad. Jour.l of Pal., vol. 11, no. 1, pp. 29-30.
- Jones, T.R., 1895. A monograph of the foraminifera of the Crag, pt. 2, Palaeontogr. Soc., London.
- McCulloch, I., 1977. Qualitative observations on recent foraminiferal tests with emphasis on the Eastern Pacific, Pts. 1-3, Los Angeles, Univ. of Southern California, x + 1079 pp.
- McCulloch, I., 1977. Qualitative observations on recent foraminiferal tests, pt. 4, with emphasis on the Allan Hancock Atlantic Expedition collections, Los Angeles, Univ. of Southern California, 360 pp.
- Montagu, G., 1803. Testacea Britannica, or Natural History of British Shells, Marina, Land and Fresh Water, Including the Most Minute. Romsey, England, J. S. Hollis, 606 pp.

Appendix 3: Taxonomy references and Plates

- Natland, M.L., 1938. New species of foraminifera from off the west coast of North America and from the later Tertiary of the Los Angeles Basin. Univ. of California, Scripps Inst. of Oceanogr. Bull., Tech. Ser., 4, no.5, pp. 137-163.
- Natland, M.L., 1950. Report on the Pleistocene and Pliocene Foraminifera, 1940 E.W. Scripps Cruise to the Gulf of California, The Geol. Soc. of America, New York, USA, pp. 55.
- Kuwano, Y., 1954. Notes on the genus *Cassidulina* and allied genera from Japan, 2; Description of new species of *Cassidulina* from the Pliocene of southern Kwanto region, Res. Inst. Nat. Res., Misc. Repts., no. 35.
- Lankford, R.R. and Phleger, F.B., 1973. Foraminifera from the nearshore turbulent zone, western North America, Jour. of Foram. Res., vol. 3, no.3, pp. 101-132.
- Linné, C., 1758. Systema naturae. 10th Edition, 1, Holmiae (Stockholm), L. Salvii, 824 pp.
- Parker, F.L., 1954. Distribution of the foraminifera in the northeastern Gulf of Mexico, Harvard Coll., Mus. Comp. Zool., Bull., Cambridge, Mass., vol. 111, no. 10.
- Parker, W. K., and Jones, T. R., 1865. On some foraminifera from the North Atlantic and Arctic Oceans, Including Davis Straits and Baffin's Bay. Phil. Trans. Royal Society, Vol. 155, pp. 325-441.
- Parr, W. J., 1950. Foraminifera. Reports B.A.N.Z. Antarctic Research Expedition 1929-1931, ser. B (Zoology, Botany), 5, 6, pp. 232-392.
- Phleger, F.P. and Parker, F.L., 1951. Ecology of foraminifera, northwest Gulf of Mexico, Part 2: Foraminifer Species. Geol. Soc. Am. Mem. 46, 64 pp.
- Phleger, F.P. and Parker, F.L., 1952. New names for northwestern Gulf of Mexico foraminifera. Cushman Found. Foram. Res., Contr. Washington, D.C., vol. 3, pt. 1, 14 pp.
- Rau, W.W., 1948. Foraminifera from the Porter shale (Lincoln formation) Grays Harber County, Washington. Jour. Pal., vol. 22.
- Redmond, C.D., 1953. Miocene foraminifera from the Tubara beds of northern Colombia, Jour. Pal., Tulsa, vol. 27, no. 5.
- Resig, J. M., 1981. Biogeography of benthic foraminifera of the northern Nazca Plate and adjacent Continental margin, Geol. Soc. of America, Mem., 154, pp. 619-665.
- Reuss, A.E., 1850. Neue Foraminiferen aus den Schichten des österreichischen Tertiärbeckens, Denkschr. K. Akad. Wiss. Wien, Math.-Nat. Cl., vol. 1, pp. 365-390.
- Reuss, A.E., 1851. Über die fossilen Foraminiferen und Entomostraceen der Septarienthone der Umgegend von Berlin. Zeitschrift der Deutschen Geologischen Gesellschaft, Berlin: 3, pp. 49-91.
- Reuss, A.E., 1863. Die Foraminiferen-Familie der Lagenideen, K. Akad. Wiss. Wien, Math.-Nat. Cl., vol. 46, no. 1.
- Reuss, A.E., 1870. Die Foraminiferen des Septarienthones von Pietzpuhl, K. Akad. Wiss. Wien, Math.-Nat. Cl., vol. 62.

Appendix 3: Taxonomy references and Plates

- Schwager, C., 1866. Fossile Foraminiferen von Kar Nikobar, Novara Exp., 1857-1859, Geol. Theil., vol. 2, pp. 187-268.
- Seguenza, G., 1862. Prime ricerche intorno ai Rizopodi fossili delle argile Pleistoceniche dei dintorni di Catania, Accad. Gioenica Sci. Nat. Catania 18.
- Silvestri, A., 1898. Foraminiferi pliocenici della Provincia di Siena, Part 2, Mem, dell'Acad. Pont. dei Nuovi Lincei, Roma, Italia, 15.
- Stewart, R. E. and Stewart, K. C., 1930. Post-Miocene foraminifera from the Ventura Quadrangle, Ventura County, California. Jour. of Pal.. vol. 4, no. 1, pp. 60-72.
- Todd, R., 1948. Subfamily Uvigerininae. In: Cushman, J. A., and McCulloch, I., The species of Bulimina and related genera in the collections of the Allan Hancock Foundation. Southern California Univ., Publ., Allan Hancock Pacific Exped. vol. 6, no. 5.
- Uchio, T., 1960. Ecology of living benthonic Foraminifera from the San Diego, California area. Cushman Found. Foram. Res., Special Publ., no. 5, 72 pp.
- Vismara Schilling, A. and Parisi, E., 1981. *Anomalinoidea minimus*, a new benthic foraminiferal species from Pleistocene and Holocene deep sea deposits of the Mediterranean Sea. Riv. Ital. Pal. Stratigr. 87, 284-286.
- Walker, G., and Boys, W., 1784. Testacea minuta varia, nuperime detecta in arena littoris Sandvicensis a Gul. Boys, arm. SA.S. Multa addidit, et omnium figures ope microscopii ampliatus curate delineavit Geo. Walker. London, 24 pp.
- Walker, G., and Jacob, E., 1798. Adams' essays on the microscope. In: F. Kanmacher, London, edition 2.
- Wiesner, H., 1931. Die foraminiferen der deutschen Südpolar Expedition 1901-1903, In: Drygalski, E. von, Deutsche Südpolar Expedition 1901-1903, vol. 20.
- Williamson, W.C., 1848. On the british recent species of the genus *Lagena*, Ann. Mag. Nat. Hist., ser. 2, I, 20 pp.
- Williamson, W.C., 1858. On the Recent Foraminifera of Great Britain, vol. 29, Ray Society London.

PLATES 1 – 7

Plates 1 – 4: optical microscope images of the species observed in the sediment samples. All images were taken with a Keyence VHX – 700 FD camera.

Plates 5 – 7: Scanning electron microscope (SEM) images of the same specimens as in Plates 1 – 4. All images were taken with a CamScan 44/EDX scanning electron microscope.

Plate 1

Optical microscope images; scale bar is 100 μ m.

- | | |
|--|---------------------|
| 1. <i>Bolivina costata</i> | Sample 52-2; 270 cm |
| 2. <i>Bolivina ordinaria</i> | Sample 47-2; 128 cm |
| 3. <i>Bolivina</i> cf. <i>seminuda</i> var. <i>humilis</i> | Sample 416; 200 cm |
| 4. <i>Bolivina seminuda</i> | Sample 416; 200 cm |
| 5. <i>Bolivina interjuncta</i> var. <i>bicostata</i> | Sample 52-2; 520 cm |
| 6. <i>Bolivina interjuncta</i> var. <i>bicostata</i> | Sample 52-2; 450 cm |
| 7. <i>Bolivinita minuta</i> | Sample 52-2; 270 cm |
| 8. <i>Bolivina</i> aff. <i>tortuosa</i> | Sample 59-1; 523 cm |
| 9. <i>Bolivina seminuda</i> var. <i>humilis</i> | Sample 47-2; 113 cm |
| 10. <i>Bolivina pacifica</i> | Sample 52-2; 270 cm |
| 11. <i>Bolivina tongi</i> var. <i>filacostata</i> | Sample 59-1; 523 cm |
| 12. <i>Buliminella</i> cf. <i>curta</i> | Sample 50-4; 100 cm |
| 13. <i>Suggrunda eckisi</i> | Sample 50-4; 110 cm |
| 14. <i>Suggrunda porosa</i> | Sample 47-2; 128 cm |
| 15. <i>Fursenkoina fusiformis</i> | Sample 50-4; 230 cm |
| 16. <i>Fursenkoina glabra</i> | Sample 50-4; 230 cm |
| 17. <i>Buliminella elegantissima</i> | Sample 416; 180 cm |
| 18. <i>Bulimina mexicana</i> | Sample 52-2; 520 cm |
| 19. <i>Bulimina pagoda</i> | Sample 52-2; 520 cm |

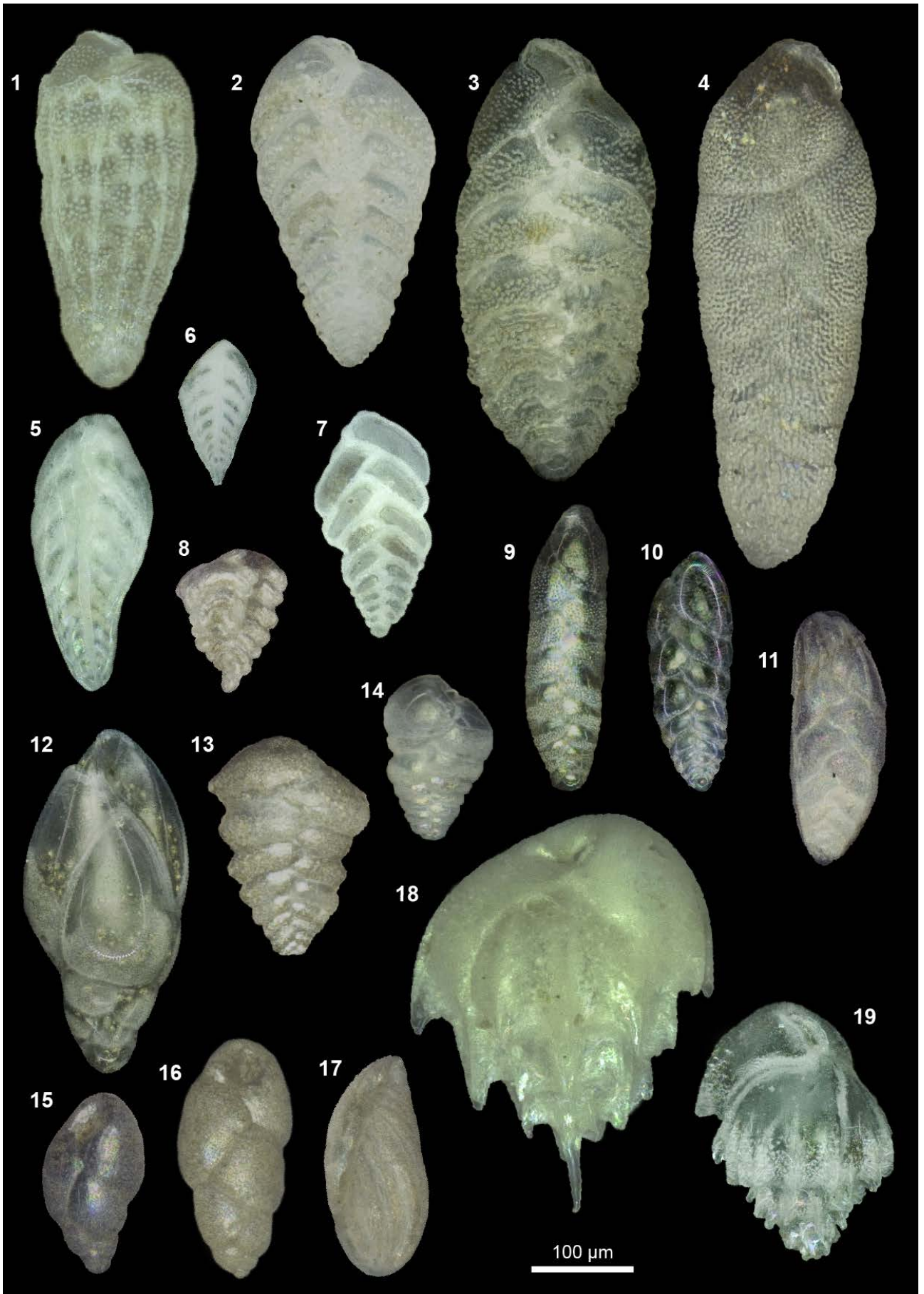


Plate 2

Optical microscope images; scale bar is 200 μ m.

- | | |
|--|---------------------|
| 1. <i>Bolivina interjuncta</i> | Sample 47-2; 168 cm |
| 2. <i>Bolivina subadvena</i> | Sample 47-2; 113 cm |
| 3. <i>Bolivina plicata</i> microspheric form | Sample 416; 200 cm |
| 4. <i>Bolivina plicata</i> macrospheric form | Sample 416; 100 cm |
| 5. <i>Bolivina argentea</i> | Sample 50-4; 350 cm |
| 6. <i>Praeglobobulimina spinescens</i> | Sample 47-2; 168 cm |
| 7. <i>Bolivina spissa</i> macrospheric form | Sample 52-2; 520 cm |
| 8. <i>Bolivina spissa</i> microspheric form | Sample 47-2; 128 cm |
| 9. <i>Stainforthia complanata</i> | Sample 50-4; 210 cm |
| 10. <i>Bolivina alata</i> | Sample 50-4; 110 cm |
| 11. <i>Buliminella tenuata</i> | Sample 50-4; 100 cm |
| 12. <i>Globobulimina pacifica</i> | Sample 52-2; 230 cm |
| 13. <i>Uvigerina peregrina</i> | Sample 416; 200 cm |
| 14. <i>Bulimina exilis</i> | Sample 50-4; 100 cm |
| 15. <i>Bulimina exilis</i> | Sample 50-4; 100 cm |
| 16. <i>Buliminella curta</i> var. <i>basispinata</i> | Sample 50-4; 350 cm |
| 17. <i>Uvigerina auberiana</i> | Sample 50-4; 350 cm |
| 18. <i>Cassidulina crassa</i> | Sample 52-2; 520 cm |

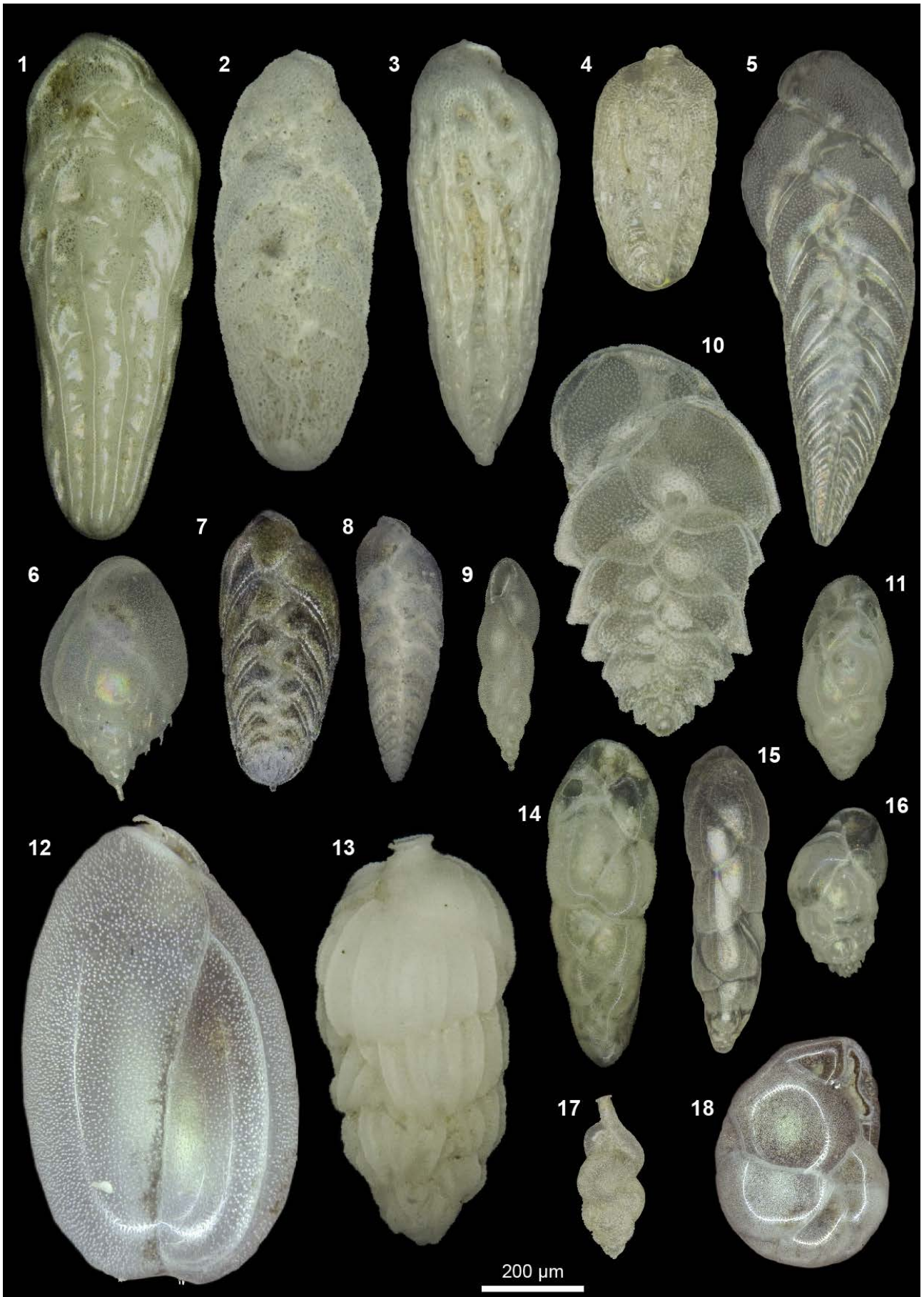


Plate 3

Optical microscope images; scale bar is 200 μ m.

- | | |
|--|---------------------|
| 1. <i>Planulina limbata</i> umbilical view | Sample 416; 100 cm |
| 2. <i>Epistominella pacifica</i> | Sample 416; 200 cm |
| 3. <i>Epistominella pacifica</i> umbilical view | Sample 416; 200 cm |
| 4. <i>Angulogerina angulosa</i> | Sample 50-4; 100 cm |
| 5. <i>Epistominella smithi</i> spiral view | Sample 50-4; 210 cm |
| 6. <i>Uvigerina striata</i> | Sample 416; 200 cm |
| 7. <i>Uvigerina hispida</i> | Sample 52-2; 120 cm |
| 8. <i>Epistominella afueraensis</i> spiral view | Sample 416; 200 cm |
| 9. <i>Epistominella afueraensis</i> umbilical view | Sample 416; 200 cm |
| 10. <i>Gyroidina rothwelli</i> umbilical view | Sample 416; 100 cm |
| 11. <i>Gyroidina rothwelli</i> spiral view | Sample 416; 100 cm |

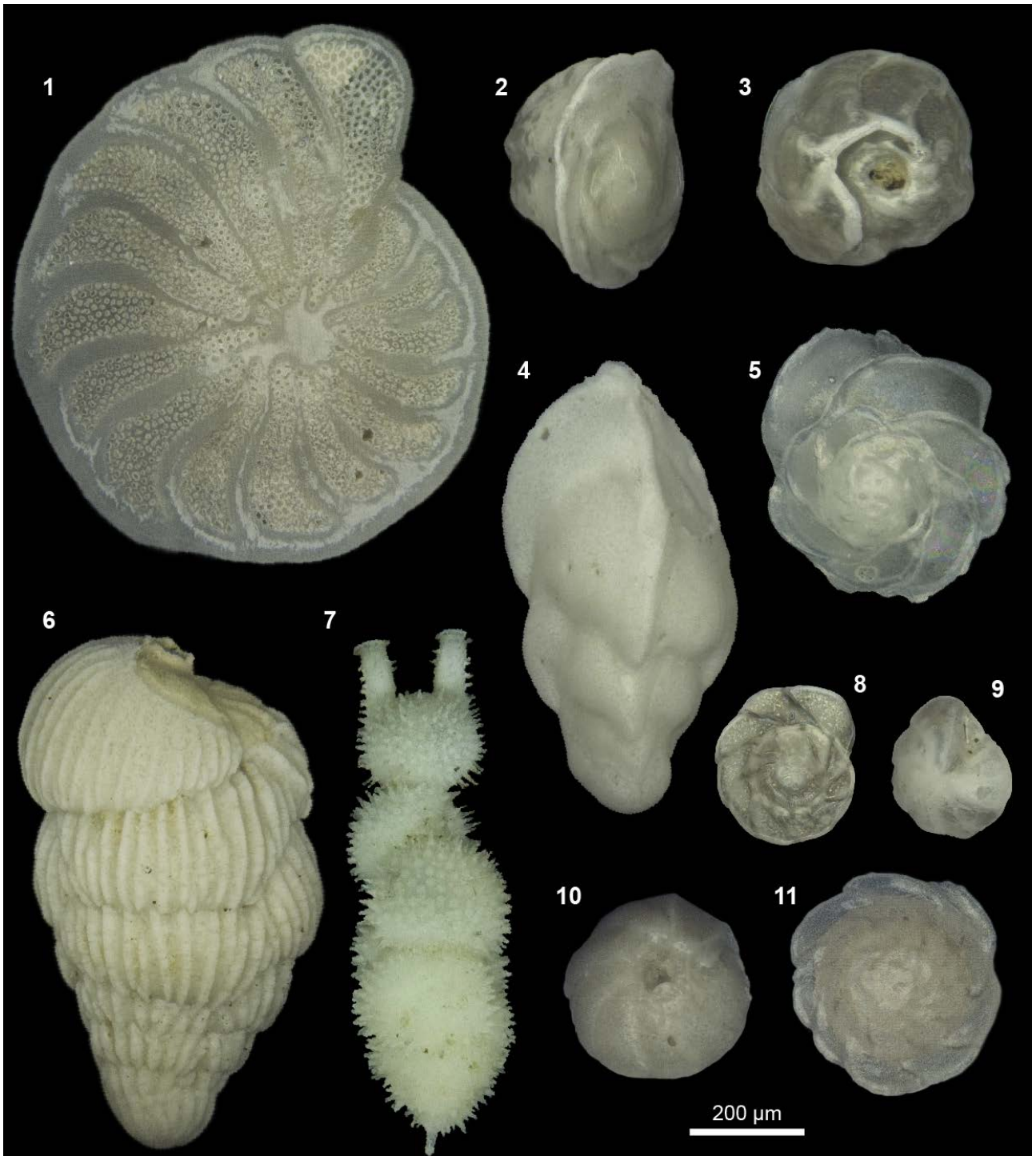


Plate 4

Optical microscope images; scale bar is 100 μ m.

- | | |
|--|---------------------|
| 1. <i>Epistominella pacifica</i> umbilical view | Sample 47-2; 128 cm |
| 2. <i>Epistominella exigua</i> spiral view | Sample 52-2; 450 cm |
| 3. <i>Epistominella exigua</i> umbilical view | Sample 52-2; 450 cm |
| 4. <i>Anomalinoides minimus</i> spiral view | Sample 59-1; 523 cm |
| 5. <i>Anomalinoides minimus</i> umbilical view | Sample 59-1; 523 cm |
| 6. <i>Epistominella obesa</i> spiral view | Sample 50-4; 100 cm |
| 7. <i>Epistominella obesa</i> spiral view | Sample 50-4; 100 cm |
| 8. <i>Epistominella obesa</i> umbilical view | Sample 50-4; 100 cm |
| 9. cf. <i>Buccella peruviana</i> spiral view | Sample 50-4; 230 cm |
| 10. cf. <i>Buccella peruviana</i> umbilical view | Sample 47-2; 113 cm |
| 11. <i>Cassidulina auka</i> | Sample 416; 100 cm |
| 12. <i>Alabaminella weddellensis</i> spiral view | Sample 52-2; 270 cm |
| 13. <i>Gyrodina subtenera</i> spiral view | Sample 52-2; 270 cm |
| 14. <i>Gyrodina subtenera</i> umbilical view | Sample 52-2; 230 cm |
| 15. <i>Cassidulina minuta</i> | Sample 52-2; 120 cm |
| 16. <i>Cassidulina carinata</i> | Sample 50-4; 210 cm |
| 17. <i>Cassidulina delicata</i> | Sample 47-2; 128 cm |



Plate 5

SEM images; scale bar is 200 µm.

* different specimens depicted in optical microscope and SEM image

1. <i>Bolivina interjuncta</i>	Sample 47-2; 168 cm
2. <i>Bolivina plicata</i> microspheric form	Sample 416; 200 cm
3. <i>Bolivina plicata</i> macrospheric form	Sample 416; 100 cm
4. <i>Bolivina spissa</i>	Sample 52-2; 520 cm
5. <i>Uvigerina peregrina</i> *	Sample 416; 200 cm
6. <i>Praeglobobulimina spinescens</i>	Sample 47-2; 168 cm
7. <i>Stainforthia complanata</i>	Sample 50-4; 210 cm
8. <i>Uvigerina auberiana</i>	Sample 50-4; 350 cm
9. <i>Uvigerina semiornata</i>	Sample 52-2; 230 cm
10. <i>Bolivina alata</i>	Sample 50-4; 110 cm
11. <i>Buliminella</i> cf. <i>curta</i>	Sample 50-4; 100 cm
12. <i>Bulimina exilis</i>	Sample 50-4; 100 cm
13. <i>Bulimina exilis</i>	Sample 50-4; 350 cm
14. <i>Uvigerina striata</i>	Sample 416; 200 cm
15. <i>Hoeglundina elegans</i>	Sample 52-2; 500 cm
16. <i>Globobulimina pacifica</i>	Sample 52-2; 230 cm
17. <i>Cassidulina delicata</i>	Sample 47-2; 128 cm
18. <i>Cassidulina crassa</i>	Sample 52-2; 520 cm
19. <i>Cassidulina auka</i>	Sample 416; 100 cm

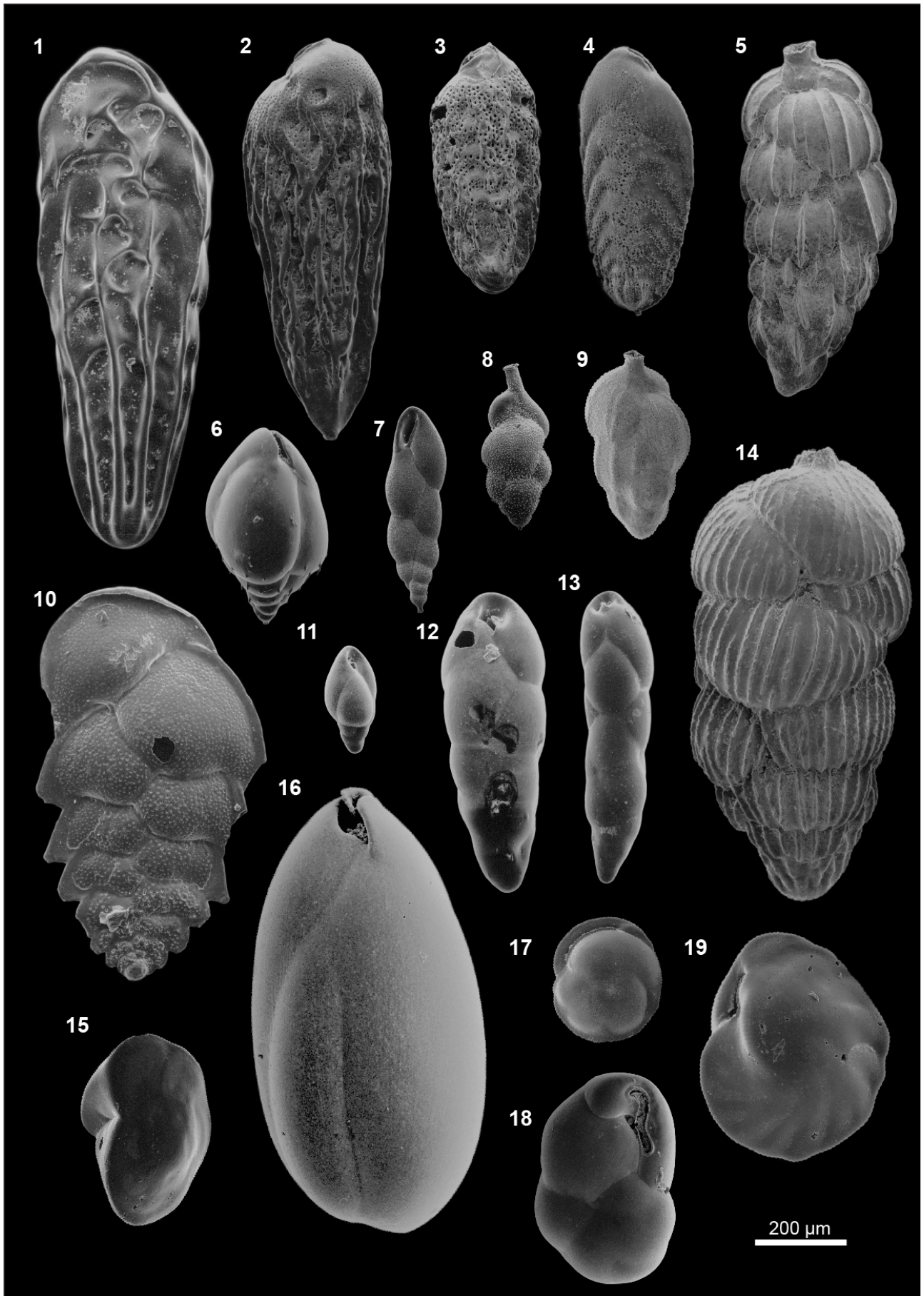


Plate 6

SEM images; scale bar is 100 μ m.

1. <i>Bolivina seminuda</i>	Sample 416; 200 cm
2. <i>Bolivina</i> cf. <i>seminuda</i> var. <i>humilis</i>	Sample 416; 200 cm
3. <i>Bolivina seminuda</i> var. <i>humilis</i>	Sample 47-2; 113 cm
4. <i>Bolivina pacifica</i>	Sample 52-2; 270 cm
5. <i>Bolivina interjuncta</i> var. <i>bicostata</i>	Sample 52-2; 520 cm
6. <i>Bolivinita minuta</i>	Sample 52-2; 270 cm
7. <i>Bolivina</i> aff. <i>tortuosa</i>	Sample 59-1; 523 cm
8. <i>Bolivina costata</i>	Sample 52-2; 270 cm
9. <i>Bolivina ordinaria</i>	Sample 47-2; 128 cm
10. <i>Bulimina pagoda</i>	Sample 52-2; 520 cm
11. <i>Fursenkoina fusiformis</i>	Sample 50-4; 230 cm
12. <i>Virgulina spinosa</i>	Sample 59-1; 963 cm
13. <i>Fursenkoina glabra</i>	Sample 50-4; 230 cm
14. <i>Animolinoides minimus</i> spiral view	Sample 59-1; 523 cm
15. cf. <i>Buccella peruviana</i> umbilical view	Sample 47-2; 113 cm
16. cf. <i>Buccella peruviana</i> peripheral view	Sample 47-2; 113 cm
17. cf. <i>Buccella peruviana</i> spiral view	Sample 50-4; 230 cm
18. <i>Epistominella exigua</i> spiral view	Sample 52-2; 450 cm
19. <i>Epistominella exigua</i> umbilical view	Sample 52-2; 450 cm
20. <i>Animolinoides minimus</i> umbilical view	Sample 59-1; 523 cm
21. <i>Epistominella afueraensis</i> umbilical view	Sample 416; 200 cm
22. <i>Epistominella afueraensis</i> peripheral view	Sample 416; 200 cm
23. <i>Epistominella afueraensis</i> spiral view	Sample 416; 200 cm
24. <i>Alabaminella weddellensis</i> spiral view	Sample 52-2; 270 cm

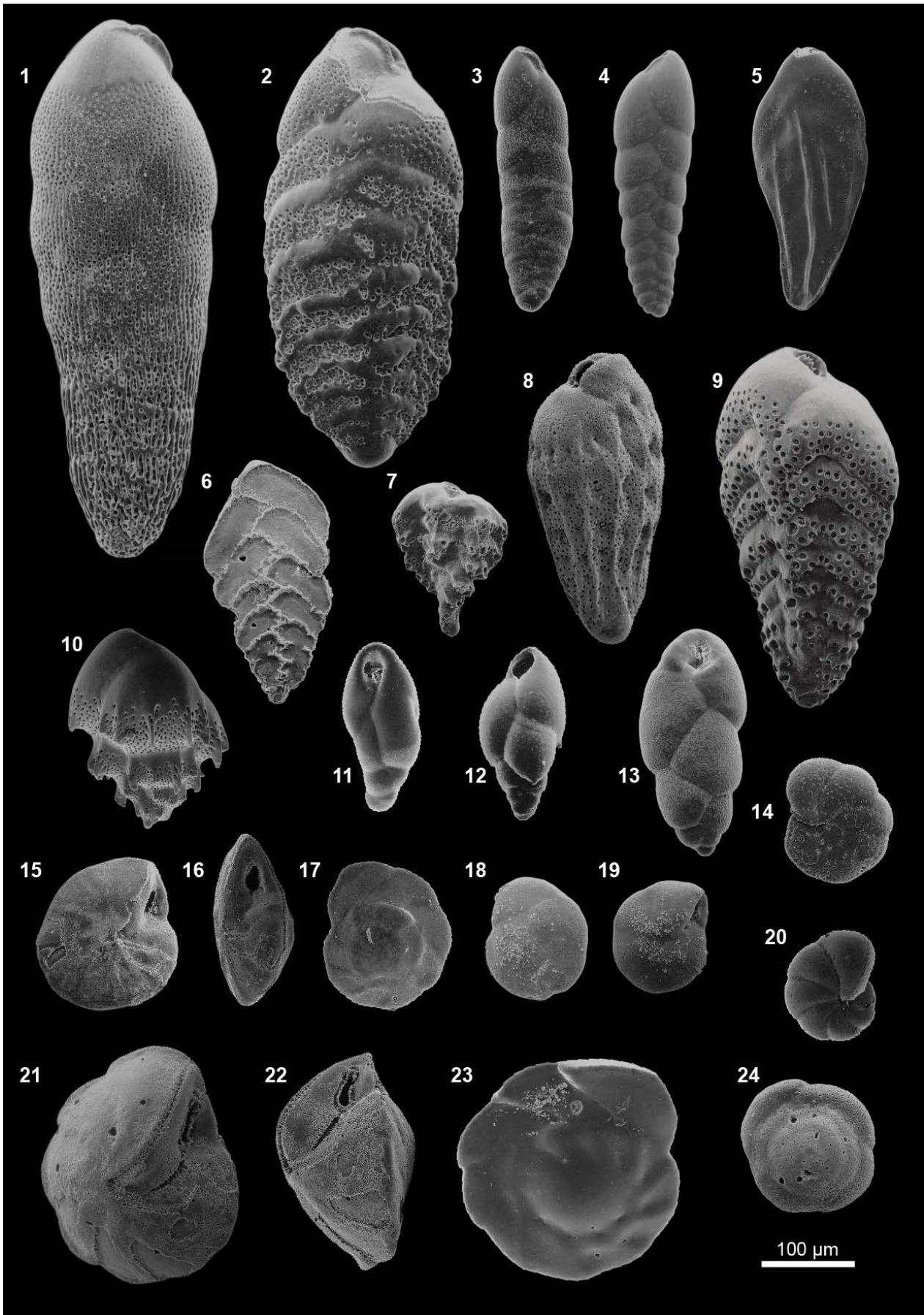
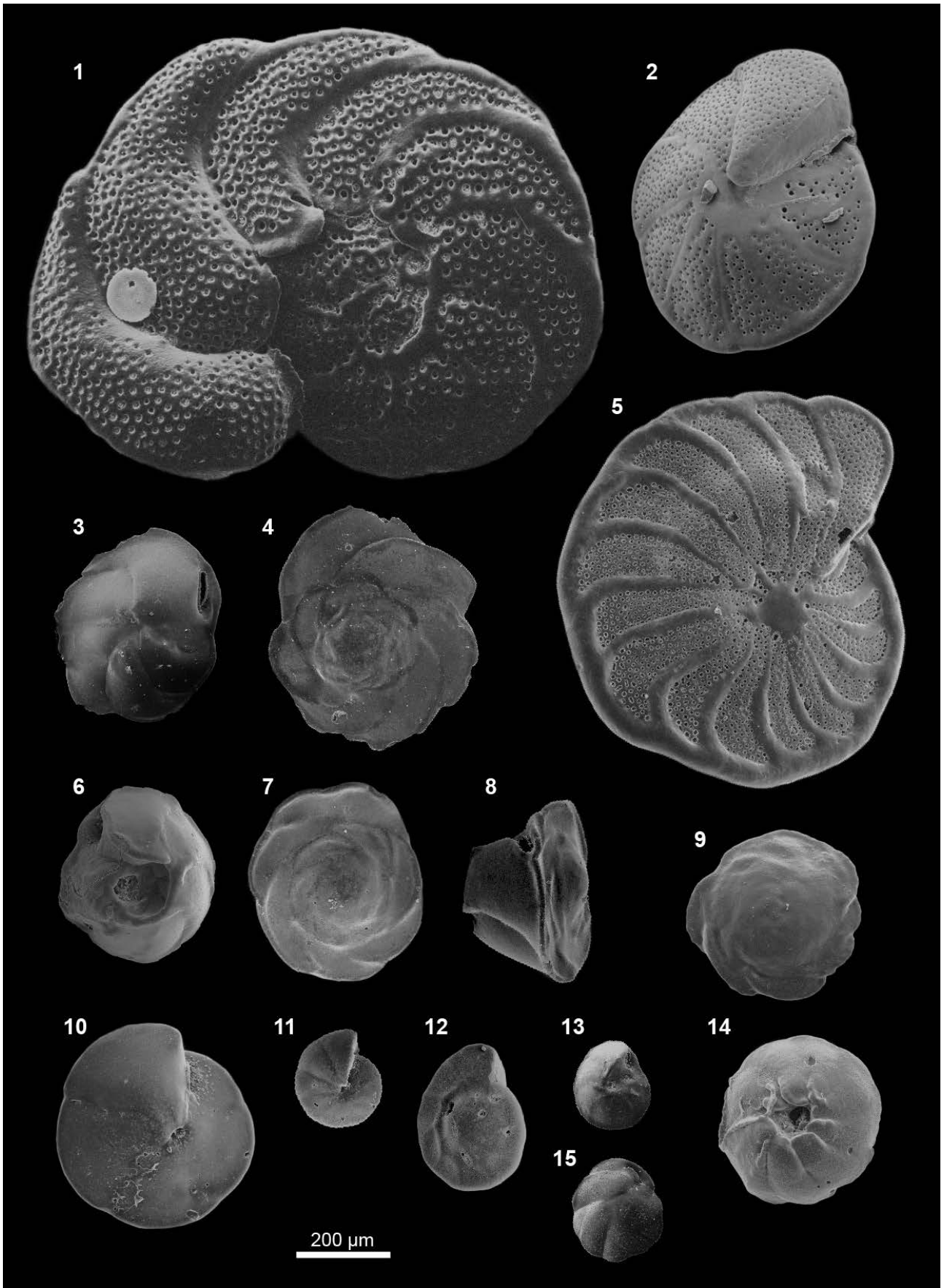


Plate 7

SEM images; scale bar is 200 μ m.

- | | |
|--|---------------------|
| 1. <i>Cibicidoides wuellerstorfi</i> spiral view | Sample 52-2; 500 cm |
| 2. <i>Cibicides mckannai</i> umbilical view | Sample 52-2; 230 cm |
| 3. <i>Epistominella smithi</i> umbilical view | Sample 50-4; 210 cm |
| 4. <i>Epistominella smithi</i> spiral view | Sample 50-4; 210 cm |
| 5. <i>Planulina limbata</i> umbilical view | Sample 416; 100 cm |
| 6. <i>Epistominella pacifica</i> umbilical view | Sample 416; 200 cm |
| 7. <i>Epistominella pacifica</i> spiral view | Sample 416; 200 cm |
| 8. <i>Epistominella pacifica</i> peripheral view | Sample 416; 200 cm |
| 9. <i>Gyroidina rothwelli</i> spiral view | Sample 416; 100 cm |
| 10. <i>Oridorsalis umbonatus</i> umbilical view | Sample 52-2; 230 cm |
| 11. <i>Gyroidina subtenera</i> umbilical view | Sample 52-2; 230 cm |
| 12. <i>Gyroidina subtenera</i> spiral view | Sample 52-2; 270 cm |
| 13. <i>Epistominella pacifica</i> umbilical view | Sample 47-2; 128 cm |
| 14. <i>Gyroidina rothwelli</i> umbilical view | Sample 416; 100 cm |
| 15. <i>Cassidulina carinata</i> | Sample 50-4; 210 cm |



Appendix 3: Taxonomy references and plates

Appendix 4: Species protocols

Species protocol of core M77/1-416							
Sediment core depth (cm)	100	120	140	160	180	200	220
species \ split	1/64	1/8	1/16	1/64	1/32	1/16	1/16
<i>Angulogerina carinata</i>							1
<i>Bolivina advena</i>				1	3		
<i>Bolivina alata</i>		1		1			
<i>Bolivina costata</i>		1					
<i>Bolivina interjuncta</i>	4	5		4	6	12	1
<i>Bolivina interjuncta</i> var. <i>bicostata</i>				1	1		
<i>Bolivina pacifica</i>		7		4		7	1
<i>Bolivina plicata</i>	2	1	1	4	7	20	9
<i>Bolivina seminuda</i>	3			2	6	8	
<i>Bolivina seminuda</i> var. <i>humilis</i>	8	16	7	17	2	47	58
<i>Bolivina serrata</i>				1		4	2
<i>Bolivina subadvena</i>	1						
<i>Bolivina</i> aff. <i>tortuosa</i>				2		5	7
<i>Bolivina</i> cf. <i>minima</i>						2	
<i>Bolivinita minuta</i>	2	2					1
cf. <i>Buccella peruviana</i>			1			1	
<i>Bulimina exilis</i>						4	
<i>Buliminella curta</i>	1	2		1		4	
<i>Buliminella elegantissima</i>		2	23	1	28	1	
<i>Buliminella tenuata</i>		6		1		6	
<i>Buliminella</i> sp.							1
<i>Cancris carmenensis</i>	1						
<i>Cancris inflatus</i>						1	2
<i>Cassidulina auka</i>	84	43	23	20	9	18	5
<i>Cassidulina carinata</i>					1		
<i>Cassidulina crassa</i>	4	2	3	1		1	
<i>Cassidulina delicata</i>	1						12
<i>Cassidulina pulchella</i>			1		4		
<i>Cassidulina</i> spp.	3		3	5			4
<i>Cibicides floridanus</i>	2	3					
<i>Cibicidoides</i> sp.			1				
<i>Ehrenbergina pupa</i>	2						
<i>Epistominella afueraensis</i>	2	70		13		24	25
<i>Epistominella exigua</i>	14	6					
<i>Epistominella obesa</i>			2		12	3	15
<i>Epistominella pacifica</i>	22	31	10	14	1	120	34

Sediment core depth (cm)	100	120	140	160	180	200	220
<i>Fursenkoina fusiformis</i>		2					
<i>Globobulimina pacifica</i>		1				1	
<i>Globocassidulina subglobosa</i>	5	1			1	1	8
<i>Globocassidulina</i> sp.	1						
<i>Gyroidina rothwelli</i>	29	28	3	20	2	8	20
<i>Gyroidina subtenera</i>		1					
<i>Gyroidina</i> sp.							1
<i>Nonionella</i> cf. <i>auricula</i>			3		2	3	
<i>Nonionella auris</i>		2	10		20		
<i>Nonionella turgida</i>		3	1		2		
<i>Nonionides grateloupianus</i>			1	2			
<i>Planulina limbata</i>	16	6	4	3	1	5	9
<i>Praeglobobulimina spinecens</i>	1						
<i>Pseudoparella subperuviana</i>			5		23	3	6
<i>Pullenia subcarinata</i>				1			
<i>Quinqueloculina</i> sp.	1						
<i>Stainforthia complanata</i>			1				
<i>Suggrunda porosa</i>		4		3			1
<i>Uvigerina excellens</i>				5		5	
<i>Uvigerina peregrina</i>		5		2		20	15
<i>Uvigerina semiornata</i>	6		1	2	1	10	4
<i>Uvigerina striata</i>	2	2			1	8	14
<i>Valvulineria araucana</i>						4	
<i>Valvulineria</i> cf. <i>olssoni</i>			4		2		
<i>Valvulineria rugosa</i>	4	3		2			6
<i>Valvulineria</i> sp.						1	
<i>Virgulina cornuta</i>				1		1	

Taxa_S	26	28	21	28	22	33	26
Individuals	221	256	108	134	135	358	262
n	0.0123	0.1405	0.0590	0.0080	0.0279	0.0634	0.0577
>63 µm weight (g)	0.6285	0.111	8.3161	0.7854	8.4869	0.9055	0.1629
Abundance (#/g sed)	28588	16415	220	21327	570	6236	27874
Fisher_alpha	7.654	8.011	7.776	10.780	7.458	8.864	7.172
Shannon_H	2.294	2.458	2.482	2.764	2.492	2.568	2.679
Dominance_D	0.185	0.138	0.121	0.089	0.116	0.148	0.098

Appendix 4: Species protocols

Species protocol of core M77/2-47-2												
Sediment core depth (cm)	108	113	118	123	128	133	138	153	158	163	168	173
species \ split	1/256	1/128	1/128	1/128	1/256	1/512	1/512	1/512	1/512	1/512	1/512	1/2048
<i>Angulogerina carinata</i>		2	1	1								
<i>Anomalinooides minimus</i>	2		1									1
<i>Bolivina advena</i>	1	1	5									
<i>Bolivina advena</i> var. <i>striatella</i>				5	2	3				2		
<i>Bolivina alata</i>	1	4	1	1	2	1	5		1	8	2	6
<i>Bolivina albatrossi</i>				3	4			2	1			
<i>Bolivina costata</i>	82	76	129	98	95	51	59	74	43	177	59	86
<i>Bolivina interjuncta</i>	7	13	7	5	11	4		5	11	22	9	8
<i>Bolivina interjuncta</i> var. <i>bicostata</i>	2					1	3					1
<i>Bolivina ordinaria</i>	4	5	13	2	5	2	1	4	2	9	2	
<i>Bolivina pacifica</i>	10	1	2			3		2	3	2	1	6
<i>Bolivina plicata</i>			2	4	1			1	2	4	1	2
<i>Bolivina</i> cf. <i>quadrata</i>									3			
<i>Bolivina seminuda</i>	7	7	13	8	4	4	5	3	8	10	7	4
<i>Bolivina seminuda</i> var. <i>humilis</i>	23	18		8	8	3	9	11	5	13	6	2
<i>Bolivina spissa</i>	3	14	10	5	6	3	4	3	1	11	2	2
<i>Bolivina subadvena</i>	9	3	10	10	10	10	3	2	10	1	9	7
<i>Bolivina</i> sp.							1					
<i>Bolivinita minuta</i>	12	16	21	25	12	7	4	9	6	17	2	6
<i>Buccella peruviana</i>	20	40	23	16	11	12	5	16	12	34	8	13
<i>Bulimina exilis</i>								1	3	1		
<i>Bulimina mexicana</i>							1					
<i>Bulimina</i> cf. <i>pagoda</i>			1						1			
<i>Bulimina</i> spp.				3			3				1	
<i>Buliminella curta</i>		2	1				3	5	1		1	4
<i>Buliminella elegantissima</i>	1						1		1			1
<i>Buliminella tenuata</i>	3	4		1	1			2	1	2		
<i>Cancris inflatus</i>	1											
<i>Cassidulina auka</i>	3	9	4	3	2	4	1	4	2	16	5	11
<i>Cassidulina carinata</i>										1		
<i>Cassidulina delicata</i>	30	54	69	65	53	28	32	27	19	77	27	20
<i>Cassidulina laevigata</i>								2		5		2
<i>Cassidulina minuta</i>	13		21		10	8	14	31	9	15	14	
<i>Cassidulina pulchella</i>						2						
<i>Cassidulina</i> spp.		2		1	1		1					
<i>Cibicides floridanus</i>				1								

Appendix 4: Species protocols

Sediment core depth (cm)	108	113	118	123	128	133	138	153	158	163	168	173
<i>Cibicides spiralis</i>			1									
<i>Epistominella afueraensis</i>	7	11	25	11			2	3	5	14	3	4
<i>Epistominella exigua</i>	5								1	1		
<i>Epistominella obesa</i>	41	71	18	10	43	38	40	55	48	62	15	21
<i>Epistominella pacifica</i>	15	11	20	16	12	5	11	10	3	13	7	2
<i>Epistominella</i> sp.						1						
<i>Eponides pusillus</i>						1	1					
<i>Fursenkoina fusiformis</i>	3			1			1			1	1	1
<i>Globobulimina affinis</i>										1		
<i>Globobulimina ovula</i>					2			1				
<i>Globobulimina pacifica</i>	1	1		1	1	2		2	1	1		1
<i>Globocassidulina subglobosa</i>		2	3	7	4				2	4		1
<i>Gyroidina altiformis</i>	3		1									
<i>Gyroidina neosoldanii</i>										1		
<i>Gyroidina rothwelli</i>	2											
<i>Gyroidina subtenera</i>		1										
<i>Gyroidina</i> sp.		1							1		1	
<i>Hoeglundina elegans</i>	1											
<i>Lagena amphora</i>									1			
<i>Lagena hispidula</i>							1					
<i>Lagena laevis</i>						1						
<i>Lagena striata</i>				1		1						
<i>Lagena sulcata</i>						1						
<i>Lenticulina convergens</i>		1										
<i>Melonis affinis</i>	1											
<i>Nonionella iridea</i>	2					2	1		1	1	1	1
<i>Nonionella stella</i>						1						
<i>Nonionella turgida</i>		1										
<i>Nonionides grateloupii</i>		1										
<i>Oolina globosa</i>			1									
<i>Oridorsalis umbonatus</i>											1	
<i>Planulina limbata</i>		4	2					1		1	3	1
<i>Praeglobulimina spinescens</i>		2	2				1		4	1	3	1
<i>Pseudoparella subperuviana</i>	36	55	51	57	30	21	19	11	42	73	10	11
<i>Pseudoparella</i> sp.	38	24	22	26	34	20	11	41	32	46	12	39
<i>Pullenia elegans</i>	1								1	3		1
<i>Pullenia subcarinata</i>												1
<i>Quinqueloculina seminulum</i>			1									

Appendix 4: Species protocols

Sediment core depth (cm)	108	113	118	123	128	133	138	153	158	163	168	173
<i>Suggrunda eckisi</i>	3		1			5		5	6	7		3
<i>Suggrunda porosa</i>	7	9	3	8	5	4	10	12	11	12	3	8
<i>Uvigerina auberiana</i>			1	1								
<i>Uvigerina excellens</i>	1				1							
<i>Uvigerina peregrina</i>	11	5	14	3	1	3	2	2	5	1	2	
<i>Uvigerina semiornata</i>		5	6	8	6		2			3	6	1
<i>Uvigerina striata</i>	3	1	3	4	2		3		1	1	2	
<i>Valvulineria araucana</i>	1								1	1		
<i>Valvulineria glabra</i>					1							
<i>Valvulineria rugosa</i>				2	1						2	
<i>Valvulineria sp.</i>			1									1
<i>Virgulina bradyi</i>								1				1
<i>Virgulina cornuta</i>			1		1			1		3	2	
<i>Virgulina sp.</i>										1		1
Unknown calcareous		1										

Taxa_S	40	37	39	36	33	34	32	33	38	45	33	37
Individuals	416	478	511	421	382	256	261	346	309	680	229	282
n	0.0043	0.0085	0.0076	0.0064	0.0031	0.0023	0.0020	0.0019	0.0016	0.0017	0.0016	0.0007
>63 µm weight (g)	0.9777	0.7414	0.5537	0.7685	0.744	0.6663	0.7548	0.8906	0.9494	2.3432	1.8588	1.4885
Abundance (#/g sed)	98951	75850	121432	85597	165626	167048	172893	204475	203418	170707	76999	270646
Fisher_alpha	10.910	9.361	9.822	9.419	8.665	10.520	9.578	8.973	11.390	10.830	10.580	11.390
Shannon_H	2.943	2.791	2.747	2.701	2.639	2.801	2.698	2.658	2.875	2.731	2.826	2.656
Dominance_D	0.082	0.090	0.108	0.111	0.115	0.095	0.107	0.107	0.085	0.113	0.102	0.133

Appendix 4: Species protocols

Species protocol of core M77/2-50-4															
Sediment core depth (cm)	60	70	80	90	100	110	130	150	170	190	210	230	330	340	350
species \ split	1/64	1/32	1/32	1/128	1/32	1/16	1/16	1/16	1/32	1/32	1/32	1/32	1/64	1/64	1/32
<i>Alabaminella weddellensis</i>	1	1						1	1				1		1
<i>Angulogerina angulosa</i>		3		1											
<i>Angulogerina carinata</i>	2	5			3			1							
<i>Bolivina advena</i>						2		3						1	2
<i>Bolivina advena</i> var. <i>striatella</i>	2					2									
<i>Bolivina alata</i>		3	1	1	2	13		1	3		2	6	1	1	10
<i>Bolivina albatrossi</i>			1	2		2	1								
<i>Bolivina argentea</i>					1	3	2	2							2
<i>Bolivina costata</i>	145	120	250	74	146	199	118	126	54	10	47	46	47	13	53
<i>Bolivina interjuncta</i>	2	5	9		8	20	7	3	6	1	7	3		1	3
<i>Bolivina interjuncta</i> var. <i>bicostata</i>				4		2			1		1	2			
<i>Bolivina ordinaria</i>			1		2	3	1	3	1			4		2	1
<i>Bolivina pacifica</i>						6		1	3		22	33	1	1	3
<i>Bolivina plicata</i>	4	4	3	1	3	5	2	3	4	1	3	10			4
<i>Bolivina seminuda</i>			5		2	5	7	2	8		3	2	2	3	3
<i>Bolivina seminuda</i> var. <i>humilis</i>	4	13	26	7	13	38	21	28	28	8	23	22	9	10	18
<i>Bolivina serrata</i>			1		5					2	1		4	1	3
<i>Bolivina spissa</i>	3	8	1		3	9	4	6	3	2	6	2	11		11
<i>Bolivina subadvena</i>	1	3				4		2							
<i>Bolivina tongi</i> var. <i>filacostata</i>															
<i>Bolivina</i> aff. <i>tortuosa</i>												3			
<i>Bolivina</i> spp.	1									1			1		
<i>Bolivinita minuta</i>	37	28	19	2	20	24	5	8	17	8	14	20	2	4	6
cf. <i>Buccella peruviana</i>			12	3		4	2	5				19	1		10
<i>Bulimina exilis</i>	2	2					5	7		4	1				2
<i>Bulimina marginata</i>							2		1		1		3		2
<i>Bulimina pagoda</i>	1	2		1	2	1		3	2		1	3			
<i>Bulimina rostrata</i>															
<i>Buliminella curta</i>			10		5	7	3	7	7	1	1	3	1		2
<i>Buliminella curta</i> <i>basispinata</i>								2	2						
<i>Buliminella elegantissima</i>								1				3		1	1
<i>Buliminella tenuata</i>	2	12	9	4	11	41	10	3	10	4	6	4	6		5
<i>Buliminella</i> spp.	1			2		3			1			10	1		
<i>Cancris inflatus</i>			5	2	4	7	2	2		2	3	1			
<i>Cassidulina auka</i>						6							14	3	11
<i>Cassidulina</i> cf. <i>auka</i>															

Appendix 4: Species protocols

Sediment core depth (cm)	60	70	80	90	100	110	130	150	170	190	210	230	330	340	350
<i>Cassidulina carinata</i>					4	12		10	4	1	10	21	20	10	33
<i>Cassidulina corbyi</i>															2
<i>Cassidulina crassa</i>				1	2	4									3
<i>Cassidulina delicata</i>	31	36	23	5	23	37	26	17	50	15	29	43	18	9	45
<i>Cassidulina depressa</i>										5	7	10	3	3	6
<i>Cassidulina laevigata</i>		4								5					
<i>Cassidulina minuta</i>	8		15	3	6	15	5	11	2						
<i>Cassidulina pulchella</i>						4	2		7			4	2		5
<i>Cassidulina</i> spp.		1			3			2					2		5
<i>Cassidulina?</i> spp.														1	
<i>Chilostomella ovoidea</i>						6	1		1		2	1		1	3
<i>Cibicides aknerianus</i>															
<i>Cibicides elmaensis</i>			1											1	2
<i>Cibicides floridanus</i>										1			2		
<i>Cibicides mckannai</i>															1
<i>Cibicoides dispars</i>											1				
<i>Cibicoides wuellerstorfi</i>		1				3	1	1	3	2		1			
<i>Cibicoides</i> spp.	2	1				1			1			1		1	
<i>Dorothia goesi</i>												1	1		
<i>Epistominella afueraensis</i>	26	5	12	4		50	3	7	19	7	12	10	6	2	3
<i>Epistominella exigua</i>	9	11	10	7	17	20		15	25	12	28	100	5	15	21
<i>Epistominella obesa</i>		8	18	11	29	49	28	33	82	12	50	60	34	25	48
<i>Epistominella pacifica</i>	1	30	33	11	22	22	6	22	13	2	5	6	9		
<i>Epistominella smithi</i>	25	10			10	23	11	18	1	3	10	1			3
<i>Epistominella</i> sp.							1								
<i>Fissurina annectens</i>															
<i>Fissurina alveolata</i>															
<i>Fissurina orbignyana</i>															
<i>Fursenkoina fusiformis</i>	3	8	5	2	11	16	8	5	5	2	21	28			1
<i>Fursenkoina glabra</i>												7			
<i>Globobulimina affinis</i>						1	1	1						1	
<i>Globobulimina glabra</i>	1									1					1
<i>Globobulimina ovula</i>															
<i>Globobulimina pacifica</i>	1			1				2	1	1	2	4		1	1
<i>Globobulimina</i> sp.		1													
<i>Globocassidulina paratortuosa</i>															
<i>Globocassidulina subglobosa</i>		2	1		5			4				2	5		1
<i>Globocassidulina</i> spp.			1		1		1								1

Appendix 4: Species protocols

Sediment core depth (cm)	60	70	80	90	100	110	130	150	170	190	210	230	330	340	350
<i>Gyroidina altiformis</i>		2		1	1	2		1		1		2			
<i>Gyroidina nitidula</i>															2
<i>Gyroidina quinqueloba</i>						1									
<i>Gyroidina rothwelli</i>		1				4						2	3	1	8
<i>Gyroidina subtenera</i>		1											1		
<i>Gyroidina sp.</i>					1		2								
<i>Hanzawaia bertheloti</i>												1			
<i>Hanzawaia mexicana</i>											1		1		
<i>Hanzawaia sp.</i>															
<i>Hoeglundina elegans</i>		1				1									
<i>Lagena amphora</i>															
<i>Lagena elongata</i>															1
<i>Lagena hispidula</i>															
<i>Lagena laevis</i>		1													
<i>Lagena striata</i>												1	1	1	1
<i>Lagena wiliamsoni</i>													1	1	1
<i>Lagena sp.</i>							1		1			1			
<i>Lagenosolenia inflatiperforata</i>												1			1
<i>Melonis barleeaanum</i>															3
<i>Nonion commune</i>	2	6					10					2			
<i>Nonion pizarrensis</i> var. <i>basispinata</i>			1												
<i>Nonionella auris</i>															
<i>Nonionella iridea</i>										1	5	10			
<i>Nonionella miocenica</i>													1		2
<i>Nonionella stella</i>											2				
<i>Nonionella turgida</i>						3		1			1	2			
<i>Nonionella sp.</i>										1					
<i>Nonionoides grateloupii</i>			7	5	4	10	3	10	4		2				
<i>Oolina globosa</i>		1				1				1	1				
<i>Oridorsalis umbonatus</i>					2				1						
<i>Planulina ornata</i>		1			1		2	5			1				
<i>Praeglobobulimina spinescens</i>		2	1	1	2	5	6	2	3	2	1	1	3	1	4
<i>Pseudoparella subperuviana</i>	25	26	35		27	39	27	37	10	24	41	41	20	4	12
<i>Pseudoparella</i> cf. <i>subperuviana</i>						6									
<i>Pseudoparella sp.</i>	2	11	25		23	9	19	22	37	12		52	2	30	27
<i>Pullenia bulloides</i>												1			
<i>Pullenia elegans</i>								1							
<i>Pyrgo depressa</i>										1					

Appendix 4: Species protocols

Sediment core depth (cm)	60	70	80	90	100	110	130	150	170	190	210	230	330	340	350
<i>Pyrgo murrhyna</i>										1			3	2	2
<i>Pyrgo serrata</i>															
<i>Quinqueloculina seminulum</i>											1	1			1
<i>Quinqueloculina triangularis</i>															
<i>Stainforthia complanata</i>	1					2						9			
<i>Suggrunda eckisi</i>	1					1									
<i>Suggrunda porosa</i>	2	1	2			5	1	4	4	4	3	11		5	3
<i>Uvigerina cf. aculeata</i>		2													
<i>Uvigerina auberiana</i>	7	6	2		2		2	2	3	1	1	5	7	1	11
<i>Uvigerina bifurcata</i>													1		
<i>Uvigerina cf. canariensis</i>															
<i>Uvigerina hispida</i>	1														
<i>Uvigerina peregrina</i>	9	10	13	3	2	4	3	2	3	3	1	4	3		18
<i>Uvigerina semiornata</i>		13	8	4	11	14	10	11	8	1	2	9	7	8	29
<i>Uvigerina cf. semiornata</i>							2	2	2		2				
<i>Uvigerina senticosa</i>												1			
<i>Uvigerina striata</i>	2	4	1		5	2					1				
<i>Uvigerina sp.</i>												1			
<i>Valvulineria araucana</i>															2
<i>Valvulineria sp.</i>	2		1		1				1				1		
<i>Virgulina bramlettei</i>											2	4		2	
<i>Virgulina cornuta</i>			4	4	5	15	7	4	4	3	23	38	6	2	8
<i>Virgulina schreibersiana</i>						1					3				
<i>Virgulina seminuda</i>												3			
<i>Virgulina spinosa</i>												3			
<i>Virgulina sp.</i>			1												
Unknown calcareous								2		2		4		2	

Taxa_S	36	44	38	28	42	58	43	53	46	41	50	62	45	37	59
Individuals	369	416	573	167	450	794	381	474	447	171	413	706	273	171	474
n	0.01	0.0238	0.0178	0.0068	0.0161	0.0409	0.0315	0.0424	0.0210	0.0116	0.0254	0.0267	0.0173	0.0147	0.0301
>63 µm weight (g)	0.2	0.1934	0.2245	0.2637	0.2176	0.1805	0.1111	0.106	0.2571	0.173	0.2711	0.2917	0.5898	0.4554	0.5949
Abundance (#/g sed)	184500	90377	143390	93132	128448	107552	108868	105465	82792	85210	59977	90648	26755	25544	26471
Fisher_alpha	9.87	12.43	9.15	9.62	11.33	14.40	12.45	15.29	12.86	17.10	14.89	16.37	15.34	14.53	17.77
Shannon_H	2.36	2.88	2.42	2.37	2.82	3.17	2.84	3.07	2.99	3.21	3.13	3.31	3.12	2.94	3.35
Dominance_D	0.19	0.11	0.21	0.22	0.13	0.09	0.12	0.10	0.08	0.06	0.06	0.06	0.07	0.08	0.05

Appendix 4: Species protocols

Species protocol of core M77/2-50-4					
Sediment core depth (cm)	370	390	410	430	450
species \ split	1/16	1/256	1/16	1/32	1/32
<i>Alabaminella weddellenensis</i>					
<i>Angulogerina angulosa</i>					1
<i>Angulogerina carinata</i>					1
<i>Bolivina advena</i>			1		
<i>Bolivina advena</i> var. <i>striatella</i>					
<i>Bolivina alata</i>	5	3	5	8	4
<i>Bolivina albatrossi</i>	1				
<i>Bolivina argentea</i>	2		1		
<i>Bolivina costata</i>	73	19	47	65	72
<i>Bolivina interjuncta</i>		1	3	9	
<i>Bolivina interjuncta</i> var. <i>bicostata</i>	1	1	1	2	
<i>Bolivina ordinaria</i>			2		2
<i>Bolivina pacifica</i>	17	1	3	4	5
<i>Bolivina plicata</i>	5	3	3	5	6
<i>Bolivina seminuda</i>	5	3	3	7	7
<i>Bolivina seminuda</i> var. <i>humilis</i>	52	12	19	19	20
<i>Bolivina serrata</i>	5	1		5	
<i>Bolivina spissa</i>	12	4	16	17	11
<i>Bolivina subadvena</i>	7	2			
<i>Bolivina tongi</i> var. <i>filacostata</i>			1		
<i>Bolivina</i> aff. <i>tortuosa</i>	3				3
<i>Bolivina</i> sp.					
<i>Bolivinita minuta</i>	12	3	10	21	26
cf. <i>Buccella peruviana</i>	30	4	9	10	36
<i>Bulimina exilis</i>			2		1
<i>Bulimina marginata</i>	3	1	5		
<i>Bulimina pagoda</i>	14	1		4	1
<i>Bulimina rostrata</i>					1
<i>Buliminella curta</i>	5	2		3	2
<i>Buliminella curta</i> <i>basispinata</i>					
<i>Buliminella elegantissima</i>	6			1	3
<i>Buliminella tenuata</i>			6		6
<i>Buliminella</i> sp.					2
<i>Cancris inflatus</i>					
<i>Cassidulina auka</i>	25	12	26	9	7
<i>Cassidulina</i> cf. <i>auka</i>	16				

Sediment core depth (cm)	370	390	410	430	450
<i>Cassidulina carinata</i>	44	4	61	48	27
<i>Cassidulina corbyi</i>					
<i>Cassidulina crassa</i>		1			
<i>Cassidulina delicata</i>	60	29	47	48	52
<i>Cassidulina depressa</i>	33	4	5	12	22
<i>Cassidulina laevigata</i>				2	4
<i>Cassidulina minuta</i>					
<i>Cassidulina pulchella</i>					3
<i>Cassidulina</i> spp.				2	7
<i>Cassidulina?</i> spp.		2	4	2	
<i>Chilostomella ovoidea</i>	3		3		
<i>Cibicides aknerianus</i>			3	4	
<i>Cibicides elmaensis</i>					
<i>Cibicides floridanus</i>	2				
<i>Cibicides mckannai</i>					
<i>Cibicidoides dispars</i>					
<i>Cibicidoides wuellerstorfi</i>		1	3	2	
<i>Cibicidoides</i> spp.	1			1	1
<i>Dorothia goesi</i>	1				1
<i>Epistominella afueraensis</i>	8	3	14	1	3
<i>Epistominella exigua</i>	76	3	44	78	55
<i>Epistominella obesa</i>	82	22	46	16	61
<i>Epistominella pacifica</i>	1		7	3	
<i>Epistominella smithi</i>			1		2
<i>Epistominella</i> sp.					3
<i>Fissurina annectens</i>			1	1	
<i>Fissurina alveolata</i>				1	
<i>Fissurina orbignyana</i>					2
<i>Fursenkoina fusiformis</i>	6	1	4	1	2
<i>Fursenkoina glabra</i>					
<i>Globobulimina affinis</i>				2	
<i>Globobulimina glabra</i>			2		3
<i>Globobulimina ovula</i>		1			2
<i>Globobulimina pacifica</i>	6		2	3	4
<i>Globobulimina</i> sp.					
<i>Globocassidulina paratortuosa</i>					2
<i>Globocassidulina subglobosa</i>	6		12	7	11
<i>Globocassidulina</i> sp.					

Appendix 4: Species protocols

Sediment core depth (cm)	370	390	410	430	450
<i>Gyroidina altiformis</i>			1		1
<i>Gyroidina nitidula</i>					
<i>Gyroidina quinqueloba</i>	2				
<i>Gyroidina rothwelli</i>	9	3		11	
<i>Gyroidina subtenera</i>	1				1
<i>Gyroidina</i> sp.					
<i>Hanzawaia bertheloti</i>					
<i>Hanzawaia mexicana</i>				1	
<i>Hanzawaia</i> sp.	1				
<i>Hoeglundina elegans</i>					
<i>Lagena amphora</i>			1		1
<i>Lagena elongata</i>					
<i>Lagena hispidula</i>	2				
<i>Lagena laevis</i>					
<i>Lagena striata</i>	1				
<i>Lagena wiliamsoni</i>					
<i>Lagena</i> sp.					
<i>Lagenosolenia inflatiperforata</i>	1				
<i>Melonis barleeaanum</i>					
<i>Nonion commune</i>					
<i>Nonion pizarrensis</i> var. <i>basispinata</i>					
<i>Nonionella auris</i>		1			
<i>Nonionella iridea</i>					
<i>Nonionella miocenica</i>	4				1
<i>Nonionella stella</i>	3	1	1	1	1
<i>Nonionella turgida</i>			1	1	
<i>Nonionella</i> sp.					
<i>Nonionoides grateloupii</i>					
<i>Oolina globosa</i>				1	
<i>Oridorsalis umbonatus</i>		2		1	1
<i>Planulina ornata</i>		4			
<i>Praeglobbulimina spinescens</i>	4		1		2
<i>Pseudoparella subperuviana</i>	22	18	28	100	61
<i>Pseudoparella</i> cf. <i>subperuviana</i>		3	7	32	
<i>Pseudoparella</i> sp.	8	9	28	27	64
<i>Pullenia bulloides</i>			1		
<i>Pullenia elegans</i>				1	
<i>Pyrgo depressa</i>					

Sediment core depth (cm)	370	390	410	430	450
<i>Pyrgo murrhyna</i>	3		2	1	
<i>Pyrgo serrata</i>			1		
<i>Quinqueloculina seminulum</i>	1	2		1	2
<i>Quinqueloculina triangularis</i>	2				
<i>Stainforthia complanata</i>					
<i>Suggrunda eckisi</i>	3			1	
<i>Suggrunda porosa</i>	9	2	7	7	12
<i>Uvigerina</i> cf. <i>aculeata</i>					
<i>Uvigerina auberiana</i>	10	2	4	1	4
<i>Uvigerina bifurcata</i>			6		
<i>Uvigerina</i> cf. <i>canariensis</i>			1		
<i>Uvigerina hispida</i>					
<i>Uvigerina peregrina</i>	10	4	6	5	10
<i>Uvigerina semiornata</i>	30	7	38	13	11
<i>Uvigerina</i> cf. <i>semiornata</i>		2		7	5
<i>Uvigerina senticosa</i>					
<i>Uvigerina striata</i>		3			
<i>Uvigerina</i> spp.					
<i>Valvulineria araucana</i>	1			1	
<i>Valvulineria</i> spp.	3				2
<i>Virgulina apertura</i>	1				2
<i>Virgulina bramlettei</i>			1		2
<i>Virgulina cornuta</i>	3	1	7	4	5
<i>Virgulina schreibersiana</i>	2		1	1	
<i>Virgulina seminuda</i>	3				
<i>Virgulina spinosa</i>	2				
<i>Virgulina</i> sp.			1		
Unknown calcareous	5				
Taxa_S	64	44	57	56	61
Individuals	774	208	566	641	672
n	0.0582	0.0028	0.0444	0.0567	0.0234
>63 µm weight (g)	0.2731	1.7647	0.4187	0.4179	0.3845
Abundance (#/g sed)	48696	42095	30446	27052	74689
Fisher_alpha	16.55	17.05	15.81	14.76	16.30
Shannon_H	3.36	3.22	3.28	3.12	3.22
Dominance_D	0.05	0.06	0.05	0.07	0.06

Appendix 4: Species protocols

Species protocol of core M77/2-052-2																		
Sediment core depth (cm)	90	110	120	130	140	230	240	250	260	270	280	350	360	370	380	390	400	410
species \ split	1/16	1/16	1/16	1/16	1/32	1/8	1/16	1/16	1/16	1/8	1/32	1/32	1/32	1/64	1/32	1/32	1/16	1/16
<i>Alabaminella weddellenensis</i>	1	3	6	5	7	6	22	4	13	10	11	6	1	13	5	1		
<i>Anomalinoides minimus</i>		1	1	1	3	2				1		1						
<i>Bolivina advena</i> var. <i>striatella</i>						1									1			
<i>Bolivina</i> cf. <i>advena</i>										1	1					2		
<i>Bolivina alata</i>	1	2	1	1		2	1	1	1			4	5		3	2	4	9
<i>Bolivina albatrossi</i>																		
<i>Bolivina argentea</i>														1	1			
<i>Bolivina costata</i>	64	144	103	142	68	307	194	103	112	223	75	18	5	4	25	8	4	7
<i>Bolivina doniezi</i>								2										
<i>Bolivina interjuncta</i>								1			1						2	8
<i>Bolivina interjuncta</i> var. <i>bicostata</i>		1	1		2		10	6	11	7	5	13	20	17	8	9	9	19
<i>Bolivina ordinaria</i>	2	3	1	3	1		11		4	7	3	2	1	3	3	3	7	3
<i>Bolivina pacifica</i>	1		3	2	1		3		3	13	3	4	4	2	13	2	10	10
<i>Bolivina quadrata</i>	1				2	1				3		3	4	6	8	11	5	6
<i>Bolivina semicostata</i>														3	1			7
<i>Bolivina seminuda</i>													1	7	2	2		
<i>Bolivina seminuda</i> var. <i>humilis</i>																2		4
<i>Bolivina serrata</i>					1			7				5				2		8
<i>Bolivina spissa</i>	10	19	25	15	9	46	35	18	29	60	22	18	17	12	16	7	22	11
<i>Bolivina subadvena</i>																		
<i>Bolivina subaenariensis</i>																		1
<i>Bolivina tongi</i> var. <i>filacostata</i>									1									
<i>Bolivina</i> aff. <i>tortuosa</i>										1			1	1	2		1	
<i>Bolivina</i> spp.	1				1		1											
<i>Bolivinita minuta</i>	4	8	9	7	10	16	49	16	29	37	25	49	86	17	33	5	18	8
cf. <i>Buccella peruviana</i>									1									
<i>Bulimina exilis</i>		1					4	1	3	9	3		4			4	13	6
<i>Bulimina mexicana</i>	3	5	6	5	2	8	6	2		4	14	1	1			3	1	
<i>Bulimina pagoda</i>		3	4	6	2	3	5	4				5	3	4	5	3	5	1
<i>Bulimina rostrata</i>																	1	
<i>Bulimina striata</i>	1				1		1	2	1	3					2		1	
<i>Buliminella curta</i>	2							3		10	2		6	6	4	7	9	15
<i>Buliminella curta</i> var. <i>basispinata</i>																		
<i>Buliminella elegantissima</i>			1				2					4		1	2		1	
<i>Buliminella tenuata</i>								3										
<i>Buliminella</i> spp.																		

Appendix 4: Species protocols

Sediment core depth (cm)	90	110	120	130	140	230	240	250	260	270	280	350	360	370	380	390	400	410
<i>Cancris inflatus</i>					2										2			
<i>Cassidulina auka</i>																		
<i>Cassidulina carinata</i>		7	7	4	12		15		3	7	6	10	9	28	22	15	22	16
<i>Cassidulina crassa</i>			2	3			2	2	3	3			4					
<i>Cassidulina delicata</i>	18	25	29	31	26	61	131	52	71	114	89	53	38	61	58	34	34	36
<i>Cassidulina depressa</i>														5	12	7	4	8
<i>Cassidulina laevigata</i>	2			2		2		4						1				2
<i>Cassidulina minuta</i>											9	2			2			
<i>Cassidulina</i> spp.											1					1		
<i>Chilostomella ovoidea</i>	2	5	2	2		10	9	8	12	24	3	10	12	9	9	3	7	7
<i>Chilostomella</i> sp.								2						1	2			
<i>Cibicides aknerianus</i>	9	2	7		1	17		7										
<i>Cibicides elmaensis</i>						8		1	5	2	2			3	1			2
<i>Cibicides floridanus</i>				1			9	3		12		4				1		3
<i>Cibicides mckannai</i>	1	14	11	10	3	32	13	18	25	31	11	19	29	27	17	5	15	6
<i>Cibicides spiralis</i>					2	5	2	9						5				
<i>Cibicides</i> spp.	2		1				4				1							
<i>Cibicoides dispars</i>																		
<i>Cibicoides mundulus</i>	2		2			2	5											
<i>Cibicoides wuellerstorfi</i>		1				6		1		1	1	2	2			1	3	1
<i>Cibicoides</i> spp.									1	1					2		4	
<i>Dentalina</i> sp.																		1
<i>Discorbis peruvianus</i>																		
<i>Dorothia goesi</i>	2	5	7	7	5	4	8	3	3	4	2	3	3		2	2	1	1
<i>Epistominella afueraensis</i>	1				1		11			6								
<i>Epistominella exigua</i>	18	13	12	28	29		19	8	10	17	16	14	12	8	20	32	60	121
<i>Epistominella obesa</i>										2			6		4	8	8	8
<i>Epistominella pacifica</i>	4	19			10	10	55	31	43	67	11	17	22	33	12	3	16	33
<i>Epistominella smithi</i>	8	18	30	28	9	17				9	12	26	35	7	41	39	31	24
<i>Epistominella</i> sp.				2			6			1		1				1		
<i>Eponides pusillus</i>																		
<i>Eponides</i> sp.						1	1			1		2						1
<i>Fissurina annectens</i>			1			2		2		6	3	2				1		
<i>Fissurina alatifundata</i>												2	2					
<i>Fissurina exsculpta</i>								1				1						
<i>Fissurina laevigata</i>		2																
<i>Fissurina marginata</i>			1				4			2								
<i>Fissurina orbignyana</i>							4	3		2	1		1			1		1

Appendix 4: Species protocols

Sediment core depth (cm)	90	110	120	130	140	230	240	250	260	270	280	350	360	370	380	390	400	410
<i>Fissurina semimarginata</i>							1											
<i>Fursenkoina fusiformis</i>		2	2	6	1	3	8	7	10	8	7	4	5	5	11	9		6
<i>Globobulimina affinis</i>	2	2	1	1	1			3	2			2		2	1			
<i>Globobulimina glabra</i>	1		4			3	1	3	5	6		2		4		2		
<i>Globobulimina hoeglundi</i>							2			2								
<i>Globobulimina ovula</i>	2								1	4				1	2		2	4
<i>Globobulimina pacifica</i>	2		5		2	3	3	5	6	6	3	1	1		2	2		3
<i>Globobulimina sp.</i>																	2	
<i>Globocassidulina subglobosa</i>		3			4		6	2	2	2	7			2				
<i>Gyroidina altiformis</i>			1			1											2	
<i>Gyroidina gemma</i>				1		2	3	2		2						1		
<i>Gyroidina lamarckiana</i>				1		1					1						1	
<i>Gyroidina neosoldanii</i>										2				4	1			
<i>Gyroidina quinqueloba</i>																		
<i>Gyroidina rothwelli</i>										1						1	8	8
<i>Gyroidina soldanii</i>								1	1									
<i>Gyroidina subtenera</i>	3	4	5	4	2	5	9	12	6	20	2	1	3		3	2		3
<i>Gyroidina sp.</i>			1				4			2		2				5		
<i>Hanzawaia bertheloti</i>																		
<i>Hoeglundina elegans</i>			1									4	5	2	1			1
<i>Lagenamphora</i>	1					1				1		1			1			
<i>Lagenadistoma</i>																	1	
<i>Lagenaelongata</i>															1			
<i>Lagenagracillima</i>					1							2			1		1	
<i>Lagenahispidula</i>		1			1	2	1	1	1			1	1	2	2	2	1	2
<i>Lagenalaevis</i>								1	1									
<i>Lagenalateralis</i>				2		1	2											
<i>Lagenameridionalis</i>																		
<i>Lagenasemistriata</i>																		
<i>Lagenastriata</i>					1				1			1			1	1		1
<i>Lagenasubstriata</i>		1				1	1	1							1			
<i>Lagenasulcata</i>							1		1			1		2				
<i>Lagenasulcata striatopunctata</i>									1									
<i>Lagenasp.</i>			1					1										
<i>Lagenosolenia inflatiperforata</i>				1		1	3	2										
<i>Lagenosolenia sp.</i>										2								
<i>Lenticulina convergens</i>											1	1		1	2		2	
<i>Martinottiella communis</i>	1	2	1					1					2				1	2

Appendix 4: Species protocols

Sediment core depth (cm)	90	110	120	130	140	230	240	250	260	270	280	350	360	370	380	390	400	410
<i>Martinottiella nodulosa</i>		1	1	2	1				1	1			1					
<i>Melonis affinis</i>																		1
<i>Melonis barleeaanum</i>																		
<i>Melonis pompilioides</i>																		
<i>Nodosaria</i> sp.																		
<i>Nonionella auris</i>									4				2		1			
<i>Nonionella iridea</i>										5								
<i>Nonionella labradorica</i>				1						7								
<i>Nonionella miocenica</i>								1	1							3		3
<i>Nonionella stella</i>																		
<i>Nonionella turgida</i>						4		1		3		2		1	2	1		
<i>Nonionella</i> sp.										1								
<i>Nonionoides grateloupii</i>	2		3			2		1	3					1	1	3	1	5
<i>Oolina globosa</i>	1	1	3		1	1	2	1	2					1	1	2		
<i>Oolina apiculata</i>			1							4	4							
<i>Oolina truncata</i>								4		2			3					1
<i>Oridorsalis umbonatus</i>		1	1	2		6	2		1	6	1	1				1	6	
<i>Planulina ornata</i>	1	2			1		1		2	3			4	1		1	4	3
<i>Praeglobobulimina spinescens</i>	3	1	1	1	3	4	5	3		11		1	2	1	1	2	1	3
<i>Pseudoparella subperuviana</i>										2					5	2	4	1
<i>Pseudoparella</i> sp.	1									1		3			1		5	7
<i>Pullenia bulloides</i>	1	5	4	1	2		3	4	6	6			1	1				
<i>Pullenia quinqueloba</i>		1	1	1														
<i>Pyrgo depressa</i>									1									
<i>Pyrgo lucernula</i>																		
<i>Pyrgo murrhyna</i>						1			1				2		2			
<i>Quinqueloculina seminulum</i>											1					1	1	
<i>Stainforthia complanata</i>		2			1	1	3	2	1	3		2		1	8		1	1
<i>Suggrunda eckisi</i>												2				1	3	4
<i>Suggrunda porosa</i>				1														
<i>Uvigerina auberiana</i>	18	42	43	36	27	41	46	29	27	45	25	25	24	22	23	21	11	14
<i>Uvigerina bifurcata</i>										6			5		6			
<i>Uvigerina curtica</i>										6	1				3		1	8
<i>Uvigerina excellens</i>		2		2		8			3	1				1				2
<i>Uvigerina hispida</i>	1						4		2		1							
<i>Uvigerina peregrina</i>		4					10	6	7	8			4		6	3	3	3
<i>Uvigerina semiornata</i>	19	29	34	34	18	39	47	44	64	45	15	29	24	46	22	26	48	22
<i>Uvigerina senticosa</i>	4	4																

Appendix 4: Species protocols

Sediment core depth (cm)	90	110	120	130	140	230	240	250	260	270	280	350	360	370	380	390	400	410
<i>Uvigerina striata</i>	9	2	5	9		7			2	14		7			4	1	7	
<i>Uvigerina</i> sp.												2						
<i>Valvulineria araucana</i>	1	3	6		1	5	13	8	7	2	9	4	2	7	7	1	6	
<i>Valvulineria californica</i>							9	1										
<i>Valvulineria glabra</i>				2														
<i>Valvulineria</i> cf. <i>involuta</i>								1										
<i>Valvulineria minuta</i>															2			
<i>Valvulineria</i> cf. <i>olssoni</i>																		
<i>Valvulineria rugosa</i>					1		2			1	6	4		2				
<i>Valvulineria</i> sp.		2						1				1						
<i>Virgulina apertura</i>					2			3		2							3	3
<i>Virgulina bradyi</i>						1		1				5				1		
<i>Virgulina bramlettei</i>		2	1		1				1	2				2	1	1		
<i>Virgulina cornuta</i>	1	3	3	7	6	1	5	6	17	7	7		5	2	4	8	5	7
<i>Virgulina pauciloculata</i>					1			2	5		4		1				2	
<i>Virgulina schreibersiana</i>										2	4	1			4	3		4
<i>Virgulina seminuda</i>		2				3	3	5	5	8				2	4	1	3	2
<i>Virgulina squamosa</i>																1		
<i>Virgulina texturata</i>													2			1		
<i>Virgulina</i> sp.	2					5			1							3		
Unknown calcareous			2		5	1	2	1	4	1	1	1		1		2	1	2

Taxa_S	45	48	50	41	48	53	62	67	60	77	46	60	50	53	69	67	59	63
Individuals	236	425	404	420	294	723	845	494	590	964	433	414	433	402	478	342	455	520
n	0.0058	0.0297	0.0408	0.0543	0.0432	0.0697	0.0552	0.0431	0.0422	0.1113	0.0217	0.0328	0.0347	0.0209	0.0312	0.026	0.063	0.0248
>63 µm weight (g)	0.121	0.118	0.125	0.129	0.148	0.231	0.230	0.216	0.230	0.230	0.217	0.183	0.150	0.234	0.231	0.339	0.292	0.557
Abundance (#/g sed)	336278	121269	79216	59960	45983	44905	66556	53064	60787	37658	91954	68972	83189	82199	66323	38802	24734	37644
Fisher_alpha	16.49	13.90	15.02	11.24	16.29	13.17	15.41	20.91	16.70	19.69	13.02	19.28	14.61	16.35	22.13	24.91	18.07	18.77
Shannon_H	2.919	2.754	2.909	2.617	2.978	2.503	3.036	3.249	3.088	3.211	2.987	3.349	3.125	3.208	3.546	3.503	3.397	3.349
Dominance_D	0.106	0.143	0.103	0.147	0.092	0.203	0.096	0.077	0.080	0.087	0.091	0.056	0.075	0.064	0.046	0.050	0.053	0.076

Appendix 4: Species protocols

Species protocol of core M77/2-052-2										
Sediment core depth (cm)	420	430	440	450	500	510	520	530	540	
species \ split	1/32	1/32	1/32	1/16	1/8	1/64	1/8	1/32	1/16	
<i>Alabaminella weddellenensis</i>								6		
<i>Anomalinooides minimus</i>									4	
<i>Bolivina advena</i> var. <i>striatella</i>	2						1			
<i>Bolivina</i> cf. <i>advena</i>	2				1					
<i>Bolivina alata</i>	7	8	5	3	9	2	9	6	1	
<i>Bolivina albatrossi</i>							1			
<i>Bolivina argentea</i>	1									
<i>Bolivina costata</i>	4	8	3	7	34	18	44	20	39	
<i>Bolivina interjuncta</i>								1		
<i>Bolivina interjuncta</i> var. <i>bicostata</i>	19	8	14	11	16	2	12	5	2	
<i>Bolivina ordinaria</i>	3	3	2	3			6	5	4	
<i>Bolivina pacifica</i>	4	10	20	7	11	7	12	9	5	
<i>Bolivina quadrata</i>	1	3	5	6	6	3	5			
<i>Bolivina semicostata</i>	3			2		1				
<i>Bolivina seminuda</i>		1			2					
<i>Bolivina seminuda</i> var. <i>humilis</i>	2		3	6		3	1		1	
<i>Bolivina serrata</i>					7	2	2			
<i>Bolivina spissa</i>	19	9	8	14	8	4	14	2	1	
<i>Bolivina subadvena</i>	6									
<i>Bolivina subaenariensis</i>	2									
<i>Bolivina tongi</i> var. <i>filacostata</i>					2	1				
<i>Bolivina</i> aff. <i>tortuosa</i>								1		
<i>Bolivina</i> spp.				4	3					3
<i>Bolivinita minuta</i>	20	4	3	4	3	1		1	1	
cf. <i>Buccella peruviana</i>								3		
<i>Bulimina exilis</i>	6	2	1		3		2	4		
<i>Bulimina mexicana</i>					12		26	19	1	
<i>Bulimina pagoda</i>		3	2	4	47	13	58	21	42	
<i>Bulimina rostrata</i>										3
<i>Bulimina striata</i>					1	2	7	3	1	
<i>Buliminella curta</i>	11		13	16	5	3	6	1	3	
<i>Buliminella curta</i> var. <i>basispinata</i>				2						
<i>Buliminella elegantissima</i>	4	2	1	3	7	3	2	6	2	
<i>Buliminella tenuata</i>		1								
<i>Buliminella</i> spp.	1									1
<i>Cancris inflatus</i>			1							
<i>Cassidulina auka</i>			2							
<i>Cassidulina carinata</i>	2	12	20	14	68	91	88	57	47	
<i>Cassidulina crassa</i>					4	2	21	8	4	
<i>Cassidulina delicata</i>	28	34	28	70	69	22	80	31	96	
<i>Cassidulina depressa</i>	5	4	6	9		16			9	
<i>Cassidulina laevigata</i>	6			12	8		30	38	91	
<i>Cassidulina minuta</i>								17		
<i>Cassidulina</i> spp.								2	1	
<i>Chilostomella ovoidea</i>	9	4		2	7	7	6	12	1	
<i>Chilostomella</i> sp.										
<i>Cibicides aknerianus</i>					1		6			
<i>Cibicides elmaensis</i>										5
<i>Cibicides floridanus</i>		1	2		4					
<i>Cibicides mckannai</i>	10	4	4	10	16	1	16	1	8	
<i>Cibicides spiralis</i>								2		
<i>Cibicides</i> spp.							1			3
<i>Cibicoides dispars</i>		1								2
<i>Cibicoides mundulus</i>		1		1	3	1	8	4		
<i>Cibicoides wuellerstorfi</i>	1			1	3	1				4
<i>Cibicoides</i> spp.						2		1		2
<i>Discorbis peruvianus</i>			1		2		10			

Appendix 4: Species protocols

Sediment core depth (cm)	420	430	440	450	500	510	520	530	540
<i>Dorothia goesi</i>	2	3		4	1				1
<i>Epistominella afueraensis</i>		1					12		2
<i>Epistominella exigua</i>	98	91	126	168	8	40	6	28	23
<i>Epistominella obesa</i>	13	3	9	7				4	
<i>Epistominella pacifica</i>	16	8	8	10			2	6	14
<i>Epistominella smithi</i>	17	16	26	9	83	23	48	22	15
<i>Epistominella</i> sp.				2		1	1		1
<i>Eponides pusillus</i>									1
<i>Eponides</i> sp.						1			
<i>Fissurina annectens</i>					3	2		1	2
<i>Fissurina marginata</i>					1		2		
<i>Fissurina orbignyana</i>			1	1				1	
<i>Fissurina semimarginata</i>									
<i>Fursenkoina fusiformis</i>	21	16	15				7	7	
<i>Globobulimina affinis</i>	2				1		4		2
<i>Globobulimina glabra</i>			3		2		1		
<i>Globobulimina hoeglundi</i>									
<i>Globobulimina ovula</i>	10			3		1	1	4	
<i>Globobulimina pacifica</i>		6				3	4		2
<i>Globobulimina</i> sp.					1		1		
<i>Globocassidulina subglobosa</i>								6	6
<i>Gyroidina altiformis</i>	1			1	3		7	1	10
<i>Gyroidina gemma</i>					1		6	5	
<i>Gyroidina lamarckiana</i>									3
<i>Gyroidina neosoldanii</i>								1	
<i>Gyroidina quinqueloba</i>					1			2	
<i>Gyroidina rothwelli</i>	1	1						1	
<i>Gyroidina soldanii</i>									
<i>Gyroidina subtenera</i>	2	1	1	2	5		5	4	
<i>Gyroidina</i> sp.		1			9	1	7	1	
<i>Hanzawaia bertheloti</i>									1
<i>Hoeglundina elegans</i>				1	6		2		
<i>Lagena amphora</i>						2	2	2	
<i>Lagena gracillima</i>			1		1				
<i>Lagena hispidula</i>	1				3	4	3	1	1
<i>Lagena laevis</i>				1					
<i>Lagena lateralis</i>							2		
<i>Lagena meridionalis</i>			1		2				
<i>Lagena semistriata</i>							1		
<i>Lagena striata</i>					1		3		1
<i>Lagena substriata</i>				2		1		3	
<i>Lagena sulcata</i>					1				2
<i>Lagena sulcata striatopunctata</i>					1		1		
<i>Lagena</i> sp.									
<i>Lagenosolenia inflatiperforata</i>				2	1	1	1	1	
<i>Lagenosolenia</i> sp.									
<i>Lenticulina convergens</i>					1		1		
<i>Martinottiella communis</i>									
<i>Martinottiella nodulosa</i>									
<i>Melonis affinis</i>									1
<i>Melonis barleeaanum</i>							1	3	
<i>Melonis pompilioides</i>								1	
<i>Nodosaria</i> sp.								1	1
<i>Nonionella auris</i>				2				2	
<i>Nonionella iridea</i>									
<i>Nonionella labradorica</i>									
<i>Nonionella miocenica</i>			7		3		2	3	
<i>Nonionella stella</i>			2						
<i>Nonionella turgida</i>		2	2					1	

Appendix 4: Species protocols

Sediment core depth (cm)	420	430	440	450	500	510	520	530	540
<i>Nonionella</i> spp.					1		1		
<i>Nonionoides grateloupii</i>		4		2	1			1	8
<i>Oolina globosa</i>									1
<i>Oolina apiculata</i>								2	2
<i>Oolina truncata</i>									
<i>Oridorsalis umbonatus</i>			1		6	9	16	3	8
<i>Planulina ornata</i>		3			5		7	2	5
<i>Praeglobobulimina spinescens</i>		3	1	1	1		1	3	2
<i>Pseudoparella subperuviana</i>	2	7				4			
<i>Pseudoparella</i> sp.						1			
<i>Pullenia bulloides</i>					9	5	8	4	3
<i>Pullenia quinqueloba</i>						1	2		3
<i>Pyrgo lucernula</i>								2	
<i>Pyrgo murrhyna</i>	1						3		
<i>Quinqueloculina seminulum</i>									
<i>Stainforthia complanata</i>	1	1		3	1				
<i>Suggrunda eckisi</i>	2	3	6	6	3	1	2	4	1
<i>Suggrunda porosa</i>							1		
<i>Uvigerina auberiana</i>	12	11	2	14	63	22	70	32	38
<i>Uvigerina bifurcata</i>					38	12	86		
<i>Uvigerina curtica</i>									
<i>Uvigerina excellens</i>		1		3	10		10		
<i>Uvigerina hispida</i>									1
<i>Uvigerina peregrina</i>	9	1			19	16	54	55	37
<i>Uvigerina semiornata</i>	27	31	23	32	141	23	63	20	39
<i>Uvigerina senticosa</i>									
<i>Uvigerina striata</i>		1							2
<i>Uvigerina</i> spp.					2				
<i>Valvulineria araucana</i>	5	2	3		2		1		2
<i>Valvulineria californica</i>					1				
<i>Valvulineria glabra</i>									
<i>Valvulineria</i> cf. <i>involuta</i>									
<i>Valvulineria minuta</i>								4	
<i>Valvulineria</i> cf. <i>olssoni</i>					2				
<i>Valvulineria rugosa</i>	1				2				1
<i>Valvulineria</i> spp.					3		6		
<i>Virgulina apertura</i>		3		5					
<i>Virgulina bradyi</i>					1	1	3		
<i>Virgulina bramlettei</i>							4		
<i>Virgulina cornuta</i>	15	8	17	11	6	3	16	8	8
<i>Virgulina pauciloculata</i>			2					4	
<i>Virgulina schreibersiana</i>		2	2	2		4	2	2	
<i>Virgulina seminuda</i>	2	3	1	2	1			1	2
<i>Virgulina squamosa</i>									
<i>Virgulina texturata</i>									
<i>Virgulina</i> spp.									1
Unknown calcareous	3	1		2	1	1	2	2	6

Taxa_S	50	51	45	50	76	50	75	73	70
Individuals	442	357	404	509	820	391	965	547	646
n	0.079	0.0301	0.033	0.0674	0.1096	0.0152	0.1004	0.0314	0.0477
>63 µm weight (g)	0.195	0.183	0.152	0.095	0.511	0.985	1.093	1.611	0.822
Abundance (#/g sed)	28692	64811	80808	79578	14641	26115	8794	10813	16476
Fisher_alpha	14.49	16.28	12.97	13.74	20.45	15.23	19.00	22.63	19.96
Shannon_H	3.197	3.107	2.846	2.829	3.243	3.027	3.446	3.543	3.203
Dominance_D	0.075	0.093	0.123	0.140	0.070	0.088	0.049	0.046	0.070

Appendix 4: Species protocols

Species protocol of core M77/2-59-1													
Sediment core depth (cm)	143	163	183	203	223	243	403	443	483	523	563	803	
species \ split	1/64	1/64	1/128	1/16	1/64	1/32	1/256	1/256	1/64	1/64	1/128	1/128	
<i>Alabaminella weddellensis</i>	34	41	14	17	25	22	7	15	18	36	20		
<i>Anomalinoides minimus</i>	21	23	9	19	11	20	10	15	32	41	38	20	
<i>Bolivina advena</i>													3
<i>Bolivina alata</i>	5	2	2	3	1	5	2		1	1	3	3	
<i>Bolivina argentea</i>													1
<i>Bolivina costata</i>										2	1		
<i>Bolivina interjuncta</i>								4	6	5	5	14	
<i>Bolivina interjuncta</i> var. <i>bicostata</i>	4	5		2	2	1	1	4	8	14	12	45	
<i>Bolivina ordinaria</i>	4	9	1	6				1	2	10	4		
<i>Bolivina pacifica</i>			1		1	1	1		1	6	3	5	
<i>Bolivina plicata</i>		1			1	1				3	1	3	
<i>Bolivina quadrata</i>	1						2	3	7	12	12	29	
<i>Bolivina</i> cf. <i>quadrata</i>													
<i>Bolivina seminuda</i>						1							
<i>Bolivina seminuda</i> var. <i>humilis</i>	4	4		1				3		9			
<i>Bolivina serrata</i>	2		2		5	6	2	3	9	10	10	7	
<i>Bolivina spissa</i>	24	13	5	9	8	23	7	8	8	25	18	9	
<i>Bolivina</i> cf. <i>spissa</i>		2											
<i>Bolivina subadvena</i>		1				2			2				
<i>Bolivina subaenariensis</i>		3					3			12	9		
<i>Bolivina tongi</i> var. <i>filacostata</i>		2	1	2		3	1	1	6	5	1	2	
<i>Bolivina tortuosa</i>													
<i>Bolivina</i> aff. <i>tortuosa</i>		3								11	2	4	
<i>Bolivina</i> spp.	3	1	2							1	2		
<i>Bolivinita minuta</i>	153	150	76	85	87	72	28	58	114	230	152	122	
cf. <i>Buccella peruviana</i>		5											
<i>Bulimina denudata</i>	4	3		1	3								
<i>Bulimina exilis</i>		1			1					1		1	
<i>Bulimina marginata</i>							3	2	2				
<i>Bulimina mexicana</i>	2	1	1	1			1	1		2			
<i>Bulimina pagoda</i>	14	10	5	1	6	7	1		1	6	4	3	
<i>Bulimina rostrata</i>							2	2					
<i>Bulimina</i> spp.													
<i>Buliminella curta</i>	2	2		1	2	3					3		
<i>Buliminella elegantissima</i>								2		2	1		
<i>Buliminella tenuata</i>	5	3		1						4			

Appendix 4: Species protocols

Sediment core depth (cm)	143	163	183	203	223	243	403	443	483	523	563	803
<i>Canceris auriculus</i>											1	
<i>Canceris inflatus</i>			1									
<i>Cassidulina carinata</i>	19	26	13	23	36	27	12	30	46	72	48	34
<i>Cassidulina cf. carinata</i>											8	
<i>Cassidulina crassa</i>				2	2	1			2	2		4
<i>Cassidulina delicata</i>	68	82	29	46	43	68	31	29	81	143	61	18
<i>Cassidulina depressa</i>	9	2					12		17	14	7	22
<i>Cassidulina laevigata</i>	10						1				6	
<i>Cassidulina cf. laevigata</i>												
<i>Cassidulina minuta</i>	58	29		6	21	12		14	8			
<i>Cassidulina spp.</i>	4							4	2	13		17
<i>Chilostomella ovoidea</i>	3	3						1		1	2	1
<i>Cibicides elmaensis</i>		2	1									
<i>Cibicides floridanus</i>	2	1				4	1					
<i>Cibicides mckannai</i>	6	3		2	5	2		8	10	13	9	1
<i>Cibicides spiralis</i>	11	7	6	3	8	7	5	3	11	2	3	
<i>Cibicides spp.</i>											1	2
<i>Cibicoides wuellerstorfi</i>								3	1		1	1
<i>Cibicoides spp.</i>				3		5				3		
<i>Dentalina advena</i>				1		2		1				
<i>Discorbis micens</i>												
<i>Discorbis peruvianus</i>							1					
<i>Dorothia goesi</i>	1				1							
<i>Ehrenbergina pupa</i>									1			
<i>Epistominella afueraensis</i>			4			23	3	20	20	17	8	19
<i>Epistominella exigua</i>	39	39	14	31	25	35	18	26	59	118	60	77
<i>Epistominella cf. exigua</i>							5			4	11	
<i>Epistominella obesa</i>	18	21	4	14	22	5				21	7	5
<i>Epistominella pacifica</i>	5	10	1						8	11	20	
<i>Epistominella smithi</i>					1	1		1				32
<i>Fissurina annectens</i>		1	3	2		2	1	1	2		1	
<i>Fissurina kergulenensis</i>									1			
<i>Fissurina laevigata</i>						2						
<i>Fissurina marginata</i>					2	3		2	3	6		
<i>Fissurina orbignyana</i>	2	2		1	1				1			
<i>Fissurina semimarginata</i>	1				2				1		1	
<i>Fursenkoina fusiformis</i>		2		2		2		1	1		3	6
<i>Fursenkoina glabra</i>												

Appendix 4: Species protocols

Sediment core depth (cm)	143	163	183	203	223	243	403	443	483	523	563	803
<i>Globobulimina affinis</i>			1	1	1				1			
<i>Globobulimina glabra</i>										2		
<i>Globobulimina ovula</i>												4
<i>Globobulimina pacifica</i>		1							1	1	2	
<i>Globobulimina sp.</i>										2		
<i>Globocassidulina paratortuosa</i>		8	6			8	5	4	6	26	28	
<i>Globocassidulina subglobosa</i>	5	8	2	10	9	9	7		27	21	10	6
<i>Gyroidina altiformis</i>					2	3	1	1	1		1	1
<i>Gyroidina cf. gemma</i>		2										
<i>Gyroidina polia</i>									7	6		
<i>Gyroidina quinqueloba</i>	7	5	1			5		9	3	4	5	3
<i>Gyroidina rothwelli</i>	8	8	5	4	3	5	2	11	10	28	21	32
<i>Gyroidina subtenera</i>												4
<i>Gyroidina sp.</i>		1	1							4		
<i>Hanzawaia bertheloti</i>									1			
<i>Hanzawaia mexicana</i>					1	1	2	1			3	4
<i>Hanzawaia sp.</i>												
<i>Hoeglundina elegans</i>	1			2	1		2					
<i>Lagena amphora</i>		1				1						
<i>Lagena distoma</i>									1			
<i>Lagena gracillima</i>	1			1			2		1			
<i>Lagena hispidula</i>	4	3		2	1	4		1	3			
<i>Lagena lateralis</i>					2					1		
<i>Lagena squamosa</i>									1			
<i>Lagena striata</i>				1				1				
<i>Lagena substriata</i>							2					
<i>Lagena sulcata</i>								1				
<i>Lagena sulcata peculiaris</i>												
<i>Lagena wiliamsoni</i>									1			
<i>Lagena sp.</i>					2							
<i>Lagenosolenia inflatiperforata</i>												
<i>Laticarinina pauperata</i>	2					1	1					
<i>Lenticulina convergens</i>	1	1				1			2	5	1	
<i>Lenticulina limbosa</i>		1		1				1				
<i>Lenticulina sp.</i>					1							
<i>Melonis affinis</i>		10	2	2	3	5						
<i>Melonis barleeaanum</i>	2	2										
<i>Melonis pompilioides</i>	1											

Appendix 4: Species protocols

Sediment core depth (cm)	143	163	183	203	223	243	403	443	483	523	563	803
<i>Nonionella iridea</i>					1				1	3	2	2
<i>Nonionella labradorica</i>										1	1	1
<i>Nonionella miocenica</i>						2						
<i>Nonionella stella</i>												
<i>Nonionella turgida</i>				1					1			
<i>Nonionella</i> sp.										1		
<i>Nonionoides grateloupii</i>			1		2		1	1		2	1	
<i>Oolina apiculata</i>		3								2		
<i>Oolina globosa</i>	2	1			1			2	1	2		
<i>Oolina truncata</i>		1				4	3		2			
<i>Oridorsalis umbonatus</i>	1	7		1	3	9	4	3	2	7	1	
<i>Planulina ornata</i>	3	3		1		3			9	1		
<i>Praeglobobulimina ovata</i>	2				2			1				
<i>Praeglobobulimina spinescens</i>	4				2			1	3	3	2	
<i>Pseudoparella subperuviana</i>	11											
<i>Pseudoparella</i> sp.		5										1
<i>Pullenia bulloides</i>	15	10	1	4	5	9		1				
<i>Pullenia quinqueloba</i>							1					
<i>Pyrgo depressa</i>												
<i>Pyrgo murrhyna</i>	1										1	
<i>Quinqueloculina seminulum</i>									1	1		1
<i>Quinqueloculina</i> sp.											1	
<i>Stainforthia complanata</i>		1		5	2	2	1	5	5			5
<i>Suggrunda eckisi</i>	1	1	1						2	2	2	3
<i>Suggrunda porosa</i>		1										
<i>Uvigerina auberiana</i>	46	50	13	24	27	41	16	19	43	61	38	21
<i>Uvigerina canariensis</i>										7	1	
<i>Uvigerina excellens</i>										1		
<i>Uvigerina peregrina</i>	2			2		3			1	7		3
<i>Uvigerina semiornata</i>	20	11	4	15	22	25	9	9	21	13	24	17
<i>Uvigerina</i> cf. <i>semiornata</i>		1	2	2		3						4
<i>Uvigerina senticosa</i>				3								
<i>Uvigerina striata</i>	4											
<i>Uvigerina</i> spp.												
<i>Valvulineria araucana</i>	16	18	11	9	12	9	6	6	21	41	33	9
<i>Valvulineria bradyana</i>			4							4	4	
<i>Valvulineria glabra</i>												
<i>Valvulineria involuta</i>		1										

Appendix 4: Species protocols

Sediment core depth (cm)	143	163	183	203	223	243	403	443	483	523	563	803
<i>Valvulineria rugosa</i>	3	1	1									
<i>Valvulineria</i> sp.												
<i>Virgulina</i> cf. <i>apertura</i>		1										
<i>Virgulina bramlettei</i>		1										
<i>Virgulina cornuta</i>									1			4
<i>Virgulina pauciloculata</i>												1
<i>Virgulina schreibersiana</i>		1				3			1			
<i>Virgulina seminuda</i>		2		1	2	2	1	1	1	1	4	
<i>Virgulina spinosa</i>										1		3
<i>Virgulina</i> sp.			1									
Unknown calcareous		2	5	2	3	2	4		7	10	3	5

Taxa_S	57	71	40	48	51	56	45	50	67	70	63	52
Individuals	701	688	257	378	433	528	231	345	681	1159	748	644
n	0.0186	0.0207	0.0095	0.0877	0.0131	0.0246	0.0038	0.0103	0.0153	0.015	0.0103	0.0095
>63 µm weight (g)	0.3873	0.4501	0.3481	0.0821	0.5353	0.3577	0.5777	0.6322	0.6718	0.6153	0.6293	0.3885
Abundance (#/g sed)	97310	73843	77715	52499	61748	60004	105227	52982	66254.55	125576	115400	174490
Fisher_alpha	14.66	19.87	13.27	14.57	15.02	15.84	16.68	16.06	18.42	16.38	16.40	13.34
Shannon_H	3.127	3.181	2.821	2.963	3.050	3.273	3.230	3.174	3.221	3.182	3.201	3.144
Dominance_D	0.081	0.083	0.119	0.091	0.079	0.061	0.059	0.066	0.069	0.079	0.073	0.073

Appendix 4: Species protocols

Species protocol of core M77/2-59-1								
Sediment core depth (cm)	843	883	923	963	1043	1163	1243	1323
species \ split	1/256	1/256	1/256	1/128	1/64	1/128	1/128	1/128
<i>Alabaminella weddellensis</i>		2			3			
<i>Anomalinoides minimus</i>	1	3	2	2	2			
<i>Bolivina advena</i>							3	
<i>Bolivina alata</i>	5	7	9	1	16	3	2	3
<i>Bolivina argentea</i>	5		1	1	3	20	3	8
<i>Bolivina costata</i>								
<i>Bolivina interjuncta</i>	17	8	8	5	10	11	1	1
<i>Bolivina interjuncta</i> var. <i>bicostata</i>	17	23	10	9	40	20	22	22
<i>Bolivina ordinaria</i>	4	1		9	13	8	4	15
<i>Bolivina pacifica</i>	9	25	17	16	11	10	18	30
<i>Bolivina plicata</i>	1	2	5			2		1
<i>Bolivina quadrata</i>	15	36	4	9	12		18	19
<i>Bolivina</i> cf. <i>quadrata</i>	8		3		18	13		
<i>Bolivina seminuda</i>		7				2		3
<i>Bolivina seminuda</i> var. <i>humilis</i>				2		7		4
<i>Bolivina serrata</i>	3	5			2			
<i>Bolivina spissa</i>	5	2				6	9	4
<i>Bolivina</i> cf. <i>spissa</i>				2	4			5
<i>Bolivina subadvena</i>						3		
<i>Bolivina subaenariensis</i>							20	14
<i>Bolivina tongi</i> var. <i>filacostata</i>	4	2		2				
<i>Bolivina tortuosa</i>								1
<i>Bolivina</i> aff. <i>tortuosa</i>	4	6	4	2	5			
<i>Bolivina</i> spp.								
<i>Bolivinita minuta</i>	39	31	8	2	74	19	6	2
cf. <i>Buccella peruviana</i>								
<i>Bulimina denudata</i>								1
<i>Bulimina exilis</i>								2
<i>Bulimina marginata</i>		2	1			1	2	
<i>Bulimina mexicana</i>								
<i>Bulimina pagoda</i>	2	3	2	5	8	8	17	9
<i>Bulimina rostrata</i>								
<i>Bulimina</i> spp.							3	
<i>Buliminella curta</i>					17	6	6	
<i>Buliminella elegantissima</i>					1			
<i>Buliminella tenuata</i>	2	1	3	9	9	7	5	
<i>Cancris auriculus</i>								
<i>Cancris inflatus</i>								
<i>Cassidulina carinata</i>	23	40		6	30	36	40	27
<i>Cassidulina</i> cf. <i>carinata</i>			15	12		16		
<i>Cassidulina crassa</i>	1		5	2	3		1	
<i>Cassidulina delicata</i>	30	19	12	12	53	77	35	56
<i>Cassidulina depressa</i>	17	7	6	3	11	5	9	13
<i>Cassidulina laevigata</i>	4				18			25
<i>Cassidulina</i> cf. <i>laevigata</i>					8		13	
<i>Cassidulina minuta</i>					3			
<i>Cassidulina</i> spp.	5			4	3			
<i>Chilostomella ovoidea</i>	2	1			1	3	4	7
<i>Cibicides elmaensis</i>								
<i>Cibicides floridanus</i>					2	3		
<i>Cibicides mckannai</i>					1			1
<i>Cibicides spiralis</i>								
<i>Cibicides</i> spp.		1				2	4	1
<i>Cibicidoides wuellerstorfi</i>								
<i>Cibicidoides</i> spp.								
<i>Dentalina advena</i>								
<i>Discorbis micens</i>				1				

Appendix 4: Species protocols

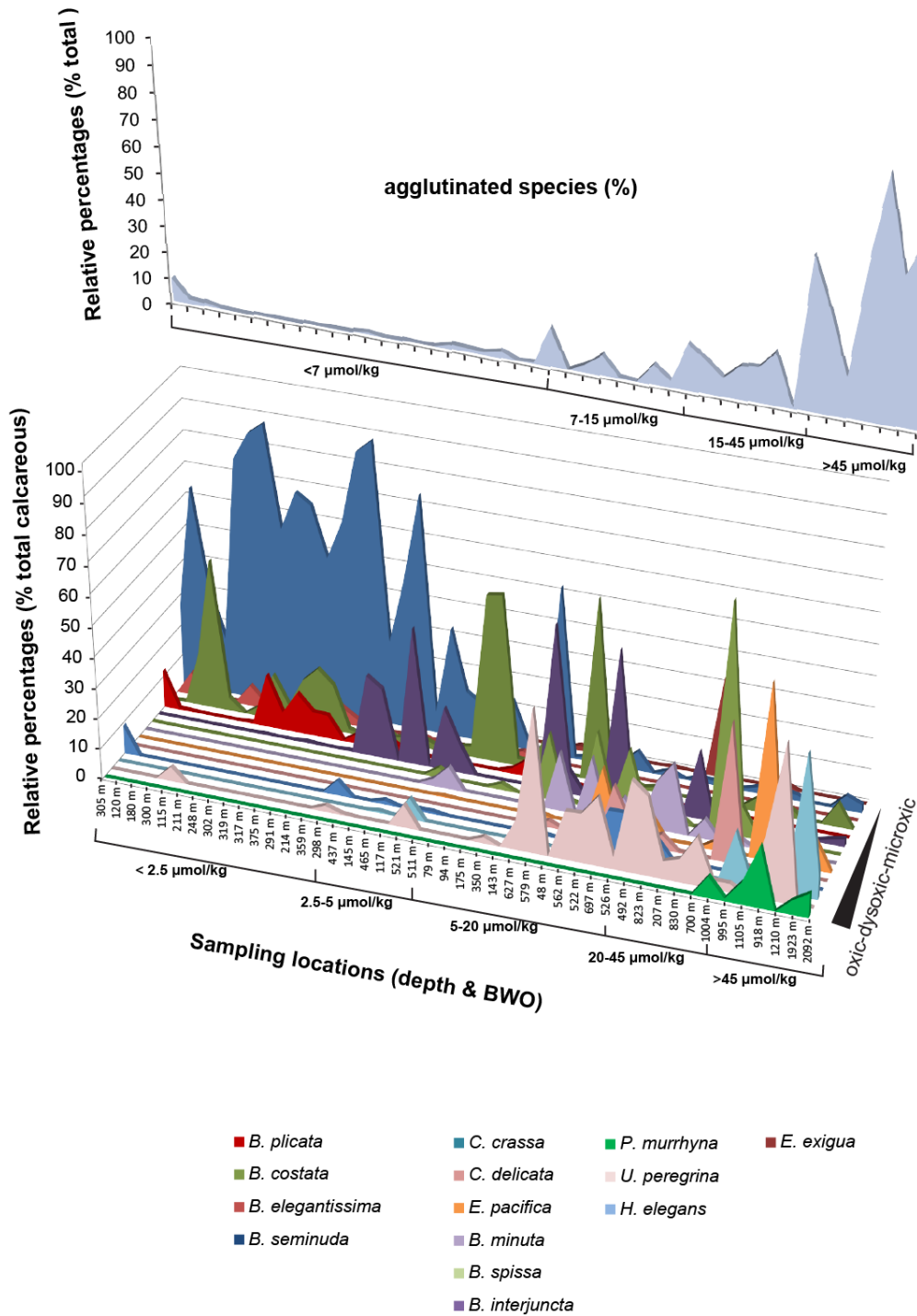
Sediment core depth (cm)	843	883	923	963	1043	1163	1243	1323
<i>Dorothia goesi</i>								
<i>Ehrenbergina pupa</i>								
<i>Epistominella afueraensis</i>	8	1		2			3	
<i>Epistominella exigua</i>	46	79	62	52	117	45	60	127
<i>Epistominella cf. exigua</i>				2				
<i>Epistominella obesa</i>	16	11	13	10	19	16	8	9
<i>Epistominella pacifica</i>	11	33	16		15	10	8	5
<i>Epistominella smithi</i>	25			14	24	14	26	28
<i>Fissurina annectens</i>							1	
<i>Fissurina kergulenensis</i>								
<i>Fissurina laevigata</i>								
<i>Fissurina marginata</i>								
<i>Fissurina orbignyana</i>								
<i>Fissurina semimarginata</i>								
<i>Fursenkoina fusiformis</i>	2	3	5		9	6	9	7
<i>Fursenkoina glabra</i>						4		
<i>Globobulimina affinis</i>							3	
<i>Globobulimina glabra</i>	2	6			3			2
<i>Globobulimina ovula</i>			2	2				
<i>Globobulimina pacifica</i>	2	2			4	3		3
<i>Globobulimina sp.</i>								
<i>Globocassidulina paratortuosa</i>		25	3	9	9	6	12	16
<i>Globocassidulina subglobosa</i>	5	2		1	2			2
<i>Gyroidina altiformis</i>						1		
<i>Gyroidina cf. gemma</i>								
<i>Gyroidina polia</i>								
<i>Gyroidina quinqueloba</i>	1	1	2			1		
<i>Gyroidina rothwelli</i>	23	27	12	10	22	23	4	9
<i>Gyroidina subtenera</i>		2						
<i>Gyroidina sp.</i>		1	2	3				
<i>Hanzawaia bertheloti</i>								
<i>Hanzawaia mexicana</i>					5		2	3
<i>Hanzawaia sp.</i>				1				1
<i>Hoeglundina elegans</i>								
<i>Lagena amphora</i>						1	1	
<i>Lagena distoma</i>								
<i>Lagena gracillima</i>								
<i>Lagena hispidula</i>								1
<i>Lagena lateralis</i>								
<i>Lagena squamosa</i>								
<i>Lagena striata</i>								
<i>Lagena substriata</i>					2	4		1
<i>Lagena sulcata</i>					1			
<i>Lagena sulcata peculiaris</i>							1	
<i>Lagena williamsoni</i>								
<i>Lagena sp.</i>								
<i>Lagenosolenia inflatiperforata</i>						1		
<i>Laticarinina pauperata</i>								
<i>Lenticulina convergens</i>								
<i>Lenticulina limbosa</i>								
<i>Lenticulina sp.</i>								
<i>Melonis affinis</i>								
<i>Melonis barleeaanum</i>								
<i>Melonis pompilioides</i>								
<i>Nonionella auris</i>			3		3	8	3	2
<i>Nonionella iridea</i>	1							2
<i>Nonionella labradorica</i>								
<i>Nonionella miocenica</i>								2
<i>Nonionella stella</i>	1	6	2	2			9	

Appendix 4: Species protocols

Sediment core depth (cm)	843	883	923	963	1043	1163	1243	1323
<i>Nonionella turgida</i>		3	1		2	4		
<i>Nonionella sp.</i>								
<i>Nonionoides grateloupii</i>	5	1		1				
<i>Oolina apiculata</i>								
<i>Oolina globosa</i>		1					1	1
<i>Oolina truncata</i>								
<i>Oridorsalis umbonatus</i>					1			
<i>Planulina ornata</i>							1	
<i>Praeglobobulimina ovata</i>								
<i>Praeglobobulimina spinescens</i>		2		1		11	9	
<i>Pseudoparella subperuviana</i>	3	3	7					3
<i>Pseudoparella sp.</i>			4					
<i>Pullenia bulloides</i>								
<i>Pullenia quinqueloba</i>								
<i>Pyrgo depressa</i>					1			
<i>Pyrgo murrhyna</i>								
<i>Quinqueloculina seminulum</i>					1		3	1
<i>Quinqueloculina sp.</i>								
<i>Stainforthia complanata</i>	1							
<i>Suggrunda eckisi</i>	10	17	3	5	7	4	4	3
<i>Suggrunda porosa</i>							2	
<i>Uvigerina auberiana</i>	14	11	3	4				
<i>Uvigerina canariensis</i>	2							
<i>Uvigerina excellens</i>								
<i>Uvigerina peregrina</i>	2		1		7	11	2	13
<i>Uvigerina semiornata</i>	7	4		5	13	4	13	7
<i>Uvigerina cf. semiornata</i>		2	5	2	5	11		
<i>Uvigerina senticosa</i>								
<i>Uvigerina striata</i>			1	2				1
<i>Uvigerina spp.</i>	1		1					
<i>Valvulineria araucana</i>	1	1	2	2	8		4	
<i>Valvulineria bradyana</i>		2		1				
<i>Valvulineria glabra</i>	1	1		1				
<i>Valvulineria involuta</i>								
<i>Valvulineria rugosa</i>								
<i>Valvulineria spp.</i>							1	
<i>Virgulina cf. apertura</i>			2					4
<i>Virgulina bramlettei</i>		1						
<i>Virgulina cornuta</i>	2	1	3	1	11	8	9	8
<i>Virgulina pauciloculata</i>				1				
<i>Virgulina schreibersiana</i>		3		1		5	5	24
<i>Virgulina seminuda</i>					1	2		1
<i>Virgulina spinosa</i>	8	37	18	65	8	3	4	
Unknown calcareous	5	1	2	2	4		2	

Taxa_S	51	54	43	49	56	49	52	53
Individuals	428	524	290	318	685	494	455	560
n	0.0036	0.0057	0.0041	0.0082	0.0147	0.0101	0.0077	0.0083
>63 µm weight (g)	0.6376	0.4207	0.3930	0.2925	0.5045	0.8499	0.7804	0.7325
Abundance (#/g sed)	186463	218516	179979	132583	92366	57549	75719	92109
Fisher_alpha	15.09	15.11	13.96	16.18	14.43	13.51	15.13	14.37
Shannon_H	3.390	3.219	3.191	3.108	3.322	3.370	3.398	3.132
Dominance_D	0.047	0.060	0.072	0.084	0.062	0.054	0.050	0.081

Supplementary Information Figure 1. Graphs showing the relative percentages (% total calcareous) of the index living benthic foraminifera and the relative percentages of the agglutinated species (% total). x-axis indicates the surface sample locations and they are grouped according to the prevailing bottom-water-oxygen concentrations.



Appendix 5: supplementary information of Chapter 5

Supplementary information Table. Results of the Approach 2 bottom water oxygenation estimations in 3 sediment cores with the core depth and calibrated age point information.

	M77/2-50-4 8°S 1013 m				M77/2-52-2 5°S 1249 m				M77/2-59-1 3°57'S 997 m			
	Core depth (cm)	Age (cal yrs BP)	BWO (μmol/kg)	error	Core depth (cm)	Age (cal yrs BP)	BWO (μmol/kg)	error	Core depth (cm)	Age (cal yrs BP)	BWO (μmol/kg)	error
late Holocene	HIATUS				90	3130	44.8	9.1	143	3024	29.1	21
					110	3845	42.9	11.9	163	3413	34.1	22.8
					120	4202	47.5	13.1	183	3801	3.9	18.3
					130	4559	45.6	11.7	203	4178	34.9	20.3
					140	4917	51.1	13.2	223	4531	32.8	20.6
									243	4877	47.9	23.6
early Holocene	HIATUS				230	8097	37.7	14.9	403	8098	52.5	21.6
					240	8486	47.9	16.8	443	8596	29.7	17.9
					250	8839	44.5	15.4	483	9095	33.7	19.1
					260	9192	49.7	14.9	523	9594	29.8	17.6
					270	9546	42.4	13.0	563	10093	24.3	17.6
					280	9899	50.9	17.2				
BA/ACR	60	12873	7.3	9.1	350	12714	39.3	17.3	803	13112	21	14
	70	13502	22.2	7.9	360	13177	29	17.7	843	13504	43.8	13.6
	80	14131	15.	7.7	370	13641	63.4	16.4	883	13867	44.5	13.5
	90	14377	20.6	7.4	380	14143	50.6	16	923	14230	57.9	16.2
	100	14622	14.7	7.6	390	14465	76.7	19.6	963	14569	60.4	13.3
Heinrich Stadial 1	110	14868	16.9	7.3	400	15147	65.4	12.1	1043	15080	38.2	11.8
	130	15359	20.9	8	410	15469	71	16.1	1163	15643	46.9	9.3
	150	15850	26.1	7.4	420	16151	71.7	16.7	1243	16330	52.3	10.9
	170	16341	32.9	8.8	430	16653	71.3	15.6	1323	17065	66.8	15.1
	190	16832	25.8	8.9	440	17155	80	18.5				
	210	17215	35.8	8.3	450	17657	97.1	19.9				
	230	17598	43.2	6.8								
Last Glacial Max	330	20095	33	7.7	500	20168	71.4	19.1	NO RECORD			
	340	20359	37.3	7.4	510	20670	67.5	15.4				
	350	20623	44.3	6.9	520	21172	63.6	18.6				
	370	20900	40.9	9	530	21674	66.3	15.3				
	390	21178	34.9	8.3	540	22176	70.3	16.9				
	410	21455	44.4	6.9								
	430	21733	35.2	10.8								
	450	22010	34.1	7.7								

Thank you

I would like to thank to my supervisor Dr. Joachim Schönfeld for giving me the opportunity to work and do my Ph.D. as a part of this interesting interdisciplinary project and also for helping me getting through in the challenging and fascinating world of benthic foraminifera. I am especially thankful and actually I feel really lucky that I was working in this project together with Dr. Nicolaas Glock who made almost everything easier during the whole Ph.D. period. With his support and help since the beginning I could cope with lots of things which were new for me, translating things from German to English or vice versa is just one example.

I would like to thank to Prof. Dr. W.-Christian Dullo who in the first place introduced me the SFB 754 project while I was looking for interesting Ph.D. topics back in Istanbul. Special thanks to Prof. Dr. Martin Frank for being there whenever there was need to talk about things, to Prof. Dr. Dirk Nürnberg for his support especially during the last days and also for including me to his scientific crew and taking me to the research cruise in the Caribbean Sea which is definitely one of the highlights of this Ph.D. period. I also want to thank to Dr. Marcus Dengler who was really patient when I was trying to understand the basics of physical oceanography.

I would like to thank to my extremely nice office mates Anna Jentzen and Swaantje Bennecke who made the office hours much more pleasant, to Theodora Pados, Judith Elger, Veit Dausmann, David Poggemann, Daniel Yirgaw and others for the nice working environment, especially the lunch breaks. I don't want to think how challenging it would have been, without all these beautiful people I met thanks to my work and Ph.D. project. Following this I would like to also thank to other side of the fjord; Allanah Paul simply for everything, Sonja Endres for all the support especially during the first months, Tim Boxhammer for being Tim, a good friend and almost a flat-mate.

I am really grateful that I am/was part of the legendary WG, sharing the flat with beautiful people Michael Sswat, Susanne Schorr, Stephanie Langer and Matias Scheinin at some point, who transformed it a wonderful, comfortable home even when home-sickness kicked in. At this point I am really happy that Serra Örey entered my life in Kiel as an intruder from Istanbul which made things much more bearable and cheerful, including possibility to talk Turkish and occasional Turkish food.

Finally, I would like to thank to my friend Mine Sim Yücel who listened me, supported me from such a distance. With her brilliant travel ideas, holidays were even better and relaxing.

I want to dedicate this thesis to my family, without their support I wouldn't have been this far in my education and career. But most of all I want to dedicate it to my father who left us too early and did not see this happening. He was smart enough to foresee the scientist in me and that I would need German in the future, already during middle school, but I was stubborn enough not to accept this fact.

Thank you all for being there during this challenging and full-of-with-new things period of my life.

*"I almost wish I hadn't
gone down that rabbit-hole
-and yet - and yet -
it's rather curious, you know
this sort of life"- Lewis Carroll*

Curriculum Vitae

Personal Data

Name: Zeynep Erdem
Address: Ringstrasse 75,
24114 Kiel, Germany
Tel: +49 (0) 176 314 38356
E-Mail: zeyerdem@gmail.com
Nationality: Turkish
Date of birth: 26.05.1985
Gender: Female

Summary

- Geologist, PhD in paleoceanography and micropaleontology, interested in multi-proxy approaches in paleoceanography and paleoclimatology.
- Knowledge in the Late Quaternary benthic foraminifera taxonomy from South East Equatorial Pacific (Peru-Ecuador), familiar with Black Sea and Marmara Sea species.
- Experience at sediment studies from both marine and lacustrine environments (e.g., radiocarbon dating, physical properties, XRF measurements).
- Basic knowledge and experience on geophysical studies and interpretation (mainly seismic)
- Experienced Microsoft Office and Adobe products user
- Nature lover, amateur photographer with good language skills.

Education and Work Experience

Ph.D.

07.2012 – ongoing **Ph.D. Student in Faculty of Mathematics and Natural Sciences**, Christian-Albrechts-University of Kiel, Germany

- Thesis title “Reconstruction of past bottom water conditions of the Peruvian Oxygen Minimum Zone (OMZ) for the last 22 kyrs and the benthic foraminiferal response to (de)oxygenation”
- Part of Integrated School of Ocean Sciences (ISOS) in Kiel.
- Expected graduation in June 2016.

07.2012 – 06.2016 **Researcher/Project Member** in Paleoceanography department at GEOMAR Helmholtz Centre for Ocean Research Kiel, Germany as part of **SFB754** Phase II subproject B7.

- Chronostratigraphies of sediment cores from the Peruvian margin
- Paleo-environmental reconstructions off Peru using benthic foraminifera.
- Field and lab work assistance to Living Benthic Foraminifera from Tidal Flats; M.Sc. lecture during winter semesters.

11. – 27.03.2013 **Researcher**; German R/V Meteor, Leg M94, Carribean Sea

- Geophysical studies & Sediment core sampling

06.2011 – 04.2012 **Administrative and Logistic support** for **EU WP7 HYPOX** project at EMCOL (Eastern Mediterranean Centre for Oceanography and Limnology), Istanbul, Turkey

M.Sc.

09.2008– 06.2011 **M.Sc. Student; Climate and Marine Science program,**

Eurasian Institute of Earth Sciences, Istanbul Technical University, Istanbul, Turkey

- Lectures on marine and climate science, earth system, marine geochemistry, paleoceanography
- Thesis title “Sedimentary Record of Mediterranean Inflow Effect on Redox Conditions of the Istanbul Strait Outlet Area of the Black Sea”

Researcher and Student assistant at EMCOL, Istanbul, Turkey.

06.2009– 06.2011 **Researcher** at **EU WP7 HYPOX** project, at EMCOL, Istanbul, Turkey.

- M.Sc. topic/analysis and data acquisition from Black Sea sediment cores. (Itrax XRF, MSCL and TOC/TIC measurements)
- Attendance to research cruises

08.2010 & 01.2011 **Student assistant** at **ICDP: PALEOVAN** Lake Van, Ahlat, Van, Turkey.

- Multi Sensor Core Logger (MSCL) measurements on ICDP cores.

& part of ICDP:PALEOVAN Scientific party at MARUM, IODP-ICDP Core Repository, Bremen, Germany.

- Laboratory work; Sampling Lake Van ICDP cores

03.2010 & 10.2010 **Student assistant;** part of **EC EMSO/ESONET** European Multidisciplinary Seafloor Observatory project, at Turkish R/V Yunus Sea of Marmara Demo Mission, Istanbul, Turkey.

- Deployment of sea floor monitoring device
- Communication between Italian scientific team – Turkish R/V crew members.

& at URANIA2010 Italian R/V Urania, part of EC EMSO/ESONET European Multidisciplinary Seafloor Observatory Project, in Sea of Marmara, Turkey.

- Geophysical studies and sediment core sampling

11.2009 & 04.2010 **Researcher**, part of **EU WP7 HYPOX project;** Turkish R/V Arar, Black Sea (Bosphorus Outlet Area), Turkey & German R/V M.S.Merian, Leg MSM-15/1, Black Sea (Bosphorus Outlet Area), Turkey

- Geophysical Studies and sediment core sampling

B.Sc.

09.2004 – 08.2008 **B.Sc. Student** in Mining Faculty, Department of Geological Engineering Istanbul Technical University, Istanbul, Turkey

- Lectures (8 semester) Geology and Engineering subjects.
- Thesis title “Geology of Kilyos (Northern İstanbul) and the Sedimentological Properties of Sand Dunes in the Region”

- 06.2007 – 08.2007 **Internship** at DSI (State Hydraulic Works) XIV. Region Headquarters, Istanbul, Turkey
- Regular visits – controls at dam construction in Istanbul, Turkey.
 - Geological mapping of the region
- 06.2006 – 07.2006 **Internship** at Eastern Mediterranean Center for Oceanography and Limnology (EMCOL) laboratories, Istanbul Technical University, Istanbul, Turkey
- Micropaleontological studies on sediment cores from Marmara Sea, Turkey.

Education

- 09.1996 – 06.2004 High School**; Kadıköy Anatolian High School, Istanbul, Turkey
- 09.2002 – 07.2003 **Student exchange program** AFS; Liceo Scientifico Ettore Majorana, Latina, Italy

Language

English - Advanced

German - Intermediate

Turkish - Mother language

Italian - Upper Intermediate

French - Beginner

Training & Certificates

- 2013 6th Course on Benthic and Planktonic Foraminifera within the International School on Foraminifera, organized by Grzybowski Foundation, in Urbino, Italy.
- 2012 Molecular Organic Biogeochemistry Summerschool at the NIOZ, Texel, the Netherlands.
- Soft skill and technical courses during Ph.D. period at ISOS and Graduate Centre of Christian-Albrechts-University of Kiel, Germany
- Basics of University teaching,
 - Scientific poster presentation and design, Adobe InDesign
 - Introduction to programming language (R, Matlab, Python), Physical oceanography, ODV

Memberships & others

- 12.2012 – 09.2014 Ph.D. students representation/GEOMAR DokTeam member
- 05.2007 – 07.2012 Part time librarian in a private collection library
- 09.2003 – 07.2012 Volunteer at AFS Student Exchange program

Publications

Papers Published in Science Journals

- 1) **Erdem, Z.**, Schönfeld, J., Glock, N., Dengler, M., Mosch, T., Sommer, S., Elger, J. and Eisenhauer, A., 2016. Peruvian sediments as recorders of an evolving hiatus for the last 22 thousand years *Quaternary Science Reviews*, 137 . pp. 1-14. DOI 10.1016/j.quascirev.2016.01.029.
- 2) Schönfeld, J., Kuhnt, W., **Erdem, Z.**, Flögel, S., Glock, N., Aquit, M., Frank, M., Holbourn, A., 2015. Records of past mid-depth ventilation: Cretaceous ocean anoxic event 2 vs. Recent oxygen minimum zones, *Biogeosciences*, 12, 1169-1189. doi:10.5194/bg-12-1169-2015.
- 3) Friedrich, J., Janssen, F., Aleynik, D., Bange, H.W., Boltacheva, N., Çagatay, N., Dale, A.W., Etiope, G., **Erdem, Z.**, Geraga, M., Gilli, A., Gomoiu, M.T., Hall, P.O.J., Hansson, D., He, Y., Holtappels, M., Kirf, M.K., Kononets, M., Kononov, S., Lichtschlag, A., Livingstone, D.M., Marinaro, G., Mazlumyan, S., Naeher, S., North, R.P., Papatheodorou, G., Pfannkuche, O., Prien, R., Rehder, G., Schubert, C.J., Soltwedel, T., Sommer, S., Stahl, H., Stanev, E.V., Teaca, A., Tengberg, A., Waldmann, C., Wehrli, B., Wenzhöfer, F., 2014. Investigating hypoxia in aquatic environments: diverse approaches to addressing a complex phenomenon, *Biogeosciences*, 11, 1215-1259. doi:10.5194/bg-11-1215-2014.

Articles, Reports published (not peer-reviewed)

- 1) Hübscher, C., Nürnberg, D., Al Hseinat, M., Alvarez Garcia, M., **Erdem, Z.**, Gehre, N., Jentzen, A., Kalvelage, C., Karas, C., Kimmel, B., Mildner, T., Ortiz, O., Parker, A. O., Petersen, A., Raeke, A., Reiche, S., Schmidt, M., Weiß, B. and Wolf, D. (2014) Yucatan Throughflow - Cruise No. M94, March 12 – March 26, 2013, Balboa (Panama) – Kingston (Jamaica) . *METEOR-Berichte, M94* . DFG-Senatskommission für Ozeanographie, Bremen, 32 pp. DOI 10.2312/cr_m94.
- 2) **Erdem, Z.**, 2015. Taxonomy Workshop on Recent benthic foraminifera (TMS2015 meeting), Foraminifera group report article in *Newsletter of Micropaleontology*, Number 92, p. 44, ISSN: 0140-6730, August 2015 issue.

Papers Presented in International Conferences (abstracts)

- 1) **Erdem, Z.**, Schönfeld, J., Glock, N., 2015. A 22,000 year record of changing redox conditions from the Peruvian Oxygen Minimum Zone (OMZ): benthic foraminifera approach, *AGU2015 Abstracts* (poster)
- 2) **Erdem, Z.**, Schönfeld, J., Glock, N., 2015. Benthic foraminifera as indicators of changing redox conditions: a 22,000 year record from the Peruvian margin, *TMS15 Abstracts*. (poster)
- 3) **Erdem, Z.**, Schönfeld, J., Voigt, S., Glock, N., Eisenhauer, A., Dengler, M., 2014. A 22 kyr record of an evolving mid-depth hiatus in sediments at the Peruvian margin, *GeoFrankfurt2014 Abstracts*. (talk)
- 4) **Erdem, Z.**, Schönfeld, J., Voigt, S., Glock, N., Eisenhauer, A., Dengler, M., 2013. SFB754: Sediments of the Peruvian Oxygen Minimum Zone as Records of Mid-Depth Ocean Dynamics, *ICP11 Abstracts*. (poster)
- 5) **Erdem, Z.**, Çagatay, M.N., Damcı, E., Ülgen, U.B., Holtappels, M., Lichtschlag, A., 2012. Holocene History of the Mediterranean Inflow and Its Influence on Formation of the Channel Network Complex and Redox Conditions in the Istanbul Strait Outlet Area of the Black Sea.

Geophysical Research Abstracts, Vol. 14, EGU2012-7068, 2012. *EGU General Assembly 2012*. (talk)

- 6) Damcı, E., Çağatay, M.N., Krastel, S., Öğretmen, N., Çukur, D., Ülgen, U.B., **Erdem, Z.**, Litt, T., Anselmetti, F.S., Eriş, K.K., 2012. Lake Level Changes of Lake Van over the Last 400 ka: Evidence from Deltas in Seismic Reflection Data and ICDP Drilling. Geophysical Research Abstracts, Vol. 14, EGU2012-626-3, 2012. *EGU General Assembly 2012*.
- 7) Çağatay, M.N., **Erdem, Z.**, Ülgen, U.B., Damcı, E., Acar, D., Holtappels, M., Lichtschlag, A., 2011. Holocene Evolution of the Channel Network Complex and Redox Conditions in the İstanbul Strait Outlet Area of Black Sea: Influence of the Mediterranean Inflow. *Abstract book of INQUA 501 Plenary Meeting and Field Trip*.
- 8) **Erdem, Z.**, Çağatay, M.N., 2011. Effect of Mediterranean Inflow on Redox Conditions of the İstanbul Strait Outlet Area of the Black Sea. Geophysical Research Abstracts, Vol. 13, EGU2011-2363, 2011. *EGU General Assembly 2011*. (talk)

Papers Presented in National Conferences (abstracts)

- 1) Damcı, E., Çağatay, M.N., Krastel, S., Öğretmen, N., Çukur, D., Ülgen, U.B., **Erdem, Z.**, Litt, T., Anselmetti, F.S., Eriş, K.K., 2012. Van Gölü'nün Son Dörtüzbün Yıldaki Göl Seviyesi Değişimleri: Sismik Yansıma Hatlarındaki Deltalar ve ICDP Sondaj Verileri. 65. *Türkiye Jeoloji Kurultayı Bildiri Kitabı, 2012*.
- 2) **Erdem, Z.**, Çağatay, M.N., 2011. Akdeniz Akıntısının Karadeniz'in İstanbul Boğazı Çıkışında Redoks Koşulları Üzerindeki Etkileri. 64. *Türkiye Jeoloji Kurultayı Bildiri Kitabı, 2011*.